

DISSERTATION

DEVELOPMENT AND OPTIMIZATION OF A STOVE-POWERED  
THERMOELECTRIC GENERATOR

Submitted by

Dan Mastbergen

Department of Mechanical Engineering

In partial fulfillment of the requirements

For the Degree of Doctor of Philosophy

Colorado State University

Fort Collins, Colorado

Spring 2008

UMI Number: 3321296

### INFORMATION TO USERS

The quality of this reproduction is dependent upon the quality of the copy submitted. Broken or indistinct print, colored or poor quality illustrations and photographs, print bleed-through, substandard margins, and improper alignment can adversely affect reproduction.

In the unlikely event that the author did not send a complete manuscript and there are missing pages, these will be noted. Also, if unauthorized copyright material had to be removed, a note will indicate the deletion.

**UMI**<sup>®</sup>

---

UMI Microform 3321296

Copyright 2008 by ProQuest LLC.

All rights reserved. This microform edition is protected against unauthorized copying under Title 17, United States Code.

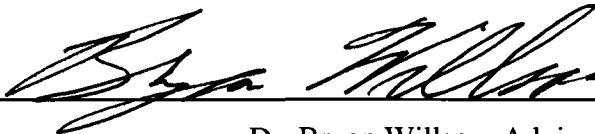
ProQuest LLC  
789 E. Eisenhower Parkway  
PO Box 1346  
Ann Arbor, MI 48106-1346

COLORADO STATE UNIVERSITY

March 12, 2008

WE HEREBY RECOMMEND THAT THIS DISSERTATION PREPARED UNDER OUR SUPERVISION BY DANIEL MASTBERGEN TITLED DEVELOPMENT AND OPTIMIZATION OF A STOVE-BASED THERMOELECTRIC GENERATOR BE ACCEPTED AS FULLFILING IN PART REQUIREMENTS FOR THE DEGREE OF DOCTOR OF PHILOSOPHY.

Committee on Graduate Work



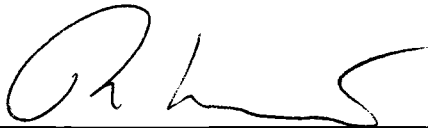
---

Dr. Bryan Willson, Advisor



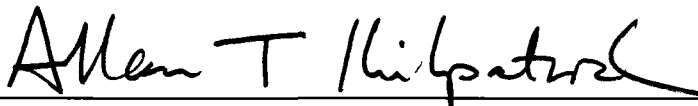
---

Dr. Daniel Olsen, Committee Member



---

Paul Hudnut, Committee Member



---

Dr. Allan T. Kirkpatrick, Committee Member, Mechanical Engineering  
Department Head

**ABSTRACT OF DISSERTATION**  
**DEVELOPMENT AND OPTIMIZATION OF A STOVE-BASED**  
**THERMOELECTRIC GENERATOR**

Almost a third of the world's population still lacks access to electricity. Most of these people use biomass stoves for cooking which produce significant amounts of wasted thermal energy, but no electricity. Less than 1% of this energy in the form of electricity would be adequate for basic tasks such as lighting and communications. However, an affordable and reliable means of accomplishing this is currently non-existent.

The goal of this work is to develop a thermoelectric generator to convert a small amount of wasted heat into electricity. Although this concept has been around for decades, previous attempts have failed due to insufficient analysis of the system as a whole, leading to ineffective and costly designs. In this work, a complete design process is undertaken including concept generation, prototype testing, field testing, and redesign/optimization. Detailed component models are constructed and integrated to create a full system model. The model encompasses the stove operation, thermoelectric module, heat sinks, charging system and battery. A 3000 cycle endurance test was also conducted to evaluate the effects of operating temperature, module quality, and thermal interface quality on the generator's reliability, lifetime and cost effectiveness. The results from this testing are integrated into the system model to determine the lowest system cost in \$/Watt over a five year period.

Through this work the concept of a stove-based thermoelectric generator is shown to be technologically and economically feasible. In addition, a methodology is developed for optimizing the system for specific regional stove usage habits.

Daniel Blair Mastbergen  
Department of Mechanical Engineering  
Colorado State University  
Fort Collins, CO 80523  
Spring 2008

## **Acknowledgments**

I would like to thank my parents for their constant support throughout my college career and especially during the past couple years of this work. I could not have done this without their help and encouragement.

I would also like to thank Sachin Joshi, Gabriel Miller, and Patrick Flynn. Each played a vital role in the field testing phases of this project, which would not have been possible without their help.

Finally, I would like to thank God for the giving me the opportunity and abilities necessary to pursue an advanced degree in a field I truly enjoy.

# TABLE OF CONTENTS

<b>Acknowledgments</b> .....	<b>iv</b>
<b>TABLE OF CONTENTS</b> .....	<b>v</b>
<b>LIST OF FIGURES</b> .....	<b>ix</b>
<b>LIST OF TABLES</b> .....	<b>xvi</b>
<b>LIST OF ABBREVIATIONS</b> .....	<b>xvii</b>
<b>1 BACKGROUND</b> .....	<b>1</b>
1.1 Problem Identification .....	1
1.2 Solution Concepts .....	4
1.2.1 Stirling Engine .....	5
1.2.2 Brayton Cycle Engine .....	8
1.2.3 Rankine Cycle Engine.....	9
1.2.4 Thermoelectric Generator .....	10
1.3 General Principles of Thermoelectricity .....	11
1.3.1 Thermoelectric Effects.....	11
1.3.2 Thermodynamics of Thermoelectric Modules .....	16
1.3.3 Thermoelectric Materials .....	25
1.3.4 Emerging Thermoelectric Materials .....	29
1.4 Construction and Analysis of Thermoelectric Generators.....	33
1.4.1 Thermoelectric Module Construction .....	33
1.4.2 Thermoelectric Generator Assembly .....	36
1.4.3 Heat Sinks .....	38
1.4.4 Interface Materials .....	42
1.4.5 Generator Thermal Analysis .....	45
1.4.6 Module Electrical Performance .....	47
1.4.7 Module Reliability and Degradation.....	49
1.5 Battery Storage .....	53
1.5.1 Battery Characteristics .....	53

1.5.2	Battery Charging .....	54
1.5.3	Battery Lifetime .....	56
1.6	Lighting.....	57
1.7	Stove Design.....	61
<b>2</b>	<b>GENERATION 1 SYSTEM DEVELOPMENT .....</b>	<b>63</b>
2.1	Cooling System Design Alternatives.....	65
2.1.1	Air-Cooled Forced Convection.....	65
2.1.2	Air-Cooled Natural Convection.....	66
2.1.3	Water-Cooled Forced Convection .....	67
2.1.4	Water-Cooled Natural Convection .....	68
2.1.5	Final Cooling System Selection.....	70
2.2	Component Selection.....	71
2.2.1	Heat Sink Evaluation .....	71
2.2.2	Module Evaluation.....	77
2.2.3	Steady State System Modeling .....	79
2.3	Stove Integration and Testing .....	83
2.4	Charging Circuit Design .....	87
2.4.1	DC-DC Converter .....	87
2.4.2	Fan Control .....	92
2.4.3	Battery Management.....	93
2.5	Complete System Analysis .....	94
2.6	Battery Selection.....	95
2.7	Prototype Kit Cost Breakdown.....	96
<b>3</b>	<b>FIELD TESTING GENERATION 1 PROTOTYPE .....</b>	<b>99</b>
3.1	Objectives .....	99
3.2	Data Acquisition .....	99
3.3	Nicaragua Field Testing.....	103
3.3.1	Test Plan.....	103
3.3.2	Installation.....	103
3.3.3	Results from Round 1 .....	105
3.3.4	Results from Round 2 .....	115
3.3.5	Post Test Component Analysis .....	124

3.4	India Field Testing .....	127
3.4.1	Test Plan.....	128
3.4.2	Results.....	128
3.5	Nepal Field Testing.....	132
3.5.1	Test Plan.....	132
3.5.2	Results.....	133
3.6	Conclusions from Field Testing.....	141
<b>4</b>	<b>Generation 2 System Development.....</b>	<b>145</b>
<b>5</b>	<b>System Model .....</b>	<b>146</b>
5.1	Component Characterization .....	146
5.1.1	Module/Heat Sink Test Bench Development .....	146
5.1.2	Module Characterization.....	150
5.1.3	Cold Sink Characterization.....	154
5.1.4	Hot Sink Modeling.....	160
5.1.5	Charging Circuit Characterization .....	173
5.1.6	Stove Temperature Characterization.....	174
5.2	System Model Architecture .....	179
5.3	Model Validation .....	180
<b>6</b>	<b>Generation 2 Circuit Design .....</b>	<b>185</b>
6.1	Peak Power Tracking .....	185
6.2	Circuit Efficiency Optimization.....	191
6.3	Variable Fan Control .....	195
6.4	Hysteresis.....	199
6.5	Battery Charge Control -- Adaptive Battery Capacity.....	202
6.6	Low Power Operation .....	204
6.7	Program Architecture.....	206
6.8	Circuit Design .....	208
6.9	Overall Net Energy Gains from Generation 2 Circuit .....	211
<b>7</b>	<b>Endurance Testing.....</b>	<b>214</b>
7.1	Test Apparatus .....	214
7.2	Test Matrix and Methodology .....	216
7.3	Results.....	218

<b>8</b>	<b>Parametric Studies and Component Optimization.....</b>	<b>222</b>
8.1	Damage Modeling -- Module and Temperature Selection .....	222
8.2	Heat Sink Selection.....	230
8.3	Over-Temperature Protection .....	235
<b>9</b>	<b>Future Work.....</b>	<b>241</b>
<b>10</b>	<b>Summary &amp; Conclusions.....</b>	<b>242</b>
<b>11</b>	<b>Works Cited.....</b>	<b>250</b>
<b>12</b>	<b>Appendix.....</b>	<b>256</b>
12.1	Microcontroller Code (PicBasic).....	256
12.2	EES Model Code .....	263
12.3	Heat sink data.....	267
12.4	Module Data .....	273
12.5	Nicaragua 5 Week Data House 7 and 8 .....	278
12.5.1	House 7 Five Week Data .....	278
12.5.2	House 8 Five Week Data .....	283

## LIST OF FIGURES

Figure 1.1: Effects of firewood gathering.....	2
Figure 1.2: Room lit by traditional stove.....	4
Figure 1.3: STC 55W free piston engines.....	6
Figure 1.4: Solar Stirling engines. Boeing 30 kW(left) Energy Innovations 50 W(right).....	6
Figure 1.5: Biowatt Stirling engine from Sunpower.....	7
Figure 1.6: Capstone 30kW micro-turbine. ....	8
Figure 1.7: Energy bands in a thermoelectric generator using n-type semiconductor	13
Figure 1.8: Electron energy levels in p-type conductor.....	15
Figure 1.9: Basic thermoelectric generator model.....	18
Figure 1.10: Differential segment within generator leg.....	18
Figure 1.11: Power and efficiency vs. $m'$ for $Z=.001$ .....	25
Figure 1.12: Power and efficiency vs. $m'$ for $Z=.007$ .....	25
Figure 1.13: Effect of charge carrier concentration on material properties [27] .....	27
Figure 1.14: Figure of Merit for Bismuth Telluride, Lead Telluride, and Silicon Germanium [32].....	28
Figure 1.15: Quantum well efficiency [2].....	32
Figure 1.16: Quantum well module construction [Hi-Z].....	32
Figure 1.17: Basic thermoelectric circuit Error! Reference source not found.....	33
Figure 1.18: Schematic of a Thermo-element Error! Reference source not found....	34
Figure 1.19: Thermo-elements in series Error! Reference source not found.....	34
Figure 1.20: Close up of element assembly .....	34
Figure 1.21: Thermoelectric module construction.....	35
Figure 1.22: Basic components of a thermoelectric generator .....	37
Figure 1.23: Schematic of generator assembly .....	37
Figure 1.24: (clockwise from upper left) extruded heat sink, bonded fin heat sink, high density extrusion, forged pin fin heat sink.....	40
Figure 1.25: Water cooling block .....	41

Figure 1.26: Heat pipe design .....	42
Figure 1.27: Heat sinks based on heat pipe technology.....	42
Figure 1.28: Effect of clamping force on thermal resistance for multiple interface materials [48] .....	44
Figure 1.29: Effect of surface finish on junction quality [48] .....	45
Figure 1.30: Thermal resistance circuit for TEG.....	46
Figure 1.31: Thermal resistance circuit with bypass .....	46
Figure 1.32: Module equivalent circuit.....	47
Figure 1.33: Power as a function of $m'$ , $200\text{ }^{\circ}\text{C } \Delta T$ , $\alpha = 0.04\text{ V/K}$ .....	48
Figure 1.34: Power as a function of current, $200\text{ }^{\circ}\text{C } \Delta T$ , $\alpha = 0.04\text{ V/K}$ .....	49
Figure 1.35: Change in module AC resistance with number of cycles [46] .....	50
Figure 1.36: Change in module AC resistance with number of cycles [47].....	50
Figure 1.37: AC resistance change at elevated temperature ( $100\text{ }^{\circ}\text{C}$ ) [45] .....	51
Figure 1.38: ZT change at elevated temperature [46].....	52
Figure 1.39: ZT change from temperature cycling [47] .....	52
Figure 1.40: Typical discharge characteristics for a sealed lead acid battery where C is the battery capacity in Ah [3].....	54
Figure 1.41: Battery charging characteristics .....	55
Figure 1.42: Effect of discharge depth on battery life .....	56
Figure 1.43: Lighting efficacy comparisons [72][73].....	59
Figure 1.44: Efficacy and cost vs. lumens for single LED bulbs [71].....	59
Figure 1.45: Light and driver cost for various lighting options.....	61
Figure 1.46: Rocket elbow combustion chamber .....	62
Figure 1.47: Basic Rocket stove (left) and Ecofogao with chimney and oven (right) 63	
Figure 2.1: Stove model used for generator retrofit.....	64
Figure 2.2: Forced convection cooling concept.....	65
Figure 2.3: Aavid 65605 extrusion .....	66
Figure 2.4: Natural convection system using heated duct to increase flow .....	67
Figure 2.5: Water cooled forced convection system.....	68
Figure 2.6: Natural convection system with water tank .....	70
Figure 2.7: Thermal circuit with calculated heat sink resistances (red) .....	72
Figure 2.8: Properties for hot side heat sink at 15 cm length .....	73
Figure 2.9: Fan operating characteristics .....	75

Figure 2.10: Heat sinks (left to right) bonded fin, pin fin, extruded fin .....	76
Figure 2.11: Specifications for Aavid 61085 at 0.2 m/s and 0.4 m/s.....	82
Figure 2.12: Exploded view of TEG stove (with one TEG unit).....	83
Figure 2.13: TEG placement within the stove .....	84
Figure 2.14: Temperatures within the system during a cooking cycle .....	84
Figure 2.15: Comparison of CSU tests to field temperature data .....	85
Figure 2.16: Module power during a cooking cycle .....	85
Figure 2.17: Power vs. load resistance.....	88
Figure 2.18: Power curves at varying temperature differential .....	88
Figure 2.19: DC-DC current limit. Specification (left), actual at 30 mΩ (right).....	89
Figure 2.20: Actual current vs. peak power current.....	90
Figure 2.21: Component and system efficiency .....	91
Figure 2.22: Module conversion efficiency vs. power (constant internal resistance 3.4 Ohm) .....	91
Figure 2.23: Comparing max power to actual power .....	92
Figure 2.24: Labeled charging circuit.....	94
Figure 2.25: Energy losses through each system component (total energy for 3 cycles per day) .....	95
Figure 3.1: In-Line Power Meter .....	100
Figure 3.2: Signal conditioner (left), charger, battery, signal conditioner, loggers (right) .....	100
Figure 3.3: Generator kits ready to be shipped .....	104
Figure 3.4: Fabrication of stoves at Prolena .....	104
Figure 3.5: Instructing Prolena in assembling and diagnosing the generators .....	104
Figure 3.6: Field data showing damaged charging circuit.....	108
Figure 3.7: Module power from house #3 for three weeks.....	112
Figure 3.8: Module and battery voltage from house #3 for three weeks .....	112
Figure 3.9: Data from house #3 by day.....	113
Figure 3.10: New stove (left) and old stove (right) .....	114
Figure 3.11: Hot side temperature data from House #7 for 5 weeks .....	118
Figure 3.12: Module power data from House #7 for 5 weeks .....	118
Figure 3.13: Module and battery voltage data from House #7 for 5 weeks.....	118
Figure 3.14: Data from house #7 by day (first week).....	119

Figure 3.15: Temperature data from House #8 for 10 weeks .....	121
Figure 3.16: Module power data from House #8 for 10 weeks .....	121
Figure 3.17: Module and battery voltage over 10 week period (House #8) .....	122
Figure 3.18: Effect of failed battery on fan/cold sink failure .....	123
Figure 3.19: Data from house #8 by day (first week).....	124
Figure 3.20: Post test photos of fan and hot heat sink. ....	127
Figure 3.21: Post test module photos. Melted solder (left), fatigued module (right). .....	127
Figure 3.22: Data from 16 W generator in India .....	130
Figure 3.23: Data from 8 W generator in India .....	131
Figure 3.24: Module hot block temperature for 2 module unit in Nepal.....	134
Figure 3.25: Module hot block temperature for 2 module unit (by day) .....	135
Figure 3.26: Hot block temperature for 1 module unit in Nepal .....	137
Figure 3.27: Module hot block temperature for 1 module unit (by day) .....	137
Figure 3.28: Module power data from House #4 for 5 weeks .....	139
Figure 3.29: Hot side temperature data from House #4 for 5 weeks .....	139
Figure 3.30: Voltage data from House #4 for 5 weeks .....	139
Figure 3.31: System data by day for House #4 for the first week .....	140
Figure 5.1: Schematic of bench top tester.....	147
Figure 5.2: Temperature distribution within the bench top testing apparatus (In Kelvin) .....	148
Figure 5.3: Temperature distribution at the hot module surface and within the vicinity of the thermocouple (In Kelvin) .....	148
Figure 5.4: Temperature distribution at the cold module surface and within the vicinity of the thermocouple (In Kelvin) .....	149
Figure 5.5: Screen shots showing method for determining open circuit voltage and voltage drift after opening the load circuit.....	151
Figure 5.6: Example of module data sheet for TEP1-0.8 .....	152
Figure 5.7: Rmt Z-meter .....	153
Figure 5.8: Variability in initial Z-meter readings for 12 TEP1-0.8 modules .....	154
Figure 5.9: Results from heat sink length test using Mechatronics fan.....	156
Figure 5.10: Heat sink thermal resistance at varying fan voltage with three different fans (16 cm length) .....	157

Figure 5.11: Heat sink thermal resistance as a function of fan power (16.25 cm length) .....	158
Figure 5.12: Comparison of extruded E1465 16.5 cm (top right) and bonded Melcor 15 cm (bottom right) heat sinks using Cooler Master and Mechatronics fans .....	159
Figure 5.13: Heat sink thermal resistance with and without filter .....	160
Figure 5.14: Hot sink thermal resistance from field data (House #8 day 1) .....	161
Figure 5.15: Hot heat sink test apparatus .....	162
Figure 5.16: Experimental and manufacturer values for thermal resistance as a function of free stream velocity .....	163
Figure 5.17: Experimental and manufacturer values for pressure drop as a function of free stream velocity .....	163
Figure 5.18: Correction term for channel aspect ratio .....	164
Figure 5.19: Comparison of fluid dynamics estimate to experimental pressure drop .....	166
Figure 5.20: Model geometry (left) and heat sink mesh (right) .....	167
Figure 5.21: Temperature contours (in Kelvin) of air entry region (left) and fin temperature (right) .....	167
Figure 5.22: Contours of pressure (Pa) from the CFD model .....	168
Figure 5.23: Comparison of CFD results and experiment for thermal resistance ...	169
Figure 5.24: Comparison of CFD results, experiment, and fluids equations for pressure drop .....	169
Figure 5.25: Effect of hot gas temperature on thermal resistance .....	170
Figure 5.26: Stove fitted with inlet shroud for anemometer readings .....	172
Figure 5.27: Stove flow rates vs. the hot gas temperature .....	172
Figure 5.28: Comparison of field data and CFD data at 2 g/s flow rate .....	173
Figure 5.29: Charging circuit characterization for original circuit with 40 mOhm current sense resistor .....	174
Figure 5.30: Averaging multiple cycles .....	175
Figure 5.31: Temperature histogram for Nicaragua field test data .....	176
Figure 5.32: Average daily cycle for Nicaragua House 7 & 8 .....	177
Figure 5.33: Resulting net power for average daily cycle .....	177
Figure 5.34: Average temperature as a percentage of Temp 1 .....	178
Figure 5.35: System power/temperature solver schematic .....	179
Figure 5.36: Thermal circuit with capacitance .....	180
Figure 5.37: Comparison of hot and cold side temperatures using hot gas data .....	181

Figure 5.38: Comparison of model with and without thermal capacitance .....	182
Figure 5.39: Gross module power from field data and from the system model .....	183
Figure 5.40: Temperature distribution during week 1 with average energy per day (House #8).....	184
Figure 6.1: Peak power tracking methods. Clockwise from upper right: direct power control, battery current control, load resistance control and open circuit voltage control. ....	189
Figure 6.2: Power drift using battery current control .....	189
Figure 6.3: Peak power tracking effectiveness of PPT circuit compared to first generation circuit with 30 mOhm and 40 mOhm current sense resistors .....	190
Figure 6.4: Effect of inductor value on DC-DC converter efficiency .....	192
Figure 6.5: Effect of PWM frequency on charger efficiency (330 uH inductor) ...	194
Figure 6.6: Effect of PWM frequency on charger efficiency (100 uH inductor) .....	194
Figure 6.7: Comparison of Gen2 and Gen1 DC-DC converter efficiency .....	195
Figure 6.8: Comparison of Gen2 and Gen1 total circuit efficiency (PPT and DC-DC) .....	195
Figure 6.9: Example of continued low temperature operation leading to near zero net power (Nicaragua house 7, day 4) .....	196
Figure 6.10: Net module power vs. fan voltage at various hot side temperatures (2 TEP1-0.8 modules in series, Thermaflo E1456 16.25 cm heat sink, Mechatronics fan, 85% efficient charger).....	198
Figure 6.11: Example of temperature spike after fan is shut off on cool-down .....	198
Figure 6.12: Battery control Hysteresis .....	200
Figure 6.13: Module start-up Hysteresis.....	201
Figure 6.14: Field data illustrating too large of battery capacity .....	202
Figure 6.15: Adaptive capacity concept -- threshold moves up.....	203
Figure 6.16: Adaptive capacity concept -- threshold moves down.....	203
Figure 6.17: Battery voltage drop from charger circuit power consumption over multiple days.....	205
Figure 6.18: Program flow chart.....	207
Figure 6.19: Generation two circuit elements and layout .....	209
Figure 6.20: Generation two circuit schematic .....	210
Figure 6.21: Resulting net power for typical day (House 7+8) using generation 1 and generation 2 circuits.....	214
Figure 7.1: Endurance test setup (heater insulation not shown) .....	215

Figure 7.2: Plot of temperature limits and typical cycle times .....	215
Figure 7.3: % change in electrical resistance with number of cycles .....	219
Figure 7.4: % change in total thermal resistance (Module + interface) with number of cycles.....	220
Figure 8.1: Trend line fits for electrical resistance increase per cycle.....	223
Figure 8.2: Damage per cycle (electrical) as a function of maximum temperature.	223
Figure 8.3: Trend line fits for total thermal resistance increase per cycle .....	224
Figure 8.4: Damage per cycle (thermal) as a function of maximum temperature ...	224
Figure 8.5: Number of cycles peaking at various temperature intervals (House #7) .....	225
Figure 8.6: Number of cycles peaking at various temperature intervals (House #8)	226
Figure 8.7: Number of cycles peaking at various temperature intervals (House #7&8, normalized for 2 cycles per day).....	226
Figure 8.8: Reduction in monthly energy as a result of module damage for different maximum temperatures.....	229
Figure 8.9: Total energy generated over a five year period with different maximum temperatures .....	229
Figure 8.10: Thermaflo E1456 16.5 cm(top) and Melcor 15 cm(bottom) heat sink thermal resistance with Mechatronics fan.....	231
Figure 8.11: Power curves for Melcor and Thermaflo heat sink comparison .....	232
Figure 8.12: Heat sink cost effectiveness at various manufacturing costs .....	234
Figure 8.13: Bimetallic bypass in closed (left) and open (right) positions .....	235
Figure 8.14: Hot sink thermal resistance as a function of temperature with three different bimetallic concepts.....	237
Figure 8.15: Module hot side temperature with three different bimetallic concepts	237
Figure 8.16: Close up of module hot side temperature with fixed and variable hot sink resistance .....	238
Figure 8.17: Module net power with fixed and variable hot sink resistance .....	238
Figure 8.18: Hot side heat sinks: Aavid 61085 (upper left), Thermaflo E1441 (upper right), Aavid 82525 (bottom). (Dimensions in mm and inches).....	240
Figure 8.19: Hot sink thermal resistance (manufacturer data at 20 C) .....	241

## LIST OF TABLES

Table 2.1: Comparison of cooling design alternatives.....	70
Table 2.2: Fan no-load efficacy .....	74
Table 2.3: Heat sink/fan thermal resistances .....	77
Table 2.4: Manufacturer module specifications.....	79
Table 2.5: Module and heat sink comparison (fixed hot sink $R = .7$ ) .....	80
Table 2.6: Module and heat sink comparison (fixed hot side temp 260 C).....	82
Table 2.7: Cost breakdown for prototype system @ 10,000 units.....	97
Table 2.8: Cost breakdown for system @ 10,000 + units.....	98
Table 3.1: Sample of weekly monitoring report .....	102
Table 3.2: House #1 results.....	105
Table 3.3: House #2 results.....	109
Table 3.4: House #2b results.....	110
Table 3.5: House #3 results.....	112
Table 3.6: House #4 results.....	115
Table 3.7: House #7 average daily energy data (includes 1-2 days/week of no use) .....	117
Table 3.8: House #8 average daily energy data (includes 1-2 days/week of no use) .....	120
Table 3.9: Post test module properties.....	126
Table 5.1: Modules tested for database.....	151
Table 5.2: Initial Z-meter readings .....	154
Table 5.3: Model % error on total energy with and without thermal capacitance...	183
Table 6.1: Comparison of PPT methods .....	190
Table 6.2: Circuit improvements to reduce operating power .....	206
Table 6.3: Resulting energy gain for circuit improvements compared to original generation 1 circuit .....	213
Table 7.1: Endurance test matrix .....	217
Table 8.1: System cost effectiveness with different heat sink lengths .....	234

## **LIST OF ABBREVIATIONS**

**TEG** – Thermoelectric Generator

**LED** – Light Emitting Diode

**CCFL** – Cold Cathode Fluorescent Light

**CFL** – Compact Fluorescent Light

**EECL** – Colorado State University Engines and Energy Conversion Laboratory

**PPT** – Peak Power Tracking

**PWM** – Pulse Width Modulation

# **1 BACKGROUND**

## ***1.1 Problem Identification***

Almost half of the world's population uses biomass for cooking and heating [4]. This enormous usage of solid fuels has a dramatic effect on air pollution, indoor air quality, health, and deforestation.

The impact of stoves on outdoor air is tremendous. This process releases levels of pollution that rivals those released by the rest of the developed world. For example, in the United States where stove use is small, the amount of CO released by stoves is equal to that released by all other sources. In Asia, the same amount of black carbon is emitted from biomass as from transportation, industry, and power generation in North America [10]. These statistics show the potential impact that cleaning up stove emissions could have on a global scale.

On an individual scale, the use of primitive cookstoves can fill houses and huts with levels of hazardous air pollutants (HAPs) that are far beyond safe levels. Stoves release high levels of formaldehyde, carbon monoxide, NO<sub>x</sub>, and other harmful chemicals. This has a devastating effect on the health of users. Exposure to smoke from stoves has been equated to smoking ten packs of cigarettes a day. This leads to reduced life expectancy and increased child mortality. In India alone, there are an estimated 1.6 million premature deaths from exposure to stoves.

Approximately 500,000 women and children under five die prematurely from this exposure [5].

Stoves also have a detrimental effect on the land. The use of inefficient cookstoves is leading to massive deforestation in many parts of the world. Approximately 800 million tons of wood is burned annually for cooking and heating [9]. Billions of dollars are spent each year in attempts to reforest hillsides, but this has typically been a losing battle. In order to keep up with reforestation, approximately 13 billion dollars would be required annually [9]. This is more than any government can afford to spend on reforestation. A more cost effective and sustainable solution is needed to prevent this deforestation.

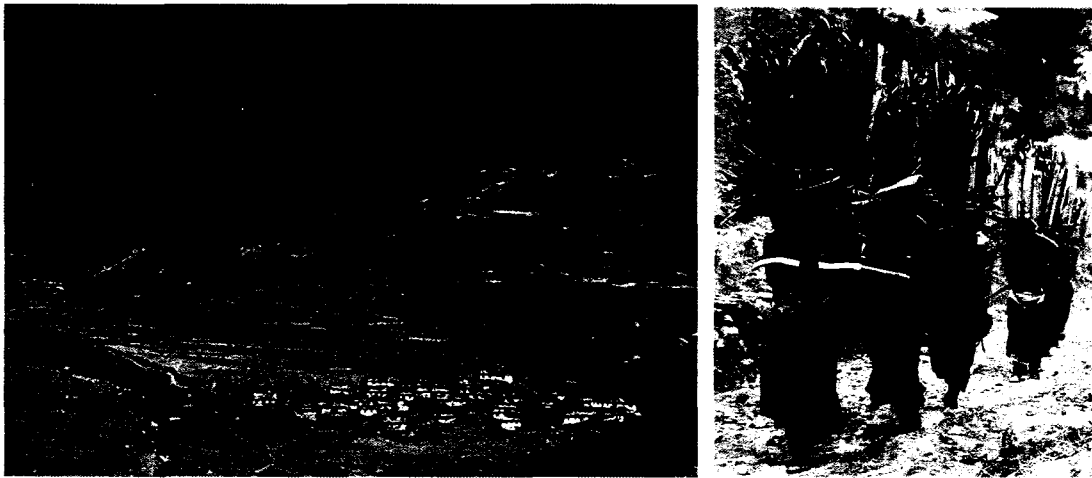


**Figure 1.1: Effects of firewood gathering**

It is expected that many countries may never be able to make the switch to fossil fuels. The only way to alleviate these problems it to develop stoves that burn biomass more cleanly and efficiently. In recent years, there has been a considerable effort to design and disseminate cleaner cookstoves [8]. Unfortunately, many of these

programs have failed. One reason why clean stoves have not been successful is that they commonly require more effort and attention from the user. Another is that they require changes in cooking habits and culture in general. Many people resist this change. Clean stoves also eliminate the light produced by the traditional open fire. Without this light clean stove users must sit in complete darkness during the evening hours. The absence of light from clean stoves is one of the biggest hurdles to acceptance in many regions. When faced with sitting in the dark by a clean stove, or sitting in a room lit by a smoky fire, many choose the latter. The generation of a small amount of electricity would alleviate this problem. It is believed that a stove that produces electricity will be so highly valued by the users that they will be more willing to make changes in cooking style and maintain the stove.

Most stoves being used for cooking produce around 1-5 kilowatts of thermal energy. If one percent of this could be converted into electricity (10-50 W) this would provide ample power for room lighting, radio, and possibly television. Some lamps being produced today using fluorescent or LED lighting require only a few watts of power. With access to high quality light, users would have the ability to participate in educational and income generating activities at night. This could have an effect on poverty reduction in addition to the health benefits of a smokeless stove. This electricity could also be used for communications such as radio, television, and cell phone charging.



**Figure 1.2: Room lit by traditional stove**

## ***1.2 Solution Concepts***

There are a number of devices capable of producing electricity from an external heat source. The most feasible were identified as the Stirling Engine, the Rankine Engine, the Brayton Engine, and a Thermoelectric Generator. In order to select the appropriate one for this specific application, it is important to look at the criteria of the user, as well as the environment in which it will be operating. The following criteria for the generator were identified:

- The generator must be virtually maintenance free. Any maintenance must require no technical expertise or understanding.
- The design must be very quiet, since it will be running inside the room with the users for a large portion of the day.

- The design must be reliable, with a lifetime of at least five years before a failure.
- The design must be very low cost. As an initial goal, the cost must be competitive with solar electricity on a cost per watt basis (\$5-\$8/W).
- The design must be easily adaptable to stove designs in use today.

### **1.2.1 Stirling Engine**

The first alternative considered was the Stirling engine, which has been studied fairly extensively for low power, low temperature differential applications. Stirling engines are external combustion engines which run on the Stirling cycle. The Stirling cycle is the closest theoretically to the Carnot cycle, with the potential to achieve very high efficiency [61]. However, in practice the ideal Stirling cycle is impossible to achieve [62]. Stirling engines have other advantages such as very low noise, low vibration operation. This is due to steady external combustion, and very low reciprocating masses. Free piston designs have no sliding friction and perfectly opposing pistons leading to even lower noise and vibration. Stirling engines also have an unequalled ability to operate on extremely low temperature differentials. The lowest demonstrated has been by Senft of 0.5 °C [65].

Stirling engines manufactured by the Stirling Technology Company (STC) are currently used in space applications using radioisotope heat sources. These engines achieve very high efficiencies and are very reliable due to their free piston design, but are very expensive. Stirling engines have also been used in solar applications at the

focal point of a solar concentrator [63][64]. However, they are currently being left behind by advances in solar photovoltaic technology and gas micro-turbines. Current solar concentrating Stirling engines are estimated to cost around \$7/W [63].

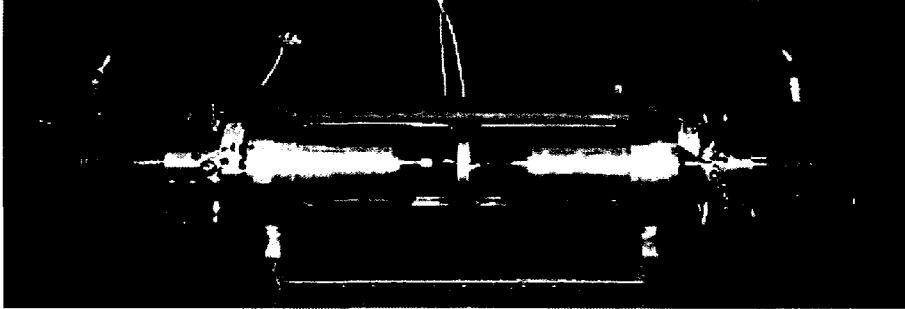


Figure 1.3: STC 55W free piston engines.

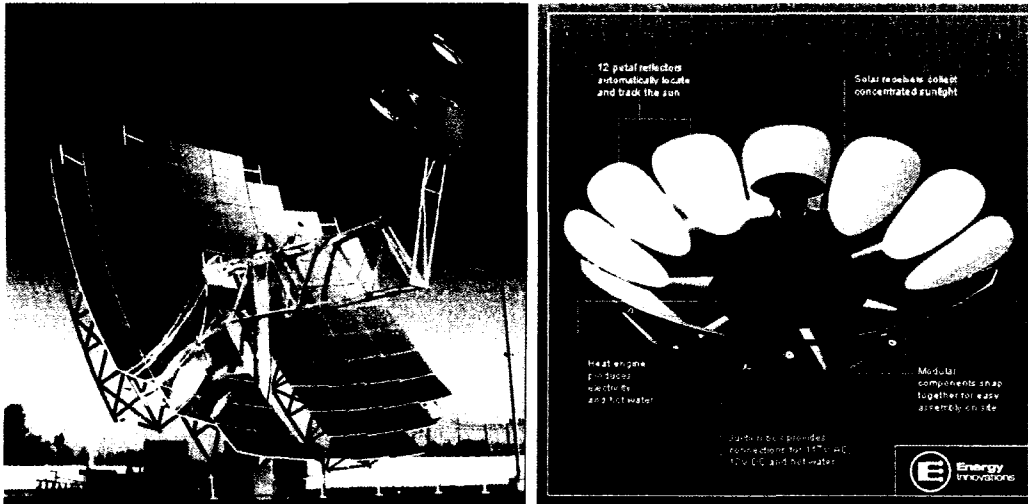
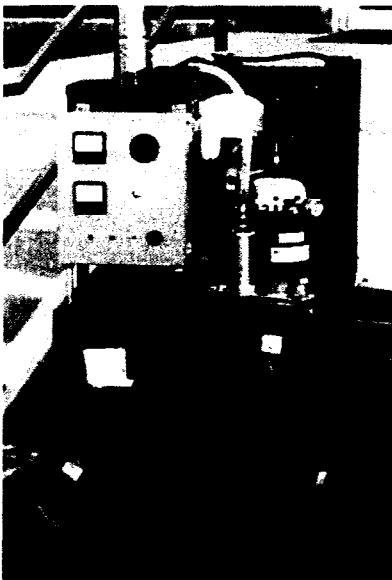


Figure 1.4: Solar Stirling engines. Boeing 30 kW(left) Energy Innovations 50 W(right)

These larger cost Stirling engines typically operate at efficiencies around 20-40%. For waste heat applications such as this, a much lower efficiency could be tolerated if the cost per watt were reduced. It is feasible that this could be accomplished through less sophisticated designs that are easier to manufacture. As of now, no one has commercialized such a design.

There have been several Stirling engines designed for the utilization of biomass [66][67][68][69]. The most promising is that developed by Sunpower called the Biowatt[68][69]. This engine generates over 1 kWe at 23% efficiency from wood chips. The most impressive aspect is that it is predicted that the system cost will come in an order of magnitude lower than most systems today. The projected cost is \$350 in production quantities, although this cost is not sufficiently justified. The projected maintenance period is 40,000 hrs. Although this system meets the cost and maintenance targets for the current stove application, it may be unsuitable in a couple of ways. First, it is not feasible that this system could be miniaturized to less than 50W at the current cost per watt. Secondly, the system requires the preparation of wood chips, and a system to feed them in at a constant rate for the engine to operate.



**Figure 1.5: Biowatt Stirling engine from Sunpower.**

## 1.2.2 Brayton Cycle Engine

The Brayton Cycle engine was also investigated as a design alternative for the stove-based generator. The Brayton cycle is most commonly used in the modern gas turbines for jet engines and large stationary power generation. Typically, gas turbines have been restricted to sizes above 1 MW. Recently, advances have been made in “micro-turbines” that have been successfully scaled down to 30 kW. This is still large compared to the desired output here, but worth considering.

### Capstone C30 MicroTurbine Generator

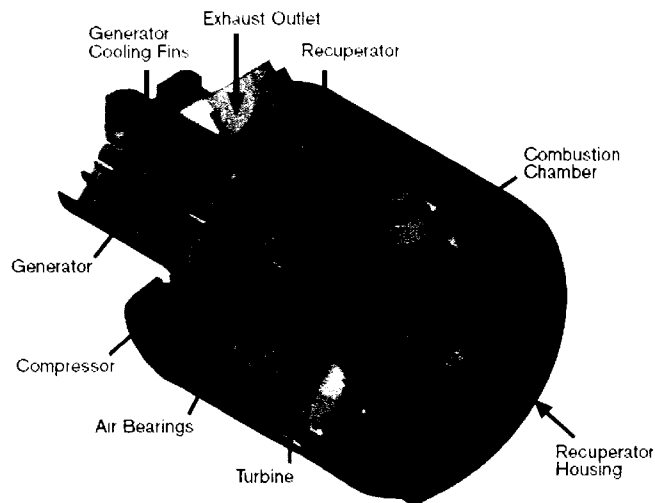


**Figure 1.6: Capstone 30kW micro-turbine.**

After a brief analysis of the Brayton engine and its components, a major hurdle to its application in small (less than 50 W) applications was identified. This is the miniaturization of the compressor and turbine. In a Brayton engine, the compressor efficiency is very important since it takes power from the turbine to run. Since the compressor is compressing a gas, the power required is significant [61]. The

compressors in gas turbines are typically multistage axial compressors. These are extremely expensive, high tolerance devices necessary for achieving high efficiencies. As an alternative, a radial centrifugal compressor was considered like those used in micro-turbines. However, for the power required in this application the diameter would be so small that the rotation would most likely need to be well over 100,000 RPM in order to get a significant pressure ratio. This is undesirable from the standpoints of manufacturability, noise and longevity. A piston or vane type compressor was considered, but these typically do not have the efficiency required for a Brayton cycle. Furthermore, they are not suited for the large volume flows required for a Brayton cycle. The potential for constructing a low cost, high efficiency, high pressure ratio compressor for this size was considered to be prohibitively low.

### **1.2.3 Rankine Cycle Engine**

The Rankine engine was also considered a potential option for generating electricity from stoves. The Rankine cycle uses water as the working fluid. The water is first compressed and heated to create high pressure steam. The steam is then expanded through a turbine or piston to create power, and is then cooled back to liquid water. The Rankine cycle has a distinct advantage over the Brayton cycle in that the compression of water requires very little work, therefore the compressor can have a lower efficiency with less effect on the cycle effectiveness [61]. Rankine cycle engines, or steam engines, have been constructed in almost every size range from 1 W to 1 GW. However, most small steam engines have not been used in working applications, but have been confined to hobby applications. In order to construct a 5-25 W Rankine engine, a very small turbine or piston expander would be

required, which is not currently available. The circulation of high temperature steam and water through all the components would also require that almost the whole device be constructed from higher cost materials such as stainless steel, aluminum, and brass. In addition, this engine would still require a very high speed operation which would generate significant noise.

#### **1.2.4 Thermoelectric Generator**

A thermoelectric generator (TEG) was the last alternative considered. A TEG is a solid state device that converts thermal energy directly into electricity. TEGs have been used for over 30 years in remote power applications such as weather stations, remote communications, navigational aids and gas pipelines [11]. The first practical use of a TEG was in 1959 for space power, which used polonium-210 as the heat source [11].

Since a TEG is a solid state device, it can produce power with no moving parts, making it very reliable and attractive for this application. However, moving parts such as fans and pumps are often incorporated into the cooling and heating system for the generator. Minimal moving parts also make TEGs very silent, which is very favorable for this application. To date, TEGs have remained very expensive and are used mostly in applications where users are willing to pay very high prices for continuous, highly reliable, maintenance free power for years. In recent years, thermoelectrics have seen commercial success being used as refrigerators. This has driven the cost of common thermoelectric materials down and brought about improvements in the materials. Several manufacturers are now making “high

temperature” bismuth telluride modules at very competitive costs (\$2-\$6/W @ qty. 10,000). Since the module is likely the most expensive component in the system, the TEG appears very promising.

Ultimately, a TEG system was selected since it met all the criteria defined initially. It is feasible in the 5-25 W power range. Its minimal moving parts make it very reliable, maintenance free and silent. With current module prices, which continue to decrease, a system cost competitive with solar power is very promising. Lastly, it is adaptable to stove design in use today, requiring only that the hot heat sink be placed in a hot gas stream.

### ***1.3 General Principles of Thermoelectricity***

#### **1.3.1 Thermoelectric Effects**

There are a number of thermoelectric effects that occur in any conductor that allow them to function both as generators and refrigerators. These effects are known as the Seebeck effect, the Peltier effect, and the Thompson effect. The thermoelectric effects are brought about by the difference in the accessible energy levels for an electron (or hole), due to temperature and atomic composition. To understand the thermoelectric effects, Figure 1.7 and Figure 1.8 depicting thermoelectric elements are helpful. A background in quantum mechanics is required to explain the significance of the conduction band, valence band, and Fermi level, as well as how they vary between metals, n-type semiconductors, and p-type semiconductors [27].

The most important effect in terms of thermoelectric generation is the Seebeck effect. The Seebeck effect refers to the voltage that is created within a conducting material with the presence of a temperature gradient. At the hot side, the electrons are at a higher energy level on average than on the cold side. The system wants to exist at the lowest possible energy state, so there is a potential established wanting to push the electrons from hot to cold. The most common application of this phenomena is in a thermocouple. In a thermocouple, two dissimilar metals are joined in the presence of a temperature that is to be measured. Therefore, each material has a temperature gradient along its length from the temperature in question, to the cold junction temperature. Because each material has a different Seebeck coefficient they each produce a different voltage. This voltage difference can then be measured and correlated to a temperature at the junction. It is a common misconception that the voltage is produced from the contact potential of the two dissimilar metals, this is incorrect [30]. The differential Seebeck coefficient ( $\alpha$ ) for a particular material is defined as

$$\alpha = \frac{V}{\Delta T}$$

**Equation 1.1**

where  $V$  is the developed voltage and  $\Delta T$  is the temperature difference applied. For most materials  $\alpha$  is defined in  $\mu\text{V}/\text{K}$ .

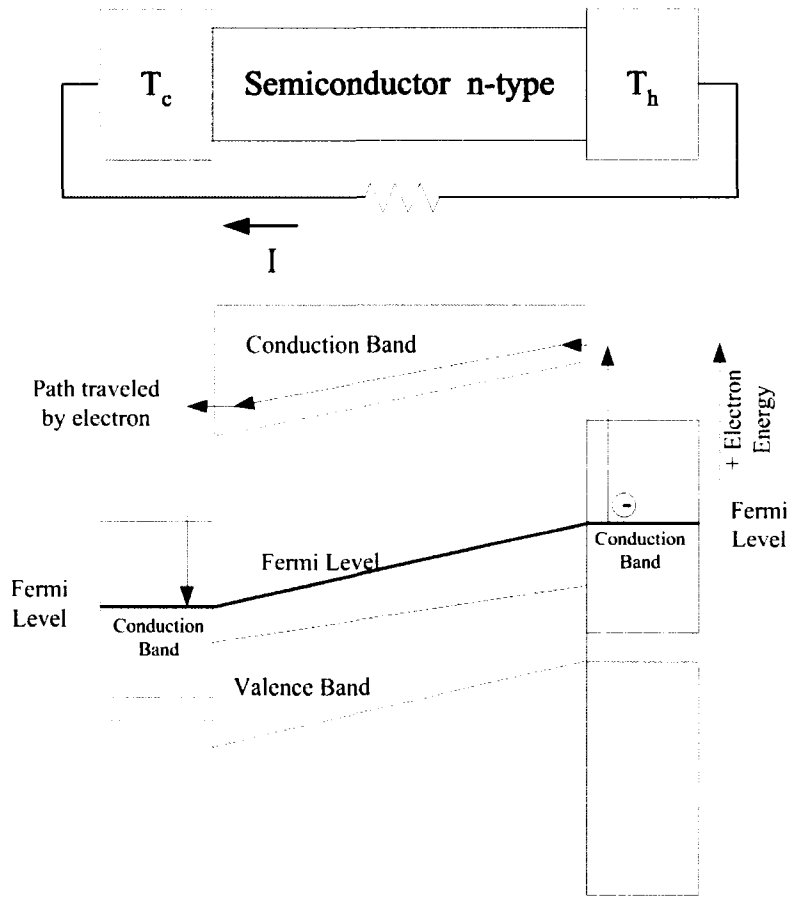


**Figure 1.7: Energy bands in a thermoelectric generator using n-type semiconductor**

The second thermoelectric effect is the Peltier effect. The Peltier effect is a result of current flow through junctions of dissimilar metals. As the charge carriers pass from one material to the other, their entropy is changed resulting in the release or absorption of energy. This can also be explained through Figure 1.8. As the charge on the left moves from the metal to the semiconductor, it must gain energy (positive

down) in order to move from the Fermi energy in the metal to the valence band in the semiconductor. This causes an absorption of energy by the electron hole, cooling the cold side. As the particle enters the metal on the hot side, it must liberate energy to work back down to the Fermi level of the metal, thus heating the hot side. It is important to note that in the case of a generator as in Figure 1.7, the Peltier effect is still present. However, it opposes the temperature gradient established by the heat sink, reducing the overall temperature difference. The Peltier effect is the basis for thermoelectric refrigeration, which is used for electronics cooling as well as personal coolers. The Peltier coefficient ( $\pi$ ) is defined as

$$\pi = \frac{I}{q}$$

**Equation 1.2**

where I is the current and q is the heat absorbed or liberated.

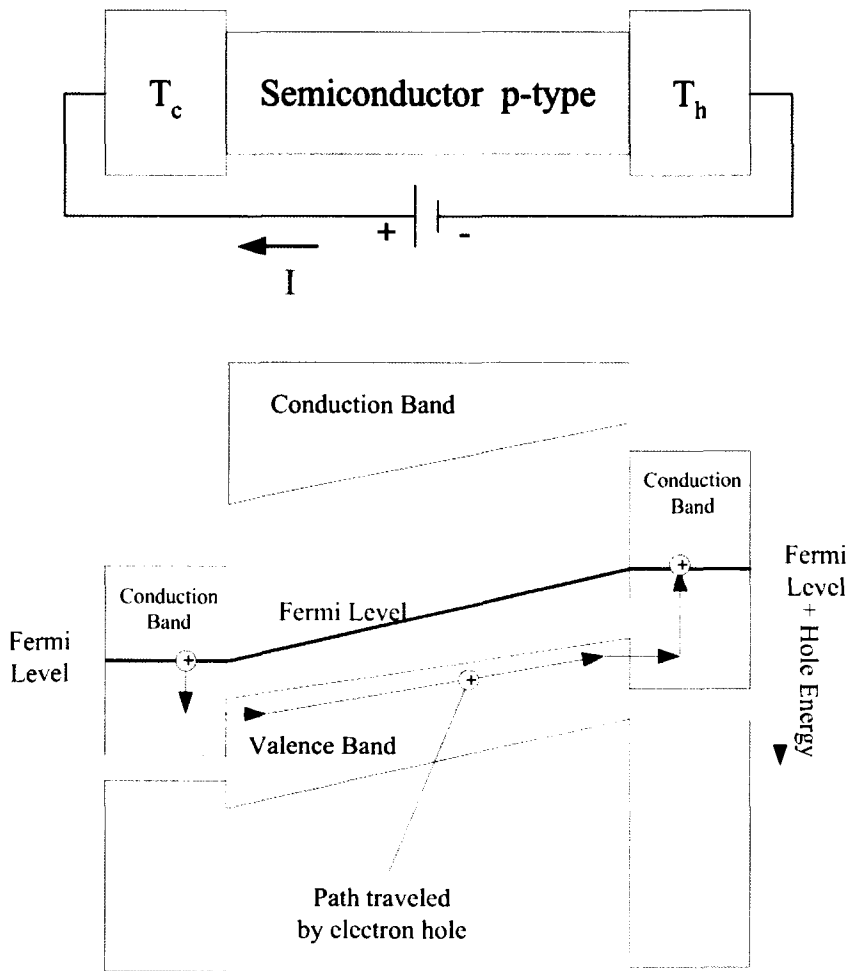


**Figure 1.8: Electron energy levels in p-type conductor**

The last thermoelectric effect is the Thompson effect. It was described by Thompson as the “specific heat of electricity.” It results in the generation or absorption of heat as current flows through a conductor with a temperature difference. As charge carriers flow against a thermal gradient they absorb heat, and vice versa. This effect can also be visualized in Figure 1.8. As the hole flows from left to right in the semiconductor it loses energy (in the amount  $eV$ ) as it moves with the electric field. It also gains energy ( $2k\Delta T$ ) as it moves to the higher temperature region. The

difference of these quantities is the energy liberated or absorbed by the electron. The Thomson effect is typically smaller than the other thermoelectric effects. It is defined by the coefficient  $\beta$ .

$$\beta = \frac{q}{I \Delta T}$$

**Equation 1.3**

These three thermoelectric effects can be related to each other through the Kelvin relationships. These relationships were initially derived by Kelvin, and have since been shown to be valid experimentally and by irreversible thermodynamics. For material pair a and b

$$\alpha_{ab} = \frac{\pi_{ab}}{T}$$

**Equation 1.4**

$$\frac{d\alpha_{ab}}{dT} = \frac{\beta_a - \beta_b}{T}$$

**Equation 1.5**

### **1.3.2 Thermodynamics of Thermoelectric Modules**

In order to understand the effects of material properties, module geometry, and operating temperatures on a generator's performance, it is necessary to develop an in-depth thermodynamic analysis of thermoelectric generation. The following analysis follows that developed in [27]. The goal of this analysis is to identify the optimal

module geometry and load resistance to achieve peak power, or peak efficiency from a material with known properties. The result can be used to predict the module performance in any configuration. We will first start analyzing a single element couple, which can be easily scaled to multi-element modules. The model generator is shown in Figure 1.9.

The following assumptions are necessary to achieve the analytical solutions desired in this analysis:

- The Seebeck coefficient is constant with temperature. This also implies that the Thompson coefficient is zero by definition. This is a reasonable assumption as it was earlier noted that the Thompson effect is small compared to the Seebeck and Peltier effects.
- The materials resistivity and thermal conductivity are constant with temperature.
- The Seebeck coefficient of the conductor strip joining the elements is zero, as well as the electrical resistance.
- The thermal and electrical contact resistances are also negligible, making the temperature difference across the elements  $T_h - T_c$ .
- All heat flow from the hot reservoir to the cold reservoir is through the elements, neglecting convection and radiation.
- The elements are of constant cross section.

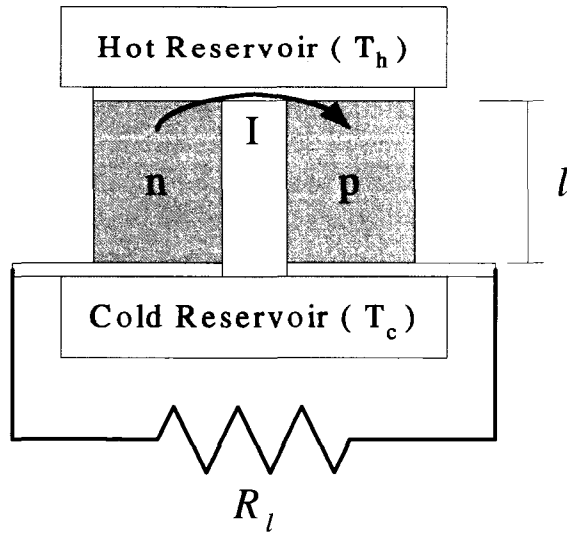


**Figure 1.9: Basic thermoelectric generator model**

To begin the analysis, it is necessary to first analyze the thermal energy flowing in and out of each leg. This quantity is comprised of three components--the heat driven through the leg by Fourier's law of heat conduction; heat generated by Joule heating; and heat generated or liberated through the Peltier effect. The first two can be determined with the following analysis.

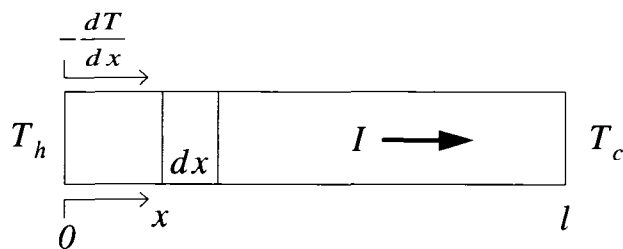


**Figure 1.10: Differential segment within generator leg**

Consider a differential segment ( $dx$ ) within one leg of the generator at arbitrary position ( $x$ ) as shown in Figure 1.10. The heat flowing across the left face can be described by

$$-\lambda \frac{dT}{dx}$$

**Equation 1.6**

While the heat flowing through the right face is expressed as

$$-\lambda \left[ \frac{dT}{dx} + \frac{d}{dx} \left( \frac{dT}{dx} \right) dx \right]$$

**Equation 1.7**

The Joule heating within the element is

$$J^2 \rho$$

**Equation 1.8**

Under steady state conditions, by conservation of energy the heat leaving the volume must equal the heat flowing in, plus the heat generated. In other words, the accumulation of energy is zero. This can be stated using the previous definitions as

$$\frac{d^2T}{dx^2} + J^2 \rho = 0$$

**Equation 1.9**

Using the boundary conditions  $T = T_h$  at  $x = 0$ , and  $T = T_c$  at  $x = l$ , the resulting solution to the differential equation in Equation 1.9 is

$$T(x) = \left[ T_h - \left( \frac{x}{l} \right) \Delta T \right] + \left[ \frac{J^2 \rho}{2 \lambda} \right] x(l-x)$$

**Equation 1.10**

From this solution the contributions from Fourier conduction and Joule heating can be seen, as the solution is the superposition of the two effects. Notice that under no applied temperature difference, the temperature distribution is parabolic within the leg due to Joule heating. With no Joule heating and a temperature difference applied, the distribution is linear from  $T_h$  to  $T_c$ . With both a temperature difference and Joule heating, the profile is non-linear, being the addition of the linear and parabolic components.

Equation 1.10 is sufficient to describe the heat flux at any point within the material. However, at the junctions the Peltier effect must also be included since the current is passing from one material to the other here. At the junction, the total heat flowing in or out is described by the heat driven due to the local temperature gradient at the junction, as well as that contributed by the Peltier effect. The amount driven by the temperature gradient can be found by taking the derivative of Equation 1.10 with respect to  $x$  and inserting into Fourier's law of heat conduction.

$$Q_0 = A \lambda \left. \frac{-dT}{dx} \right|_{x=0} = \gamma \lambda \Delta T - \frac{1}{2} I^2 \frac{\rho}{\gamma}$$

**Equation 1.11**

$$Q_L = A \lambda \left. \frac{-dT}{dx} \right|_{x=L} = \gamma \lambda \Delta T + \frac{1}{2} I^2 \frac{\rho}{\gamma}$$

**Equation 1.12**

This analysis presents an interesting result. At the hot junction,  $x = 0$ , half of the total Joule heating term is subtracted from the Fourier term. This does not imply that the heat actually flows against the temperature gradient, it is simply another case of the joule heating superimposed on the Fourier heat transfer. On the cold side, the other half of the Joule heating term appears flowing with the Fourier term.

To complete the analysis at the junction, the Peltier term needs to be included. The total heat from both junctions, p-leg to conductor and conductor to n-leg is defined by

$$Q = -(\pi_p + \pi_n) I_{pn} = -\pi_{pn} I_{pn}$$

**Equation 1.13**

By introducing one of Kelvin's relationships (Equation 1.4), Equation 1.13 becomes

$$Q = -\alpha_{pn} T I_{pn}$$

**Equation 1.14**

Now that expressions for the heat flux at the junctions have been developed, an analysis of the entire generator can be developed. The thermal efficiency of the system is defined as

$$\eta_{th} = \frac{\text{Electrical power}}{\text{Thermal energy in}} = \frac{I^2 R_l}{K\Delta T + \alpha T_h I - \frac{1}{2} I^2 R_i}$$

**Equation 1.15**

Where  $R_l$  is the load resistance,  $K$  is the conductivity of the entire module and  $R_i$  is the module internal resistance. These are defined as

$$K = \frac{\lambda_n A_n}{l_n} + \frac{\lambda_p A_p}{l_p} = \lambda_n \gamma_n + \lambda_p \gamma_p$$

**Equation 1.16**

$$R_i = \frac{\rho_n l_n}{A_n} + \frac{\rho_p l_p}{A_p} = \frac{\rho_n}{\gamma_n} + \frac{\rho_p}{\gamma_p}$$

**Equation 1.17**

$$\gamma = \frac{A}{l}$$

**Equation 1.18**

The goal of this derivation is to express the efficiency strictly in terms of its geometric and material properties. Therefore, the following substitution is made for current  $I$ .

$$I = \frac{\alpha \Delta T}{R_i + R_l}$$

**Equation 1.19**

Equation 1.19 is then substituted into Equation 1.15. After significant rearrangement and the introduction of the term  $m'$ , the following equation results.

$$\eta_{th} = \frac{m' \left( \frac{\Delta T}{T_h} \right)}{\frac{R_i K}{\alpha^2 T_h} (1 + m')^2 + (1 + m') - \frac{\Delta T}{2T_h}}$$

**Equation 1.20**

$$m' = \frac{R_l}{R_i}$$

**Equation 1.21**

Equation 1.20 can now be used to optimize the module geometry, material and load resistance for maximum efficiency. Looking at the module geometry first, recall that  $R_i$  and  $K$  both contain the geometric information of the elements as well as the material properties. For a given value of  $m'$  and  $\alpha$ , efficiency is maximized when the product  $R_i K$  is minimized. This results in the following expression

$$(R_i K)_{\min} = \left[ (\rho_n \lambda_n)^{\frac{1}{2}} + (\rho_p \lambda_p)^{\frac{1}{2}} \right]^2$$

**Equation 1.22**

If  $\alpha$  is considered as well, then efficiency is maximized when the quantity  $Z$  is maximum. Where  $Z$ , termed the figure-of-merit, is defined by

$$\frac{\alpha^2}{R_i K} = Z$$

**Equation 1.23**

Finally, the value of  $m'$  that results in the maximum efficiency can be determined by differentiating Equation 1.20 with respect to  $m'$  and setting the result equal to zero. The resulting expression for  $m'$  is simply

$$m'_{opt} = (1 + Z T_{av})^{\frac{1}{2}}$$

**Equation 1.24**

Note that the value of  $m'$  for peak power is easily shown to be one, where  $R_l$  is equal to  $R_i$ . The expression for the fully optimized system can be written as

$$\eta_{t\max} = \frac{(m'_{opt} - 1) \frac{\Delta T}{T_h}}{m'_{opt} + \frac{T_c}{T_h}}$$

**Equation 1.25**

From this development, the performance of an ideal thermoelectric generator can be fully analyzed to study the effects of variations in geometry, load resistance and material properties. In addition, an important term has been defined, the figure-of-merit, which is valuable in assessing a materials effectiveness in thermoelectric applications. In most cases, the figure-of-merit appears in the pair  $ZT$  as in Equation 1.24 and Equation 1.20. Therefore, if temperature is considered a variable then the quantity  $ZT$  needs to be maximized for optimal efficiency.

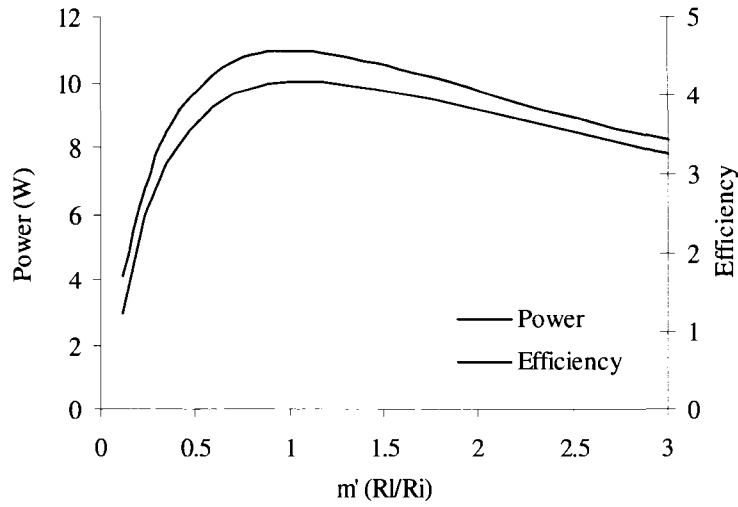


**Figure 1.11: Power and efficiency vs.  $m'$  for  $Z=.001$**

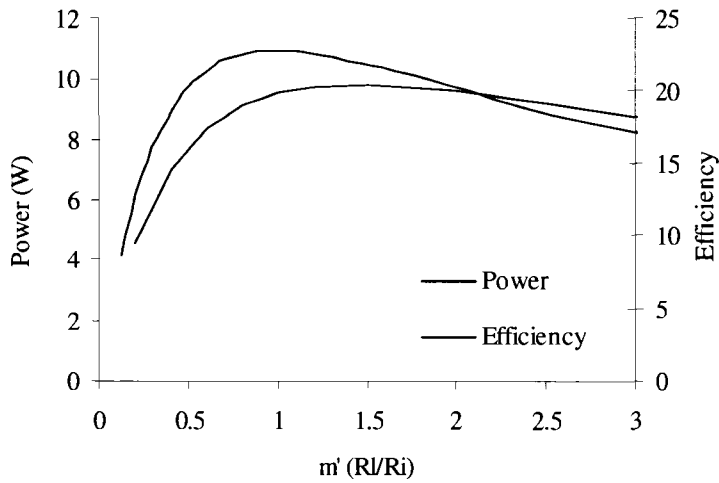


**Figure 1.12: Power and efficiency vs.  $m'$  for  $Z=.007$**

### 1.3.3 Thermoelectric Materials

There are currently dozens of materials being researched for thermoelectric power generation. Technically, any conductive material exhibits a Seebeck effect and could be used for thermoelectric generation. Clearly, some materials are more effective than others. When evaluating thermoelectric

materials, the figure-of-merit ( $Z$ ) is used as an indicator of a material's effectiveness as a generator (see section 1.3.2). The quantity  $ZT$  is also used as a dimensionless figure-of-merit that accounts for the materials operating temperature. It has been recognized that metals have too high of a charge carrier concentration to be used for generation. Insulators, on the other hand, have too few charge carriers. Semiconductor materials have carrier concentrations between the two, in the optimal range of  $10^{19}/\text{cm}$  [28][29]. Furthermore, the charge carrier concentration in semiconductors can be controlled by the amount of doping used. A significant amount of effort has gone into creating materials with optimized  $Z$  values within various operating temperature ranges. The most common materials used today for thermoelectric generation are bismuth telluride ( $\text{Bi}_2\text{Te}_3$ ), lead telluride ( $\text{PbTe}$ ), and silicon germanium ( $\text{SiGe}$ ). The figure-of-merit for these materials is shown in Figure 1.14 [32].

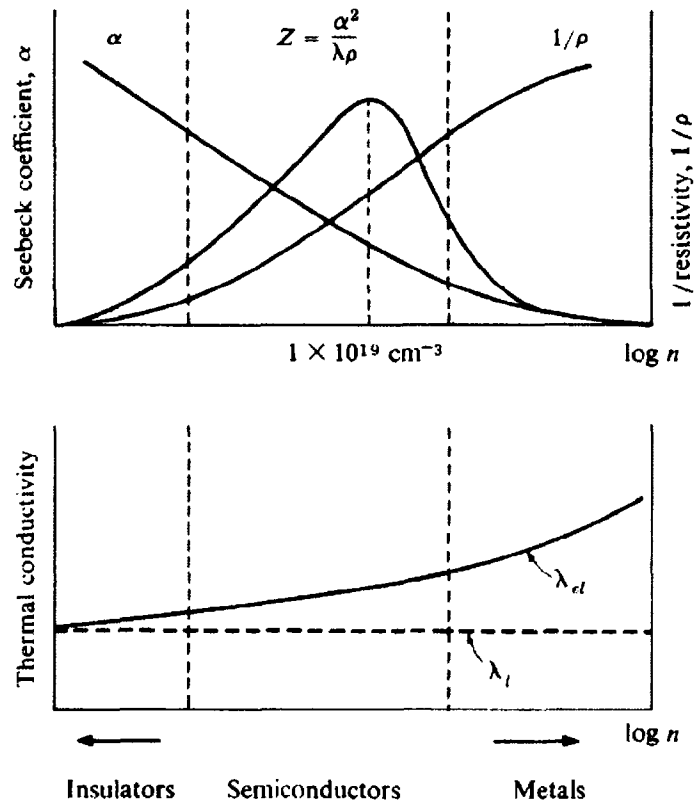
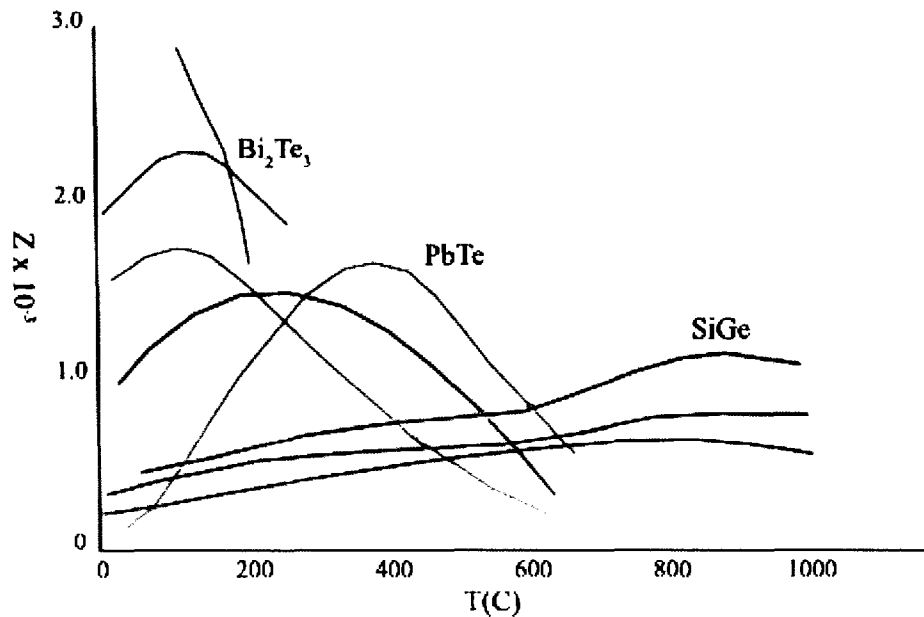


Figure 1.13: Effect of charge carrier concentration on material properties [27]



**Figure 1.14: Figure of Merit for Bismuth Telluride, Lead Telluride, and Silicon Germanium [32]**

Although the  $Z$  values for the three materials vary significantly, the  $ZT$  values are similar ( $ZT \text{ Bi}_2\text{Te}_3 < 1.2$ ,  $ZT \text{ PbTe} < 1.1$ ,  $ZT \text{ SiGe} < 0.9$ ). It is also important to notice the effective operating range of each material ( $\text{Bi}_2\text{Te}_3 < 260 \text{ C}$ ,  $\text{PbTe} < 700 \text{ C}$ ,  $\text{SiGe} < 1000 \text{ C}$ ). Bismuth telluride is clearly the best material at lower temperatures, which is why it is used in refrigeration. For generation, the appropriate material depends on the temperature of the heat source. For fossil fueled applications, PbTe is a logical choice. Global Thermoelectric, currently the only commercial manufacturer of TEGs, uses PbTe for its natural gas fuelled generators to achieve efficiencies of around 9% [12]. However, at these temperatures it is necessary to hermetically seal the module in an inert atmosphere to prevent the PbTe from oxidizing [12]. For

waste heat recovery,  $\text{Bi}_2\text{Te}_3$  or  $\text{PbTe}$  would be appropriate depending on the temperature of the fluid stream. Currently, there are no manufacturers selling  $\text{PbTe}$  modules at competitive prices, while there are several manufacturing  $\text{Bi}_2\text{Te}_3$  modules for high temperature operation. These high temperature modules are optimized for high temperature generation both in the material properties and the element geometry.

It is also important to note that the temperature within the module varies from the hot side temperature to the cold side temperature. For this reason, properties are commonly evaluated at the average module temperature. This gives a good approximation, but can lead to significant error if the temperature distribution or material properties are highly non-linear.

#### **1.3.4 Emerging Thermoelectric Materials**

During the past decade, significant advances have been made in thermoelectrics which promise much higher efficiencies than the traditional semiconductor materials available today. These advancements have mostly come about through new materials and nano-structures with enhanced thermoelectric properties.

There have been a number of materials recently developed with ZT values exceeding the traditional  $\text{Bi}_2\text{Te}_3$ ,  $\text{PbTe}$ ,  $\text{SiGe}$  systems. Several of primary interest are known as skutterudites, clathrates, and complex chalcogenides [38][39]. These materials have been developed through experimentation, and with the aid of very sophisticated computational programs that can predict thermoelectric behavior for different atomic arrangements.

Skutterudites are composed of binary compounds in the form  $\text{MX}_3$ , where the M atom is a metal Co, Rh, or Ir, and the X atom is a non-metal P, As, or Sb. These compounds form complex cubic structures with a large unit cell. This unit cell contains large voids that can be filled with other metal atoms known as “guests”. These guests “rattle” within the atomic cage, acting as phonon scattering centers. This gives the skutterudite material a much lower thermal conductivity, and a significantly improved figure-of-merit. Currently skutterudite compounds have ZT values exceeding one, with values reaching 1.5 at 900 K [38][39].

Clathrate compounds are similar to skutterudites in that the atoms form a cage-like structure that is filled with rattlers or guest atoms. The cage structure can be made of silicon or germanium, and the rattler is an alkali metal. The presence of the rattler results in “glass-like” thermal properties for the compound. Both skutterudites and clathrates have glass-like phonon behavior and the electron behavior of a semiconductor crystal. For this reason, they are commonly referred to as “phonon glasses.” Currently clathrate materials can achieve ZT values of around one at 400 °C. This is not especially high, but for a new material it is encouraging[39].

Complex chalcogenide structures are also being developed for high ZT values. These materials consist of complex arrangements of heavy atoms such as Ag, Pb, Sb, Se, Te, and alkali metal atoms. Synthesis of complex structures consisting of these atoms has traditionally been very difficult since they tend to proceed to the most thermodynamically favorable state, typically a binary compound. However, the use of molten salts as a solvent has made the creation of these complex structures possible. The molecule  $\text{AgPb}_{18}\text{SbTe}_2$  can achieve a ZT value of  $\sim 2.5$  at 800 K [38].

This incredibly high figure of merit has been attributed to several possible explanations. The molecule consists of loosely bonded, heavy atoms. These atoms can have large displacements and cause large structural disorder, which leads to low conductivity as in the case of rattlers [39]. The Seebeck coefficient is very high due to an asymmetry in the density of states [38][39].

In addition to engineering new materials, significant advancements have been made in creating nano-scale structures with very high figures of merit. The contribution of size effects, specifically grain size, on conductivity was observed over 60 years ago. This is mainly due to the scattering of phonons at grain boundaries, lowering their mean free path. This lower conductivity enhances the thermoelectric figure of merit as observed by several researchers [39][42].

The most recent advancements have been made in creating 1-D and 2-D structures such as nano-wires, thin films, and quantum wells. In these structures the material thickness is on the order of the de Broglie wavelength of the carriers, around 100 angstroms thick [39][43]. The creation of these low dimensional structures allows the engineer to affect properties that are essentially fixed in the bulk material. These are the scattering parameter, density of states, the charge mobility and the position of the Fermi level [39]. Theoretical calculations show values of ZT as high as four could be achieved for quantum wires[38]. However, the production of these nano-structures on scales large enough for multi-watt generation has been problematic. Figure 1.15 shows the potential improvement in efficiency and range of operation for quantum wells versus traditional  $\text{Bi}_2\text{Te}_3$  modules [2]. Figure 1.16 shows a quantum well module construction [2].

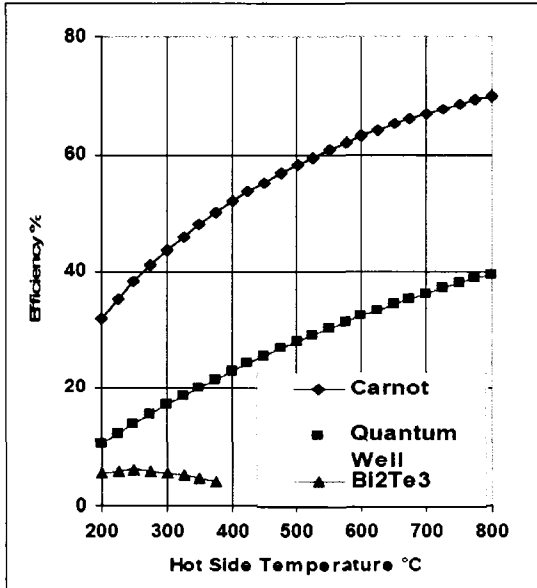


Figure 1.15: Quantum well efficiency [2]

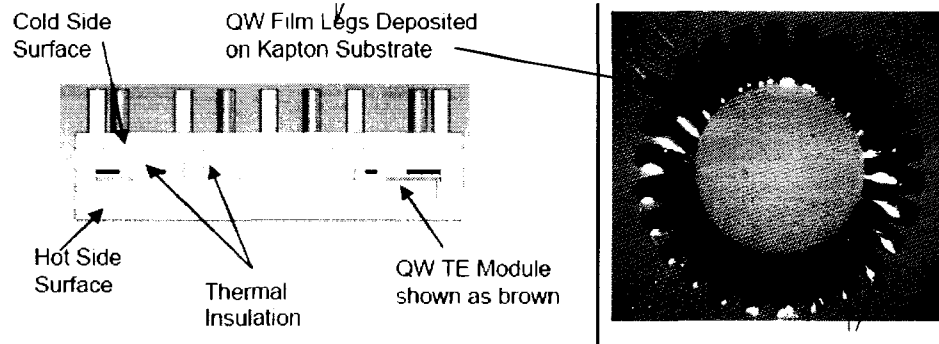
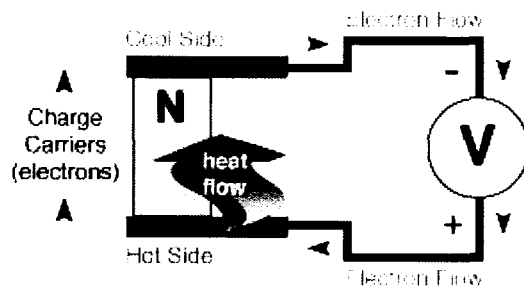


Figure 1.16: Quantum well module construction [Hi-Z]

## 1.4 Construction and Analysis of Thermoelectric Generators

### 1.4.1 Thermoelectric Module Construction

In order for a thermoelectric material to function well as a generator or refrigerator, it must first be configured into what is termed a thermoelectric module. Thermoelectric modules are composed of individual legs of material called elements. A single element forming a basic thermoelectric circuit is shown in Figure 1.17. Since most thermo-elements produce only millivolts, they need to be combined electrically in series and thermally in parallel. To accomplish this, n-type and p-type materials are combined in series as shown in Figure 1.18. In this configuration, the electrons act as the charge carriers in the n-type materials, while holes act as charge carriers in the p-type material. By using this configuration, many element pairs can be combined easily as shown in Figure 1.19. A close up of an element assembly is shown in Figure 1.20.



**Figure 1.17: Basic thermoelectric circuit [1]**

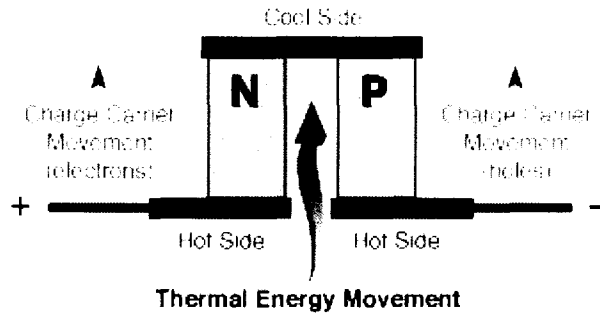


Figure 1.18: Schematic of a Thermo-element [1]

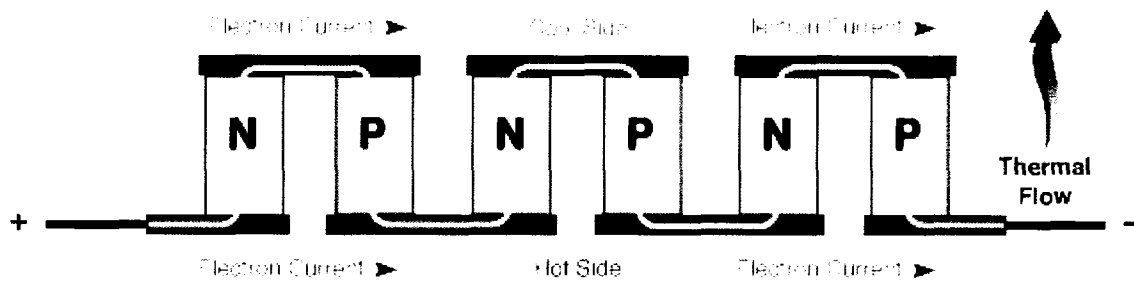


Figure 1.19: Thermo-elements in series [1]

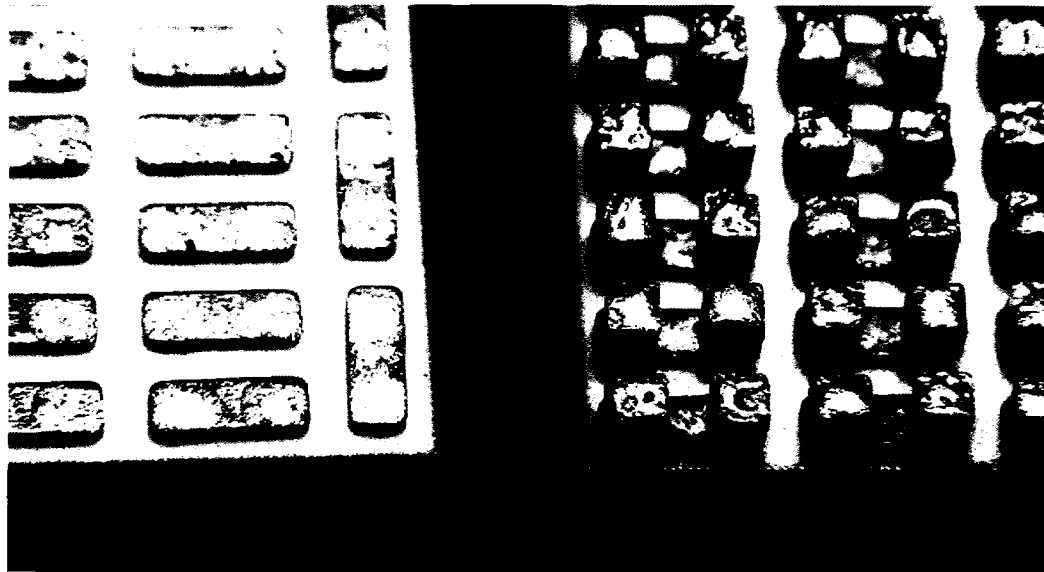
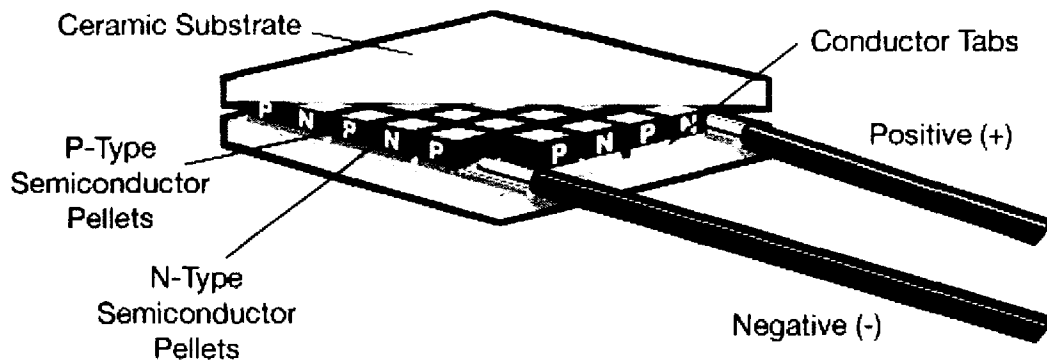


Figure 1.20: Close up of element assembly [1]

To maintain a temperature difference across the module, it is necessary to attach heat sinks to each side. Since the heat sink is electrically conductive, it will short the modules unless an insulator is placed between the two. The most common way to accomplish this is through the use of a ceramic wafer. It is desirable to find a material that is electrically insulating, yet thermally conductive. For this, the most common material is aluminum oxide  $\text{Al}_2\text{O}_3$ . Some have also experimented with surface coatings on the heat sink such as anodizing to isolate the heat sink electrically [44].



**Figure 1.21: Thermoelectric module construction**

As discussed in Section 1.3.3, the temperature within the module varies in a nearly linear fashion from the hot side to the cold side. This means the material properties such as the figure-of-merit vary within the element legs. As seen in Figure 1.14, the figure-of-merit can vary significantly within relatively small ranges of temperature. This means part of the module may be operating at a high figure-of-merit while another section may be at a low figure-of-merit. For this reason some modules are constructed with segmented legs, to ensure each portion is operating in its optimal temperature range. Unfortunately, this adds additional complexity to the

construction of the modules and increases cost. This is done when efficiency or power density are of utmost importance.

#### **1.4.2 Thermoelectric Generator Assembly**

To maintain a temperature difference across a module, it is necessary to attach heat sinks on both sides. Typically the hot heat sink will be placed in a hot gas stream, while the cold sink is cooled by natural convection or a fan. Typical system components are shown in Figure 1.22. In order to ensure good contact between the heat sinks and the module, significant clamping forces are required. The clamping system is typically comprised of several components. The first is fiber washers to minimize heat traveling through the screws and bypassing the module. The second is spring washers to allow for thermal expansion of the heat sink and module as they heat up. A thermal spreader block is also commonly placed between the hot and cold heat sinks to separate the two to reduce convection between the two heat sinks. It is also necessary if the assembly must pass through an insulated wall. Detailed views of these assemblies are shown in Figure 1.23.

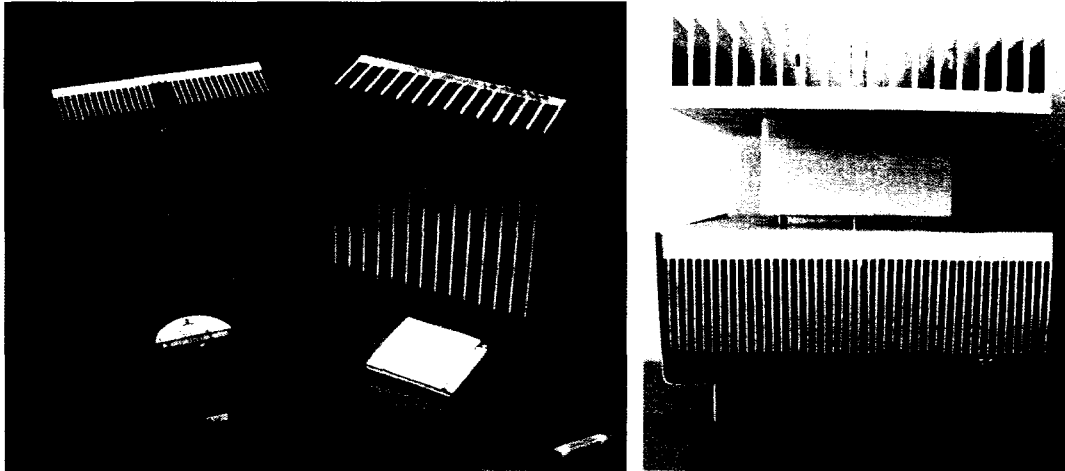


**Figure 1.22: Basic components of a thermoelectric generator**

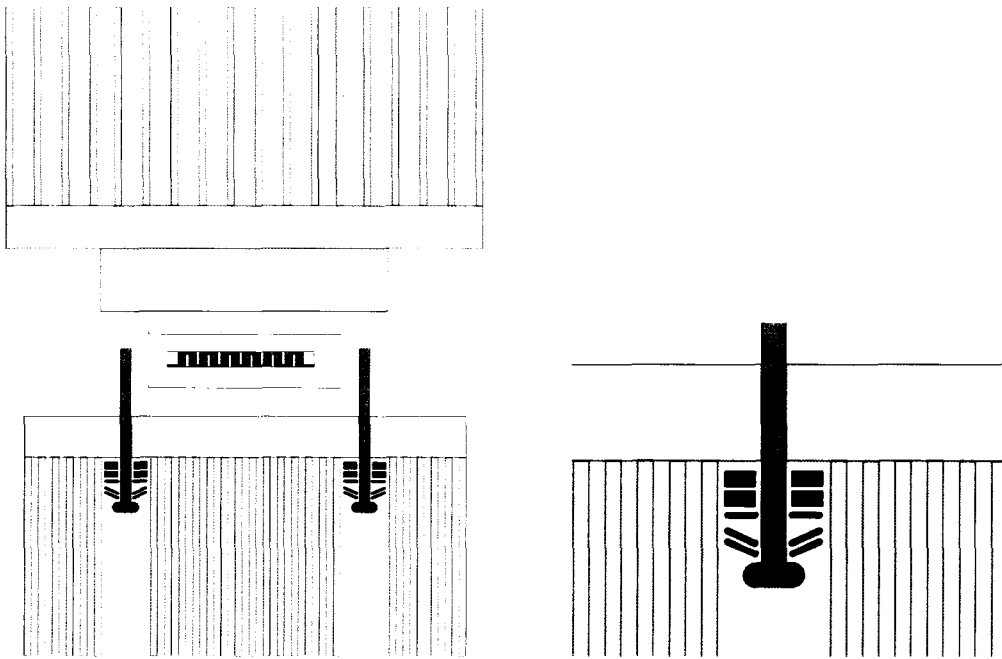


**Figure 1.23: Schematic of generator assembly**

### 1.4.3 Heat Sinks

Selection of an appropriate heat sink is critical for a successful thermoelectric design. There is a multitude of heat sink styles, shapes and configurations. There are several common methods of manufacturing heat sinks, resulting in different thermal performance, cost, temperature limitations and geometry. The most common are extruded and bonded fin heat sinks. Forged pin, folded fin and die cast heat sinks are also used for high power dissipation.

Extruded heat sinks are typically the most common for general cooling applications due to the ability to form a wide range of custom geometries at very low cost. Although extruded heat sinks excel in the category of cost, they have two major disadvantages. The first is the limiting fin aspect ratio (height/width). The second is a limit on fin density. As fin aspect ratio and fin density become too large, the extrusion die cannot support itself under the applied loading. The limiting fin aspect ratio is not a fixed value, but rather depends on the skill of the manufacturer and the cost of the process.

The second most common style used is bonded fin. In bonded fin heat sinks, an extrusion with small slots is produced that fins of any length can be bonded into, typically using a conductive epoxy. This method gets around the limitation on fin aspect ratio, but introduces new thermal interfaces. In addition, the bonding epoxy limits the heat sinks maximum temperature and can degrade over time. This method also allows for the use of different materials for the base and fin materials. Bonded fin heat sinks are typically more expensive than an extrusion of the same weight.

However, due to the larger fin area they can be cost competitive from a performance standpoint.

Folded fin heat sinks also provide very high densities and large aspect ratios. In this method fins are constructed from a sheet of metal folded accordion style into a stack of fins. The fins are then epoxied or brazed on to the heat sink base. These heat sinks are capable of dissipating very large amounts of power, but require large fans to push air through the tightly spaced fins. As with the bonded heat sinks, the bond can limit temperature and lifetime, but allows for different materials to be used.

Forged fin and die cast heat sinks are typically made in a pin configuration. This is advantageous because the thermal boundary layer is broken up as the air flows past each pin. This results in a more efficient heat sink if the air is ducted properly through the heat sink. These heat sinks are typically used in the impinging configuration. From a cost standpoint they are typically more expensive than extrusions, due to the tool cost and the fact that they are commonly custom designs.

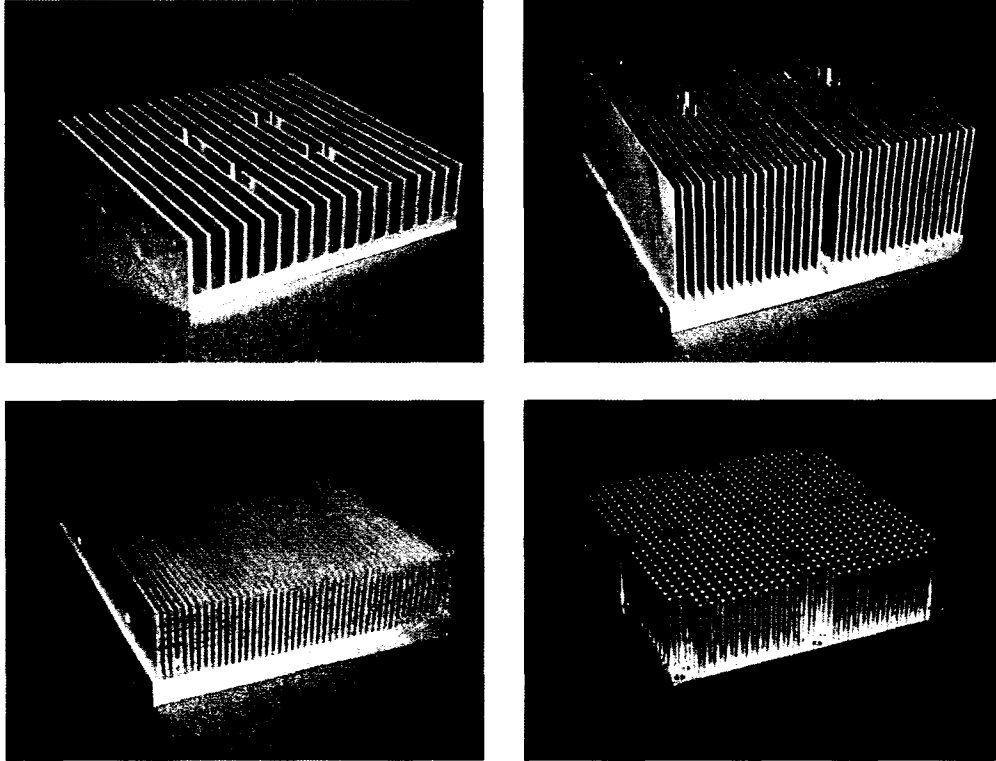


**Figure 1.24: (clockwise from upper left) extruded heat sink, bonded fin heat sink, high density extrusion, forged pin fin heat sink**

The previous heat sinks all utilize air as the cooling medium. Heat can also be removed from the module using water cooling blocks and heat pipes. However, both of these devices simply remove heat from the source to another location. Unless the reservoir is infinite, they both require an additional heat exchanger to dissipate the heat into the atmosphere. They are simply means of transferring heat from one location to another.

Liquid cooling blocks are much simpler in their construction. Typically they consist of a small block of aluminum or copper with a loop drilled into the block, or a pipe soldered onto the block. These heat sinks can be much more compact due to the high specific heat of water, or any other liquid, compared to air.

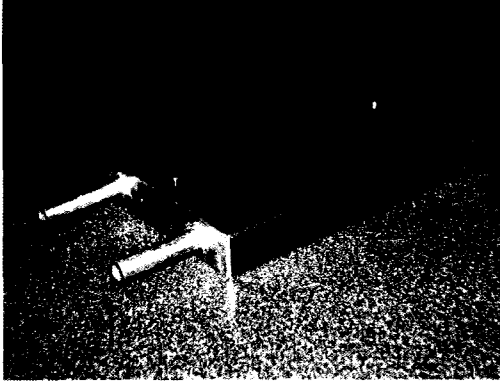


**Figure 1.25: Water cooling block**

Heat pipes operate by evaporating a liquid at the heat source, and condensing it at a remote location. These are very effective due to the high thermal energy required for phase change processes. The apparent conductivity of a heat pipe can be 1000 times that of a copper bar of the same geometry. Because the condensed fluid needs to make it back to the heat source, many heat pipes will only work in a vertical or slanted orientation. More sophisticated heat pipes use a wick within the pipe to draw the liquid back to the source. Heat pipes are commonly used in electronics cooling where space is limited, as in laptop computers. Here the heat pipe is used to transfer the heat away from the source to a location where there is room for an array of cooling fins. Although the heat pipe itself is very efficient at transferring heat, the total thermal resistance of the system is still comparable to a similar sized bonded fin heat sink located directly on the source.

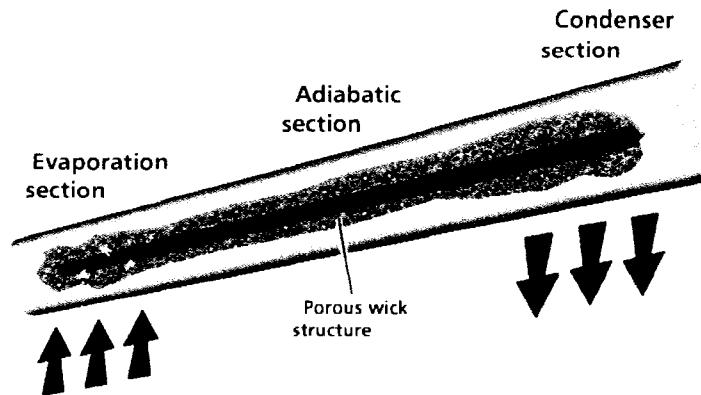


Figure 1.26: Heat pipe design

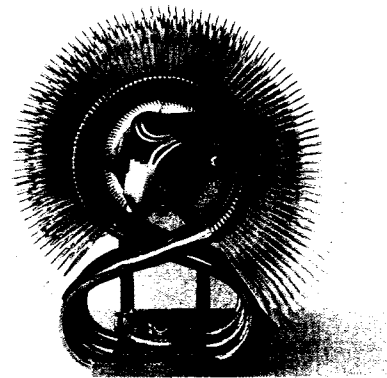
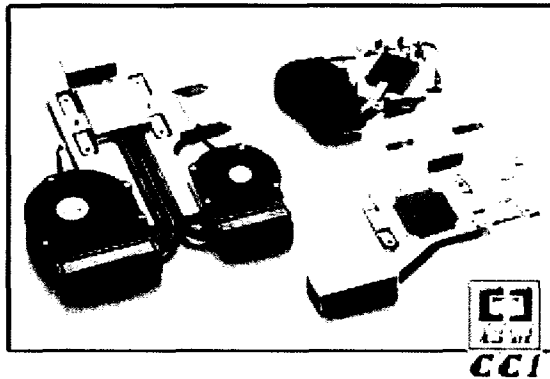


Figure 1.27: Heat sinks based on heat pipe technology

#### 1.4.4 Interface Materials

In order to effectively transfer heat from the module to the heat sink, thermal interface materials are necessary to compensate for surface roughness and flatness. At the microscopic scale, low conductivity air gaps exist between the module and heat sink leading to a large thermal resistance. A number of different materials are used to fill these gaps and create a high conductivity junction. A few of the most common materials are:

- Silicon-based thermal grease

- Non-silicon based thermal grease
- Thermally conductive adhesives
- Graphite foil patches

Silicon thermal grease is the most common interface material for general applications; however, it has a fairly low temperature limitation ( $\sim 150\text{ }^{\circ}\text{C}$ ) making it unsuitable for high temperature generation.

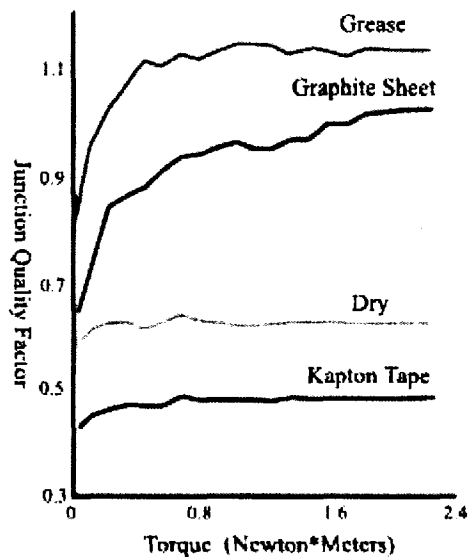
Non-silicon greases can be made to withstand much higher temperatures without significant evaporation, up to  $350\text{ }^{\circ}\text{C}$ . Unfortunately, high temperature grease is much more expensive than silicon-based grease. Even grease rated for high temperature operation will slowly evaporate or degrade.

Thermally conductive adhesives are also restricted to very low temperatures. They are a simple and clean way to join two materials, but generally have poor thermal performance.

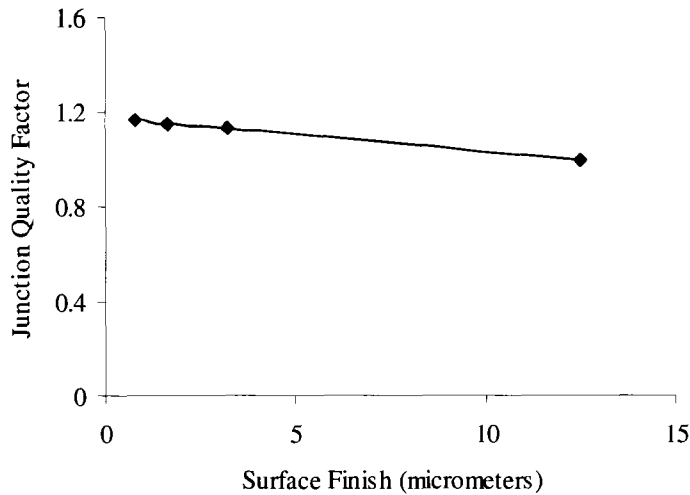
Graphite pads are also used as an interface material. Graphite pads can withstand very high temperatures, up to  $450\text{ }^{\circ}\text{C}$ . Since the graphite can be compressed, it does a good job of filling large gaps caused by bowing or curved surfaces, but not the microscopic voids. Also, because it needs to be conformed to the shape of the surface to do its job, higher clamping forces are required for graphite pads than for thermal grease.

Figure 1.28 was created by Ritzer et al. by using a pulse test method to test junction quality [48]. This clearly demonstrates the difference between the different interface materials, and the effect of clamping force (torque on clamping screws

shown). It is interesting to notice that the grease reaches a maximum at about 0.6 Nm, while the graphite sheet continually increases and would most likely continue the trend at higher pressures. Ritzer et al. also studied the effect of surface finish on junction quality. The authors remarked that even a fairly poor surface finish, 3.2  $\mu\text{m}$ , had a minimal effect on junction quality. From 3.2  $\mu\text{m}$  to 0.8  $\mu\text{m}$  the interface only improves by about 5%. Another interesting observation in this study was the impact of a human hair contaminating the interface during assembly which reduced the junction quality to about half of the typical value. Similar results were reported for small metal burs as well.



**Figure 1.28: Effect of clamping force on thermal resistance for multiple interface materials [48]**



**Figure 1.29: Effect of surface finish on junction quality [48]**

### 1.4.5 Generator Thermal Analysis

In order to calculate the power and efficiency of the thermoelectric module as outlined in sections 1.3.2 and 1.4.6, the module operating temperatures need to be determined first. Typically the TEG assembly will be placed between a hot gas or liquid stream and atmospheric air. To calculate the temperature of the hot and cold side of the module, a thermal resistance circuit is used as shown in Figure 1.30. In addition to the thermal resistances of the heat sinks and module, the thermal interfaces are also included as they can lead to significant temperature drops from the heat sink to module surface. With good practice, interface temperature drops can be kept to around 15° C with  $\Delta T$  of 200 °C [44]. Thermal resistance is typically expressed in units of °C/W. The thermal resistance circuit is easily solved by using traditional methods [70].

In some cases, a significant amount of heat bypasses the module going straight from the hot sink to the cold sink as in Figure 1.31. This can be from convection and radiation between the two, as well as through the clamping screws. It is important to keep this amount to a minimum, since it creates additional loading for the cold sink and reduces the overall temperature difference across the module.

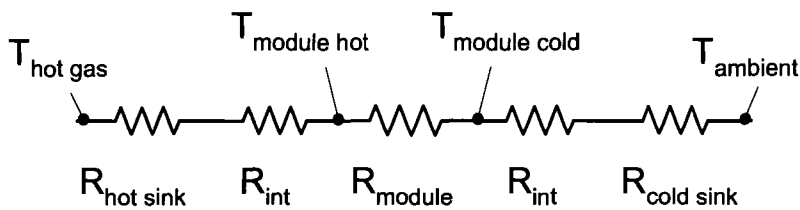


**Figure 1.30: Thermal resistance circuit for TEG**

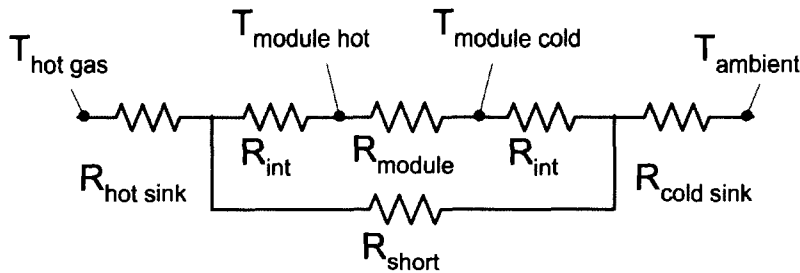


**Figure 1.31: Thermal resistance circuit with bypass**

It should be noted that the thermal resistance of the heat sinks, as well as the module can change with temperature or heat flux due to non-linear thermal effects. Typically, the resistance of the module will decrease with increasing temperature due to natural convection and radiation within the module. Convection and radiation will also increase between the heat sinks at high temperature resulting in a lower  $R_{short}$ .

It should also be noted, as described in section 1.3.2, that the electrical and thermal effects in a module cannot be separated. This is due to the effect of current on the Peltier and Joule heating effects. Therefore, the apparent thermal resistance of the module will change depending on the amount of current flowing in the module. Most manufacturers give properties at a specific operating condition. If the module is operating near this design condition, the properties can be considered constant within small temperature ranges.

#### 1.4.6 Module Electrical Performance

Once the operating temperatures of the module are determined, a simplified electrical model can be used to determine the electrical power produced by the system. The module can be treated as a voltage source, arising from the Seebeck effect, and an internal resistance. The load can be treated as a resistive load with an equivalent resistance. This is shown schematically in

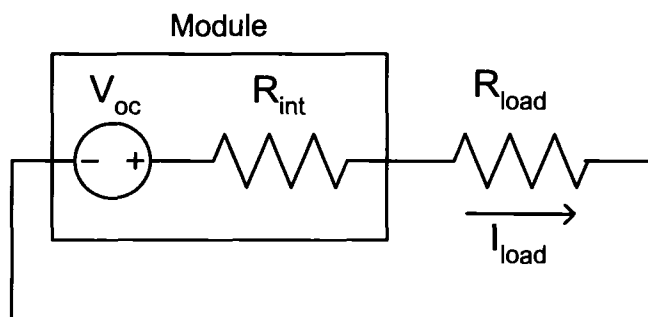


Figure 1.32: Module equivalent circuit

By analyzing this representative circuit, several important principles can be demonstrated. At a given hot side and cold side temperature, the open circuit voltage is

$$V_{oc} = \alpha \Delta T$$

**Equation 1.26**

Where the power delivered to the load can be calculated as

$$\left( \frac{\alpha \Delta T}{R_i + R_l} \right)^2 R_l$$

**Equation 1.27**

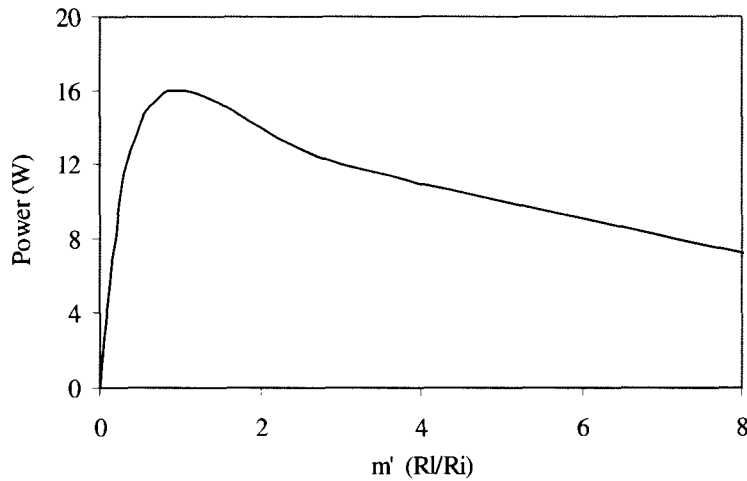


**Figure 1.33: Power as a function of  $m'$ ,  $200\text{ }^\circ\text{C } \Delta T$ ,  $\alpha = 0.04\text{ V/K}$**

From Figure 1.33, it is apparent that the power is maximum when  $m'$  is equal to 1, where  $R_l = R_i$ . This is referred to as matched load operation. However, peak efficiency occurs at  $m' > 1$ , and is dictated by Equation 1.24. This figure also shows that the power decreases much slower at  $m' > 1$  than  $m' < 1$ . Power is also shown as a function of current in Figure 1.34. At very high currents, the voltage at the load is very low leading to little power. At high voltages, the current is low leading to low power.

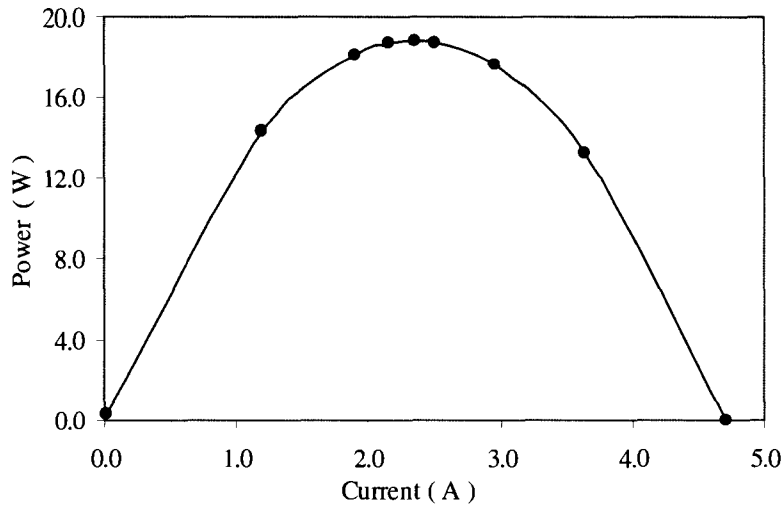


**Figure 1.34: Power as a function of current, 200 °C  $\Delta T$ ,  $\alpha = 0.04$  V/K**

### 1.4.7 Module Reliability and Degradation

A very important consideration in the design of this system is the lifetime. To be viable as a competitor to other alternative energy sources such as wind and solar, it must have a lifetime of at least five years with minimal cost on maintenance. Although there are no moving parts within the thermoelectric module, there are still several mechanisms that can lead to degradation and failure of a module over time. These mechanisms act primarily on the electrical conductivity of the module and the thermal conductivity of the interface.

A number of researchers have studied the effects of temperature cycling on the module electrical resistance [46][47]. Both studies found a significant increase in electrical resistance after just a few hundred cycles. This degradation varies significantly from one manufacturer to another. Most showed less than 20% increase after 2000 cycles, with one showing a 60 percent change after 1500 cycles. This

increase in resistance has been attributed to cracking/separation at the interface between the element and the conductor strip. This occurs due to thermal stresses leading to fatigue [49].

Ritzer et al. also observed large variations in the electrical contact resistance in the modules as they came from the manufacturer. They present a non-destructive test method to evaluate the junctions with a thermally activated paper [47].

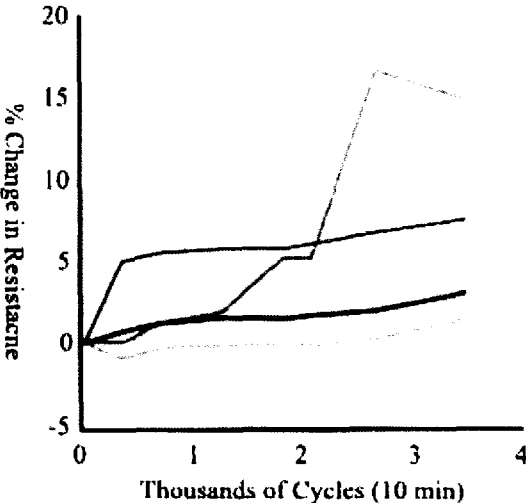


Figure 1.35: Change in module AC resistance with number of cycles [46]

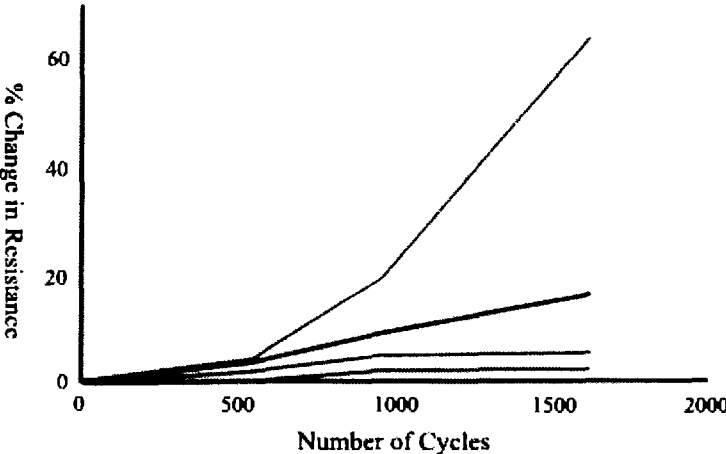
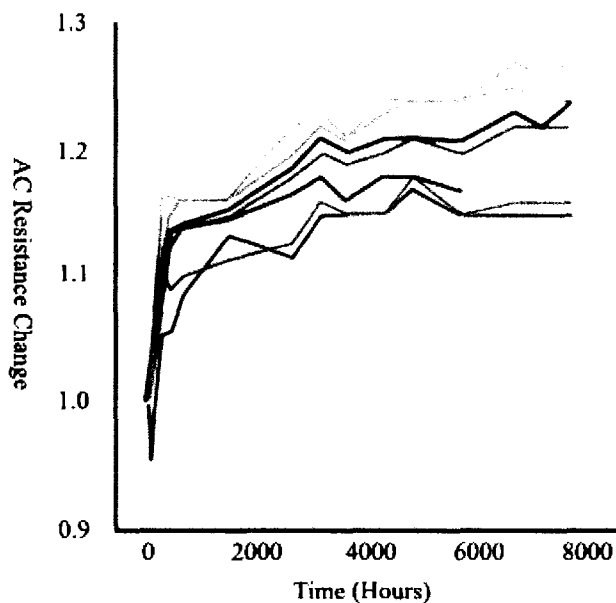


Figure 1.36: Change in module AC resistance with number of cycles [47]

It has also been shown that module AC resistance can increase from time spent at high temperature as shown in Figure 1.37 for several different modules. Most of this increase occurred during the first 700 hours and leveled off significantly. This was attributed to being near the melting point of the solder, and mostly to compositional and structural changes in the vicinity of the junctions [45].



**Figure 1.37: AC resistance change at elevated temperature (100 °C) [45]**

Another failure mechanism for a module is degradation of the Seebeck coefficient of the thermoelectric material. Stapfer and Truscello monitored the change in Seebeck coefficient for a SiGe generator over 100,000 hrs (11.4 years) [54]. An increase of less than 10% was measured over the 100,000 hr test period. This was attributed to precipitation of the n-material dopant. Other work has shown the overall change in ZT due to elevated temperature and cycling [46][47]. However, the effect on the

Seebeck coefficient was not isolated, and the trends appear to closely follow those for the electrical resistance which contributes to ZT (Figure 1.38).

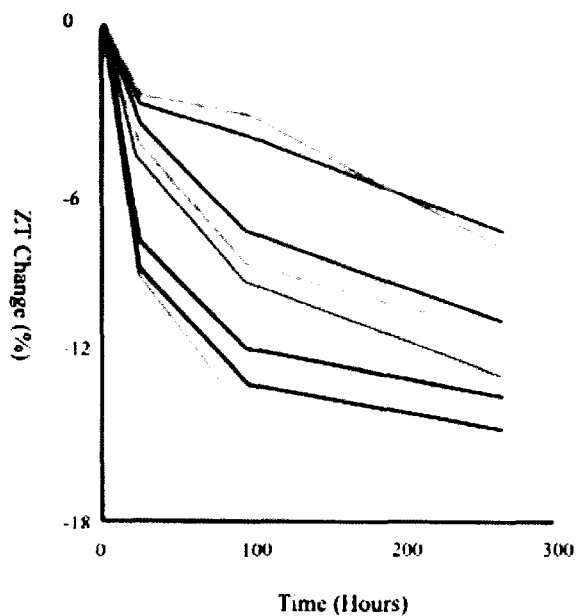


Figure 1.38: ZT change at elevated temperature [46]

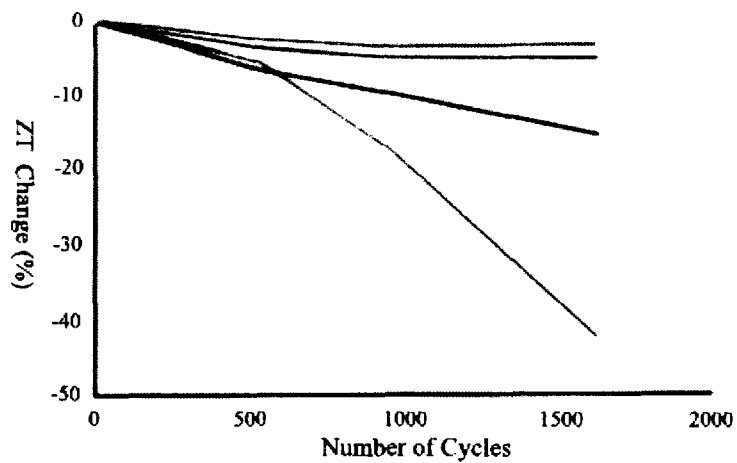


Figure 1.39: ZT change from temperature cycling [47]

## **1.5 Battery Storage**

### **1.5.1 Battery Characteristics**

Since the generator will be operating during the day, and at varying power, it is necessary to use a battery for energy storage. Selecting the appropriate battery capacity and material is very important to meet the performance and cost targets. The battery types considered were the lead-acid battery, Ni-Cd, Ni-mH, and Li-ion. These types vary in cost, energy density, cycling characteristics, lifetime, rate of charge/discharge, etc. In this application cost is the dominant factor, followed by lifetime. It was determined that the sealed lead-acid battery has the most favorable characteristics for this application.

Batteries are classified by their amp-hour (Ah) rating, which is a measure of how much energy they can deliver from the fully charged state to a specified discharge voltage. Typically the Ah rating is at the 20 hour rate to 1.75 V/cell. The amount of energy a battery can deliver depends on the current requirement. At larger currents the battery capacity is less. The discharge current also affects the final voltage that the battery reaches when it is fully discharged as shown in Figure 1.40.

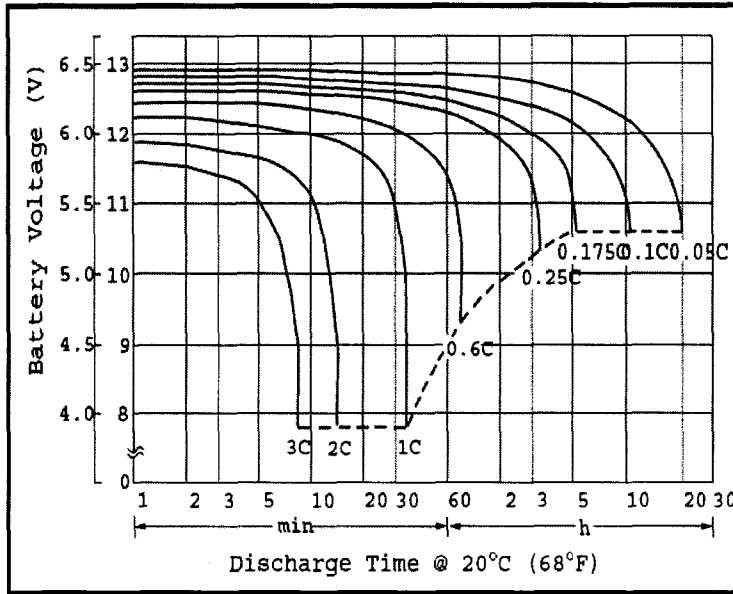


**Figure 1.40: Typical discharge characteristics for a sealed lead acid battery where C is the battery capacity in Ah [3]**

### 1.5.2 Battery Charging

The process of charging a battery is dependant on the battery capacity, charging strategy and usage. Selection of the appropriate charging current and voltage are important in maintaining battery capacity over its lifetime. It is very important to ensure that the battery is fully charged every few cycles, and that the battery is not over charged. There are three primary methods for charging a battery, fast charge, float charge and constant current charge. In fast charge, the voltage applied to the battery is around 14.5 V (for a 12 V battery). The battery will accept charge until it reaches about 13.8 V. Here the charging current drops off significantly (to around 80 mA). This is the fastest way to charge a battery; however, the charger must sense when the battery is fully charged and turn off to prevent damage to the battery.

In float charge mode, the voltage is set to 13.8 volts to maintain the battery in the fully charged state. This is used in backup power applications where the voltage can be applied continuously.

Batteries can also be charged in constant current mode. Here the current is controlled typically at a fraction of the battery capacity, until the battery is fully charged and the current is shut off.

A batteries voltage during charging will be higher than its equilibrium voltage as shown in Figure 1.41. The equilibrium voltage will be achieved about 20 minutes after the charger is disconnected. Similarly, when a battery is being discharged, its voltage is lower than the equilibrium voltage. These effects make it difficult to know the state of charge of a battery when it is being charged or discharged.

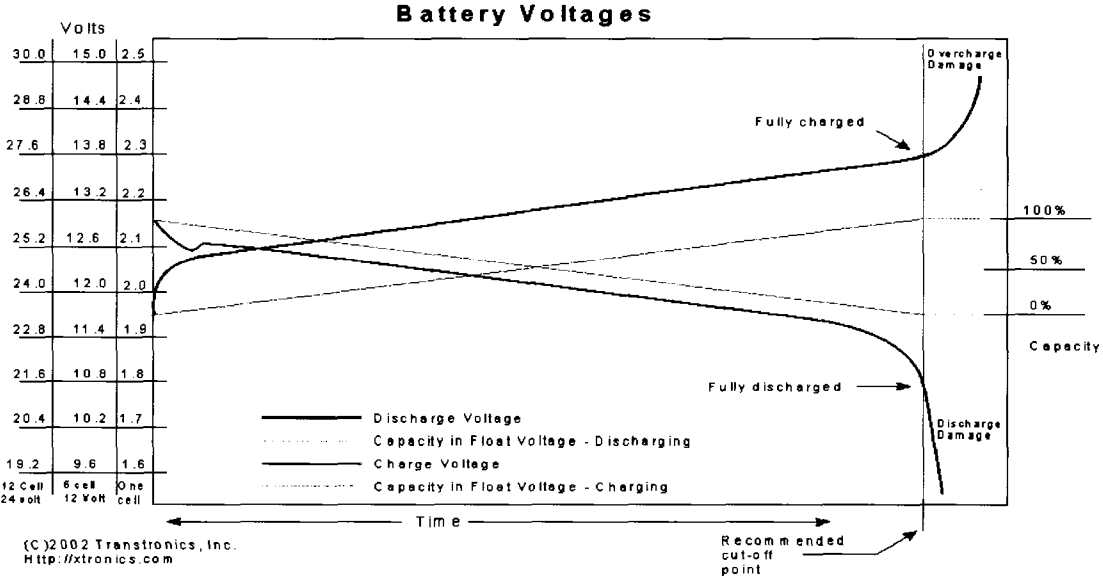


Figure 1.41: Battery charging characteristics

### 1.5.3 Battery Lifetime

Battery lifetime is influenced by the discharge/charging rate, the level of charge achieved when cycling, and the level of discharge when cycling. Most important is the level of discharge. Discharging the battery past its safe discharge voltage (around 1.7 V/cell) will significantly reduce its lifetime. If a battery is left at this charge it may be ruined. Even when a battery is cycled within the safe range, the level of discharge will affect the number of cycles the battery is good for as shown in Figure 1.42. Although a battery may not be ruined by over discharging, the capacity of the battery will continue to be reduced.

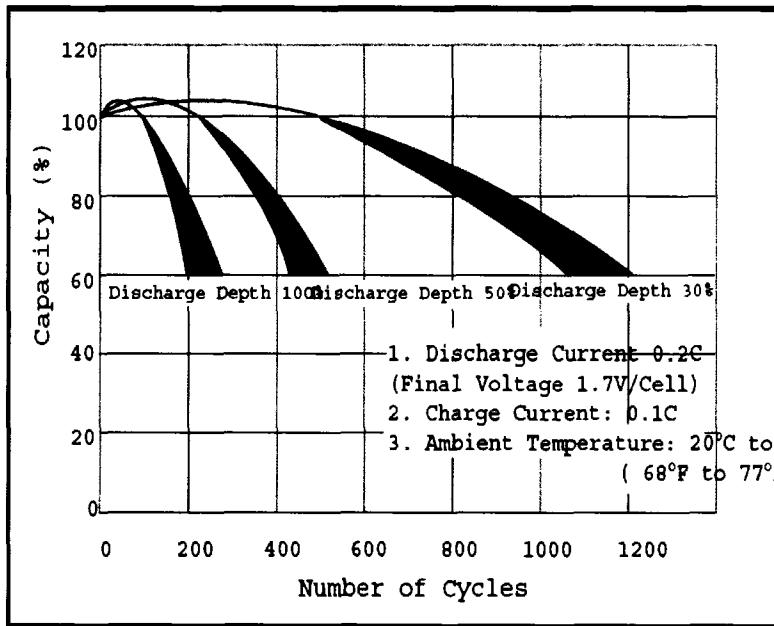


Figure 1.42: Effect of discharge depth on battery life

## **1.6 Lighting**

The issue of lighting efficiency continues to be of utmost importance in both the developed and undeveloped world. Up to 20% of the electricity usage in the developed world is for lighting. In developing countries the percentage is even higher [74]. Every year, advancements in lighting are made, making lighting more affordable and efficient. For this work, selecting the appropriate light source is very important to maximize the effectiveness of the design. Ultimately the goal is to maximize the lumen/\$ of the entire system.

There are several potential styles of lighting that can be used with the proposed system. Since the lights will be powered by a battery, this limits the types that can be used and what is available. The available lighting options considered are LED, Cold Cathode Fluorescent (CCFL), Compact Fluorescent (CFL), and straight tube fluorescent. The most important parameters for comparing the different styles are cost, power range, efficiency and lifetime.

In the past few decades, the largest leaps have been made in light emitting diodes (LED). However, LEDs have yet to surpass fluorescent lights in efficiency and cost. The greatest strength of LED lights is the potential lifetime of over 50,000 hrs [71]. In the near future it is anticipated that LED lighting will surpass CFL lighting in efficiency and cost [72]. Every year significant advances are made in LED manufacturing and performance. In the past, LEDs have been limited to very low light outputs, less than 10 lumens or so. The push to incorporate LEDs in more than just electronics applications to commercial and residential applications has led to the development of high power LED's. At the moment, the highest power LED's

deliver up to 100 lumens per bulb [71]. This is still smaller than a typical household incandescent or CFL bulb which deliver between 500-2000 lumens.

CCFL lighting is commonly left out of the discussion as a future residential and industrial lighting source, despite its many advantages. As with LEDs, CCFL lights have traditionally been used for lower power electronics applications such as backlit LCD displays on phones or laptops. CCFL lights lie in between LEDs and CFL lights in the areas of cost, efficiency, and lifetime. They are typically used in lower power applications from 10 to 200 lumens. Lifetime for CCFL can be greater than 20,000 hours, over twice that of CFL lights. This is due to more robust solid metal cathodes used in CCFL compared to thin wire cathodes used in CFL lamps [73]. This more robust cathode also helps the CCFL resist fatigue from cycling on and off, a known weakness of CFL bulbs.

CFL bulbs are now the dominant replacement for incandescent bulbs in residential applications due to their high efficiency and low cost. Although CFLs are still more expensive than comparable incandescent bulbs, the money saved on electricity and replacement makes them much more economical over their lifetime [74]. CFLs have a much longer lifetime than an incandescent bulb, but less than LED or CCFL bulbs. Typical lifetime is around 6000-8000 hrs [74]. CFL bulbs are currently more efficient than LEDs and CCFLs.

A comparison of efficacy of the lighting options considered is shown in Figure 1.43. These ranges represent the highs and lows of what is currently on the market. For LEDs the higher values of lm/W are for smaller output bulbs. Therefore, it is difficult to use the 60 lm/W bulbs for room lighting. This trend is shown in Figure

1.44. CFLs tend to follow the opposite trend with higher power bulbs being more efficient.

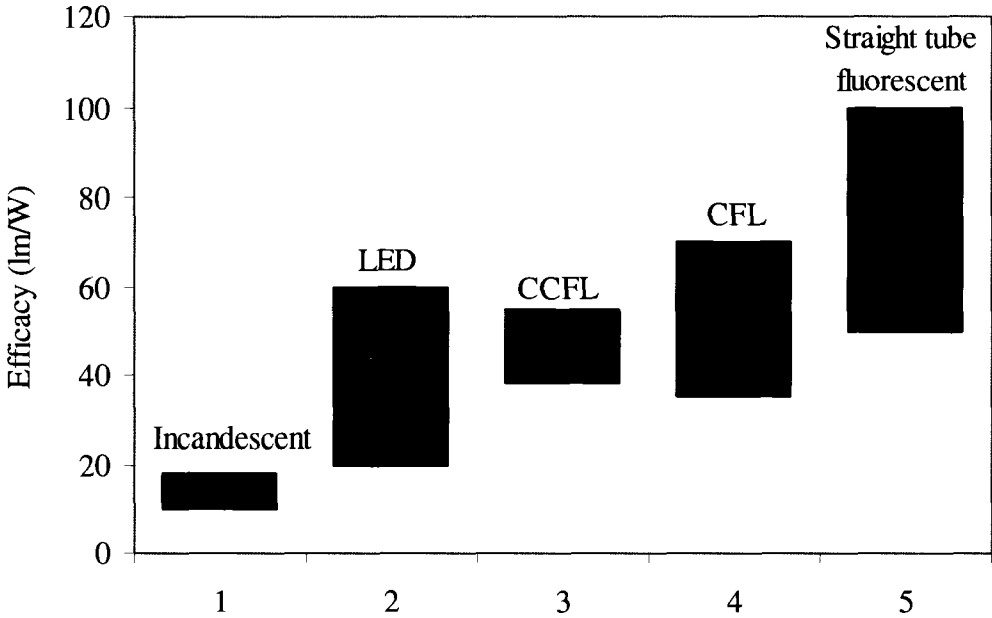


Figure 1.43: Lighting efficacy comparisons [72][73]

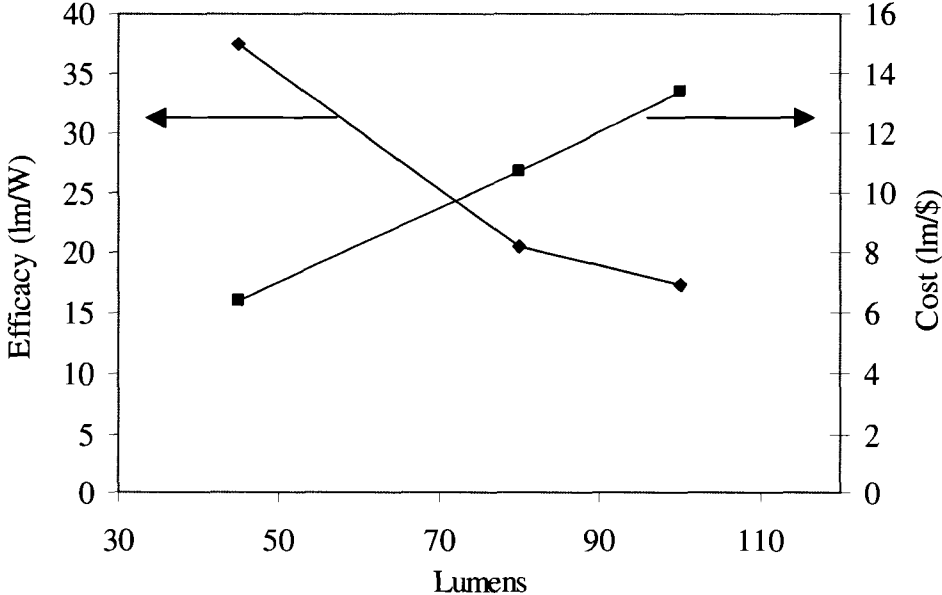
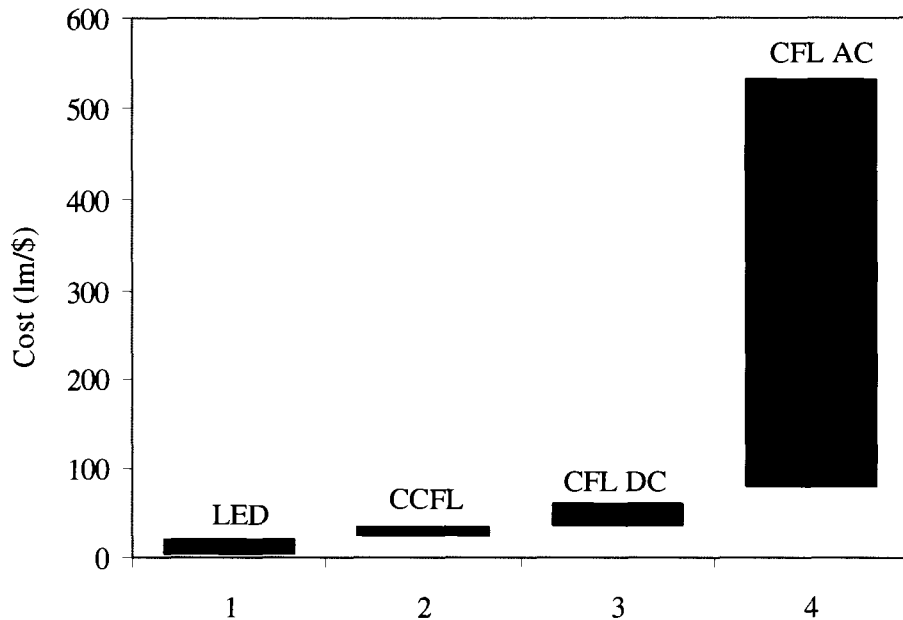


Figure 1.44: Efficacy and cost vs. lumens for single LED bulbs [71].

Cost effectiveness is also an important consideration in this selection process. In the 500-2000 lumen range CFLs have the highest lm/\$ and lm/W. Unfortunately, in DC applications the cost of the ballast used to drive the bulb is significantly more, making them less cost competitive with CCFL. This is due to higher current requirements, DC-AC conversion, and a much smaller market. CCFL lights have a favorable lm/\$ in sizes smaller than 500 lumens. LEDs currently have a lower cost effectiveness than fluorescents; however, this is quickly changing. In just the past couple years the cost of high power LEDs from Luxeon has dropped by 50% [71]. Unfortunately, as the lumens/\$ increases with higher output lights, the efficiency decreases as shown in Figure 1.44. This creates an interesting dynamic between cost and efficiency. The cost of an LED system also includes a driver for the light to regulate the current. These drivers are also currently more expensive than those on CFL and CCFL lights. Cost effectiveness can be increased if multiple LEDs are run off of the same driver. The cost effectiveness in lm/\$ for light and driver/ballast is shown in Figure 1.45. These are based on consumer costs.



**Figure 1.45: Light and driver cost for various lighting options**

## ***1.7 Stove Design***

In order for this stove-generator to be successful in the market, it must be clean burning, efficient and conform to users cooking styles and habits. Over the past 20 years, there has been a large effort to develop and distribute clean cookstoves in developing countries. From these experiences several principles have been realized that contribute to an efficient, clean burning stove.

Traditional cookstoves usually consist of a ring of bricks that a pot or pan can be rested on with wood fed in from the side. This type of stove produces significant smoke and results in low efficiency due to weak combustion. The “rocket elbow” (Figure 1.46) has been developed to address these issues in multiple ways. First of all, the diameter of the magazine and chimney are kept as small as possible while

keeping an acceptable power output for the stove. This keeps the air velocity in the stove high to promote vigorous and complete combustion. This also limits the amount of excess air drawn in to keep the overall fuel/air ratio closer to stoichiometric. This improves combustion and results in very high temperatures. The fuel is also placed on a shelf to make sure there is always a free path for air to be drawn in even when the mouth of the magazine is full. The air is also preheated as it flows into the combustion chamber. This combustion chamber is also designed to burn the tips of the sticks only. This prevents the stove from burning too rich, leaving unburned smoke. Finally, the chamber is made from the most insulative materials possible that can withstand the heat over time.

There are many stoves that incorporate this rocket chamber design. The style of the stove will vary depending on the local materials, acceptable cost of the stove, and the cooking style of the user. Examples of these stoves are shown in Figure 1.47

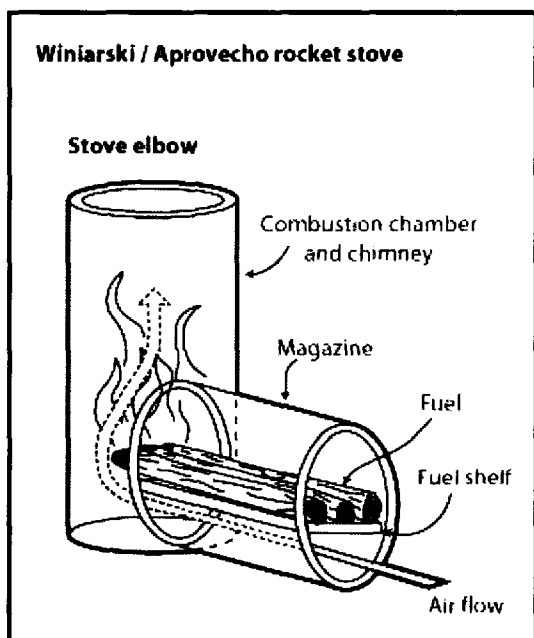
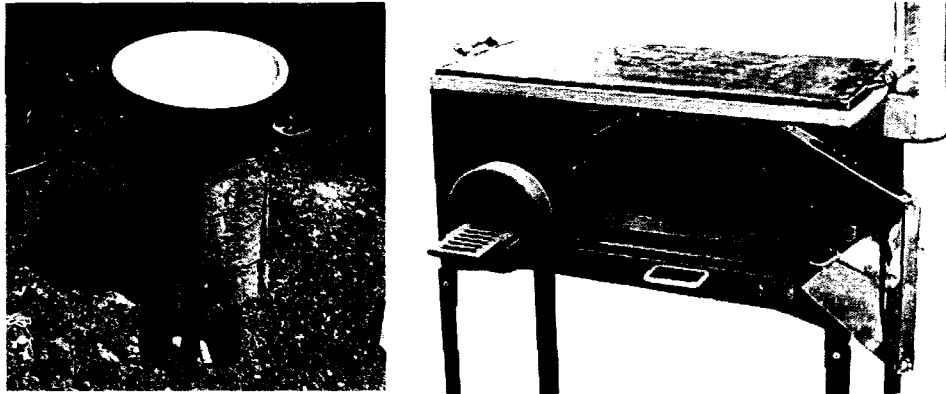


Figure 1.46: Rocket elbow combustion chamber



**Figure 1.47: Basic Rocket stove (left) and Ecofogao with chimney and oven (right)**

## **2 GENERATION 1 SYSTEM DEVELOPMENT**

To begin the design process of the first thermoelectric stove, some basic criteria had to be laid out pertaining to power output, stove configuration and user habits. The first target market considered was Latin/South America. In many of these countries, programs are currently in place to subsidize the purchase of solar photovoltaic kits for rural electrification. In addition, many of these people already own radios, TVs and other small devices that they run off of car batteries. For this first prototype, the goal was to create a system that would be competitive with current solar systems being installed in these countries. Many of the solar systems being installed are quite large, around 50 Watts. For the first design, this was considered too aggressive and costly for development work. Therefore, the objective was changed to provide approximately 3 hours of lighting using a 15 Watt compact fluorescent bulb. This requires 45 W-hr of energy to be generated and stored in the

battery. It was decided that enough power should be generated to power a fluorescent bulb due to their lower cost and higher efficiency than LED lights. This would improve the overall cost effectiveness of the system in terms of lumen/\$ (see section 1.6).

For the first generation prototype of the thermoelectric stove, we chose to work with the Brazilian stove manufacturer Ecofogao, which is well established in several Latin American and South American countries. Most of the stoves made by Ecofogao are plancha stoves, meaning the cooking is done directly on the stove surface. The basic stove form used to adapt the TEG to was the Ecoforno stove shown in Figure 2.1. The objective was to use the space currently occupied by an oven for placement of the TEG.

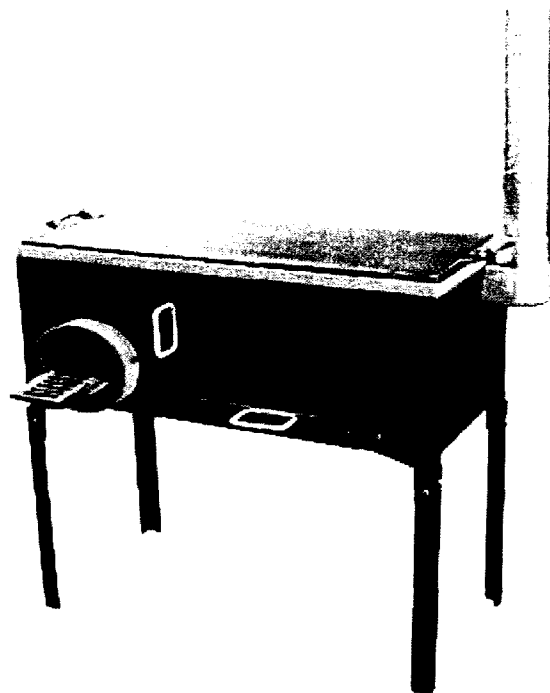


**Figure 2.1: Stove model used for generator retrofit**

## **2.1 Cooling System Design Alternatives**

Several potential design concepts were evaluated for cooling the thermoelectric module. These were air-cooled forced convection, air-cooled natural convection, water-cooled forced convection, and water-cooled natural convection. These different systems were evaluated on their ability to meet the design objectives of power output, reliability, cost and maintenance.

### **2.1.1 Air-Cooled Forced Convection**

The air cooled forced convection model consists of the cold side being cooled by a finned heat sink and a fan as shown in Figure 1.22 and Figure 1.23. This is the most common technique, and the most straightforward. The advantages of this system are that it requires the fewest parts, and that fairly low thermal resistances can be achieved on the cold heat sink. Some disadvantages are that it adds a moving part to the system, the fan, which can break down and cause module overheating and failure. It also requires that something turn the fans on and off automatically when the stove is running.

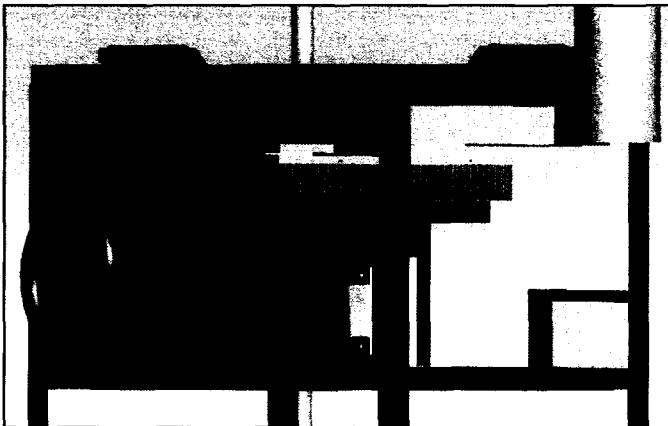


**Figure 2.2: Forced convection cooling concept**

### 2.1.2 Air-Cooled Natural Convection

The second alternative considered was the air cooled natural convection system. Having a natural convection system has several advantages. First, it requires no moving parts, eliminating the possibility for a failure in the cooling system. This also results in completely silent operation.

It was evident early on that a natural convection alone on a heat sink would not be sufficient for the size of system intended here. Even with one of the largest extrusions available, the Aavid 65605 at 18 cm length, the thermal resistance is still 0.5 C/W. This is too high to achieve the target system power as will be shown in section 2.2. In addition, it would be difficult to get the heat sink in the proper orientation for natural convection given the current stove design.

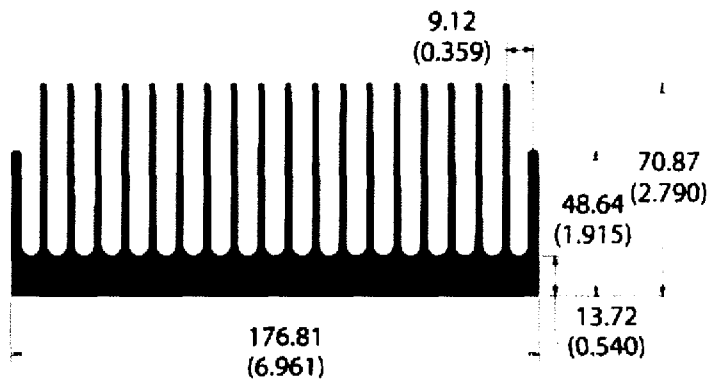


**Figure 2.3: Aavid 65605 extrusion**

Another alternative for natural convection was considered that would use additional draft provided by the stove. Natural convection is driven by the temperature change of the air, resulting in buoyant forces. Within a natural convection heat sink the temperature change is small, resulting in a very small flow rate of air. The goal of this design was to heat the air further after it exits the heat

sink by ducting it into a pipe that passes through the chimney. This concept would significantly increase the air flow across the heat sink and lower the thermal resistance.

A prototype of this configuration was constructed as shown in Figure 2.4 with no heat sink present. The flow rate through the natural convection duct was measured with an anemometer to be approximately  $0.3 \text{ m}^3/\text{min}$ . This air flow would reduce the thermal resistance from  $.5 \text{ C/W}$  to about  $.3 \text{ C/W}$ . Unfortunately, this is still not enough for the power desired, especially if this flow is split between two modules. This may still be a very attractive option for lower power systems being designed in the future.

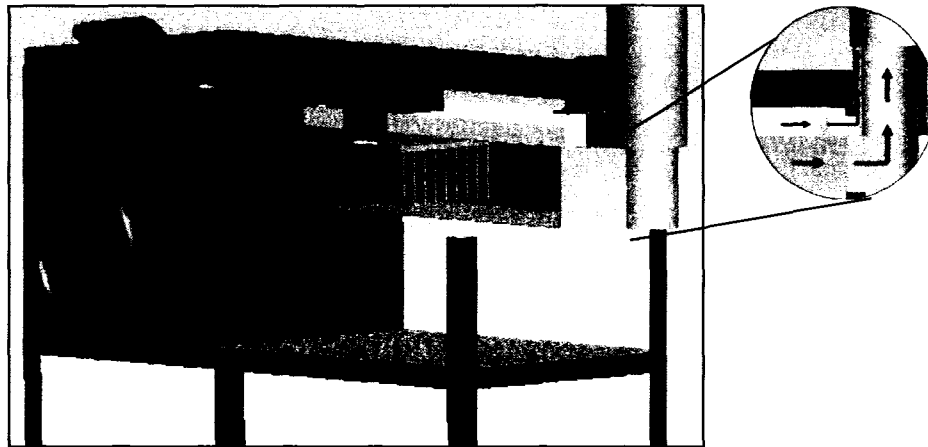


**Figure 2.4: Natural convection system using heated duct to increase flow**

### **2.1.3 Water-Cooled Forced Convection**

Water cooling methods were also considered using a cooling block and pump system. Water cooling blocks are able to achieve very low thermal resistances, lower

than those possible with air cooled systems. This would allow the use of a single larger module in place of two smaller modules. A water cooling method reduces the amount of space needed for the cold sink, allowing much more design flexibility. However, the water simply carries heat away from the module. It must still be dumped elsewhere in some type of radiator. This increases the total number of parts to a pump, cooling block, radiator and possibly a fan.

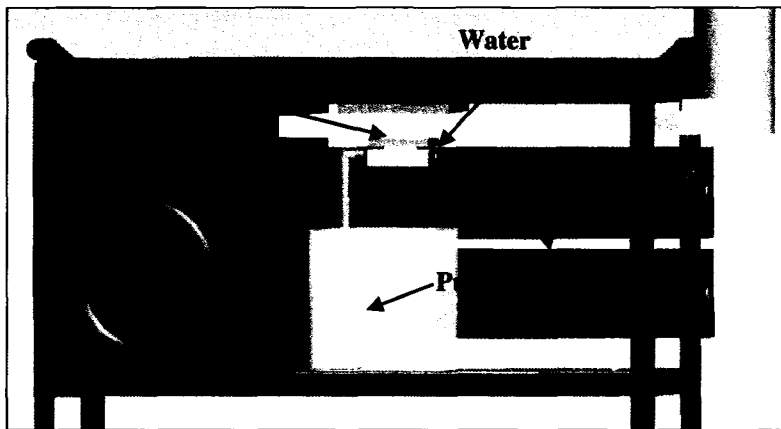


**Figure 2.5: Water cooled forced convection system**

#### **2.1.4 Water-Cooled Natural Convection**

The last configuration considered was a water-cooled natural convection system. This is commonly referred to as a thermosyphon system, where water is circulated by buoyant forces. This alternative has the same advantages as the air-cooled natural convection system. It has no moving parts, requires no control and is silent.

In a thermosyphon system, the velocity is established when the buoyant force equals the fluid friction force. These are typically low velocity systems favoring

large temperature differentials. However, in this application the temperature differential of the water passing through the heat sink would need to be kept small, resulting in a weak thermosyphon. In addition, an external radiator would still be required to deliver the heat to the atmosphere and keep the system from heating up.

Another option for a natural convection system was considered that would use a large water reservoir in direct contact with the cold heat sink. In this design the water's thermal mass would be used to absorb all the energy delivered by the module, eliminating the need to dump the heat to the atmosphere. A natural circulation would be developed within the tank to keep the heat sink cool. This concept is shown in Figure 2.6.

One disadvantage of this system is that during the day the water would continue to warm during each meal cooked, resulting in decreasing power. It is also possible that if the stove were used too much, the entire system would get hot enough to exceed the module's maximum operating temperature on the hot or cold side. Another disadvantage of this design is that it would depend on the water cooling significantly at night, or being used and replaced with cold water. If the hot water was intended to be used, it is possible the stove could be run without sufficient water resulting in the module overheating.

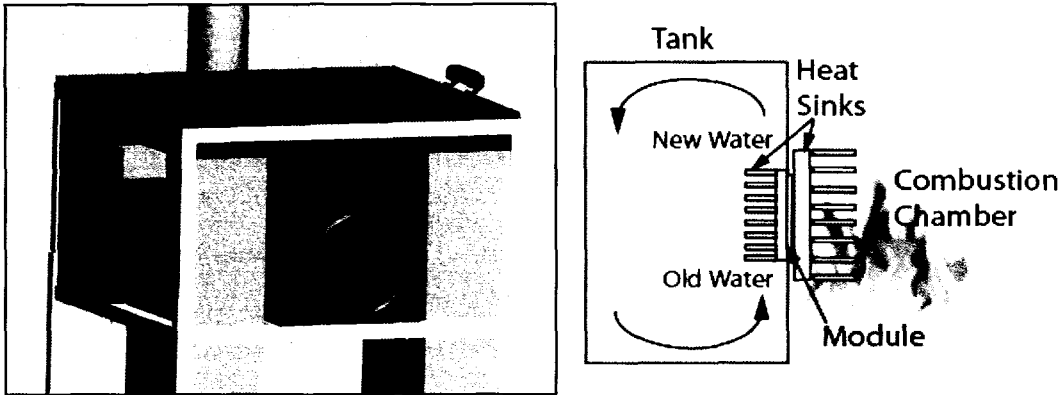


**Figure 2.6: Natural convection system with water tank**

### 2.1.5 Final Cooling System Selection

Considering the previous discussions, the following selection matrix was created to select the best alternative for the design criteria outlined in Sections 1.2. Each category was given a score of 1-5. The results were very close, with each design having unique strengths and weaknesses. The highest total was for the air-forced convection design, followed by the air natural convection and water natural convection. However, in this case the air natural convection is not capable of meeting the power objective.

**Table 2.1: Comparison of cooling design alternatives**

	Cost	Noise	Reliability	Power	Total
Air Forced Convection	4	4	4	5	16
Air Natural Convection	3	5	5	2	15
Water Forced Convection	1	3	4	5	13
Water Natural Convection	3	5	4	3	15

## **2.2 Component Selection**

Proper selection of the proper module, heat sinks and fan for the desired performance is very important to achieve an efficient and cost effective design. In order to achieve the target net power, all components must be considered together as the performance of one component affects the other. To accomplish this, each component is evaluated individually and then as a part of the system. In order to accomplish the goal of 45 W-hr per day, 15 W-hr need to be generated each meal (assuming 3 meals per day). Preliminary field test data from Ecofogao showed approximately 1.5 hr cooking periods. This means the power should average about 10 W. However, the warm up period and cool down period are very large. To compensate for this, it was estimated that a peak power of around 20 W would be necessary to result in this average power. This should also account for inefficiency in the charging system.

### **2.2.1 Heat Sink Evaluation**

To identify potential heat sinks for use in the thermoelectric system, it is first necessary to make preliminary guesses of operating conditions and module properties. There is currently only one module on the market that can produce 20W of power to meet the design conditions. However, this is at a cold side temperature of 30 °C which is nearly impossible with an air cooled system. Therefore, it was decided to use two 10 W modules with separate heat sinks. This also makes the design more adaptable to smaller systems.

Using the specifications for the Thermonamic 10 W module, the following thermal circuit was modeled to find the target thermal resistance for the hot and cold sink. The steady state hot gas temperature was measured to be around 450 °C at the intended location of the generator. The cold side was assumed to be at 20 °C ambient temperature. The interface resistance value of 0.04 C/W was estimated, based on preliminary testing and published values. The module thermal resistance was provided by the manufacturer at 230 °C. It was also assumed that the best temperature of the module hot side for peak power would be the maximum continuous temperature specified by the manufacturer of 260 °C. A target cold side temperature of 70 °C was selected to provide a module power of around 11 W. Using these values, the hot and cold heat sink resistances were calculated to be 0.7 °C/W and .15 °C/W, respectively.

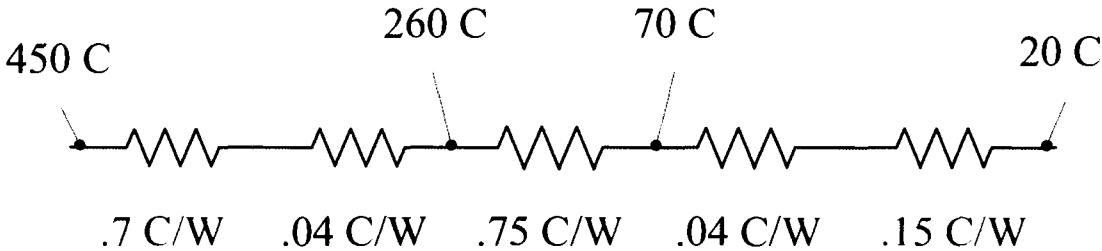


**Figure 2.7: Thermal circuit with calculated heat sink resistances (red)**

A number of heat sinks were considered on the hot and cold side to meet these target values. The hot side heat sink thermal resistance is several times larger than the cold side, since there is a much larger temperature leverage on the hot side. The hot-side heat sink value is easily met by many extrusions for low air velocities. For

this heat sink a fairly common extrusion was selected with a thermal resistance of 0.7 C/W at about .2 m/s (a reasonable flow velocity within the stove).

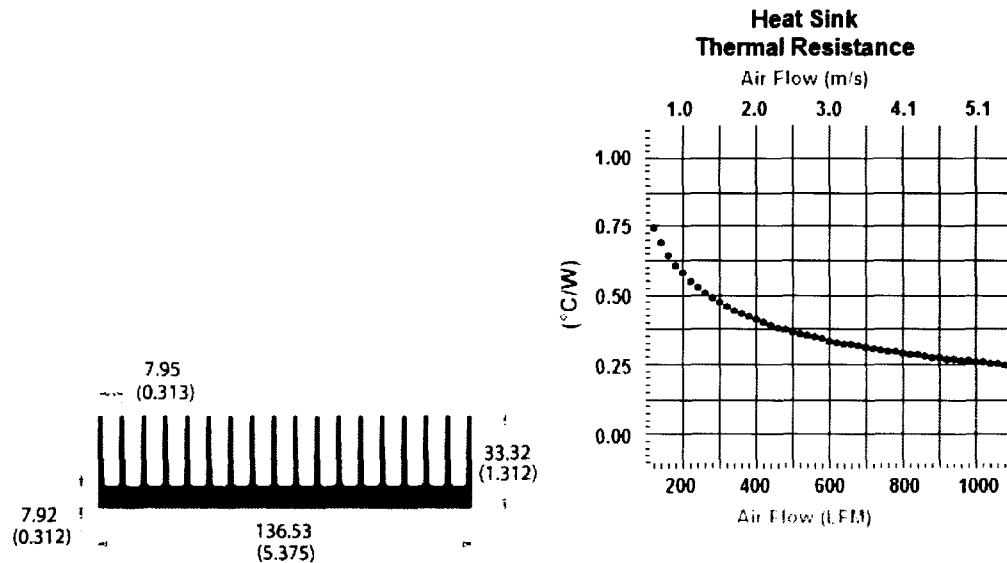


**Figure 2.8: Properties for hot side heat sink at 15 cm length**

Selection of the cold sink involved much more analysis and testing to find the most effective solution. There are two reasons for this. The first is that a thermal resistance of 0.15 C/W is difficult to achieve, even with a fan. The second is that the fan power required to achieve this resistance is a parasitic loss of the system. This means there is typically some balance between fan power and net module power, leading to an optimal fan for each application. The fan selection is commonly overlooked and has received little attention. The only work to justify the fan selection is [13].

There are hundreds of small fans available for electronics cooling applications. These vary in the size, air flow, static pressure and power consumption. Fans were

evaluated based on no-load flow rate per watt of power consumed. The highest values of (m<sup>3</sup>/min)/watt were the largest 120 mm fans since they spin at much slower velocities. A few that were identified were made by Panaflo, Papst, Cooler Master, Mechatronics and Sunon. The fan with the most efficient no-load performance was the Cooler Master fan. However, it was initially unclear how much flow or pressure would be needed to achieve the target thermal resistance. For testing, three fans covering a wide range of flows were chosen. These were the Cooler Master, Sunon and Mechatronics fans.

**Table 2.2: Fan no-load efficacy**

	m <sup>3</sup> /min	Power (W)	(m <sup>3</sup> /min)/W
Panaflo 92mm med	1.3	1.8	0.72
Panaflo 92mm low	1.25	1.32	0.95
Panaflo 120mm med	2.6	3.36	0.77
Panaflo 120mm low	1.9	2.04	0.93
Pabst 120mm	1.4	1.3	1.11
Mechatronics 120mm	1.55	1	1.61
Sunon 120mm B3	2	2.4	0.83
Cooler Master 120mm SUF-F12	1.2	.6	1.98

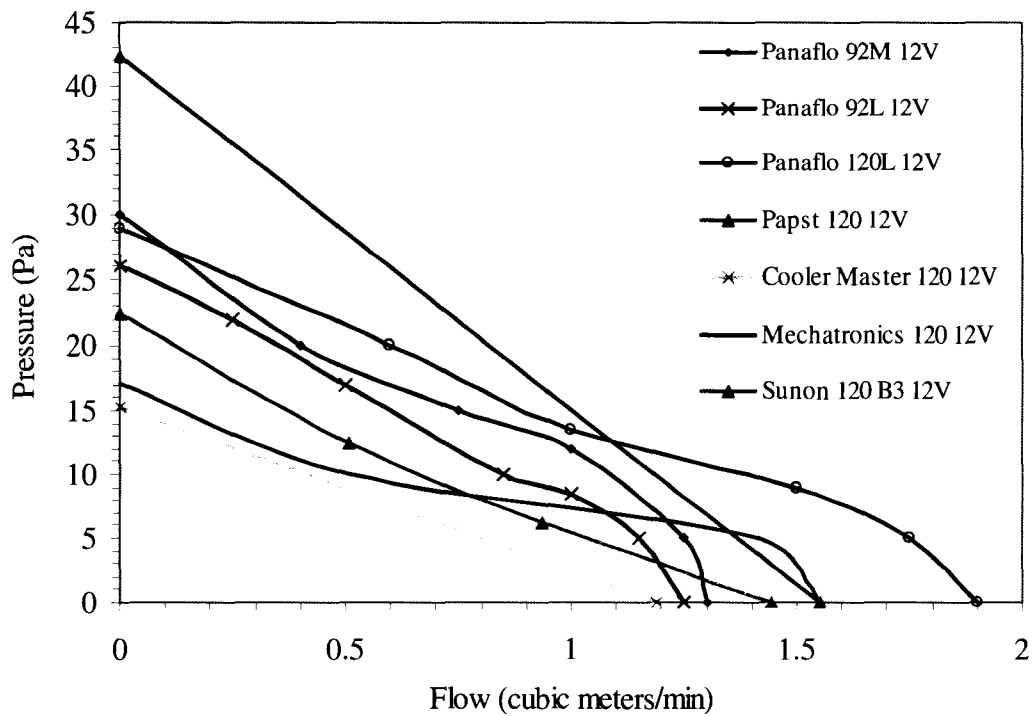


**Figure 2.9: Fan operating characteristics**

Several potential heat sinks were identified that could possibly meet the target value of .15 C/W based on manufacturer specifications. However, manufacturer specifications can be different than those achieved in an application. First, manufacturer specifications are sometimes defined for cross flow, which typically gives larger thermal resistance than impinging flow. Secondly, some specifications are for much larger fan flow rates where parasitic losses are not as important as in most electronics cooling applications.

The top three potential heat sinks were selected for further testing in a bench top apparatus. The heat sinks tested were the bonded fin HX5-301 sold by Melcor, the extruded E1456 from Thermaflo at 16.5 cm length and the 2-505017R pin fin heat

sink from Cool Innovations. They are shown in Figure 2.10. The bench top tester is described in detail in Section 5.1.1. Each heat sink was tested with three fans of different air flows. The thermal resistance values from these tests are shown in Table 2.3.

The heat sink with the best performance with all three fans was the extruded heat sink from Thermaflo. Therefore, this was the heat sink selected for further system development.

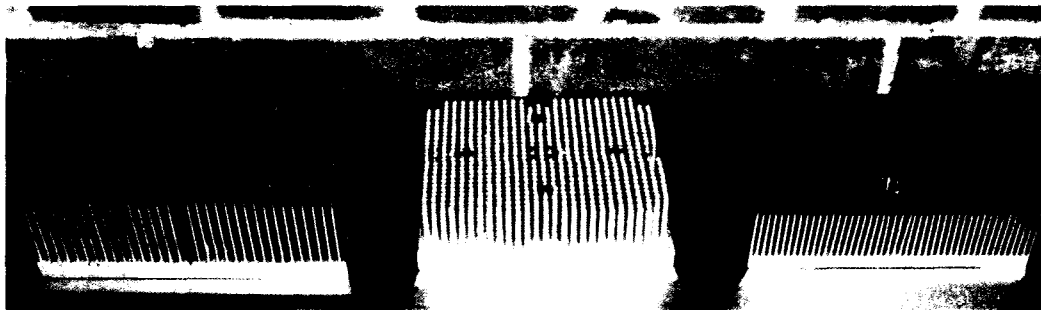


**Figure 2.10: Heat sinks (left to right) bonded fin, pin fin, extruded fin**

**Table 2.3: Heat sink/fan thermal resistances**

Heat sink	Fan	R cold sink (C/W)
Bonded	Cooler	0.17
Bonded	Mech.	0.14
Bonded	Sunon	0.13
Pin fin	Cooler	0.24
Pin fin	Mech.	0.19
Pin fin	Sunon	0.16
Extruded	Cooler	0.17
Extruded	Mech.	0.13
Extruded	Sunon	0.11

### **2.2.2 Module Evaluation**

Selecting the appropriate module for the desired power, heat sink configuration and application is critical to generating a cost effective solution. The major choices involved are the material and module size. As far as materials go, there are no commercially available materials that can currently compete with bismuth telluride in cost vs. performance. Both high temperature and cheaper low temperature modules were considered. Typical low temperature modules will operate up to 100-120 °C, while high temperature modules can operate continuously at 250 °C with transients up to 400 °C. The major differences between these modules are the melting temperature of the solder used to join the elements, and what operating temperature the material and element geometry are optimized for (see sections 1.3.2, 1.3.3)

[15][33][35]. Low temperature modules are optimized for cooling, not generation. Although the low temperature modules are cheaper, they would not be a good selection for power generation. There are two reasons for this. The first is the fact that power is a function of temperature difference squared, therefore a module operating at one half the temperature difference as a high temperature module will make only one quarter the power. In addition, the efficiency is significantly reduced at lower temperature. Therefore, the low temperature module will have to move much more heat to make the same power. Nuwayhid et al. found that a system based on low temperature modules could generate less than 1 W per module [4]. Based on the cost of the modules alone, low temperature modules appear to be competitive with high temperature modules. However, the heat sinks can contribute as much to the cost of the system as the module. In the case of low temperature modules, the heat sinks would need to be very large since the module is operating at a much lower efficiency. This quickly overwhelms any initial advantage of using cheaper low temperature modules. For this work only high temperature modules were considered.

A number of potential high temperature modules were considered that could meet the 10 W peak power objective. The modules considered are manufactured by Thermonamic of China, and Hi-Z of the United States. The manufacturer specifications are shown in Table 2.4. In the case of the thermonamic modules, the 10.5 W module and the 14.7 W module are the same price since they have the same footprint. The 14.7 W module actually has less material since the legs are shorter. For the Hi-Z modules, the 14 W module is cheaper than the 9 W module since it also has shorter legs and fewer elements. Although it appears that the larger module

would be the obvious choice, it is not necessarily. The selection depends on the heat sinks used. Since power is a function of  $\Delta T^2$  it is possible that for a given heat sink combination more power could be generated by the smaller module. This was the case in the work done by Killander and Bass where two 20 W modules were placed directly on the stove surface with no hot heat sink [14]. The result was that the modules together generated only 4-7 W. It is likely that more power could have been generated with one 10 W or 14 W module than with the two 20 W modules. Nuwayhid et al. showed how the power generated in their system actually decreased with the number of modules for a given heat sink [16]. Although their module performance was better, they still only achieved 5 W from a 10 W module, indicating that the module was still oversized. These examples show how the selection of the proper module size can only be accomplished along with a thorough heat sink analysis.

**Table 2.4: Manufacturer module specifications**

Module	Hot side (C)	Cold side (C)	Power (W)	Thermal resistance (C/W)	Electrical resistance (ohm)
Thermonamic TEP1-12656-0.8	230	50	10.5	0.75	1.7
Thermonamic TEP1-12656-0.6	230	50	14.7	0.51	1.2
Hi-Z HZ-9	230	30	9	0.922	1.15
Hi-Z HZ-14	230	30	14	0.53	0.21

### 2.2.3 Steady State System Modeling

In order to make the final module, heat sink and fan selection, each module was modeled with each heat sink/fan combination. In order to predict power of the system the manufacturer specifications for thermal resistance, electrical resistance

and Seebeck coefficient (calculated), were used in the analysis outlined in sections 1.4.5 and 1.4.6. In the analysis, the module properties were assumed constant with temperature up to 260 °C. This is not entirely correct, but is acceptable for a first order analysis. The analysis was performed using two methods. The first assumes constant hot gas temperature and fixed hot side heat sink. The results from this analysis are presented in Table 2.5.

**Table 2.5: Module and heat sink comparison (fixed hot sink R = .7)**

	Module resistance (C/W)	Cold Heat Sink Resistance (C/W)	T hot air (C)	T hot mod (C)	T Cold Mod (C)	T amb (C)	Heat Flow (W)	Voc (V)	Module elec res. (C/W)	Power (W)	Fan Power (W)	Net Power (W)
HZ-9	0.922	0.17	450	280	68	20	230	6.9	1.15	10.3	0.6	9.7
HZ-9	0.922	0.14	450	277	62	20	233	7.0	1.15	10.6	1.0	9.6
HZ-9	0.922	0.13	450	276	60	20	235	7.0	1.15	10.8	2.4	8.4
HZ-14	0.53	0.17	450	235	81	20	291	2.7	0.21	8.6	0.6	8.0
HZ-14	0.53	0.14	450	231	73	20	297	2.8	0.21	9.0	1.0	8.0
HZ-14	0.53	0.13	450	229	71	20	299	2.8	0.21	9.1	2.4	6.7
TEP1-.6	0.51	0.17	450	232	82	20	295	7.0	1.2	10.2	0.6	9.6
"14 W"	0.51	0.14	450	227	74	20	301	7.1	1.2	10.6	1.0	9.6
	0.51	0.13	450	226	71	20	303	7.2	1.2	10.8	2.4	8.4
TEP1-.8	0.75	0.17	450	263	73	20	253	8.8	1.7	11.5	0.6	10.9
"10 W"	0.75	0.14	450	259	66	20	257	9.0	1.7	11.9	1.0	10.9
	0.75	0.13	450	258	64	20	259	9.1	1.7	12.1	2.4	9.7

From this analysis the optimal module/fan/heat sink combination is the TEP1-0.8 module, and the Mechatronics or Cooler Master fan. The peak net power achieved by this system is 10.9 W, or 21.8 W for two assemblies. In this analysis, with the current hot heat sink, the higher power modules (HZ-14 and TEP1-0.6) actually make less power than the modules of lower power rating. This is because the larger modules have a smaller thermal resistance, resulting in a much smaller temperature difference.

Also, these modules are not able to achieve the maximum operating temperature of 260 °C, while the TEP1-0.8 module hits it almost exactly.

The system was also evaluated in a fixed hot side temperature at 260 °C. However, this means the hot-side heat sink must be of variable resistance, as shown in Table 2.6. In this analysis, the larger modules result in higher powers, with the highest being the TEP1-0.6 at 13.2 W net power. Although the 14 W module looks appealing in this analysis, the drawback is the hot sink resistance required to meet this operating condition. Although the thermal resistance only drops from 0.7 C/W to 0.5 C/W, the length of the heat sink must roughly double from 15 cm to 30 cm as shown in Figure 2.11. This adds additional cost to the system, and also creates significantly more drag through the stove which has been observed to have adverse effects on the combustion. For these reasons, the TEP1-0.8 module was selected for additional testing and development, along with the Mechatronics fan.

**Table 2.6: Module and heat sink comparison (fixed hot side temp 260 C)**

	Hot Sink Res. (C/W)	Module Res. (C/W)	Cold Sink Res. (C/W)	T hot mod (C)	T Cold Mod (C)	T amb (C)	Heat Flow (W)	Voc (V)	Module elec res. (C/W)	Power (W)	Fan Power (W)	Net Power (W)
HZ-9	0.86	0.922	0.17	260	65	20	212	6.4	1.15	8.8	0.6	8.2
HZ-9	0.83	0.922	0.14	260	59	20	218	6.5	1.15	9.3	1.0	8.3
HZ-9	0.82	0.922	0.13	260	57	20	220	6.6	1.15	9.4	2.4	7.0
HZ-14	0.55	0.53	0.17	260	88	20	324	3.0	0.21	10.8	0.6	10.2
HZ-14	0.52	0.53	0.14	260	81	20	338	3.1	0.21	11.7	1.0	10.7
HZ-14	0.51	0.53	0.13	260	78	20	343	3.2	0.21	12.0	2.4	9.6
TEP1-.6	0.53	0.51	0.17	260	90	20	333	7.9	1.2	13.1	0.6	12.5
"14 W"	0.51	0.51	0.14	260	83	20	348	8.3	1.2	14.2	1.0	13.2
	0.50	0.51	0.13	260	80	20	353	8.4	1.2	14.7	2.4	12.3
TEP1-.8	0.72	0.75	0.17	260	73	20	250	8.7	1.7	11.2	0.6	10.6
"10 W"	0.70	0.75	0.14	260	66	20	258	9.0	1.7	12.0	1.0	11.0
	0.69	0.75	0.13	260	64	20	261	9.1	1.7	12.2	2.4	9.8

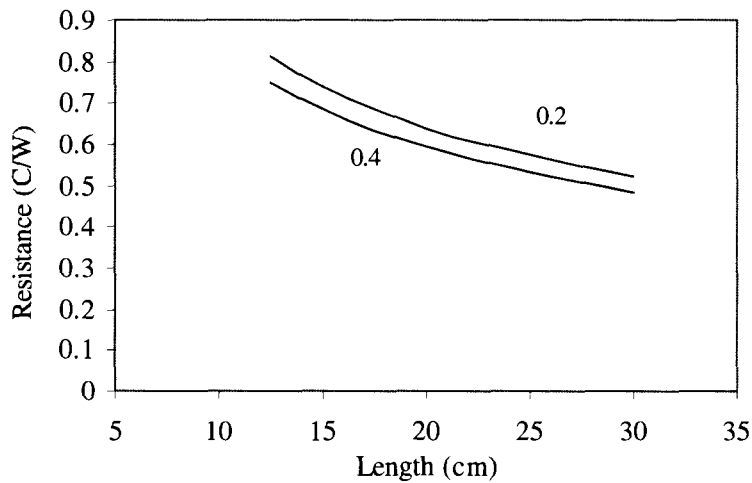


**Figure 2.11: Specifications for Aavid 61085 at 0.2 m/s and 0.4 m/s**

## 2.3 Stove Integration and Testing

The stove chosen to incorporate the generator into was the Ecoforno stove made by Ecofogao, Brazil. This particular stove has a somewhat long, narrow channel flowing underneath the griddle cooking surface ideal for placing the hot heat sinks into. The existing stove was modified to accept the TEG unit as shown in Figure 2.12 and Figure 2.13.

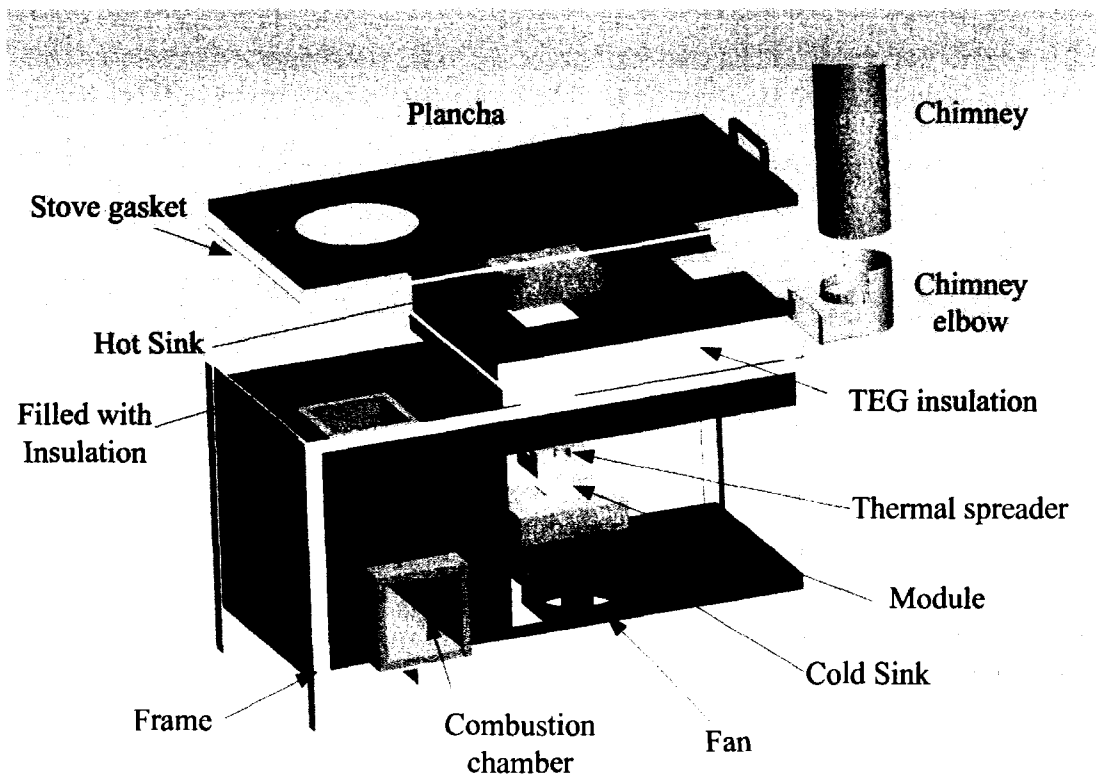
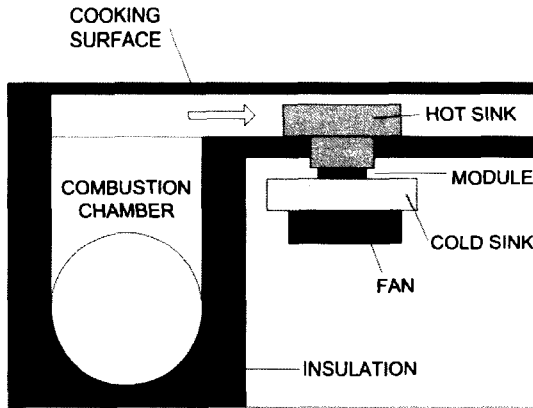
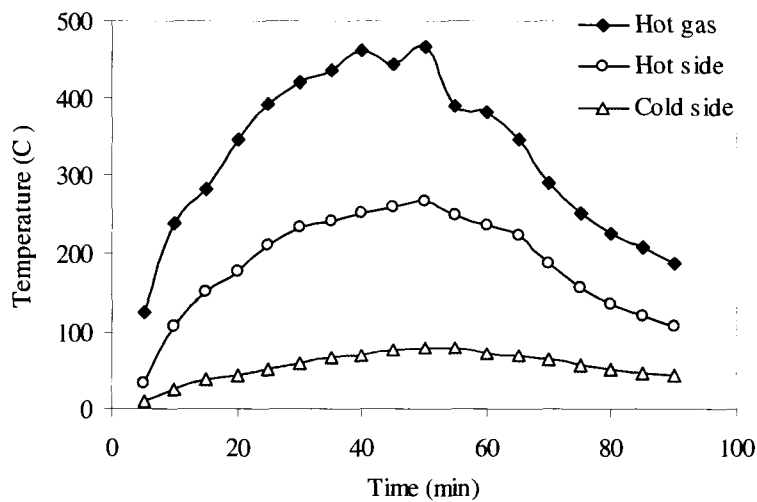


Figure 2.12: Exploded view of TEG stove (with one TEG unit)



**Figure 2.13: TEG placement within the stove**

The stove was run through a “typical” cooking cycle with the generator installed (see Figure 2.15 for comparison). The module was connected to a resistor equal to the internal resistance of the module to maintain peak power from the generator. Temperatures were taken for the hot gas stream, the hot side of the module and cold side of the module. These are shown in Figure 2.14. The corresponding power was measured from the module throughout the cycle as shown in Figure 2.16. Open circuit voltage was estimated from the module voltage under matched load.



**Figure 2.14: Temperatures within the system during a cooking cycle**

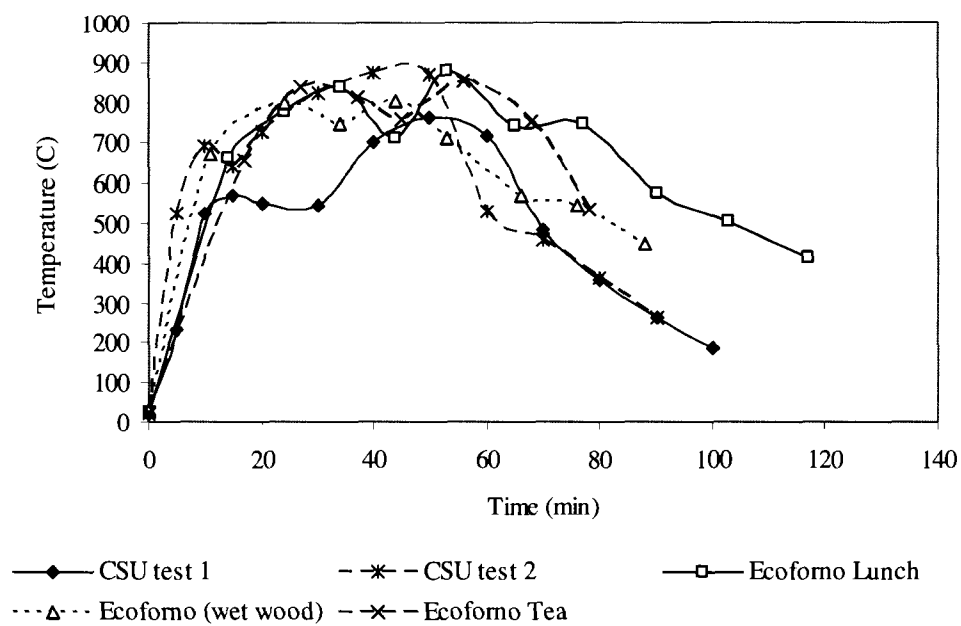


**Figure 2.15: Comparison of CSU tests to field temperature data**

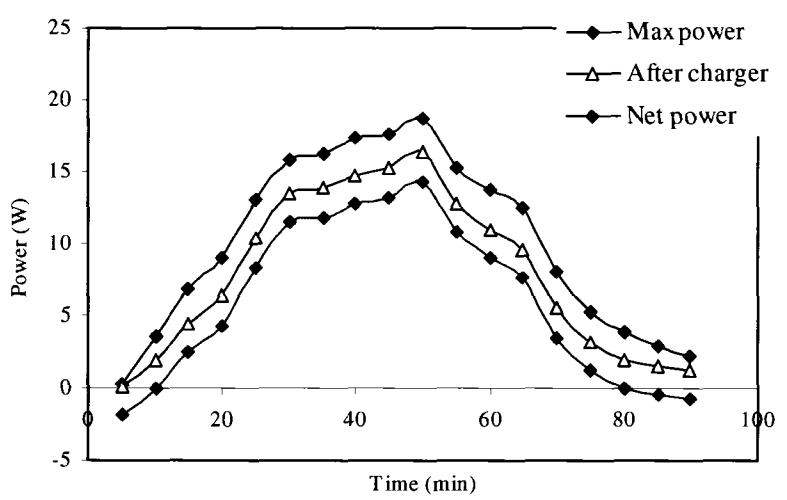


**Figure 2.16: Module power during a cooking cycle**

The stove behavior was very transient, taking approximately one half hour to fully heat up and cool down. This is seen in the temperature data and is more pronounced in the power data since power is a function of  $\Delta T^2$ . The system is well matched to the stove reaching a maximum hot side temperature of around 270 °C. This is the measured temperature but after passing through the thermal resistance the actual module temperature is closer to 260 °C. The power data shows a maximum gross power of about 19 W. This is lower than the prediction of about 21.8 W gross in section 2.2.3. This has been identified as the result of discrepancies between the module properties at elevated temperatures versus the properties specified at lower average module temperatures. Most important, are a smaller thermal resistance and a larger electrical resistance (see section 5.1.1). This results in a hotter cold side temperature and more electrical power dissipation within the module.

Another important consideration in integrating the TEG into the stove is the fraction of the stove thermal energy that is being consumed by the generator. This is important in understanding the effect of the TEG on cooking, as well as determining a maximum feasible power that could be generated from the stove. The average stove thermal output was calculated by measuring the mass flow rate of wood as it was fed into the stove. This was determined to be approximately 6 kW of thermal energy. With the two 10 W modules at 260 C, 600 W of thermal energy is drawn from the stove, or 10% of its thermal output.

## **2.4 Charging Circuit Design**

Many thermoelectric generator designs use battery storage. Unfortunately, little analysis has been reported on the charging process [13][19]. The design of a charging circuit for a thermoelectric generator presents several challenges. First, the charger must maintain the module current near the peak power operating point to utilize as much power from the module as possible. Second, it must manage the battery voltage to prevent overcharging and over discharging. Lastly, it must turn on the cooling fans when the generator is heating up and turn them off when it is cooling down.

### **2.4.1 DC-DC Converter**

For the generator used in this work, the matched load output voltage of the two modules in series is 8 V. In order to charge a 12 V battery, a DC-DC converter is used to boost the voltage to 13.8 V for float charging as described in section 1.5.2. This means the unit does not have to turn off once the battery reaches 13.8 V since no damage can be done to the battery at this voltage. In addition to boosting the voltage, the DC-DC converter also limits the current supplied by the module. Without a current limit, the current demanded can be very high, especially when the battery is discharged. This can reduce the module output voltage to a point where the DC-DC converter cannot operate. The operating characteristic of the two modules in series is shown in Figure 2.17. The internal resistance of the battery is only 0.2 Ohms, which would result in almost zero power if connected directly.

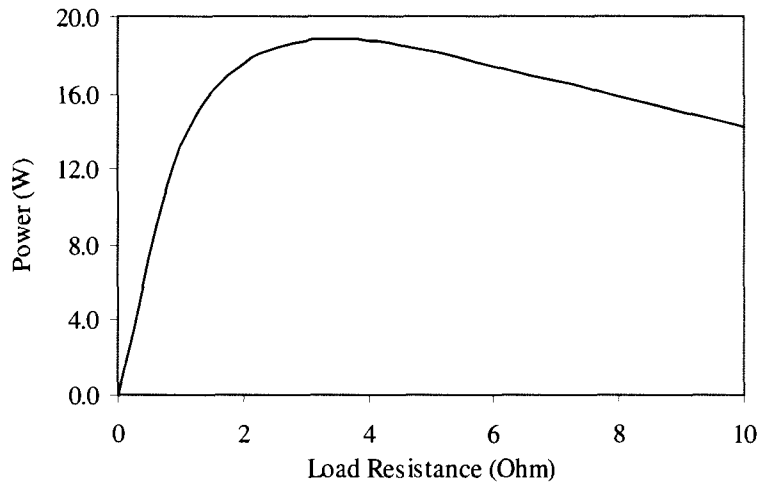


**Figure 2.17: Power vs. load resistance**

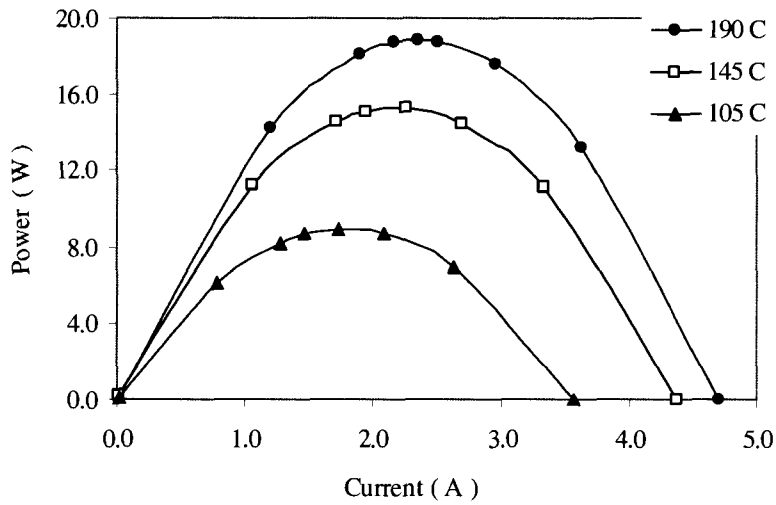


**Figure 2.18: Power curves at varying temperature differential**

For every operating temperature of the module there is a corresponding current that results in the peak power as shown in Figure 2.18. The goal of the charger design was to be operating near that point throughout the typical operating range. For the first design iteration, a DC-DC converter with a current limit was chosen

(MAX1771, Maxim Integrated Products Inc.). The current limit is set by a current sense resistor in the DC-DC converter circuit. Although this circuit does not perform peak power tracking, the current limit can be set to provide near peak power through a narrow operating range. The current limit was set to match the peak power current when the module was at the maximum continuous temperature. Figure 2.19 shows how the current limit changes as the supply voltage is varied.

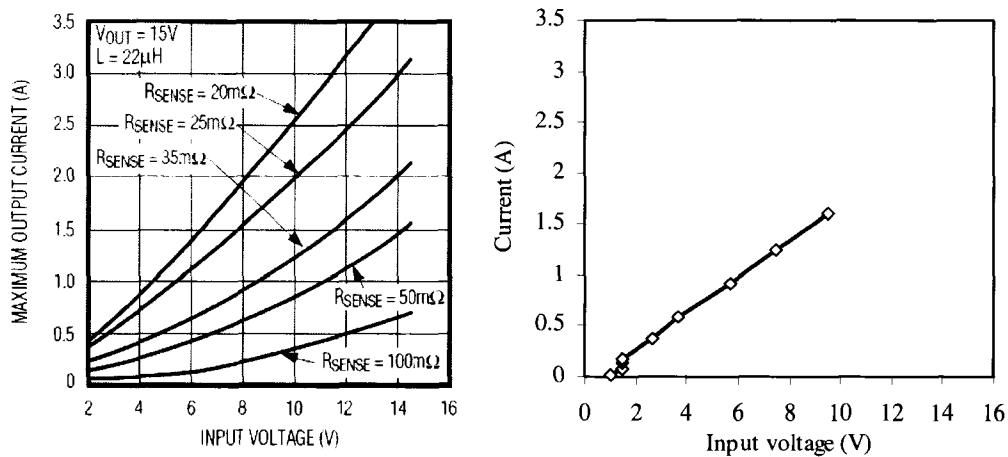


**Figure 2.19: DC-DC current limit. Specification (left), actual at 30 mΩ (right)**

This DC-DC converter was tested in a battery charging test with a simulated module as in Figure 1.32. The internal resistance was 3.4 Ohms as it would be with 2 TEPI-12656-0.8 modules in series (at peak temperature). At the peak continuous operating temperature, the two modules generated an open circuit voltage of around 17 V. At this point the peak power current is 2.5 A, therefore the DC-DC current limit was set as near as possible to 2.5 A at an input voltage of 8.5 V (matched load voltage).

In order to see how the module, DC-DC converter and battery system would function at various temperatures, the open circuit voltage was varied and efficiencies were calculated. Figure 2.20 shows the theoretical peak power current, along with the actual current from the module while charging the battery. It can be seen that from 8-12 volts open circuit, the actual current is significantly higher than the peak power current. This causes the modules voltage delivered to decrease and the power is reduced. Figure 2.21 shows how the modules efficiency is affected by non-optimal operation. Also shown in Figure 2.21 is the efficiency of the DC-DC converter, and the whole system. It should be noted that module conversion efficiency is the ratio of power actually generated by the module to the maximum possible. It is not the thermal efficiency.

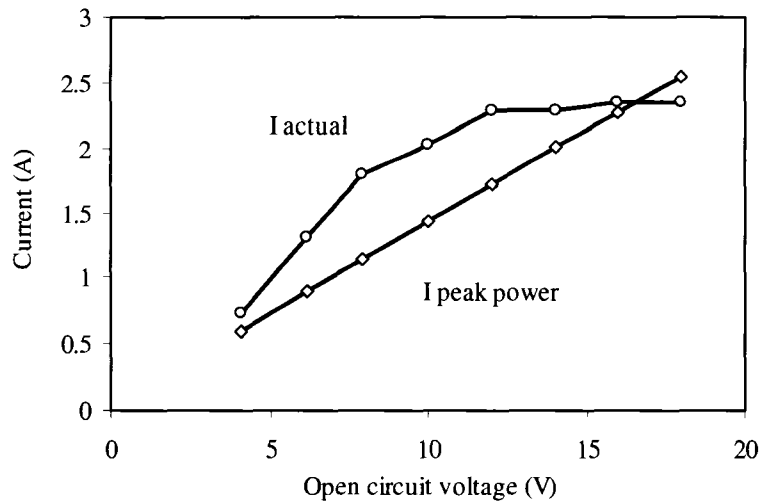


**Figure 2.20: Actual current vs. peak power current**

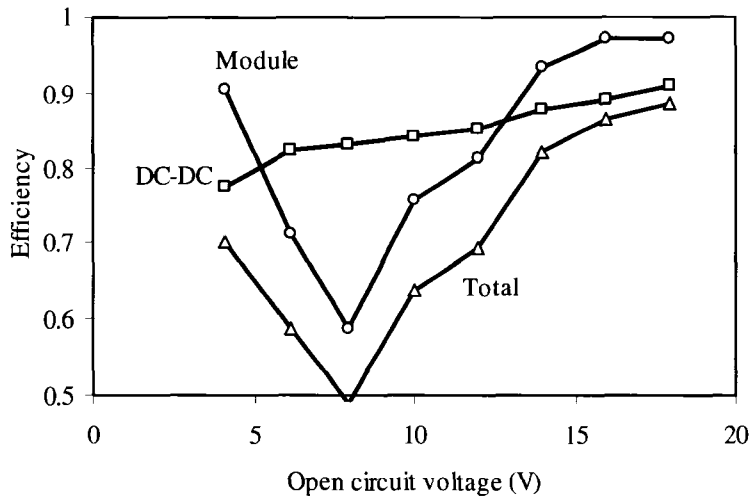


**Figure 2.21: Component and system efficiency**

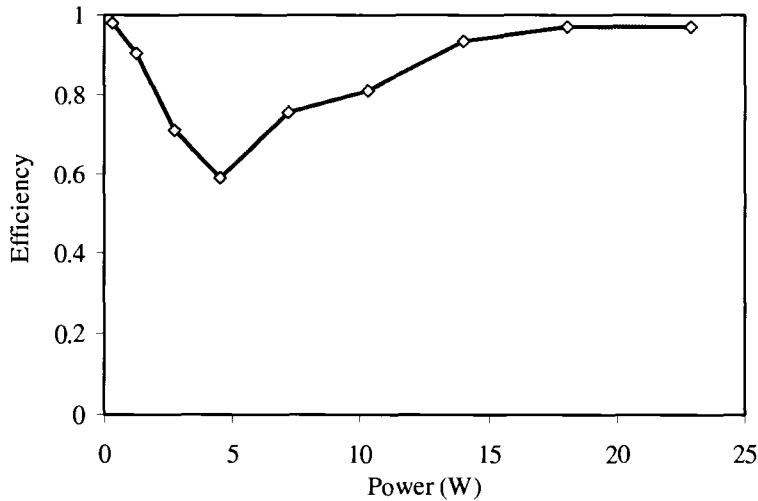


**Figure 2.22: Module conversion efficiency vs. power (constant internal resistance 3.4 Ohm)**

From Figure 2.22 it can be seen that the current limit on the DC-DC converter keeps the module operating at over 70% of its peak power through a wide operating range (7-22 W), with very good performance near max power.

From these tests, it was possible to predict the average efficiency of the system over a typical burn cycle, given the open circuit voltage measured during testing.

Figure 2.23 shows the maximum power compared to the actual power delivered to the battery during a cooking cycle. It was found that the total energy through the charger was 24 W-hr out of 30.4 W-hr possible. This results in a 78% total efficiency of the charging system.

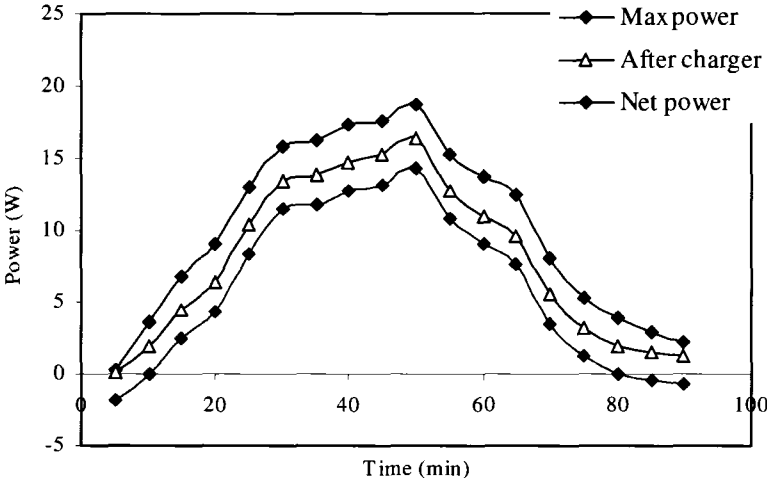


Figure 2.23: Comparing max power to actual power

### 2.4.2 Fan Control

Since the fans consume power from the battery, it is important to turn them on only when the generator is being used. It is also preferred that the fans only run when the generator is making enough power to run them to prevent negative net power. In the first prototype design, the fans are controlled by a comparator that compares the module voltage to a specified reference. When the module voltage exceeds the reference voltage, a digital signal is sent to bias a MOSFET which in turn sends power to the fans. Selecting the appropriate reference voltage is important to maximize the power generated by the module throughout the cycle. Turning the fans

on too early and off too late will result in large durations with negative net power. On the other hand, if the set point is too high the fans may never come on. When the fans are not running the cold sink is very ineffective, therefore there is a limit to how much voltage the module can make without the fans running. This is significantly smaller than the maximum operating voltage. For the current system, a very safe voltage set point was chosen of 1.25 V. With this setting there is a period of negative net power, but it is very short (< 5 min) on startup. However, it can be longer on shutdown, or during low temperature operation. The fan control portion of the circuit is shown in Figure 2.24.

### **2.4.3 Battery Management**

To protect the battery and ensure a long lifetime, several precautions were included into the charging circuit. The output of the DC-DC circuit was set to 13.8 V so it could not damage the battery from overcharging. The battery was also protected from undercharging by a buzzer and cutoff circuit. The buzzer was designed to come on at 10.7 V, just before power is cut. This is accomplished by a comparator which compares the battery voltage to a reference. If the voltage drops below the reference the buzzer comes on. The buzzer was also configured so that it would shut off if the user turned the light off. This was accomplished by incorporating a current sense resistor in the comparator circuit. If the circuit detected no current was flowing the buzzer was disabled. Lastly, the battery would be cut off from the load if the voltage reached 10.5 V, taken to be the safe discharge limit as discussed in section 1.5. The battery protection portion of the circuit is shown in Figure 2.24.

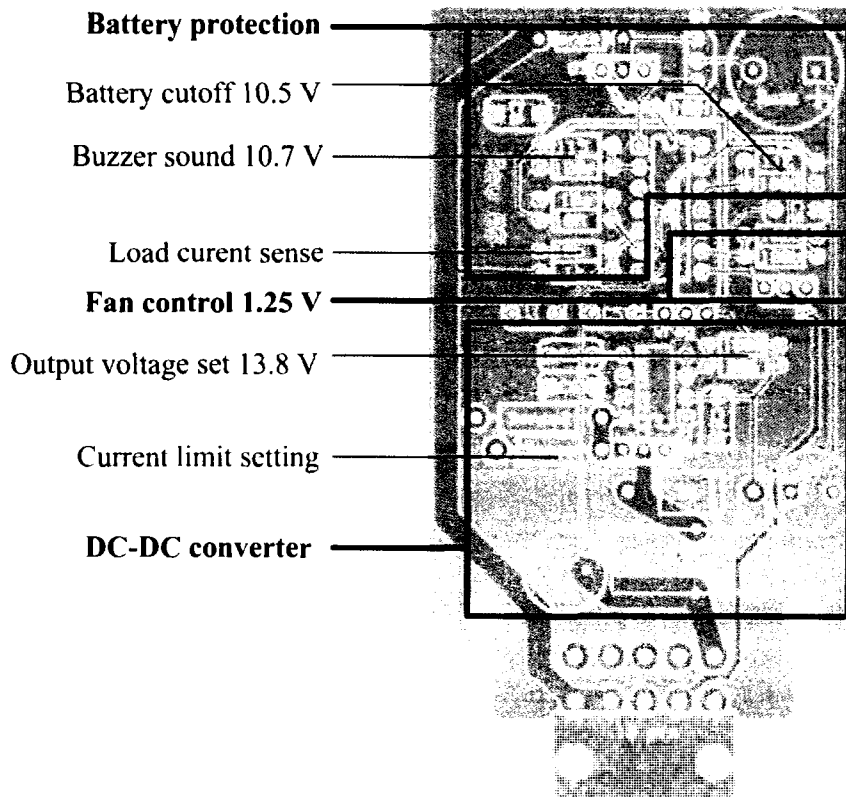


**Figure 2.24: Labeled charging circuit**

## ***2.5 Complete System Analysis***

With all the components of the system in place, a final analysis of the losses contributed from each component was performed. The results are shown in Figure 2.25. From the fixed property system model, the predicted W-hr per day from the module is 58 W-hr. This is reduced to 45 W-hr with the real module properties. There is also a significant loss of energy since the module is not operating at peak power. This reduces the energy to 39 W-hr. The next loss is through the DC-DC converter, which is about 90% efficient, reducing the energy to 37 W-hr. The fans

also draw a significant amount of power (about 15% at max power). This reduces the energy to 27 W-hr. The next subtractions are for the energy consumed by the charger and power meter circuits. Finally, the efficiency into and out of the battery is approximately 95% using good battery charging practices. The final result of this analysis is that the actual energy delivered to the user is about one third of the potential energy generated from the module using ideal properties. The second generation design addresses each one of these system losses.

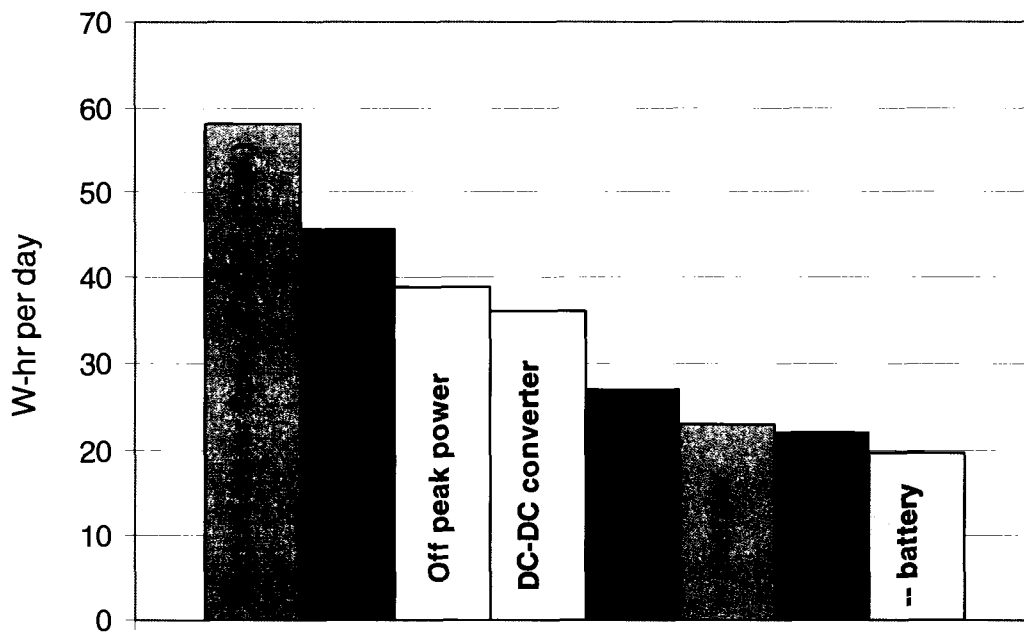


Figure 2.25: Energy losses through each system component (total energy for 3 cycles per day)

## 2.6 Battery Selection

In selecting the proper battery, both capacity and maximum charge current were considered. The battery selected for this application was a 7 A-hr sealed lead acid

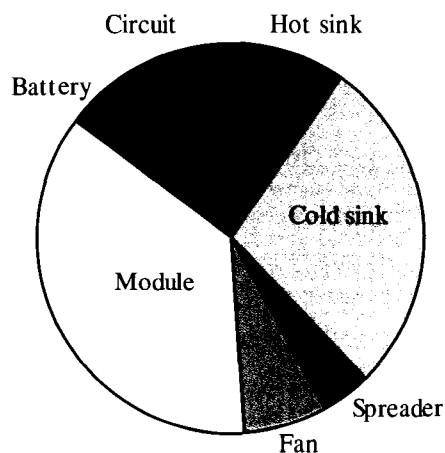
battery. The 7 A-hr battery is the most common used in this size range, and is therefore cheaper than many smaller batteries in a similar range. At a discharge current of 1.2 A the capacity is reduced to 6 A-hr, corresponding to roughly 72 W-hr. This is larger than the 45 W-hr goal; however, it is also possible that the users would run the stove for more than the projected 4.5 hr/day, making use of the extra battery capacity. The safe charging current for the battery was specified as .2C, or 1.4 A. Although the current from the module could be as high as 2.5 A, after the DC-DC converter it would be reduced to 1.66 A, just higher than the recommended charge current. This would only occur for short periods of time, so it should not damage the battery.

## ***2.7 Prototype Kit Cost Breakdown***

A summary of the component costs for the entire system are presented in Table 2.7. The costs are based on quotes from the current component manufacturers for quantities of 1000-10,000 units. The final system cost is \$143, which results in a per watt cost of \$9.53/W. This makes the thermoelectric generator slightly higher than complete solar systems (\$5-\$8/W).

**Table 2.7: Cost breakdown for prototype system @ 10,000 units**

Item	#	Cost @ 10,000 units	Cost total
Hot heat sink	2	\$7.00	\$14.00
Cold heat sink	2	\$20.00	\$40.00
Thermal spreader	2	\$3.00	\$6.00
Fan	2	\$5.00	\$10.00
Module	2	\$26.00	\$52.00
Battery	1	\$6.00	\$6.00
Power Circuit	1	\$15.00	\$15.00
TEG System Cost			\$143.00
Cost / Watt @ 15 W			\$9.53



Although this cost analysis was based on manufacturer quotes, it is believed that the unit could be produced for much less. A further cost analysis has been prepared based on the following assumptions.

It is assumed that at 10,000 units or more, the cost of manufacturing the heat sinks could be reduced to near commodity prices. The cost of the heat sinks was estimated at 200% of the raw material cost of \$2.50/kg.

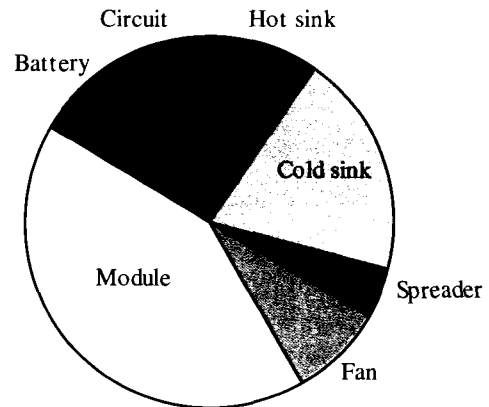
For the module, it is believed that the cost of high temperature modules will continue to fall as production volume increases. Low temperature modules using the same amount of raw materials are less than half of the cost. The primary difference is in the soldering techniques used to join the elements. As this process is evolved and production increases, it is expected that the high temperature module will come much closer to the low temperature module cost.

Reduction in the electronics cost could be accomplished by integrating the DC-DC controller with comparator circuit. Also, a more thorough component cost/efficiency analysis could be conducted.

The resulting cost prediction from this analysis is a system cost of \$72, which comes to \$4.80/Watt. Here the TEG unit looks competitive with a solar PV system, however, this does not include the cost of the stove. Ultimately, the advantage of a TEG system versus a PV system will depend on the stove usage and geographic location of the user since both systems will not generate peak power all day long.

**Table 2.8: Cost breakdown for system @ 10,000 + units**

Item	#	Cost @ 10,000 + units	Cost total
Hot heat sink	2	\$3.50	\$7.00
Cold heat sink	2	\$7.00	\$14.00
Thermal spreader	2	\$1.50	\$3.00
Fan	2	\$3.00	\$6.00
Module	2	\$15.00	\$30.00
Battery	1	\$6.00	\$6.00
Power Circuit	1	\$6.00	\$6.00
TEG System Cost			\$72
Cost / Watt @ 15 W			\$4.80



## **3 FIELD TESTING GENERATION 1 PROTOTYPE**

### ***3.1 Objectives***

There were several primary objectives in the field testing of the generation one prototype. These were as follows:

- To identify and understand any failure mechanisms of the generator system, maintenance issues, and shortcomings.
- To compare predicted W-hr, and peak power values from lab testing to those realized in the field.
- To gather data on user habits such as hours of stove use and peak stove temperatures to be used in subsequent system modeling.
- To get user feedback on the stove performance, what they liked and disliked, and how it could be improved. This applies to the stove itself as well as the generator.
- To establish partnerships with local stove manufacturers that could be involved in future scale up.

### ***3.2 Data Acquisition***

There were several methods used to gather data from the prototype units in the field. The first was a power meter that logged and displayed instantaneous power, energy accumulated and time since last reset. This device was designed to be read out by a field technician on a weekly or bi-weekly basis. It was also intended that the

field technicians could use this device to diagnose problems with the system. The power meter circuit is shown in Figure 3.1.

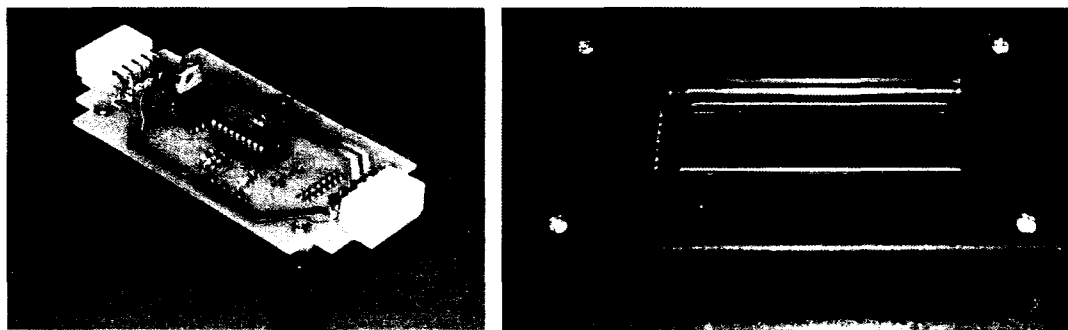


**Figure 3.1: In-Line Power Meter**

The second method for data logging used a number of HOBO brand data loggers. The first data logger used was a 4-channel voltage logger. A signal conditioner circuit was also built to output the module voltage, battery voltage, module current, and current from the battery in 0-2.5 V signals. Current sense amplifiers and RC filters were required for signal conditioning of the current measurements. In some cases thermocouple loggers were also used. The signal conditioner circuit and the data loggers are shown in Figure 3.2

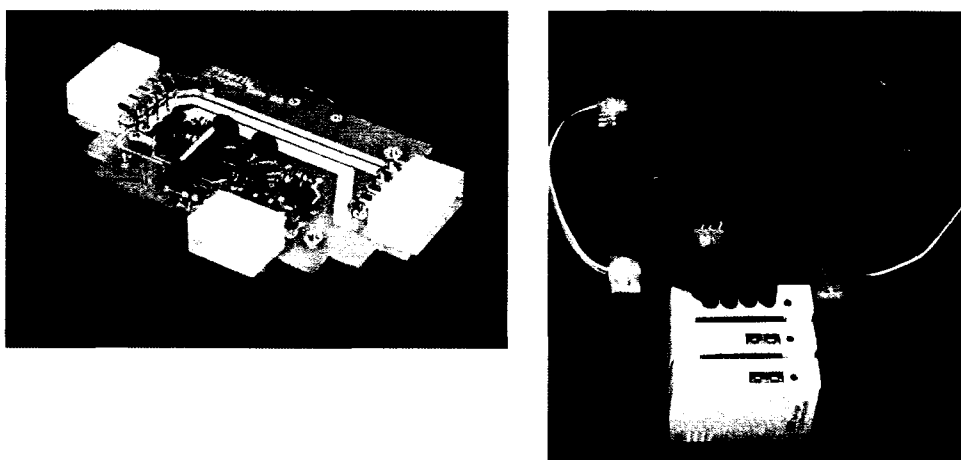


**Figure 3.2: Signal conditioner (left), charger, battery, signal conditioner, loggers (right)**

The last method for gathering data was based on user feedback recorded by the field technicians. The users would be asked to approximate their hours of stove usage and hours of light/TV usage. This was done on a bi-weekly basis so it would be fresh in their memory.

**Table 3.1: Sample of weekly monitoring report**

Date	19-Dec-06			
	HOUSES			
	1	2	3	4
NAME	Nicasio Barrios	Jose Emiliano Barrios	Freddy Perez	Jose A. Aleman
Is the light working	yes	yes		yes
Is the T.V working	yes	yes		yes
How long have you been running the light	2 h	2 h		3,5 h
How long have you been running the t.v	3 h	doesn't have		2,5 h
Has the Buzzer gone of	yes	yes		yes
How many hour a day, do you use the stove	6 h	5 h		6 h
How often have you cleaning the heat sink	every day	every day		every day
Do you have any other comments / problems about the stove or generator	all is ok.	all is ok.	the stove is in proleña	all is ok

**SYSTEM CHECK**

Are the fans running when the stove is hot	yes	yes	yes	yes
Battery	12324	n/a	n/a	12188
Energy (w-m)	6780	n/a	n/a	23117
Time	95, 31, 38	n/a	n/a	159, 42 , 52
V	3564	n/a	n/a	3272
I	2198	n/a	n/a	2000
P	7140	n/a	n/a	6400
reset	no			yes
observation		n/a = doesn't apply	n/a = doesn't apply	

### ***3.3 Nicaragua Field Testing***

The first field test site was in a village called Tempisque in Nicaragua. This test was initiated by Rogerio Miranda and funded by Winrock International. Testing began in November of 2006, and concluded in October 2007.

#### **3.3.1 Test Plan**

The test plan was to install four stoves in rural homes in the village of Tempisque, and one unit at Prolena for testing and demonstration. An additional two units were installed after the first round of testing incorporating minor changes, but with increased data logging functions. The generators were prepared by CSU, and the stoves were produced by a local stove manufacturer called Prolena. Prolena was also responsible for bi-weekly monitoring of the stoves and data collection. The stoves were to be monitored for 3-6 months, or until a failure occurred that could not be repaired.

#### **3.3.2 Installation**

The generator components were sent ahead of time and installed in the stoves by the CSU team when they arrived in Nicaragua. Workers at Prolena were instructed in how to assemble and install the generators, as well as how to monitor and diagnose the generators.

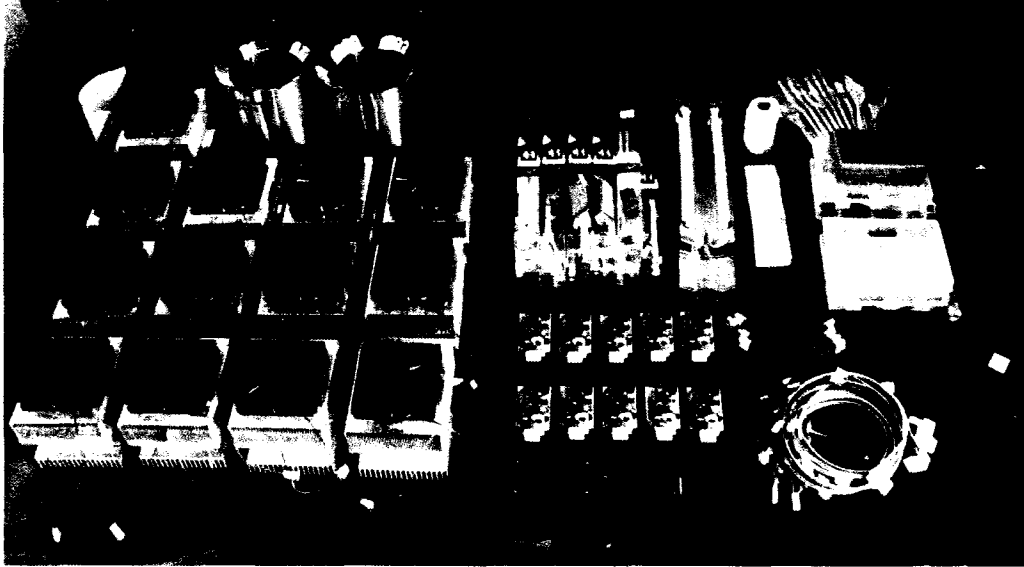


**Figure 3.3: Generator kits ready to be shipped**

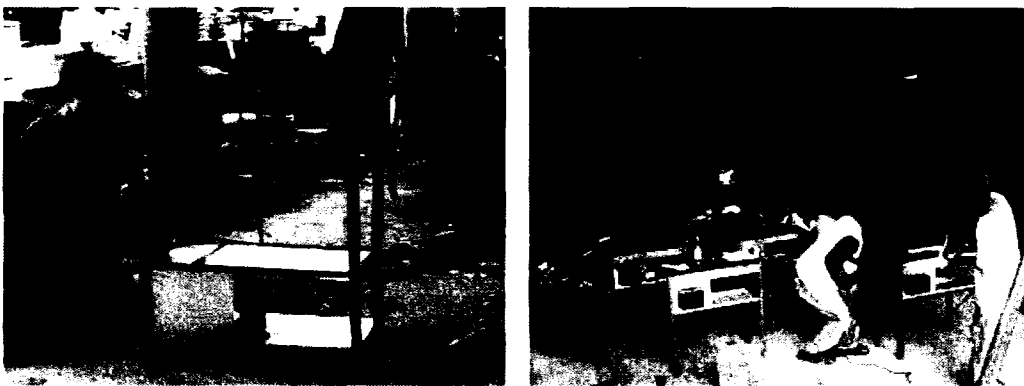


**Figure 3.4: Fabrication of stoves at Prolena**



**Figure 3.5: Instructing Prolena in assembling and diagnosing the generators**

### 3.3.3 Results from Round 1

The results from the field test in Nicaragua are presented below on a house by house basis. The type of data, and conclusions made from each house vary depending on the type of data gathering used as well as the individual users habits. In addition, a general post test component analysis is presented.

**Table 3.2: House #1 results**

House #	1	
Method of data logging	Power meter Bi-weekly report	
Generator life	Still working (7+ months)	
Known failures	Battery failure (not holding charge) Loose screws between hot sink and hot block (tightened regularly) Increased thermal resistance at module interfaces	
Average stove use (according to user)	4.8 hrs/day	
Average W-hr consumed (according to user)	42 W-hr/day	8.8 W-hr/hr use
Average W-hr generated (power meter)	53 W-hr/day	11 W-hr/hr use

Overall the generator performed very well at house #1. The performance was very consistent for the first six weeks, then significant reductions in output were observed. The reductions in energy available were a result of reduced battery capacity, as well as increased thermal resistance at the module surfaces. Due to the

design of the generator, the cold-sink screws could not be regularly tightened as the screws on the hot sink could. The hot sink screws regularly became loose due to the expansion of the hot heat sink and stretching of the screws. The screws on the hot-sink only had one very small Bellville washer that did not provide sufficient travel for the expansion of the heat sink.

After seven months, a return visit was made to House #1 to observe the generator and get feedback from the user. The generator appeared to be in good condition, except the battery was completely dead. When replaced with a new battery the stove began generating power again, only at a lower value than initially. The peak hot side and cold side temperatures were measured as 309 °C and 62 °C. At this temperature difference the open circuit voltage was measured as 15.27 V, and the power was only 10.9 W. At this temperature differential the open circuit voltage should be closer to 17.2 V. Therefore, it is evident that the actual temperature difference seen by the module is lower as a result of poor thermal contact.

The users said that they did not use the stove every day, which could have contributed to the damaged battery. The draw from the charging circuit can drain the battery to unsafe levels after a few days of inactivity (see results for house #3 Nicaragua and India results). They also noted that the light/TV would only work when the stove was running (another effect of the dead battery). They did not use the stove every day because it was slower in cooking their food. This was due to the fact that the pot was not in direct contact with the stove.

In House #2, the generator performance was very poor. After two weeks the light was no longer working. It was believed that this was due to the fact that the stove was being used less than two hours a day. Therefore, the stove and generator were switched to a new house. From an analysis of the data from the loggers, it has been determined that the charging circuit was damaged during installation, and the DC-DC converter was not functioning. It is possible to damage the charging circuit if the signal conditioner is connected backward, even momentarily (this was discovered during the India testing). Analysis of the data supports this conclusion as shown below. The only time the module generates power is when the module voltage exceeds the battery voltage, since the DC-DC converter is not boosting the voltage. Therefore, very little power is generated until the battery voltage drops below about 8V. At peak operating temperature it should be possible for the modules to generate an open circuit voltage of new 17 V, so it should be possible to charge the battery even when it is at 12 V. However, at this high voltage the current is low, leading to little power. This is seen just after the switch to the new user who ran the stove hotter and more often. This second user was able to generate more consistent power; however it was very low averaging about 3 W.

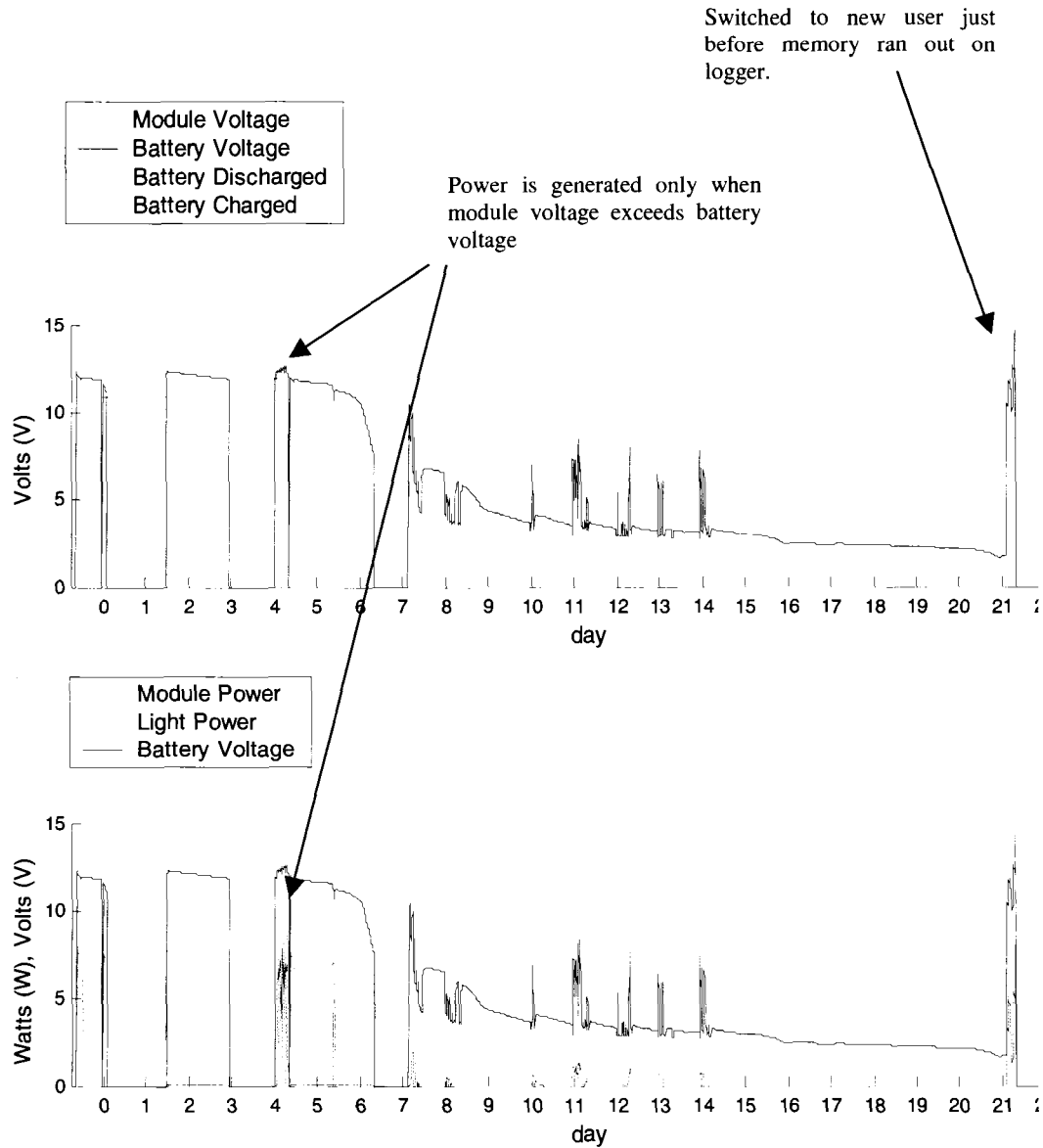


**Figure 3.6: Field data showing damaged charging circuit**

**Table 3.3: House #2 results**

House #	2a	
Method of data logging	Data logger Bi-weekly report	
Generator life	Two weeks, then transferred users at 1 month	
Known failures	Damaged charging circuit during installation, DC-DC converter not working lead to very low power  Stove used very little and at low temperatures	
Average stove use (according to user)	1.7 hrs/day	
Average W-hr consumed (according to user)	15.8 W-hr/day (All from initial battery charge. Only lasted a couple weeks)	9.3 W-hr/hr
Average W-hr generated (logger)	Net 0, all light from initial battery charge	

**Table 3.4: House #2b results**

House #	2b	
Method of data logging	Data logger Bi-weekly report	
Generator life	1 month	
Known failures	Damaged charging circuit during installation, DC-DC converter not working lead to very low power	
Average stove use (according to user)	5.6 hrs/day	
Average W-hr consumed (according to user)	17.3 W-hr/day	3.1 W-hr/hr use
Average W-hr generated (logger)	Data logger ran out of capacity before switch	

House #3 was also equipped with a voltage data logger. This house used the stove much more, resulting in several hours of light and TV each day. The results from House #3 are shown in Table 3.5. The data from the data loggers is presented by month in Figure 3.8 and by day in Figure 3.9. The values next to the daily figures are defined as:

$E_g$  is the gross energy generated (W-hr)

$E_c$  is the energy after passing through the charger (Avg. 85% efficient) (W-hr)

$E_n$  is the net energy after subtracting the fan power (W-hr)

$E_u$  is the energy utilized by the user (W-hr)

There are a number of important observations that can be made from the data presented. The first observation is the large voltage drop from day to day after the voltage has dropped below the battery cutoff (purple line). This drain is due mostly to the draw of the charging circuit and signal conditioner. This amounts to about 4

W-hrs per day. This can also be seen in the fact that the energy utilized is typically 5-10 W-hr less than the net energy.

Also important to note are the occasions where the battery charge exceeded 13.8 V (green line) as on day 9 and day 16. Both of these effects, undercharge and overcharge, contributed to the failure of the battery. Evidence of a bad battery can be seen after day 10 in the daily plots. From this point on, the battery goes from fully discharged to fully charged in less than an hour, which would not be possible at the power level of the generator. This means the battery capacity has been significantly reduced. Likewise, after the stove cools down the battery quickly goes from a fully charged voltage to a fully discharged voltage with no external power draw (except the fans and charger).

Another important observation is the amount of time the generator spends at a negative net power (see day 8). This occurs when the power required for the fans is more than the generator is producing. This happens mainly on cool down which can take over one hour. This is due to the fact that the fans are on/off only, and cannot be regulated with the current circuit. If the fans are turned off sooner, there is a risk of overheating the module. This problem was addressed in the second generation circuit. The effect of the fan power draw is also illustrated in the daily total energy values beside each figure.

In most cases, the net energy is only half of the energy delivered through the charger. This was a much larger effect than expected, since at full power the fans consume only 15% of the module power. However, long periods of time spent at low power contribute to this dramatically reduced energy value.

**Table 3.5: House #3 results**

House #	3	
Method of data logging	Data logger Bi-weekly report	
Generator life	1 month	
Known failures	Battery damaged and lost capacity. Loose hot heat sink screws	
Average stove use (according to user)	4 hrs/day	
Average W-hr consumed (according to user)	45 W-hr/day	11 W-hr/hr use
Average W-hr generated (logger)	30 W-hr/day	7.5 W-hr/hr use
Average W-hr consumed (logger)	18 W-hr/day	4.5 W-hr/hr use

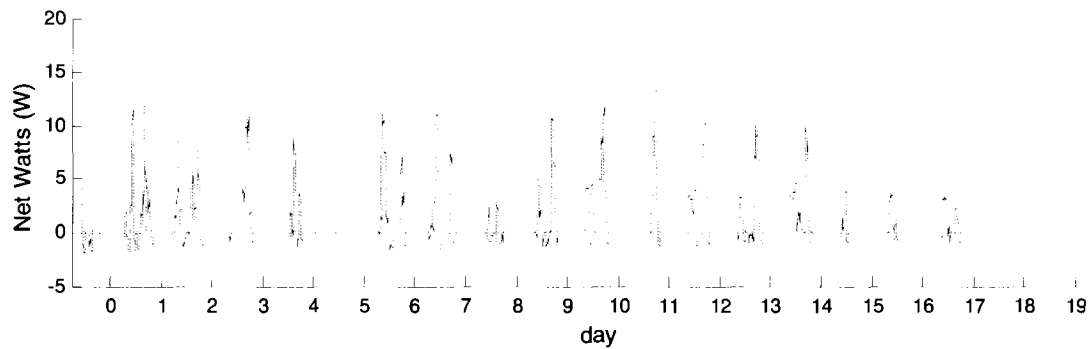


**Figure 3.7: Module power from house #3 for three weeks**

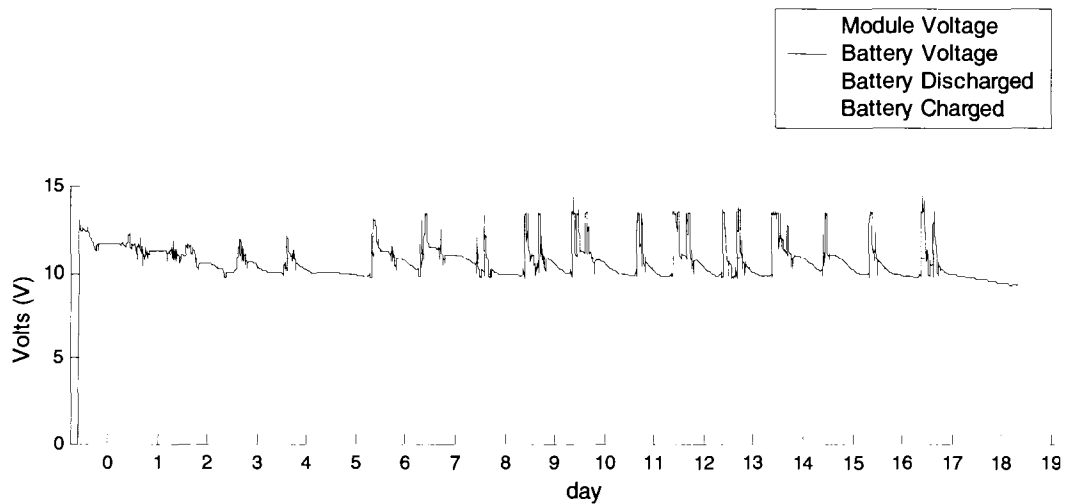


**Figure 3.8: Module and battery voltage from house #3 for three weeks**

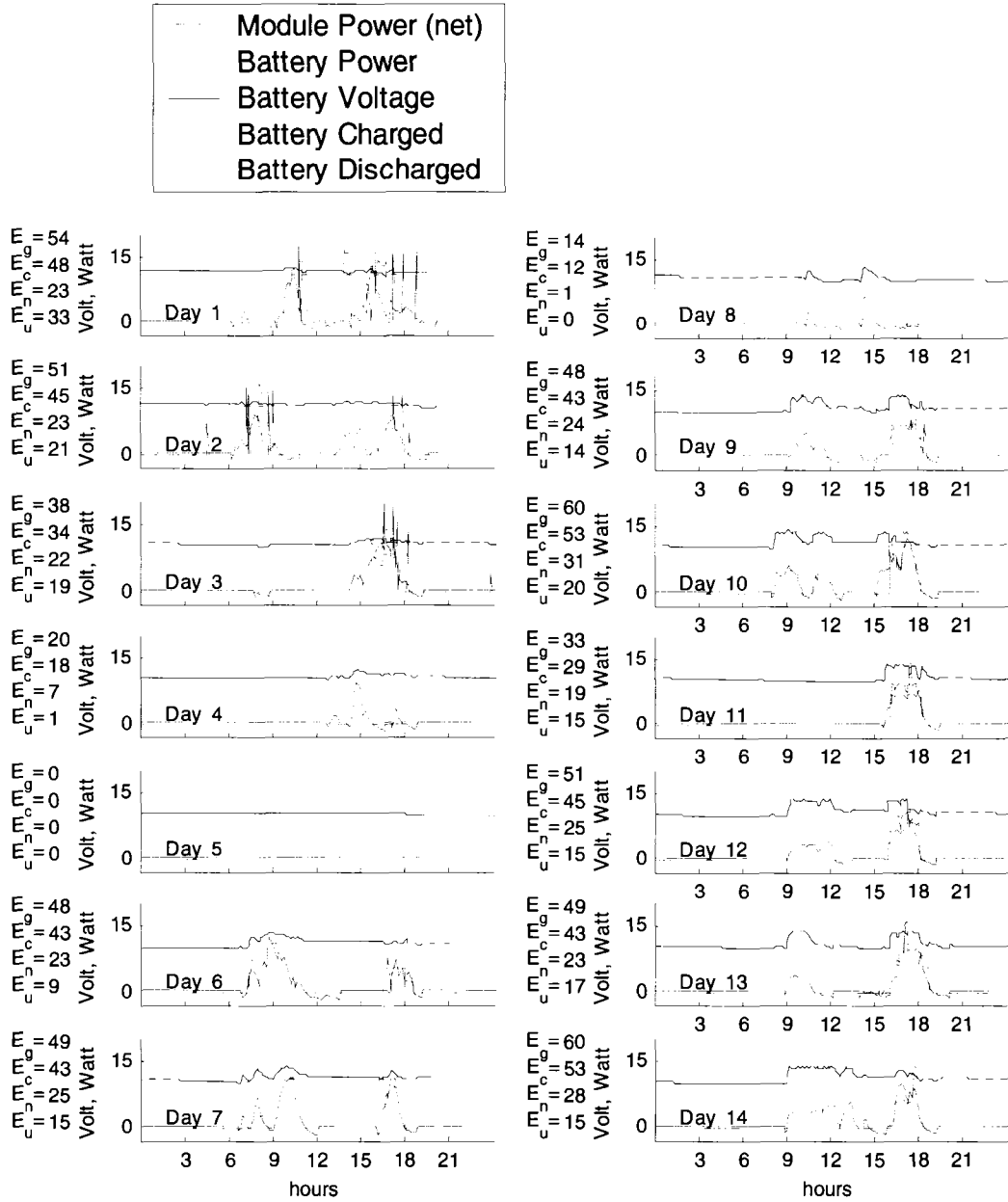


**Figure 3.9: Data from house #3 by day**

House #4 had the most hours per day on the stove, and ultimately the most energy delivered to the user. House #4 consisted of a family with several kids. The mother would be in the kitchen for the majority of the day cooking for the family. This family also had an abundance of firewood that they would sell to the local market, so keeping the stove running was not a problem. This house was also the most sealed up of all the homes, leading to a very smoky environment when the traditional stove was used. For this reason, this family was the most appreciative of the new clean stove, even without its electricity generating capabilities.

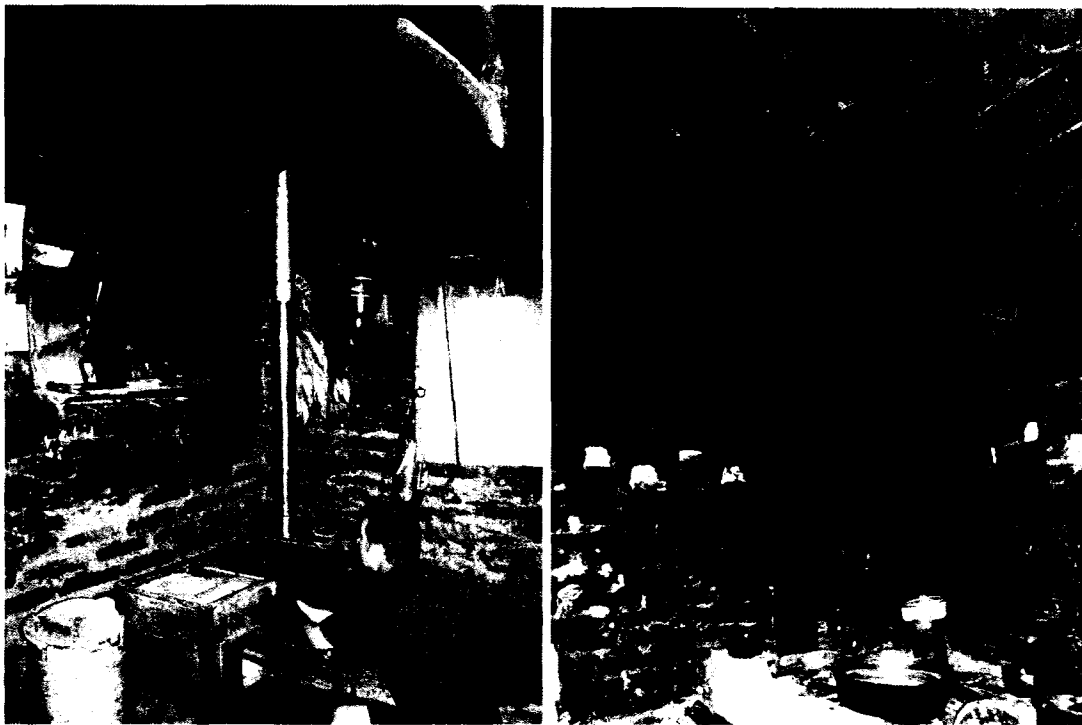


**Figure 3.10: New stove (left) and old stove (right)**

**Table 3.6: House #4 results**

House #	4	
Method of data logging	Power Meter Bi-weekly report	
Generator life	2 month	
Known failures	Loose hot heat sink screws Solder on module wires melted Module pellets loose from melted solder or fatigue	
Average stove use (according to user)	5.8 hrs/day	
Average W-hr consumed (according to user)	58 W-hr/day	10 W-hr/hr use
Average W-hr generated (meter)	75 W-hr/day	13 W-hr/hr use

The major failure of this generator was the melting of the solder on the module wires, most likely from overheating of the hot side of the module. It was also noticed that several of the module pellets were loose. This may have happened before or after the melting of the wires, since once the wires melted the fans would no longer get the signal to turn on. However, it was interesting that the pellets were loose on the cold side, with no apparent melting of the solder. This could possibly be a fatigue failure, but there is not enough information to confirm this.

### 3.3.4 Results from Round 2

In July of 2007, a second round of testing was performed to obtain better data of temperature distribution within the system, and the corresponding module power. Thermocouples were installed in the hot gas stream, in the module hot side, and in the module cold side. These temperatures helped in understanding and tracking the

degradation of the thermal interfaces. The hot and cold side temperature data were also used to determine if the module was overheating on either the hot or cold side of the module. This data was also required to validate the system level model.

For this test, several small modifications were made to the original generator to minimize the loosening of the components as seen in previous testing. It was believed that this would not only maintain the power as high as possible, but also reduce the chance of overheating since the module would always have good contact to the cold heat sink. The screws clamping the module were inverted so the screw head and Bellville washers would be on the cold-side heat sink, rather than on the hot block. It was noticed that with the Bellville washers on the hot side of the module as they previously were, that they would loose their temper and soften. Another advantage to moving the screw heads to the cold side is that they can be accessed to tighten without removing the hot heat sink. On the hot-side heat sink, larger screws and five large Bellville washers were used to prevent loosening over time. These modifications proved to be effective through the duration of the 10 weeks that data was recorded. Ultimately, the only way to prevent separation of the hot sink and hot block will be to die cast them as a single piece.

The first house tested in the second round was designated as House #7. Energy data for the first five weeks of testing is shown in Table 3.7. The temperature data from the first 10 weeks of testing is shown in Figure 3.11. Voltage and power data was only acquired for the first five weeks due to a logger malfunction, and is shown in Figure 3.12 and Figure 3.13. Daily data for the first week is shown in Figure 3.14. The full data set is shown in the appendix.

In House #7 the stove was used on a fairly regular basis, but the temperatures achieved within the stove were typically not high enough to reach maximum system power. In fact, the stove spent so much time operating at lower temperatures that during some days the net module power would total to zero. Again, this pointed to the need to better control the fan voltage to eliminate net negative power at low temperatures, and maximize power at these conditions. Days 4 and 7 are good examples of this condition. Over the entire five week period, the energy delivered to the user was only about one fifth of the gross energy generated by the module. At these lower operating temperatures with less daily usage, the parasitic losses (fan and charger) make a much larger relative reduction in energy than anticipated.

**Table 3.7: House #7 average daily energy data (includes 1-2 days/week of no use)**

House 7 week 1-5			
Energy gross	Energy through DC-DC converter	Energy net	Energy used
26.6	23.44	10.52	6.6

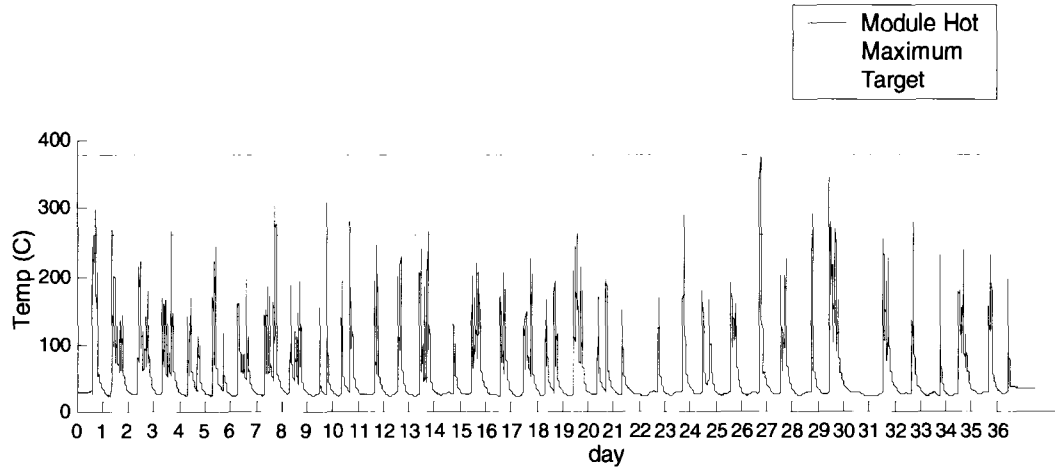


**Figure 3.11: Hot side temperature data from House #7 for 5 weeks**

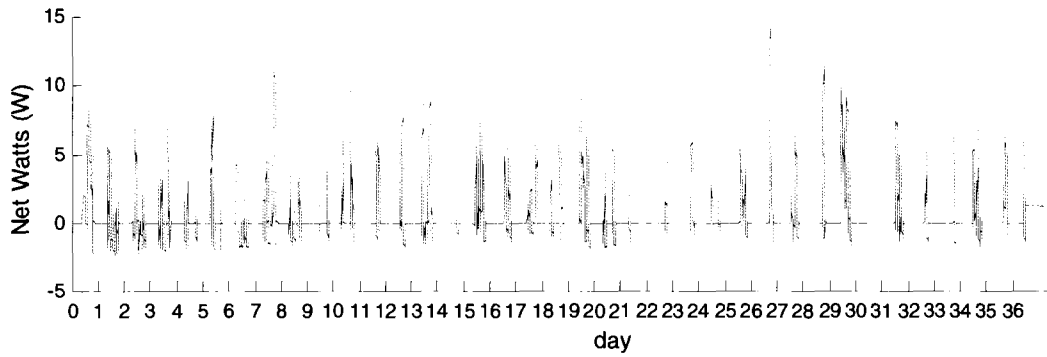


**Figure 3.12: Module power data from House #7 for 5 weeks**

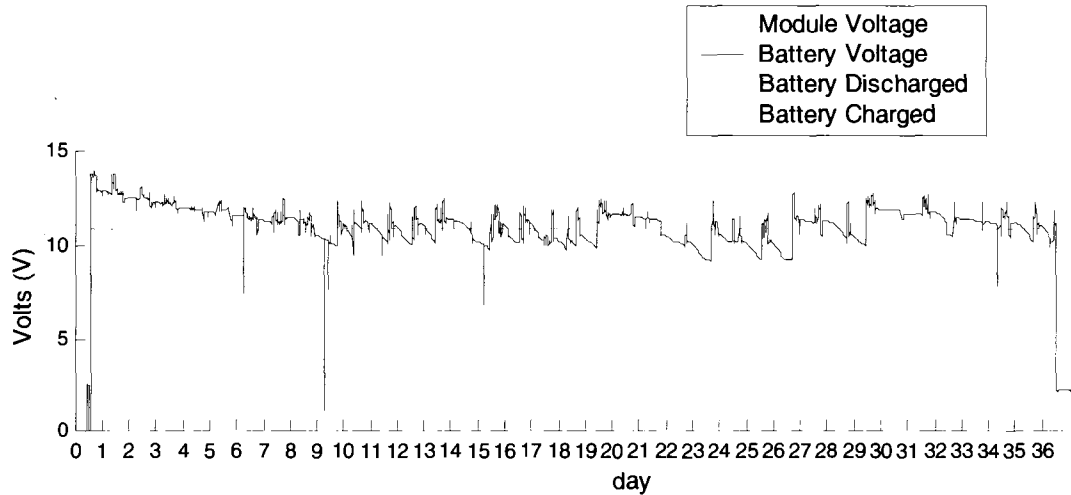


**Figure 3.13: Module and battery voltage data from House #7 for 5 weeks**

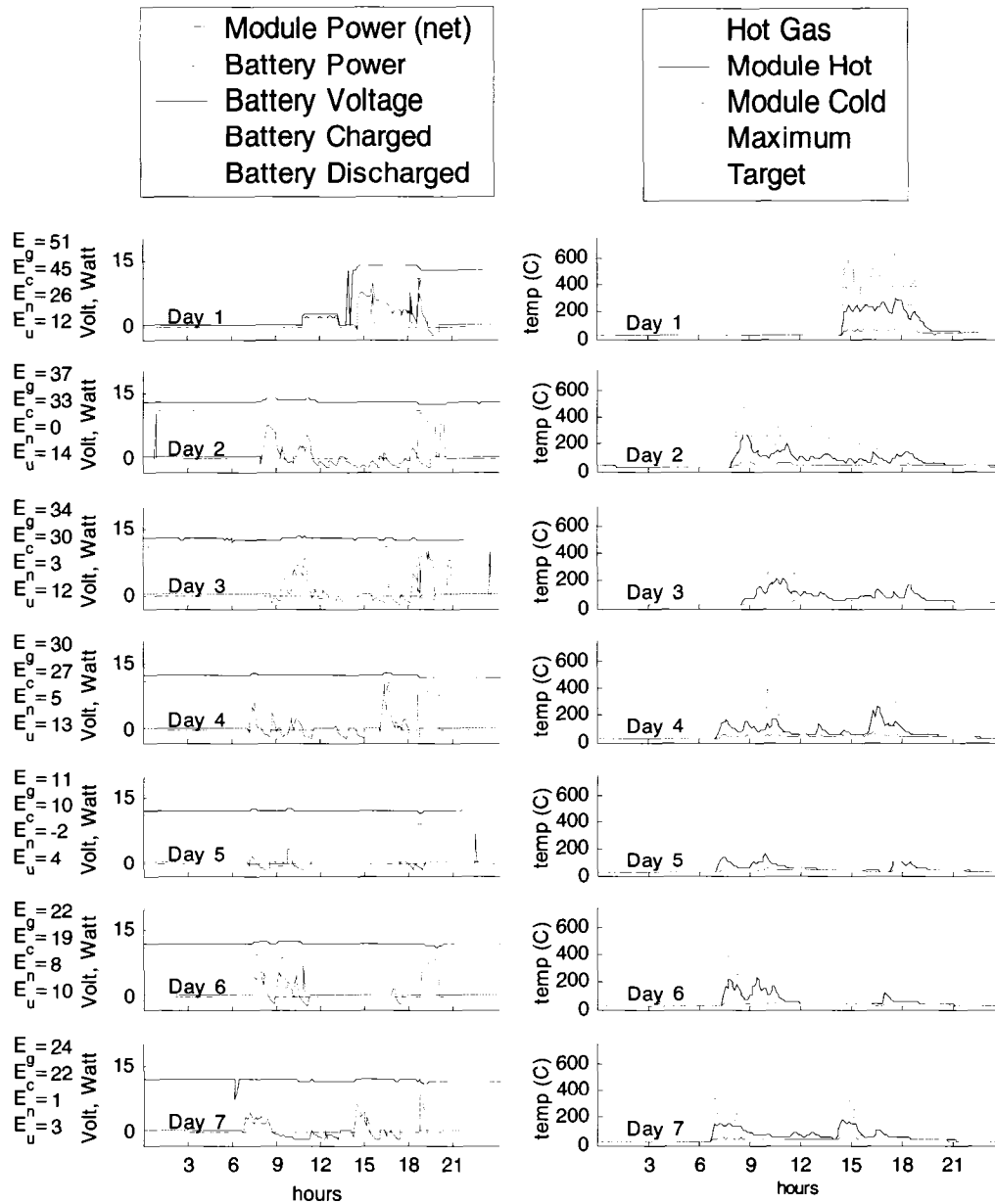


**Figure 3.14: Data from house #7 by day (first week)**

House #4 from the first round of testing was selected for follow up testing in round 2. For the second round the house was designated as House #8. The results from the 10 weeks of testing at House #8 are shown in Figure 3.15(temperature), Figure 3.16(power) and Figure 3.17(voltage). The daily data from the first week are shown in Figure 3.19.

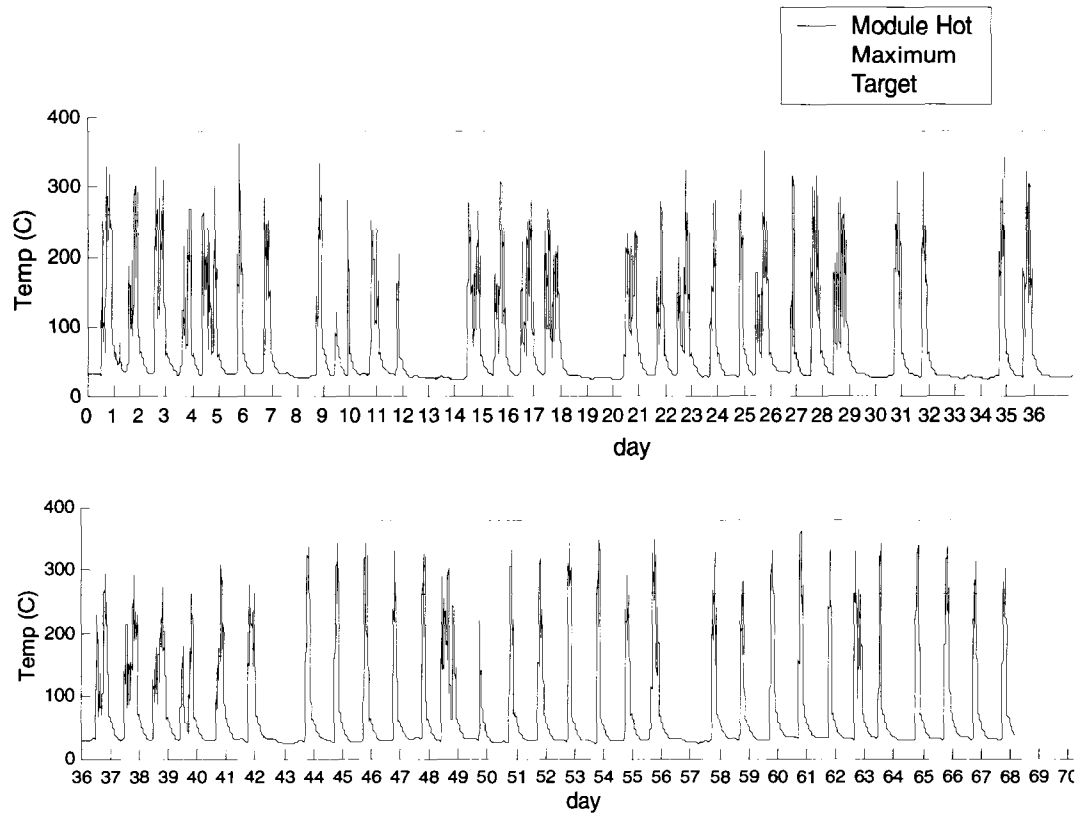
One interesting observation from this test is the steady battery voltage. It can be seen that any time the stove was running either the light or TV was also running, therefore the battery was never able to become fully charged. Again, the stove was run for many hours (5-9) each day, and at a fairly high temperature. This resulted in large amounts of energy being generated each day.

**Table 3.8: House #8 average daily energy data (includes 1-2 days/week of no use)**

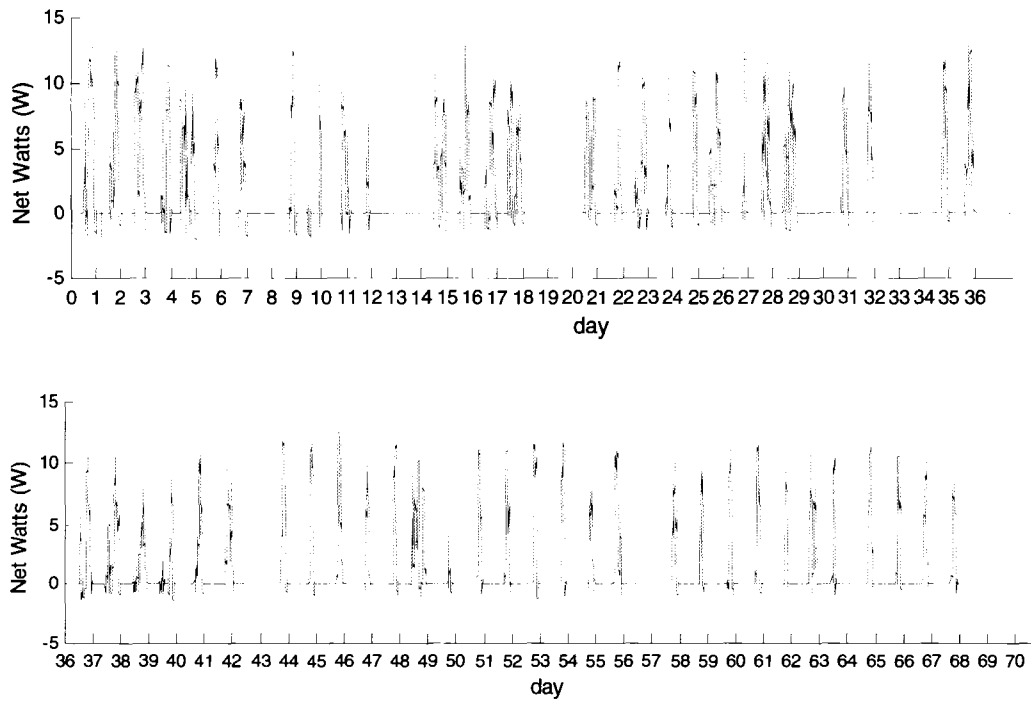
House 8 week 1-5			
Energy gross	Energy through DC-DC converter	Energy net	Energy used
51	45	30	25.5

House 8 week 6-10			
Energy gross	Energy through DC-DC converter	Energy net	Energy used
38	33.5	23.5	18.9



**Figure 3.15: Temperature data from House #8 for 10 weeks**



**Figure 3.16: Module power data from House #8 for 10 weeks**

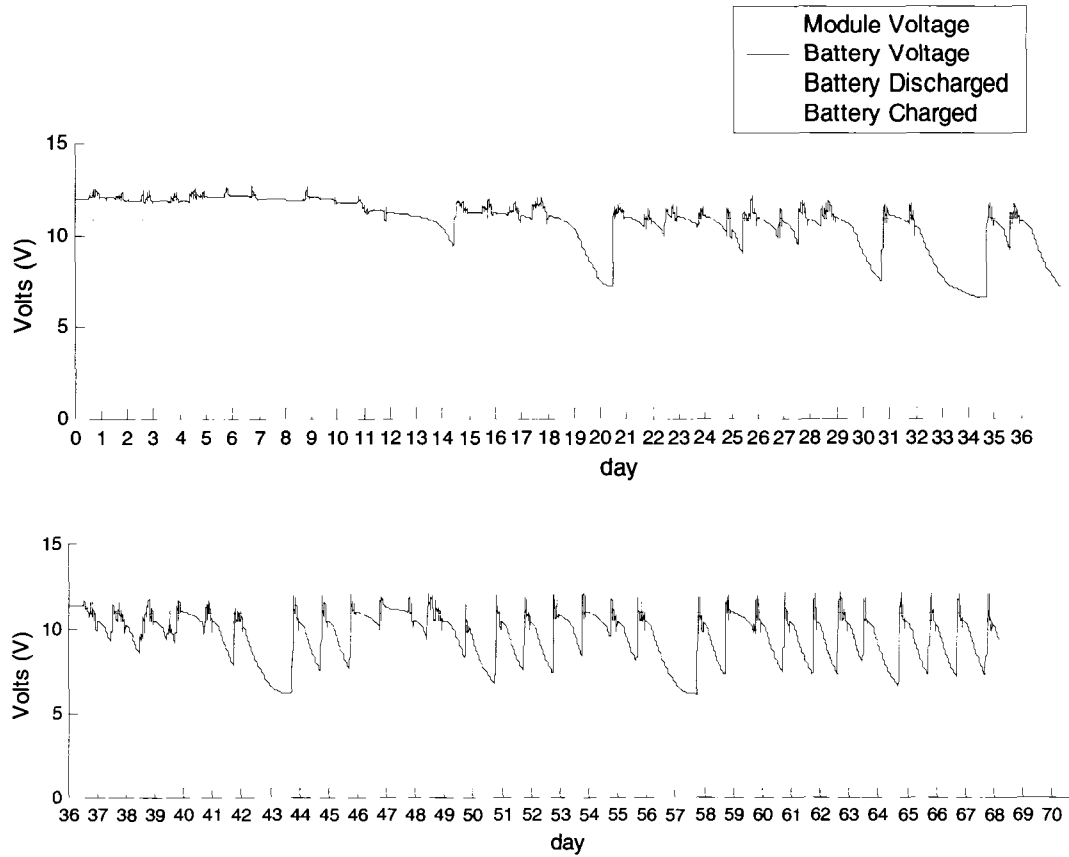


**Figure 3.17: Module and battery voltage over 10 week period (House #8)**

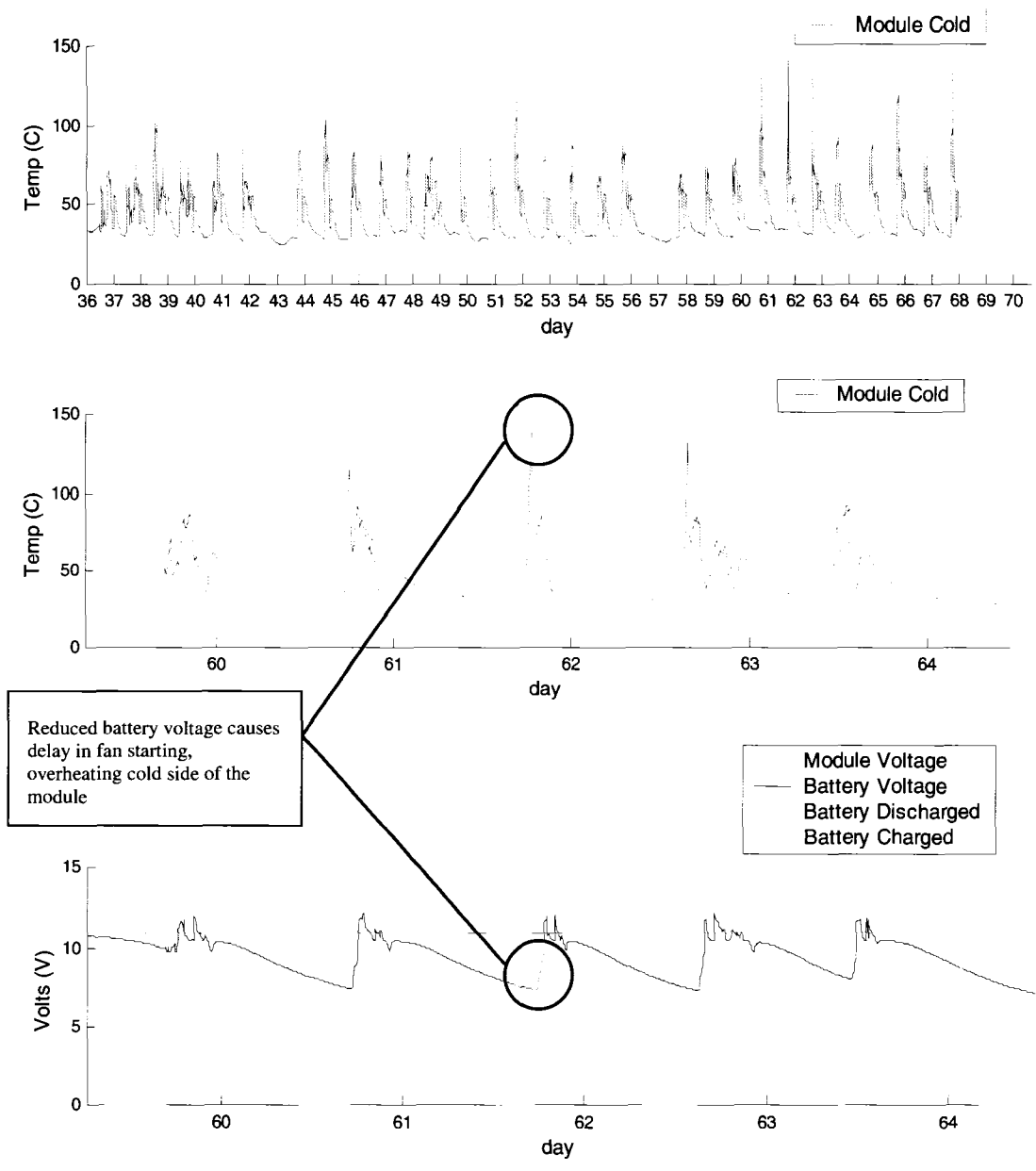


**Figure 3.18: Effect of failed battery on fan/cold sink failure**

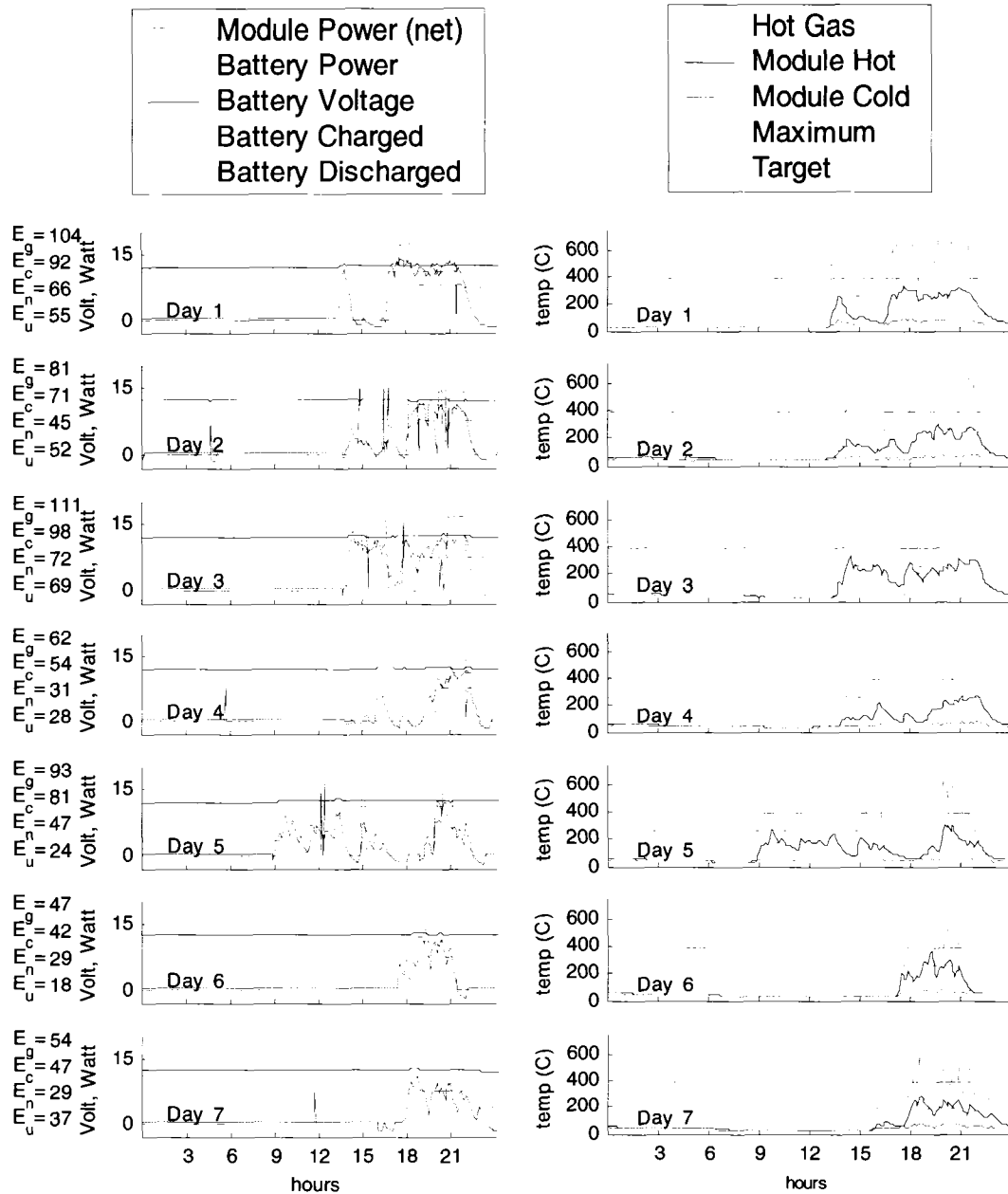


Figure 3.19: Data from house #8 by day (first week)

### 3.3.5 Post Test Component Analysis

On the return trip made in June 2007, many of the components from the first round of testing were gathered at Prolena. Unfortunately, the components were

mixed up so it was not clear which stove they went to. It was still possible to learn some additional information from these components by checking their performance and comparing to new components.

The first components tested were the fans. It was first observed that the fans had become extremely dusty from operation in homes with dirt floors. Of the 10 fans tested, all were still functioning and drawing the same power. However, three of the fans were making significant noise and seemed to be sticking on occasion. This is most likely due to dust getting into the fan bearing. If the fan was resting near a sticking position, it was possible that the fan would not turn on. There is a possibility that this could have lead to a module failure, but could not be determined without more data.

The charging circuits were also tested as well. Of the five original chargers, all were still able to turn on the fans at 1.25 V from the module as when they were new. However, two of the chargers had malfunctioning DC-DC converters. The first was from the demo unit at Prolena, and it can be concluded that the second was from House #2 as was indicated by the data. The most likely cause of this would be connecting the inline power meter or signal conditioner backwards, a flaw that has been subsequently corrected.

Finally, the modules were tested using a Z-meter and compared to readings from other new modules. Two of the modules from house #4 could not be tested due to missing leads and loose pellets. One module had an internal resistance four times the original value ( $4\Omega$ ), most likely from fatiguing the soldered connections. Another module showed a further stage of fatiguing with an internal resistance of  $1k\Omega$ ,

although the module was still together. One of the modules from the demo unit at Prolena had visibly melted solder, and measured as an open circuit. Finally, the remaining three modules from the field measured within the range of new modules, and appeared to be in good condition. The results from the post test module testing are presented in Table 3.9. The modules are listed in order of increasing damage. Unfortunately, the particular temperature and cycle history for each module was unknown. However, fatigue testing was subsequently performed in the laboratory to better understand these processes.

**Table 3.9: Post test module properties**

Module	Resistance ( $\Omega$ )	Z (*1000/K)	Comments
New module average	.9	1.9	
1	.91	1.96	
2	.92	1.94	
3	1.01	1.76	
4	3.99	.45	Fatigued. Change in Z due to resistance change only (Seebeck unchanged)
5	1000	---	Fatigued module
6	Open	---	Prolena (melted solder)

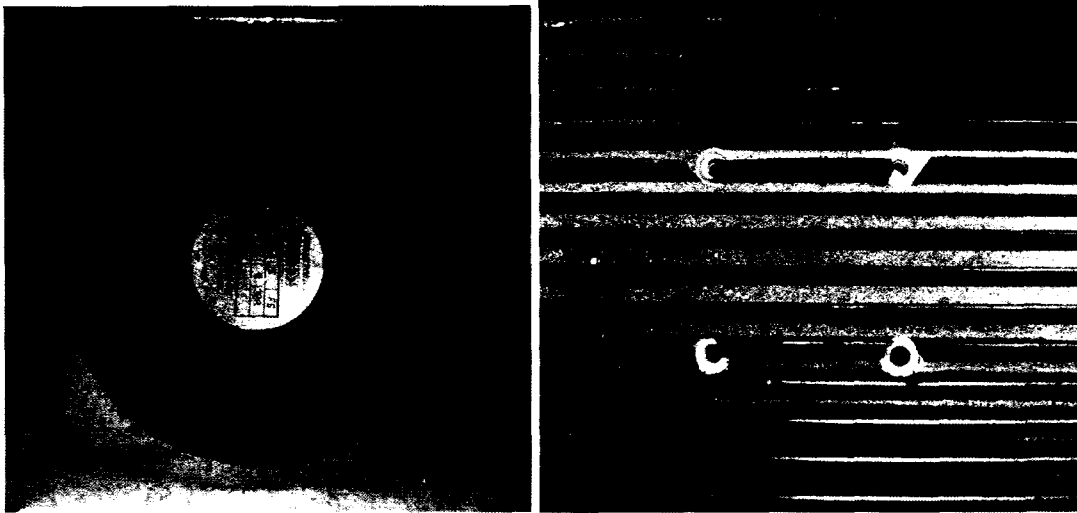


**Figure 3.20: Post test photos of fan and hot heat sink.**



**Figure 3.21: Post test module photos. Melted solder (left), fatigued module (right).**

### ***3.4 India Field Testing***

The second round of testing occurred in India during the month of December 2006. This field test was initially proposed as a demonstration, but eventually became a more involved field test. The funding was obtained as an award from NCIIA for a business plan revolving around the TEG stove. Unfortunately, the in-

country support for this test was not as effective as in Nicaragua since the project did not budget for their time.

### **3.4.1 Test Plan**

As in Nicaragua, the TEG kits were prepared at CSU and sent to India where the stoves were fabricated locally. Four kits were sent to India for testing. Because the users in this case were expected to have less income and subsidies than in Nicaragua, the size of the kits were reduced from 16 W to 8 W by using only one module. Ultimately only one 16 W unit was installed and two 8 W units were installed. The 16 W unit and one 8 W unit were outfitted with voltage and temperature data loggers. The temperature loggers measured only the hot side temperature of the module to track overheating.

### **3.4.2 Results**

The amount of data received from the field technicians in India was minimal. Therefore, the only data to analyze is that from the data loggers. Unfortunately, the stoves were used very sparsely during the first few weeks that they were installed. This was because they were taking too long to boil water compared to the traditional stove. It was soon realized that this was due to the fact that the users had round pots sitting on the hot plate of the stove. On the follow up visit holes were cut into the stove tops and the users were very happy with the stoves. This occurred after the data loggers had finished logging and had to be taken on to Nepal. In addition, the homes selected for testing had access to electricity and had stoves placed outdoors so they did not appreciate the electricity generating and smokeless aspects of the stove.

These selections were made despite the recommendations of the team at CSU. The data from the first two weeks for one 8 W unit and one 16 W unit are presented here.

From the power readings shown in Figure 3.22 it can be seen that the module was not generating close to the expected power of 16 W at 300 °C. However, the stove was not run often enough or long enough to charge the battery. In addition, the long periods of inactivity drained the battery well below 10 V, damaging the battery. As in Nicaragua, this is caused by the power consumed by the charger and logger circuit. This figure also shows the hot side temperature reaching the maximum temperature limit on the hot side (although the actual temperature of the module is less than the reading). This unit soon failed from melted solder after the stove was modified and used more often. From this data the stove was clearly getting too hot. This may be due to slight differences in the channel height from the stoves in Nicaragua (as a result in different manufacturers).

The amount of light reported by the users for this stove was approximately one hour per hour of operation, although the data logger does not show this much usage of the light.

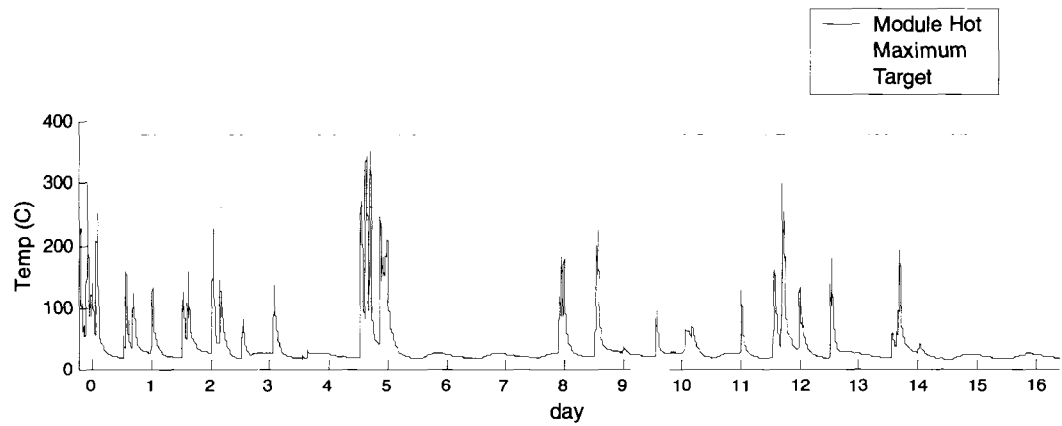
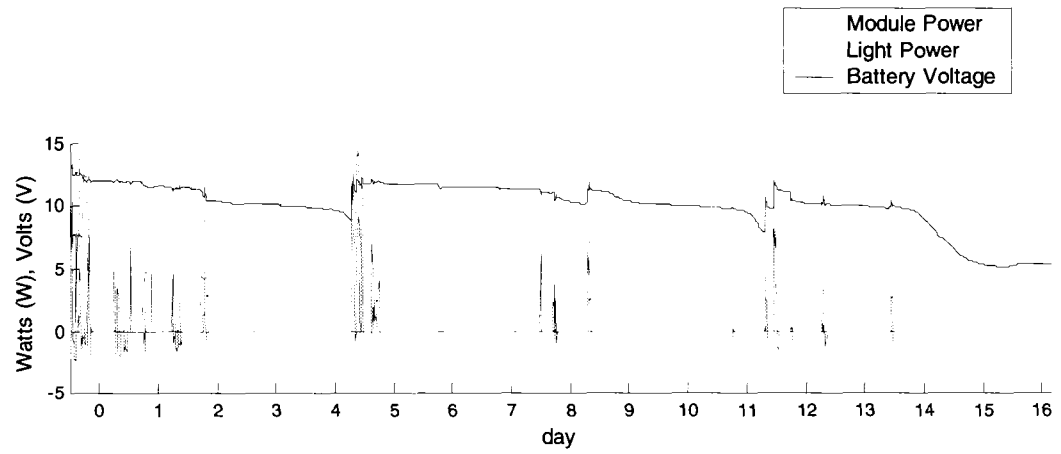
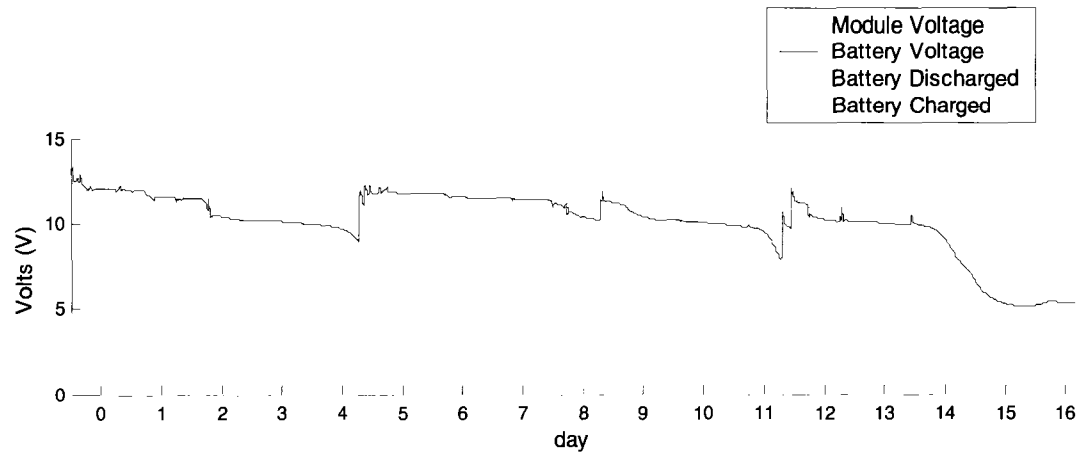


**Figure 3.22: Data from 16 W generator in India**

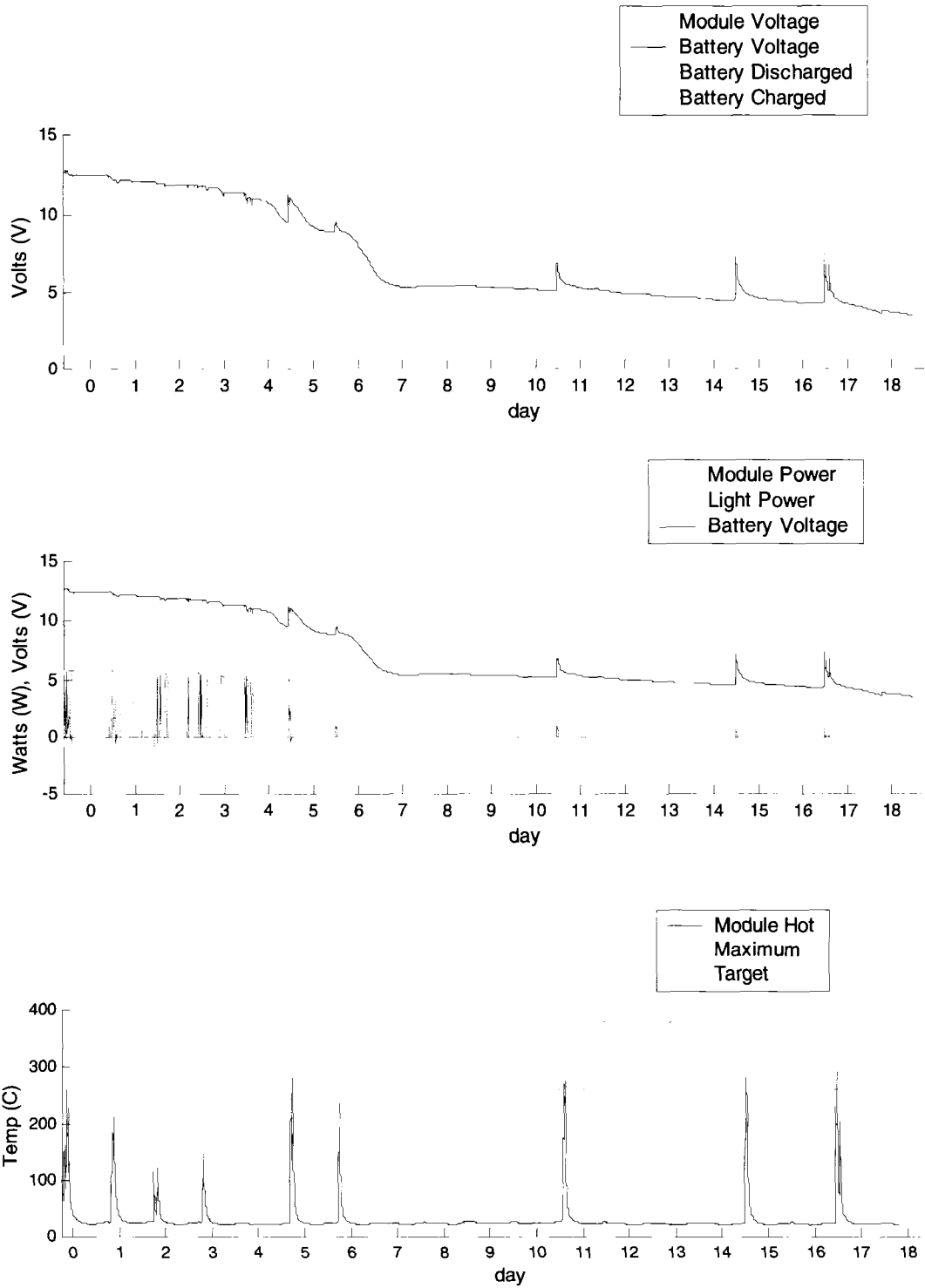


Figure 3.23: Data from 8 W generator in India

As can be seen from both sets of data from India, the stove was not used often enough or run hot enough to generate sufficient power for lighting. This was due to poor thermal contact between the round pots and flat cooking surface. Users also commented that they would prefer the stove to be much shorter since they prepare food and cook sitting down. After the follow up visit from the CSU team, stoves were modified by cutting a hole in the stove top and shortening the legs. The users were very happy with the stoves after these modifications, and used them much more frequently. Unfortunately, the batteries had already been damaged and possibly the modules from low fan voltage. No additional data was collected after the modifications since the data loggers were taken onto Nepal for field testing there. Users reported similar performance as before (one hour light per hour cooking), but the modules soon failed due to melted solder on the wire connections.

### ***3.5 Nepal Field Testing***

#### **3.5.1 Test Plan**

Field testing of four more TEG stoves took place in Nepal during the months of January 2007 to October 2007. As in the other field tests, generator kits were assembled at CSU and shipped to Nepal. Stoves were made locally by a company called STARIC. The stoves were taken to a remote village named Gatlang. The TEG units were installed by CSU team members along with STARIC members to train them in installation and monitoring.

Of the four units, one 16 W (two module) generator and three 8 W (one module) generators were installed. For the 8 W units only one light bulb (5W) was used

instead of two. Also, a smaller battery of 3A-hr was installed instead of the 7 A-hr used on the 16 W units. Two of the units were installed with power meters, and two were installed with data loggers. Unfortunately, the voltage logger conditioner circuits were left behind in India, so only the hot side temperature readings could be logged. However, this data highlighted the vast differences between usage in Nepal compared to India. As a result of lessons learned in India, holes were cut in the stove surface for direct contact between the flames and the pot.

### **3.5.2 Results**

Overall results in Nepal were very positive. The reactions to the stove were very favorable. Users were very enthusiastic about the lighting, smoke free operation, cooking efficiency and heat radiated from the stove. Most stoves were used for the majority of the day for both cooking and heating, since they were installed in the winter months.

The temperature data from the 16 W (two module) unit are shown in Figure 3.24 and Figure 3.25. A slight modification was made to this stove during initial testing to increase the temperature of the module hot side as it did not seem to be reaching the target temperature of 300 C. A baffle was inserted above the heat sink to direct more heat through the heat sink. However, the data shows that this modification was unnecessary, and may have contributed to the failure of the module. In the figure, the hot block temperature can be seen reaching the limit of 380 C several times. The unit ultimately failed after about a month due to exceeding the maximum temperature multiple times around days 21-24. It is not clear from this data whether

the temperature was exceeded on these days because the stove was run hotter (higher hot gas temperature), or if the module contact with the cold sink was reduced. For this reason, the hot gas temperature was also measured in the second round of testing in Nepal. In Figure 3.25 it can be seen that the stove is run on average 12-15 hours per day, which is significantly higher than in Nicaragua or India due to the heating demand and the local culture. This high stove usage resulted in over 4 hours of lighting per day reported by the users (around 36 W-hr per day to the user).

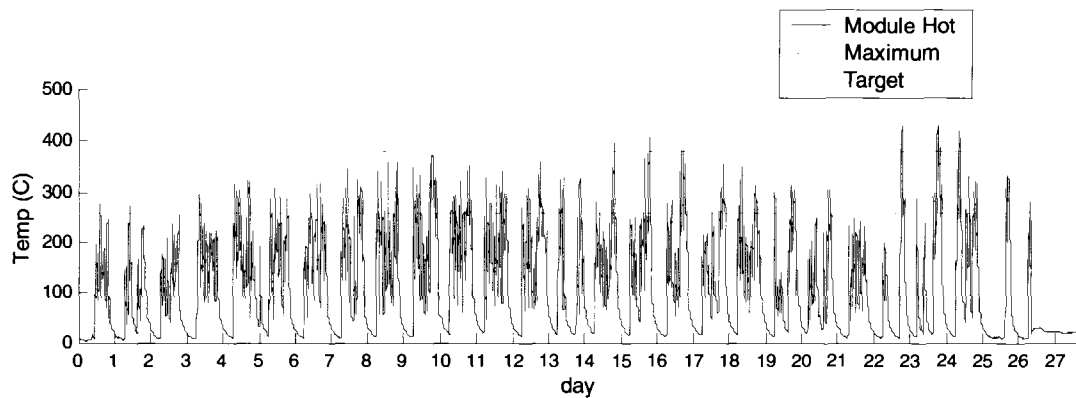


**Figure 3.24: Module hot block temperature for 2 module unit in Nepal**

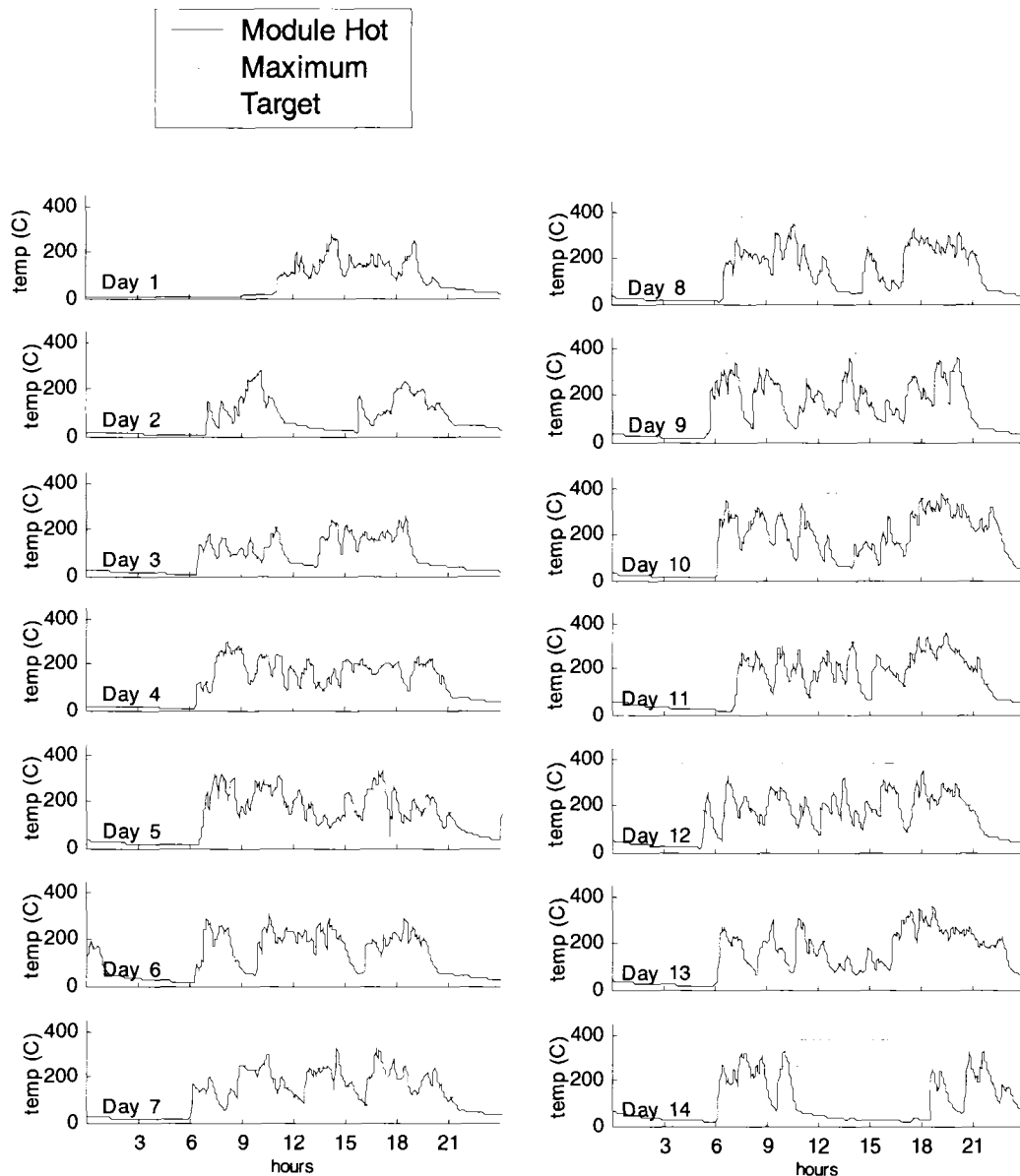


**Figure 3.25: Module hot block temperature for 2 module unit (by day)**

The results from the 8 W (one module) unit in Nepal were similar to the eight watt. In this unit, the baffles were set up almost perfectly to achieve a hot side temperature that hovered around 260-300 C, but did not reach 380 C. This unit lasted for over four months, and delivered around 3 hours of light each night (with a single CCFL bulb as opposed to two bulbs for the 16 W unit). This amounts to about 15 W-

hr per day delivered to the user. This unit was used slightly less, but still for the majority of the day. The stove was kept warm for around 12 hours a day; however the users claimed to use the stove for only six hours for cooking. After a couple of months it was determined that the battery at this location was not working.

Some additional observations from the users regarding the stoves was that the hole was not properly sized for very large pots for making Dhido (local staple food), Rakshi (local home made alcohol) and other items which need bigger pots to cook. They also had difficulty when using smaller pots that were too small for the cut hole. These comments highlight the need for multiple pot rings of different sizes. Also, metal portions of the rocket elbow and wood shelf became distorted from heat, and ultimately damaged the bricks used for the elbow.

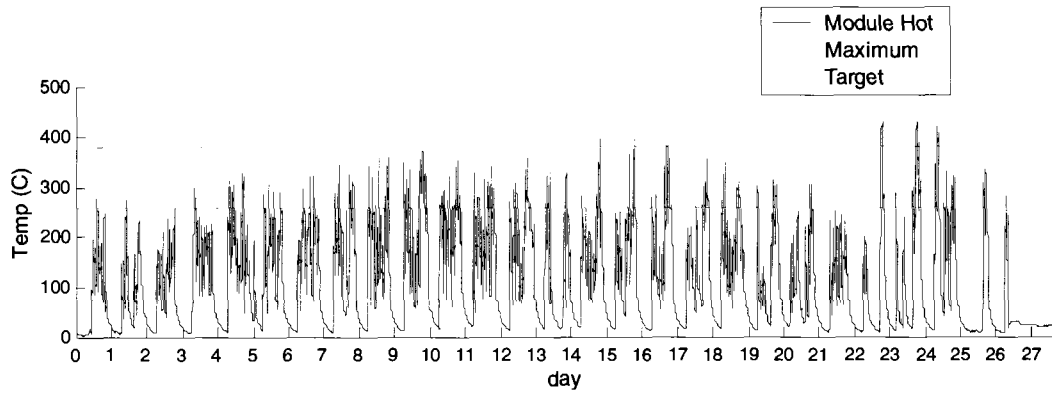


**Figure 3.26: Hot block temperature for 1 module unit in Nepal**

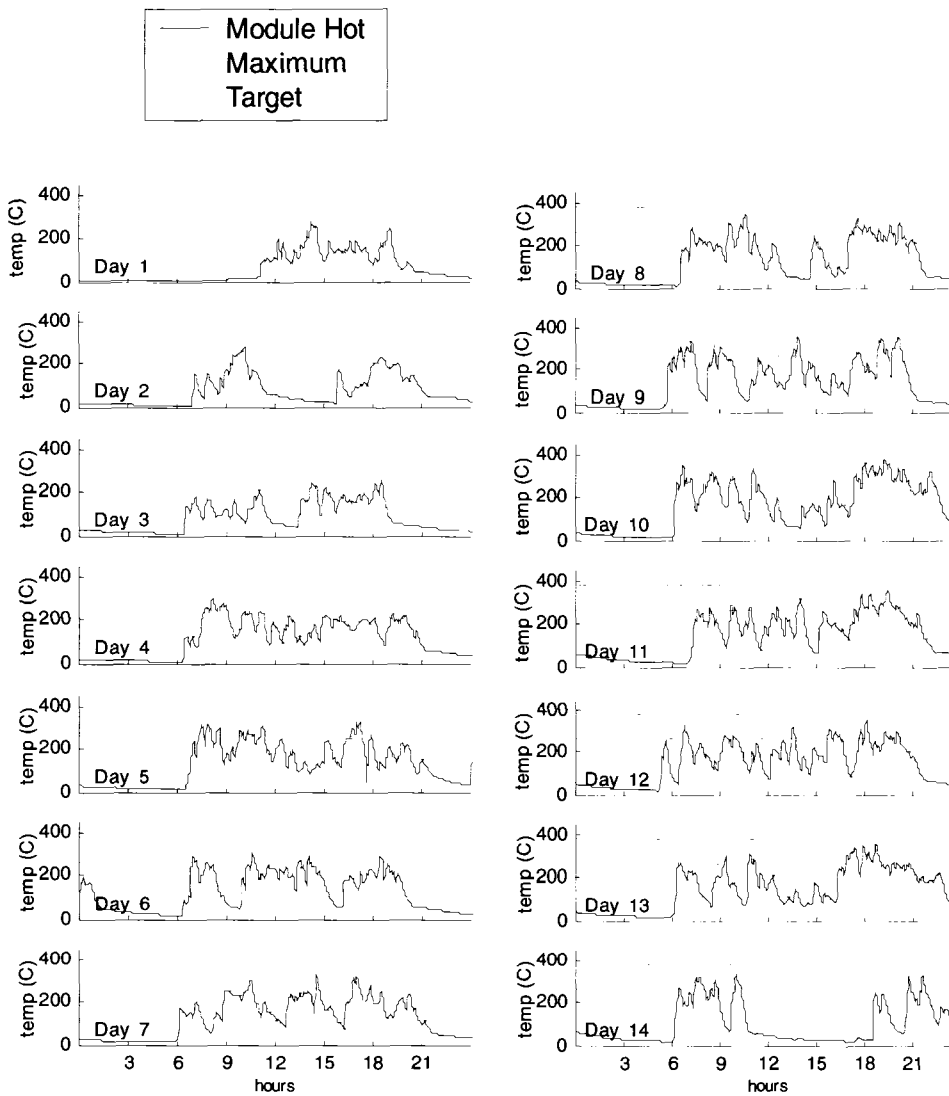


**Figure 3.27: Module hot block temperature for 1 module unit (by day)**

As in Nicaragua, a second round of field testing was conducted with one additional generator being installed with the same improvements as described in Section 3.3.4. The new generator was also installed with full data logging capability (3 system temperatures and voltages). This installation will be referred to as House #4 in Nepal. The field data is presented below.

This data is significantly different from the first round of testing. The most significant difference is in the amount the stove is used each day. Since this unit was installed in warmer weather (August – September) the stove was not needed for heating as seen before. This reduced the daily usage from about 15 hours per day to about 5 hours per day. Although this should still be enough time to generate a reasonable amount of energy, the module was not getting quite hot enough to reach peak power as seen in Figure 3.29. Although the temperature did not hit the target value, the consistency of the temperature achieved was much better than any of the previous data from Nepal, Nicaragua or India. Over the entire five-week period, the users ran the stove twice each day for nearly the same duration and to the same temperature.

Since this unit was a single module generator, the maximum net power should have been around 7.5 W. However, with the lower temperatures the peak was around 5 W, this was also due to the fact that the charger was not optimized for a single module unit. With this resulting power level, the average energy accumulated per day was just over 6 W-hr. Since the circuit had such a large parasitic draw, the net energy per day was a mere 2.5 W-hr. This would have provided less than one hour with the single CCFL bulb.

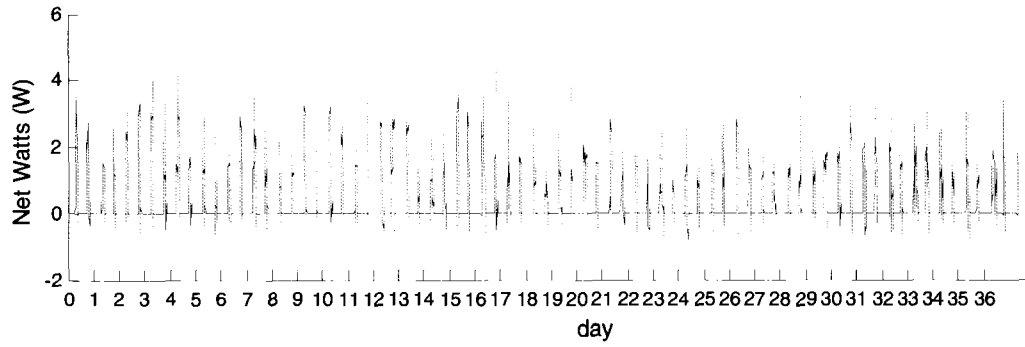


**Figure 3.28: Module power data from House #4 for 5 weeks**

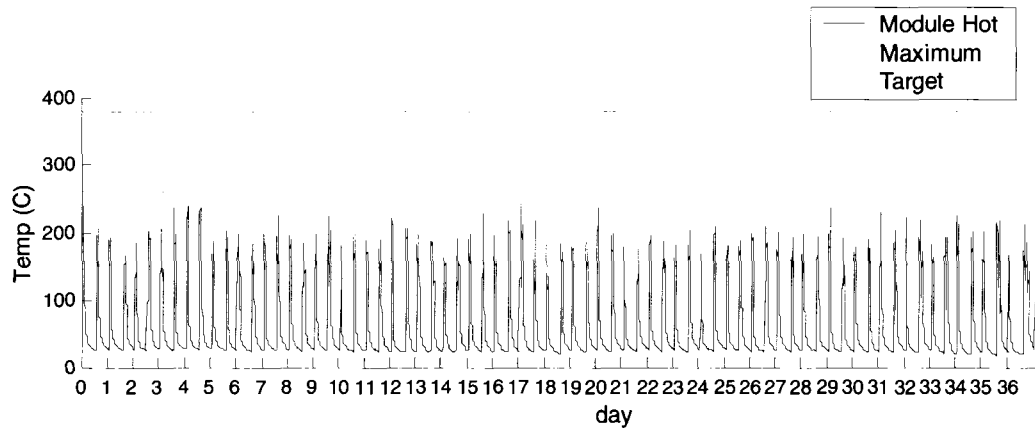


**Figure 3.29: Hot side temperature data from House #4 for 5 weeks**

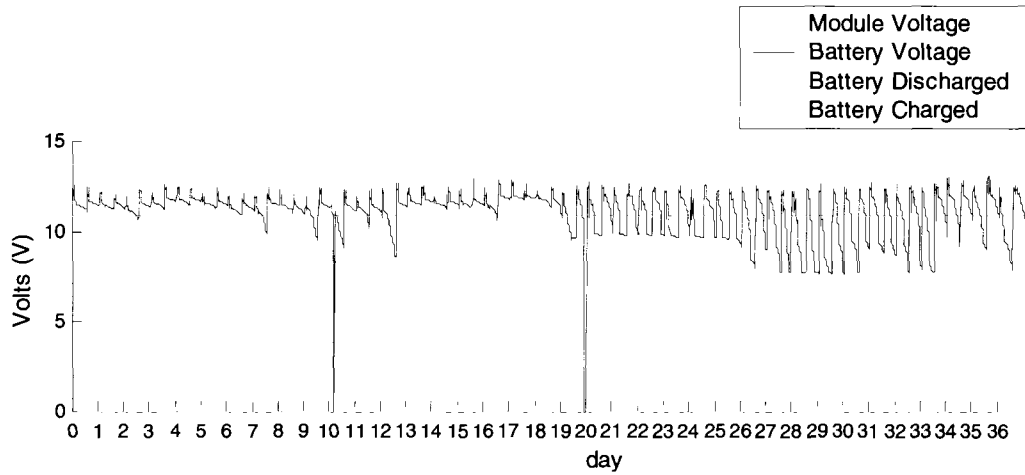


**Figure 3.30: Voltage data from House #4 for 5 weeks**

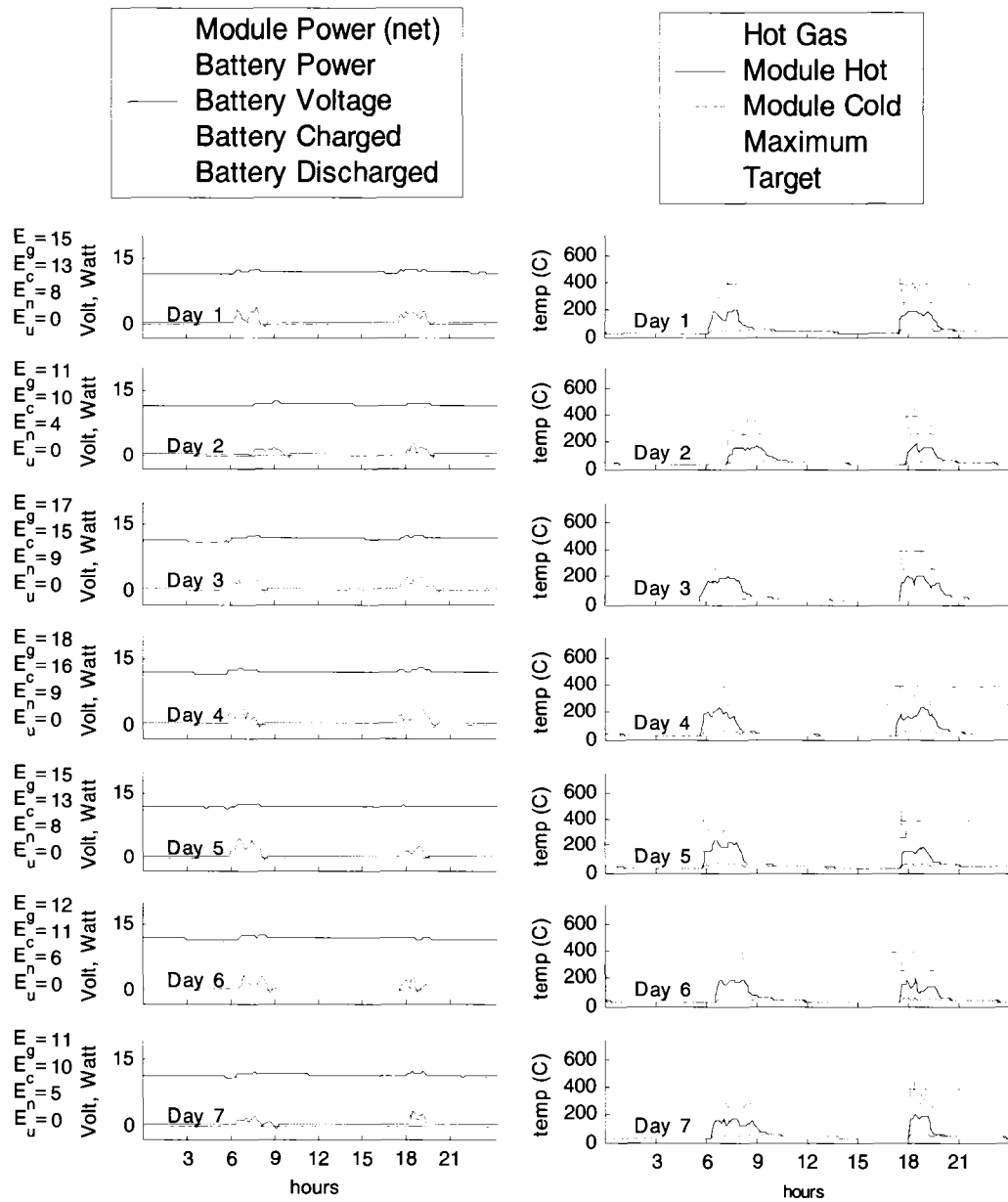


**Figure 3.31: System data by day for House #4 for the first week**

### **3.6 Conclusions from Field Testing**

Many important lessons were learned through the multiple field tests performed. These lessons related not only to the generator components, but also the stove, the users, the local partners, the data gathering tools and the methods for conducting the field tests. The highlights from testing will be divided into the categories of generator components and design, stove usage and design and data collection.

#### **Generator Components and Design**

- Overall the power generated by the stoves in the field was very close to tests done in the lab, with peak power around 16 W.
- Average power delivered to the user was around 6-8 W-hr per hour of stove use (for 2 modules). This was lower than predicted due to higher parasitic losses in the system than expected.
- Power draw from the meter and charger led to over discharging the battery, especially if the stove was not used every day.
- Overcharging the battery occurred, which damaged the battery since the maximum no load voltage was around 17 V.
- The stoves spent significant time at low temperatures where the power draw of the fan led to little or negative net power.
- Several module failures occurred from both over temperature (melting solder), and module fatigue.

- The thermal interface from hot sink to thermal spreader, and on the hot and cold side of the module were seen to degrade over time. This led to reduced power and possibly over temperature on the hot or cold side.
- The design of the power meter and signal conditioner needs to be changed to prevent a backwards connection which damages the charger.
- There were no apparent failures of the charging circuits after installation.
- No fan failures were observed; however, some appeared to have bearings close to failure due to dust.
- All components had significant coatings of dust and signs of weathering.
- Most batteries lost their capacity after a few weeks due to either over charging, over discharging, or too rapid of a charge.
- No problems were noticed with the maintenance of the hot side heat sink (soot or melting)
- Overall the peak hot side temperatures seemed to be about right (just below 380 C) when all the thermal interfaces were good. However, absolute peak values could be significantly different than average peak values, making design difficult.
- The temperature versus time profiles in the field were very different than those produced in the lab. Furthermore, the temperature profiles varied significantly from day to day, and from one user to another.

## **Stove Usage and Design**

- Most users preferred a hole cut in the stove top to reduce the time required to boil water and cook food.
- The optimal size of the hole varies with the type of pot being used.
- Some users did not want to have a hole cut in the stove top since it would be a source of smoke leakage into the room.
- Some users preferred a smaller stove that would heat up quicker, and viewed the extra space on the stove top as unnecessary thermal mass. Other users complained that the stove top was not big enough to cook all the courses of their meal at the same time.
- In India and Nepal a stove with no legs was preferred.
- Metal components in the stove elbows in Nepal warped significantly from heat.
- Small differences in the stove construction (particularly the combustion chamber) from place to place required on-site modifications to get the generator to target operating temperature.
- In places where the stove was outside or in a well ventilated area, fuel efficiency was much more important than no smoke.

## **Data Collection**

- The power meters were useful only when the stoves were within less than an hour away where they could be read weekly. However, these were of no help in determining the cause of system failure.
- Additional metrics on the power meter would make it much more useful--such as peak power, maximum battery voltage, minimum battery voltage, hours of stove usage and average power.
- In order to fully understand the root causes of system failure, it is critical to have data logged for system voltages, currents, hot gas temperature, hot side temperature and cold side temperature. No future tests should be conducted without each unit having these minimum logging capabilities.
- Data gathering and monitoring of the stoves by locals was very intermittent and unreliable. This was due to remoteness of the stoves, conflicting priorities and varying dedication of the local teams.
- Given the time and money spent on getting each unit in the field, a CSU team member should be present to take field data in the future for at least the first two weeks of testing to collect data and to make any necessary immediate changes to the system. This would prevent simple things like bad chargers or bad batteries from ruining a whole test.

## 4 Generation 2 System Development

Based on the data and feedback collected during field testing, a second generation generator was developed. For the second generation system, a comprehensive system model was developed to better understand the results of changes to the design on its performance. Specifically, it was important to understand how new designs would address the large variations in user habits, both in temperatures achieved and frequency/duration of use. The system level model also required developing more refined component tests and more complete characterization of the components tested. It was also recognized that a better understanding was needed of how cycling and high temperatures effect the degradation of the module. For the generation 2 design, an endurance test was conducted which evaluated different module construction techniques and different peak temperatures.

From the field testing, one of the major weaknesses of the system was the charging circuit. An in depth analysis was conducted to optimize the DC-DC converter circuit, and add many new features essential for peak generator performance and maximized battery lifetime.

Finally, a small database of modules, heat sinks, fans, and charging circuits was created and used in a parametric optimization. With the parametric studies the sensitivity of the module type, module temperature and heat sink length were examined in detail.

## **5 System Model**

For generation 2 system design, a system level model was developed to re-evaluate component alternatives given the wide variations in temperature and frequency of usage between different homes and different regions. Given the lessons learned during the field testing phase, the model was used to evaluate the effectiveness of design modifications in addressing the deficiencies of the original design. The system model incorporates individual component tests for the heat sink/fan combinations, modules, charging circuits and the stove. The final model was validated against transient data from the field tests, as well as accumulative field test data during the duration of the monitoring.

### ***5.1 Component Characterization***

#### **5.1.1 Module/Heat Sink Test Bench Development**

In the development of the system model, a bench top tester was designed to measure all the critical module and heat sink properties. The bench tester used an insulated hot block heated by cartridge heaters to create a known heat flux through the module and heat sink. For module testing, the modules were connected to a precision resistive load to accurately determine module current, module resistance and open circuit voltage. The resistive load was selected to match the modules internal resistance as closely as possible through the range of temperatures experienced.

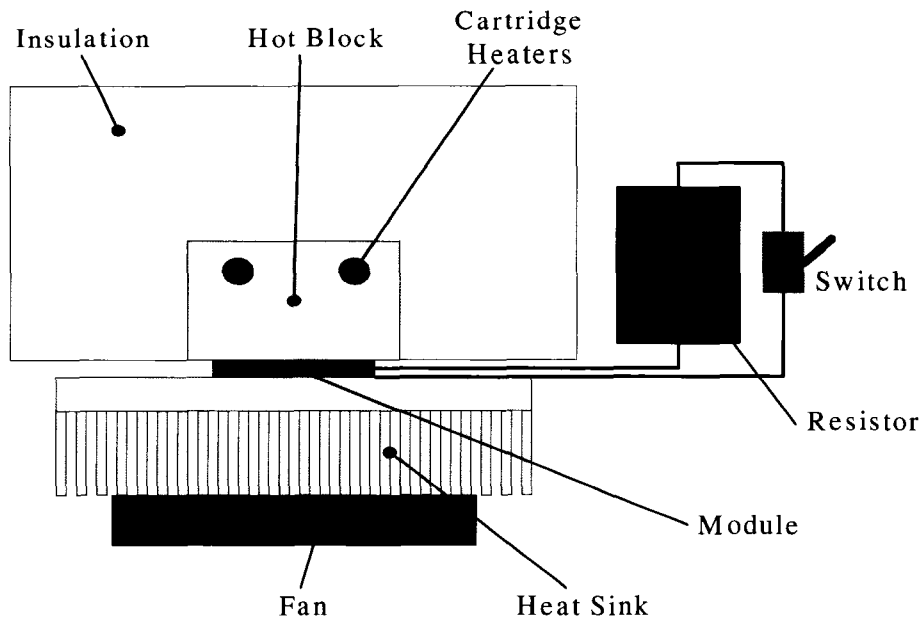


**Figure 5.1: Schematic of bench top tester**

To ensure that the readings taken using the bench top tester were accurate, a two dimensional CFD model of the apparatus was created. The purpose of the model was to examine two things. The first was to ensure that the heat generated by the cartridge heaters would create a uniform temperature across the face of the module. The temperature distribution at the hot module surface is shown in Figure 5.2 and Figure 5.3. From this analysis, the temperature distribution from the cartridge heaters is very uniform and will give accurate readings of module properties. Also, the temperature at the thermocouple location is only about 3° C higher than at the module surface at a 400 W heat flux. Therefore, the added thermal resistance due to the thermocouple location is less than .01 °C/W.



**Figure 5.2: Temperature distribution within the bench top testing apparatus (In Kelvin)**

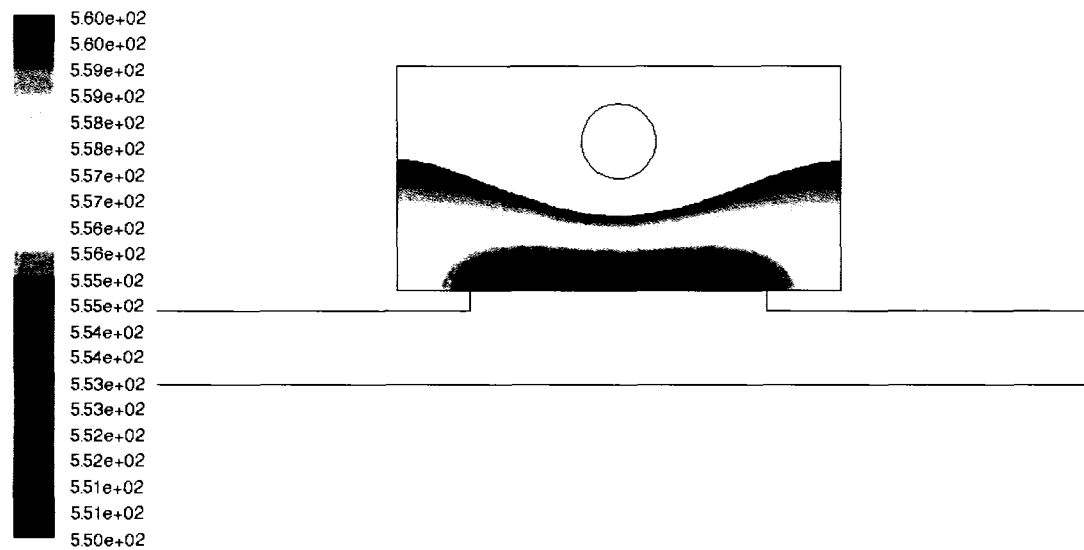


**Figure 5.3: Temperature distribution at the hot module surface and within the vicinity of the thermocouple (In Kelvin)**

For the cold heat sink, the surface was modeled as a forced convection boundary condition with a value chosen to give the same overall thermal resistance of

the heat sink. The distribution on the cold side is shown in Figure 5.4. Again, the temperature at the thermocouple location is within 4 °C from the module surface temperature at 400 W. This results in an added .01 °C/W thermal resistance to the measured thermal resistance. Also of interest in the analysis of the cold side, is the large temperature gradient from the middle of the heat sink to the outer edges. This demonstrates the cause of diminishing returns when it comes to adding length to the heat sink, since the fins at the outer edge of the heat sink operate at a much lower temperature differential. From Figure 5.2, the heat sink base temperature at the center is around 385 K, whereas at the edges it was down to 353 K for a difference of 32 °K. With an ambient temperature of 300 K, this is a 37% reduction of the temperature differential at the outer fins for the 16 cm long heat sink modeled.

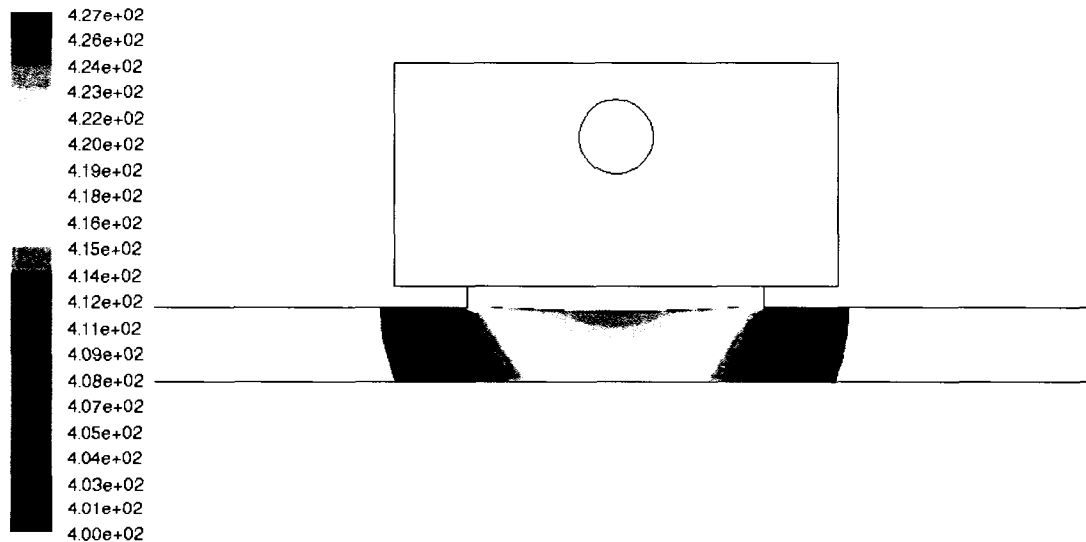


**Figure 5.4: Temperature distribution at the cold module surface and within the vicinity of the thermocouple (In Kelvin)**

### 5.1.2 Module Characterization

Using the bench top tester, a number of different modules were tested. In order to accurately model the performance of the module in the entire system, it was necessary to measure the internal electrical resistance, the Seebeck coefficient and the thermal resistance. Although these are typically given by the module manufacturer, the data is typically limited (at one operating temperature) and does not always accurately represent the module in its actual environment (effects of thermal bypass of the heat sink and non-uniform temperature distribution). It is known that the module properties vary significantly with temperature. Although these properties depend on both the hot and cold side temperatures (and all in between), the lumped properties are expressed as a function of average module temperature. For each module tested, a data sheet was created listing all the critical properties, as well as curve fits to the properties to be used for modeling. An example is shown in Figure 5.6. In all, five modules were tested and are listed in Table 5.1. The data from all the modules tested is presented in Appendix 12.4.

The module readings were taken at various hot side temperatures from approximately 100 C to 280 C. At each temperature setting, the temperatures would take 1-2 hours to reach equilibrium values. The temperature history of the module would be recorded for approximately 10 minutes. Once the temperature was steady for 10 minutes, a reading would be taken. In order to measure the internal resistance, the procedure outlined in [44] was used. Load voltage across the resistive load was measured directly, and the current could be calculated from the known resistance. To determine the open circuit voltage, the load would be quickly switched of and on.

Since the module current induces a Peltier effect, the module will reach a different equilibrium temperature once the load is switched off. Therefore, the voltage readings would be taken every 100 ms. After the switch was opened and closed, the program would be stopped to zoom in on the voltage peak as shown in Figure 5.5. As seen here, after only 0.5 seconds the voltage has increased by 1%. The reading that is recorded is the first reading after the switch is opened.

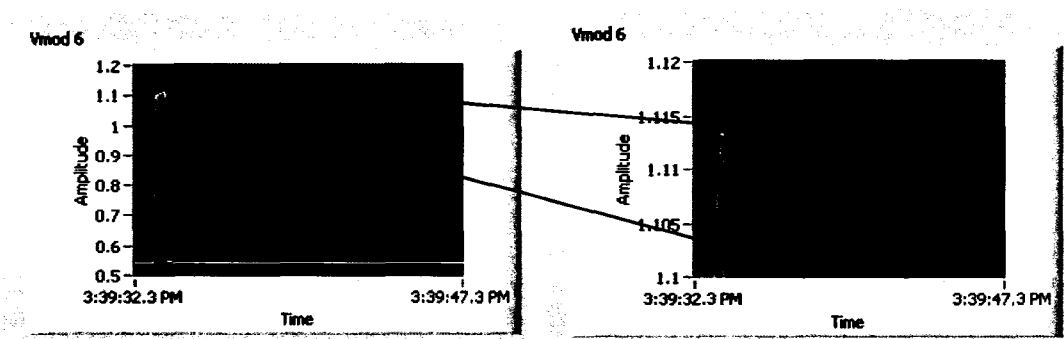


**Figure 5.5: Screen shots showing method for determining open circuit voltage and voltage drift after opening the load circuit**

**Table 5.1: Modules tested for database**

Module	Nominal Power	Manufacturer
TEP1-1.5	5.9 W	Thermonamic
TEP1-0.8	10.7 W	Thermonamic
TEP1-0.6	14 W	Thermonamic
HZ-9	9 W	Hi-Z
HZ-14	14 W	Hi-Z

**Module** **TEP1-0.8**

---

**Manufacturer Specs**

T hot (C)	230
T cold (C)	50
T avg (C)	140
Thermal Watts	240
Thermal Res @match load (C/W)	0.75
Electrical Res (Ohm)	1.7
Voc @match load (V)	8.4
I @match load (Amps)	2.5
Seebeck coef. (V/C)	0.046667
Efficiency	0.04375
Power (W)	10.5

**Test Conditions**

Heatsink	E1456 @ 6.5"
Fan	Mechatronics
Fan Voltage	12V

**Test Data**

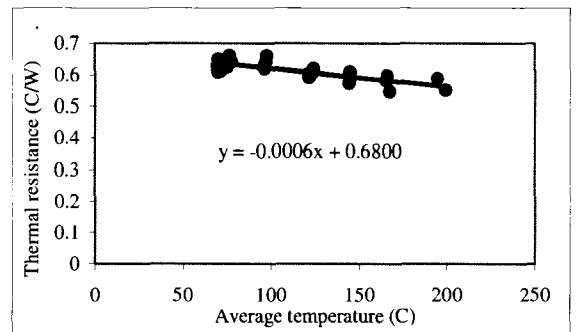
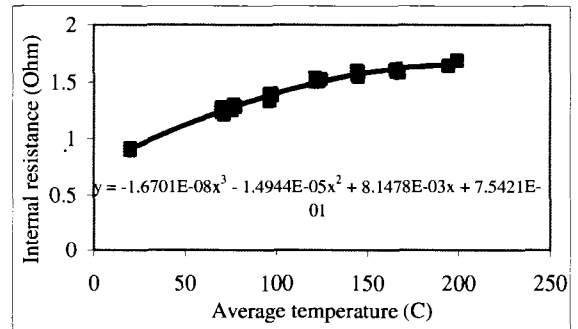
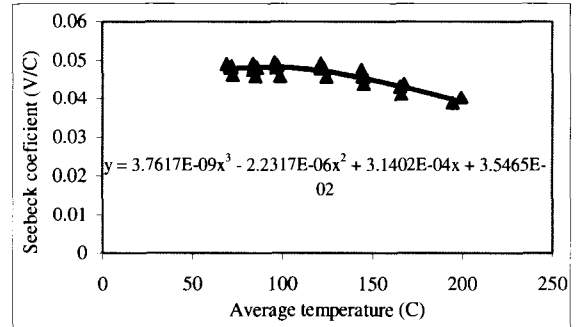


**Figure 5.6: Example of module data sheet for TEP1-0.8**

In addition to measurements taken by the bench top tester, a commercially available Z-meter made by RMT Ltd. was used to measure the initial internal resistance and Z value for the modules. The Z-meter uses the Harman approach to

determine the thermoelectric properties of the module [55][56]. This method uses a small square wave current applied to the module, and monitors the modules transient voltage response to the excitation. A curve is then fit to the module voltage profile which can be used to back out the Z value of the module. Unfortunately, this tester could not be used during the endurance test since the modules are clamped between the heat sinks. The test method works on the assumption that the module is thermally isolated, so it can only measure the Z value for a stand alone module.

For the Thermonamic modules used in the generation 1 design, 12 new TEP1-0.8 modules were tested to observe the variability from one module to the next. The results from this test are shown in Table 5.2 and Figure 5.8. Of the modules tested the maximum deviation of the Z value was + 6% / -8%.

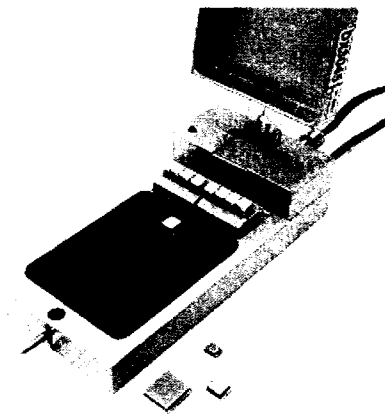


**Figure 5.7: Rmt Z-meter**

**Table 5.2: Initial Z-meter readings**

Module type	Module #	Z (1000/K)	% from average	Resistance	% from average
TEP1-0.8	1	1.94	2%	0.83	-7%
TEP1-0.8	2	1.83	-4%	0.98	10%
TEP1-0.8	3	1.75	-8%	0.75	-16%
TEP1-0.8	4	1.92	1%	0.92	3%
TEP1-0.8	6	1.95	3%	0.9	1%
TEP1-0.8	7	1.86	-2%	0.93	4%
TEP1-0.8	8	1.93	2%	0.92	3%
TEP1-0.8	9	1.86	-2%	0.91	2%
TEP1-0.8	10	1.91	0%	0.95	7%
TEP1-0.8	11	2.01	6%	0.82	-8%
TEP1-0.8	12	1.93	2%	0.91	2%
TEP1-0.8	13	1.92	1%	0.87	-2%
Average		1.90		0.89	

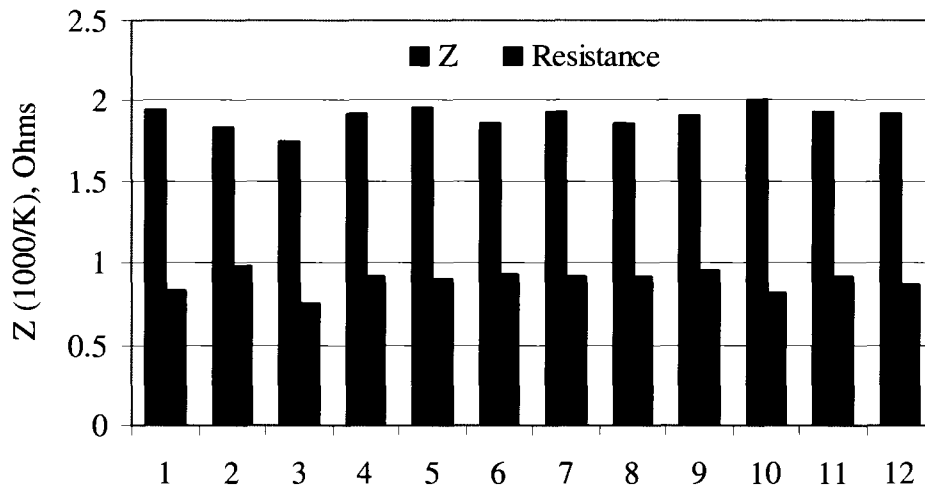


**Figure 5.8: Variability in initial Z-meter readings for 12 TEP1-0.8 modules**

### 5.1.3 Cold Sink Characterization

Compared to the thermoelectric modules, there are many more possible variations for the cold heat sink. As highlighted in the generation 1 design, the cold-side heat sink selection is as important as selecting the correct module. The cold heat

sink can vary in type, geometry, length, fan, and fan voltage. In order to better understand the optimization process, only one heat sink extrusion was used for testing. Since the E1456 heat sink by Thermaflo was shown to be the best of the original heat sinks tested, this one was chosen for the heat sink parametric study. The heat sink was tested in 9.4 cm, 12.5 cm, 16.25 cm, 20 cm and 25 cm. For the 9.4 cm heat sink a fan shroud was created to funnel the air into the middle of the heat sink, since the fan diameter was larger than the heat sink. Each heat sink was tested with three fans with varying flow rates and power consumptions. These were the Mechatronics fan, the Sunon fan and the Cooler Master fan. Each fan was tested at 6, 9, 12, and 13.8 V. The results from the heat sink length study using the Mechatronics fan are presented in Figure 5.9. This study led to an interesting and unexpected result. It was expected that as the heat sink length increased the added benefit would decrease. However, it was not expected that after a point the thermal resistance would actually increase. Coincidentally, this inflection occurred after a 16.25 cm length, the heat sink used in the generation 1 design. The cause of this behavior is that the added heat transfer surface is too far away from the source, so its effectiveness is reduced (as seen in the CFD model of Section 5.1.1). In addition, the air passing over the added length has already been heated somewhat, further reducing its effectiveness. Finally, the added length causes more flow restriction and a smaller overall flow rate. These results indicate that there is a limit to the thermal resistance that can be achieved with a fan cooled heat sink (when fan power is a consideration). The only way to reduce the thermal resistance any further would be to redesign the

heat sink to better distribute the heat to the fins and create the same surface area while reducing the restriction to flow.

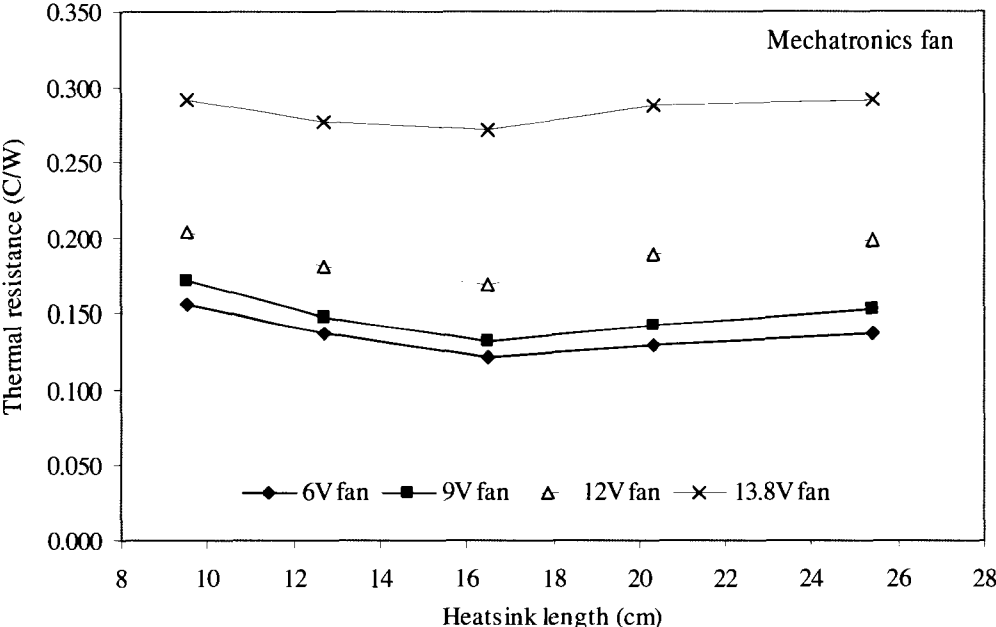


**Figure 5.9: Results from heat sink length test using Mechatronics fan**

The data from varying the fan voltage and fan type for the 16 cm long heat sink is shown in Figure 5.10. Although the Sunon fan clearly leads to the lowest thermal resistance, it also takes about twice the power of the Mechatronics fan, and four times the power of the Cooler Master fan. In order to select the best fan, the full system model is necessary to determine which leads to the maximum net power. The data from all the heat sink /fan combinations tested are presented in Appendix 12.3.

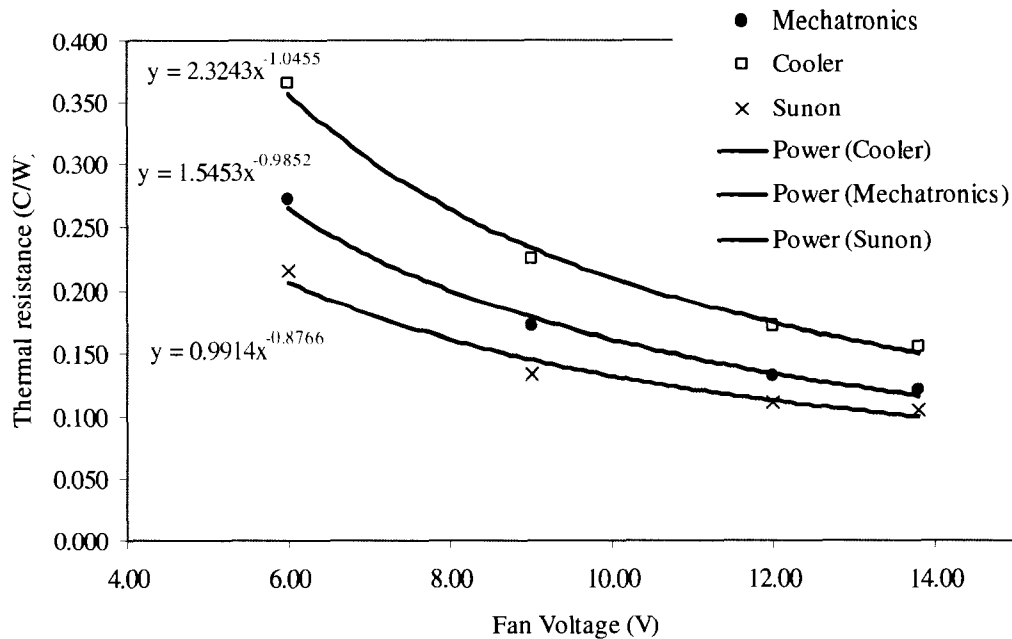


**Figure 5.10: Heat sink thermal resistance at varying fan voltage with three different fans (16 cm length)**

It is also interesting to look at the thermal resistance as a function of fan power. For the three fans tested (which had similar flow rate to power ratios) there was a fairly consistent trend line between the three fans. Each curve diverts from the trend at 6 V where the fan is no longer operating near its design condition. This data is shown in Figure 5.11. At the lowest power (.5 W) the Mechatronics fan has better performance than the Cooler Master fan. At high power (up to 1.5 W), the Mechatronics fan has better performance than the Sunon Fan. Although the Sunon fan reaches a lower value eventually, it is only slightly lower, and at a much higher power level. Therefore, the Mechatronics fan is the covers the broadest range with the best performance.

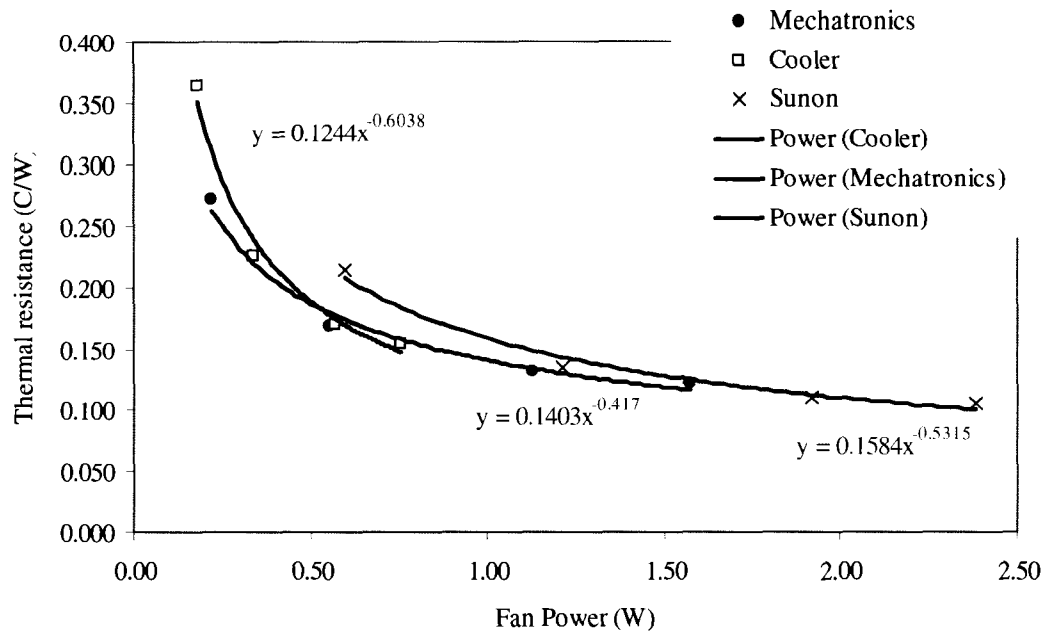


**Figure 5.11: Heat sink thermal resistance as a function of fan power (16.25 cm length)**

Although the bonded fin heat sink sold by Melcor was shown to have a larger thermal resistance than the E1456 heat sink (Section 2.2.1), it was re-tested at varying fan voltages to see how it performed at the lower flow rates. The Melcor heat sink has much longer fins with wider channels formed between the fins. This makes for a more free flowing heat sink with a comparable surface area. These heat sinks are shown in Figure 5.12. The results from this comparison are also shown in Figure 5.12. As seen before, at high fan voltages the E1456 heat sink has a lower thermal resistance. However, at low fan power the free flowing Melcor heat sink has a much lower thermal resistance. In addition, this larger fin spacing will result in a much lower thermal resistance when the fans are not on (natural convection). This superior performance at low fan power makes the Melcor heat sink more competitive when modeled with the complete system as in Section 8.2.

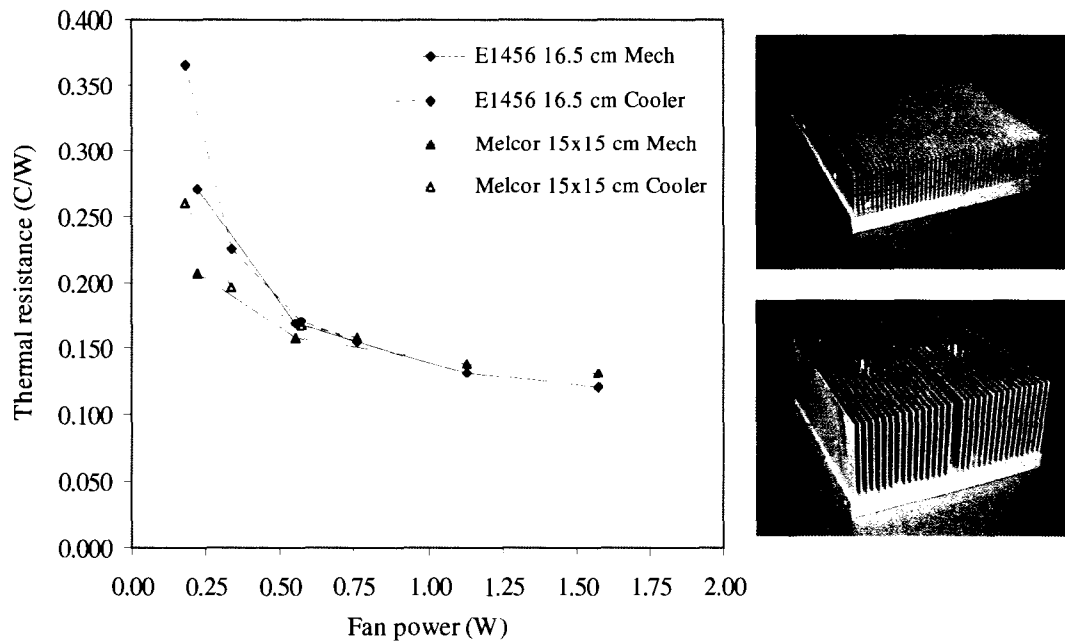


**Figure 5.12: Comparison of extruded E1465 16.5 cm (top right) and bonded Melcor 15 cm (bottom right) heat sinks using Cooler Master and Mechatrinics fans**

The final study in the heat sink characterization was to observe the effect of adding a foam filter to the fan. As seen in the field test, a large amount of dust accumulated on the fan and heat sink over several months which could lead to fan failure and reduced heat sink effectiveness. The comparison of the heat sink thermal resistance with and without the filter is shown in Figure 5.13. At each fan voltage, the heat sink with the filter had about twice the thermal resistance of the heat sink without the fan. This is an unacceptable increase in thermal resistance which would cripple the generator performance. Although adding a filter will ultimately be necessary, a much higher flow design will need to be developed such as a cylindrical filter with a much higher area and less restriction.

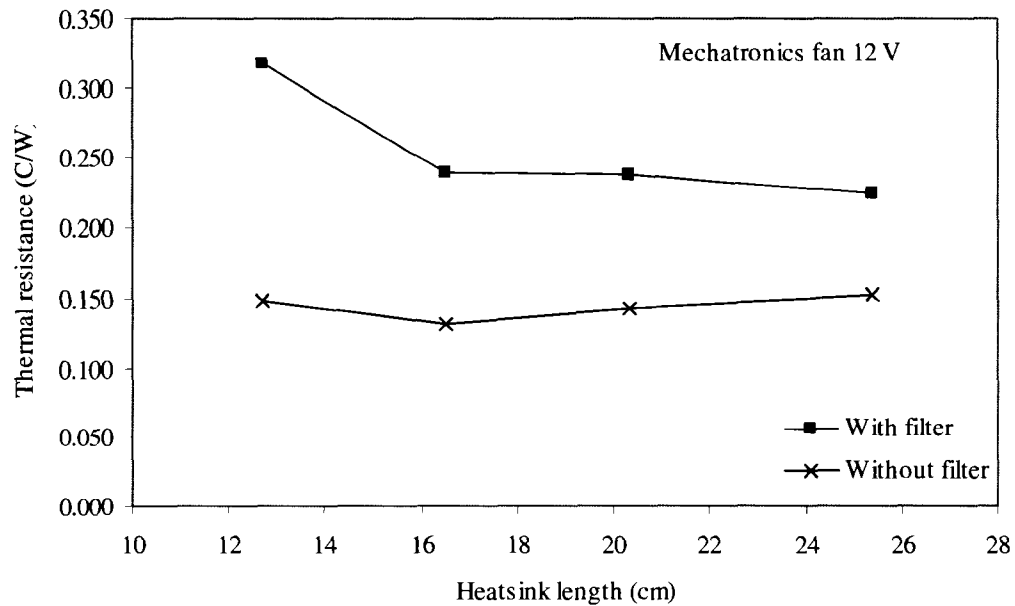


**Figure 5.13: Heat sink thermal resistance with and without filter**

### 5.1.4 Hot Sink Modeling

For the module hot sink, manufacturer data for thermal resistance was used for initial development. However, for further refinement of the design more accurate models are necessary to incorporate the complexities seen in the stove during operation. The model of the hot side heat sink must incorporate:

- Actual stove mass flows and velocities at varying hot gas temperatures
- Bypass of air around the heat sink through the channels above or beside the heat sinks.
- Variation of heat sink thermal resistance due to varying fluid properties as a result of elevated temperatures and changing composition from combustion

From the field test data, the apparent thermal resistance of the hot heat sink could be calculated at varying hot gas temperatures. The result from this calculation for the first day of House #8 is shown in Figure 5.14. From this data, it can be seen that the thermal resistance varies significantly even from one moment to the next at the same hot gas temperature. Also of interest, is the fact that the average thermal resistance is nearly constant over the temperature range of 200 C to 600 C. This is surprising considering the fluid properties such as density and thermal conductivity vary significantly across this temperature range.

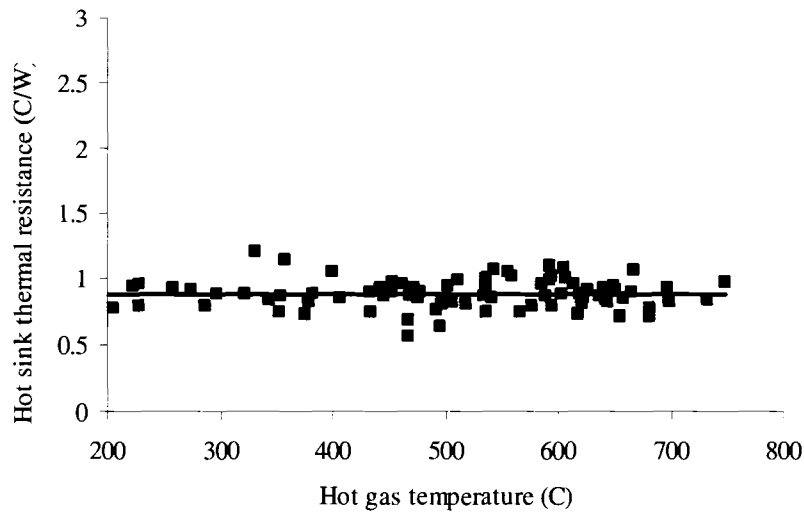


**Figure 5.14: Hot sink thermal resistance from field data (House #8 day 1)**

The first step in developing a model for the hot heat sink was to compare the manufacturer data to a bench top experiment in the laboratory. The lab experiment was setup as shown in Figure 5.15. The heat sink was heated with the same hot block assembly used for testing cold sinks.

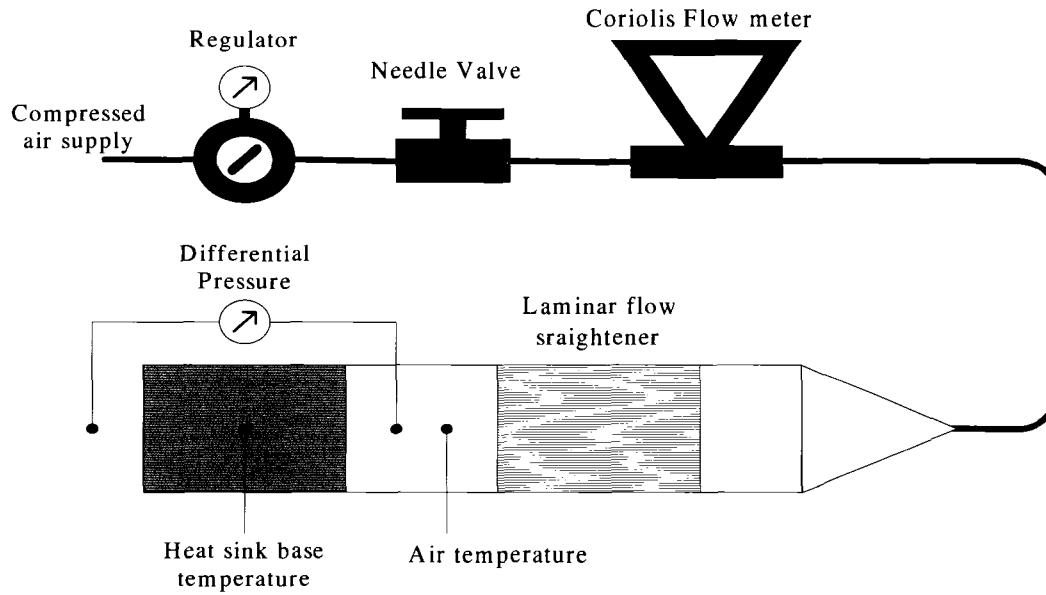


**Figure 5.15: Hot heat sink test apparatus**

The results from the heat sink testing for thermal resistance and pressure drop are shown in Figure 5.16 and Figure 5.17. From this test, it is clear that the manufacturer data is not accurate enough for detailed design work, and a more accurate model is necessary.

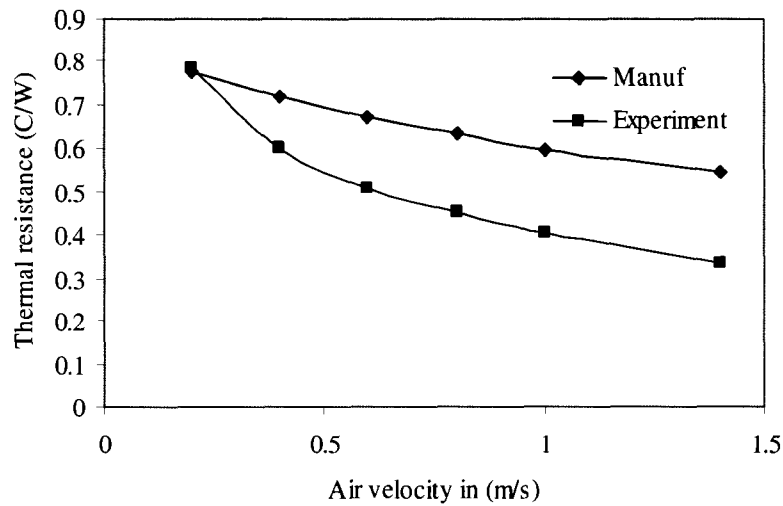


**Figure 5.16: Experimental and manufacturer values for thermal resistance as a function of free stream velocity**

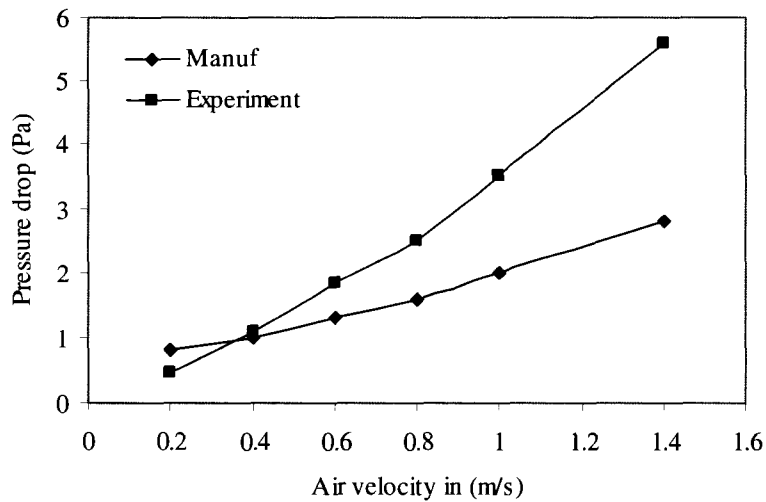


**Figure 5.17: Experimental and manufacturer values for pressure drop as a function of free stream velocity**

In addition to the manufacturer data, a fluid dynamics approach was used to estimate pressure drop through the heat sink. For each channel within the heat sink and bypass a development as described in [75] for a rectangular channel was used.

The resulting equation for pressure drop through a channel is:

$$\Delta P_{chan} = \frac{V \mu L C}{2 D_h^2}$$

**Equation 5.1**

Where :

- $\Delta P_{chan}$  is the pressure drop through the channel
- $V$  is the channel velocity
- $\mu$  is the fluid viscosity
- $L$  is the channel length
- $D_h$  is the channel hydraulic diameter
- $C$  is a correction term for the channel aspect ratio (height/width)

The correction factor (C) for a rectangular channel as a function of its height to width ratio (h/w) is shown in Figure 5.18.

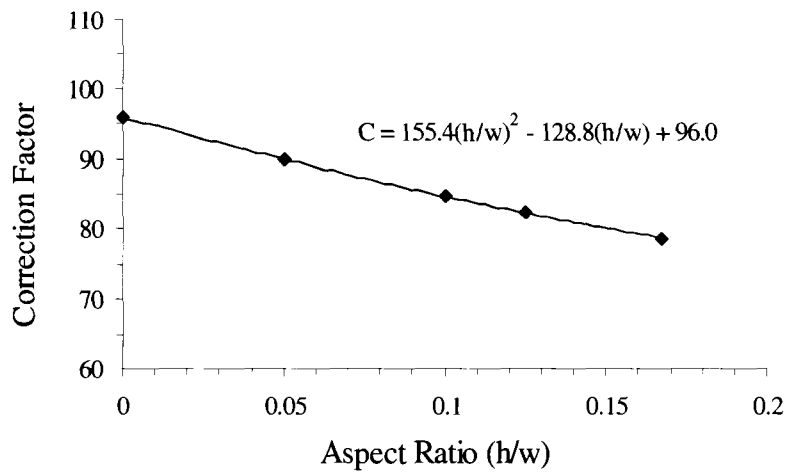


**Figure 5.18: Correction term for channel aspect ratio**

In addition to the pressure drop through the channel, an entry/exit loss coefficient was added. The pressure drop contributed by the entry/exit loss is described by:

$$\Delta P_{entry} = \frac{\rho K_{entry} V^2}{2}$$

**Equation 5.2**

*Where :*

$\rho$  is the fluid density  
 $K_{entry}$  is the minor loss coefficient  
 $V$  is the velocity in the channel

For the minor loss coefficients at the entry and exit, the value for a sharp contraction (.15) and sharp expansion (.15) were used. This gave a total K value of .3. As can be seen in Figure 5.19, a K value of .3 predicts a much lower pressure drop than the experiment, but is very close to the manufacturer value. If the K values for a sharp entry (.5) and a sharp exit (1) are used, the agreement with the experiment is very good. However, the flow entering and leaving the heat sink is not an infinite reservoir, but has some velocity, so these K values are slightly higher than they should be.

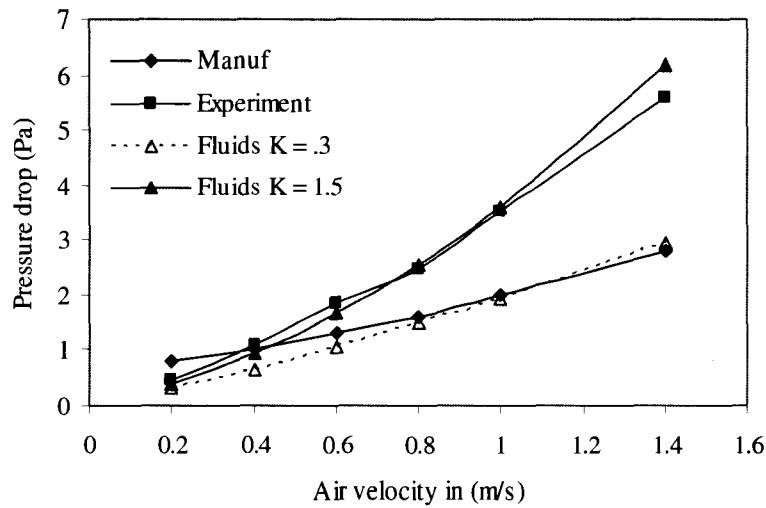


**Figure 5.19: Comparison of fluid dynamics estimate to experimental pressure drop**

To get a more accurate model of the thermal resistance through the heat sink and make predictions at elevated temperatures a CFD model was created in the program FLUENT. The mesh for the model was created in GAMBIT, and is shown in Figure 5.20. To reduce computational time, a single channel of the heat sink was modeled, with periodic boundary conditions on the side faces of the model. The inlet to the heat sink was specified as a uniform velocity inlet, and the outlet was a pressure outlet. The hot block was specified with a uniform temperature. After the model was run, the heat flux through the hot block was computed to calculate the thermal resistance of the heat sink. The area weighted average pressure at the inlet and outlet were calculated to determine the pressure drop through the heat sink. For the air properties, third order curve fits were used for conductivity, viscosity and specific heat. The ideal gas model was used for density. For the solver settings, second order upwind was used for the energy and momentum equations. The

SIMPLE model was used for pressure-velocity coupling. The viscous model used was laminar flow, which is accurate for these velocities.

The temperature contours of the gas stream and the heat sink fins are shown in Figure 5.21. The contours of static pressure are shown in Figure 5.22. From this figure it can be seen that approximately 4/5 of the pressure drop occurs at the entry, 1/2 of the pressure drop occurs through the heat sink, with the remaining 1/5 at the exit.

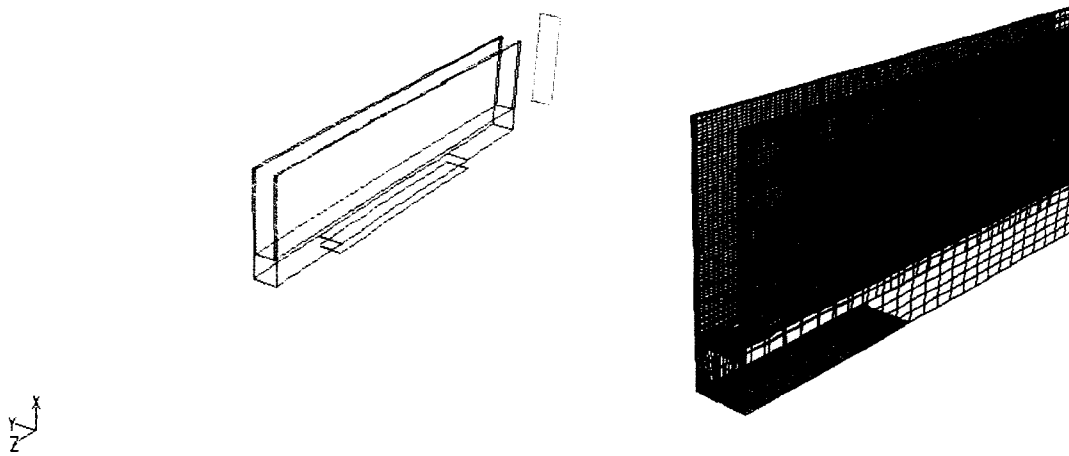


Figure 5.20: Model geometry (left) and heat sink mesh (right)

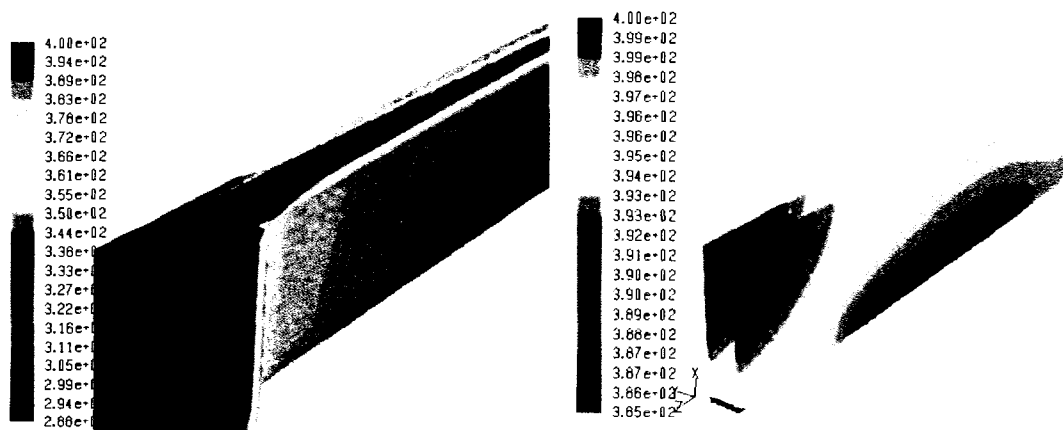
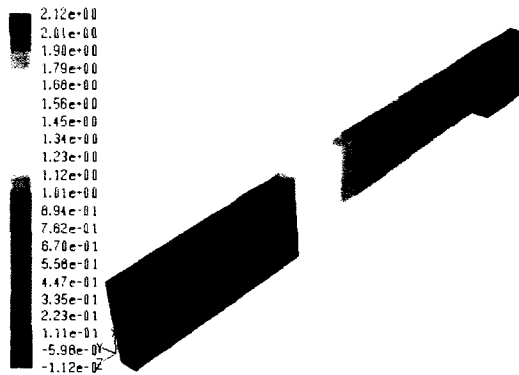
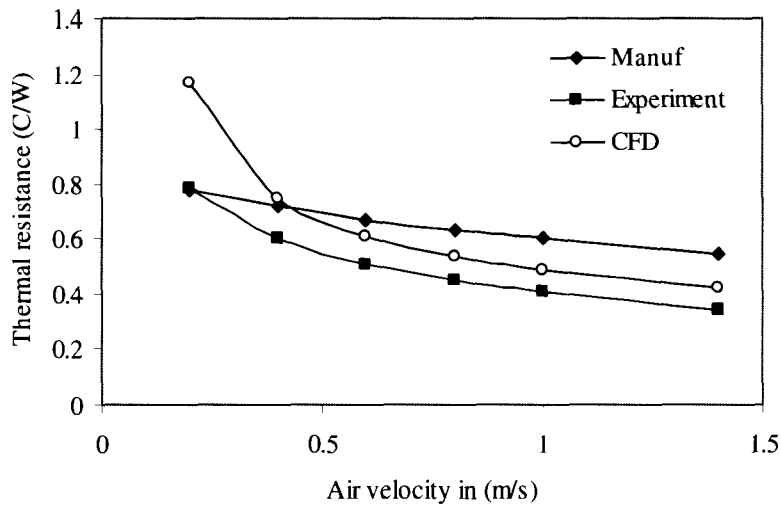


Figure 5.21: Temperature contours (in Kelvin) of air entry region (left) and fin temperature (right)



**Figure 5.22: Contours of pressure (Pa) from the CFD model**

The results from the CFD model are compared to those from the experiment and the manufacturer data in Figure 5.23(thermal resistance) and Figure 5.24(pressure drop). The thermal resistance results from the CFD are in pretty good agreement with the experiment, although they are approximately 20 % higher. Overall the trend is very accurate, especially compared to the manufacturer data. The pressure drop predictions are a bit off from the experiment, with an average error of about 25%. However, the overall trend is very accurate. Possible sources of error in the model could be the laminar model, idealized boundary conditions, mesh refinement and solver settings. Sources of error in the experiment could include non-uniform velocity, turbulence and pressure measurement errors. The pressure transducer used for the experiments was the smallest value available of .1” H<sub>2</sub>O, while the readings varied from .0015 to .016 “H<sub>2</sub>O. Clearly the measurements of pressure could have significant error at these values.



**Figure 5.23: Comparison of CFD results and experiment for thermal resistance**

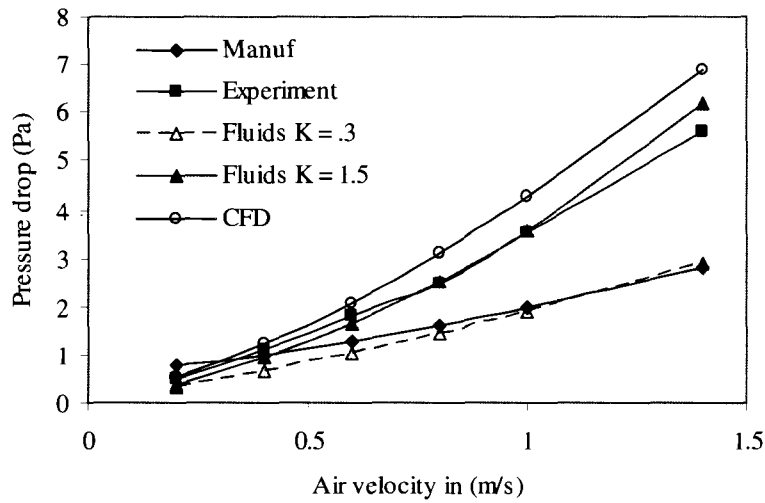


**Figure 5.24: Comparison of CFD results, experiment, and fluids equations for pressure drop**

Although the CFD model was not in exact agreement with the experimental results, it was considered good enough to investigate the effect of the gas temperature on thermal resistance. As the temperature of the gas increases its density is reduced, while its conductivity, specific heat and viscosity are all increased. The model was

run with three sets of input conditions (600 C gas--300 C module, 400 C gas—200 C module, 100 C gas— 0 C module). The results from this study are shown in Figure 5.25. The effect of temperature on thermal resistance is significant, especially at low velocities. There could also be an effect of the total heat flux on the thermal resistance. At higher temperatures the heat flux is higher. This effect was also captured in the model by the selection of the module temperature.

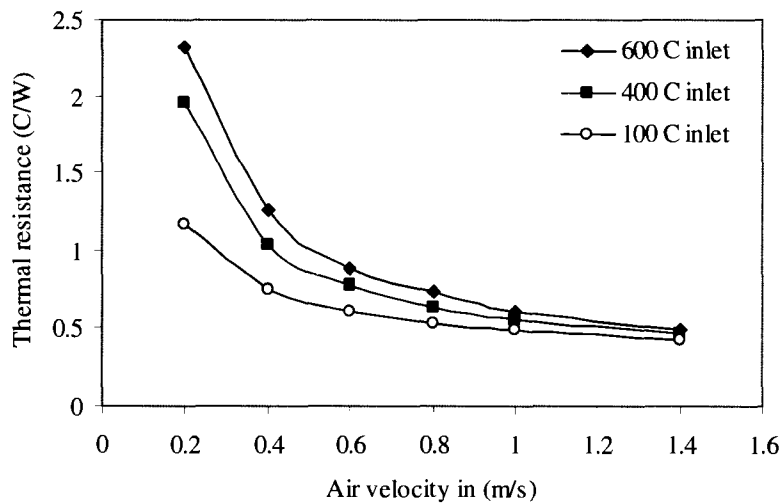


**Figure 5.25: Effect of hot gas temperature on thermal resistance**

To compare the values from the CFD to those from the field test data, the velocity of the gas through the heat sink at each hot gas temperature was required. To make this calculation, the mass flow rate through the stove at each hot gas temperature must be known.

Since the flow rate was not recorded during the field test, an experiment was run in the lab to see if the flow rate could be correlated to the hot gas temperature measured. To measure mass flow, a shroud was placed on the stove inlet to seal

against an anemometer (Figure 5.26). The velocity through the anemometer was measured and used to calculate mass flow rate. The velocity measurements taken with the anemometer were then correlated to a mass flow rate using a similar setup while measuring the flow through a Micro-Motion coriolis mass flow meter. Although the anemometer could effect the flow rate by adding a restriction, this was still considered the best option available for measuring mass flow at such low velocities. The flame within the combustion chamber was observed when the anemometer was placed on the inlet, and no visible change in the flame, temperature or smoke could be observed. Unfortunately, there was not a good correlation between the measured temperature and the flow rate as shown in Figure 5.27. This is due to the fact that there is a significant thermal mass in the stove and chimney after where the temperature measurement is taken. The flow rate through the stove is governed by the temperature difference between the inlet and outlet, and the pressure drop at every point in between. The added thermal mass beyond the heat sink causes the temperature at the outlet of the chimney to lag behind the temperature at the heat sink. Fortunately, all the stove flow rates were within a fairly narrow band so for modeling purposes the average value of 4 g/s was used (2 g/s to each heat sink).



**Figure 5.26: Stove fitted with inlet shroud for anemometer readings**

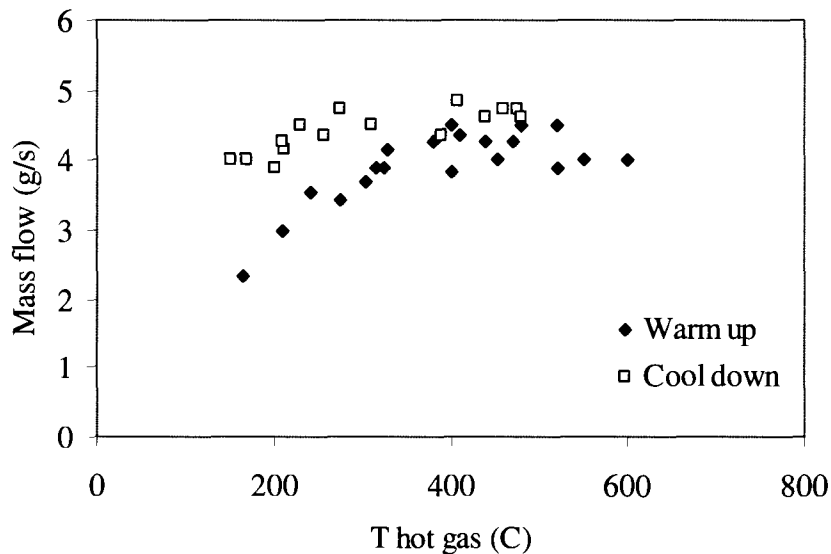


**Figure 5.27: Stove flow rates vs. the hot gas temperature**

Given an average mass flow rate of 2 g/s per heat sink, the predicted thermal resistance from the CFD model was compared to the field test data. The comparison is shown in Figure 5.28. It is encouraging that the CFD results also show a nearly linear thermal resistance at the different flow temperatures, even through the curves are very different. Overall the prediction from the CFD is approximately 15% lower than the field test data. It is also understood that gas composition will have an effect on the heat sink thermal resistance. This has been left as a topic for future work.

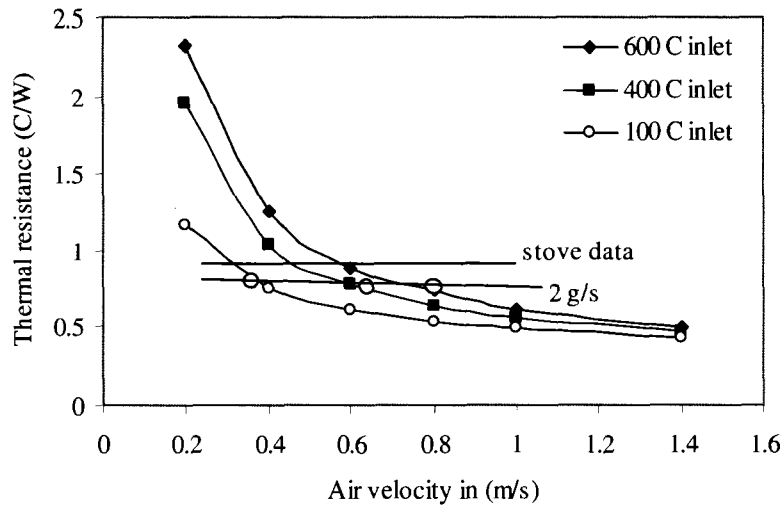


**Figure 5.28: Comparison of field data and CFD data at 2 g/s flow rate**

### 5.1.5 Charging Circuit Characterization

The charging circuit was characterized as in Section 2.4.1. The module was simulated with a power supply and an adjustable power resistor to represent the internal resistance of the module. The resistance was varied according to the open circuit voltage to match the results of the module tests. At each open circuit voltage value the maximum possible power, actual power in and actual power out were calculated. From this the efficiency in (maximum possible power / actual power in) was calculated. This quantity is a measure of how well the charger keeps the module near the peak power operation. The DC-DC converter efficiency was also calculated as the power out to power in. This efficiency is primarily reduced by resistance losses through the inductor, MOSFET, and capacitors. An example of a charger characterization is shown in Figure 5.29 for the original charging circuit with a 40 mOhm current sense resistor.

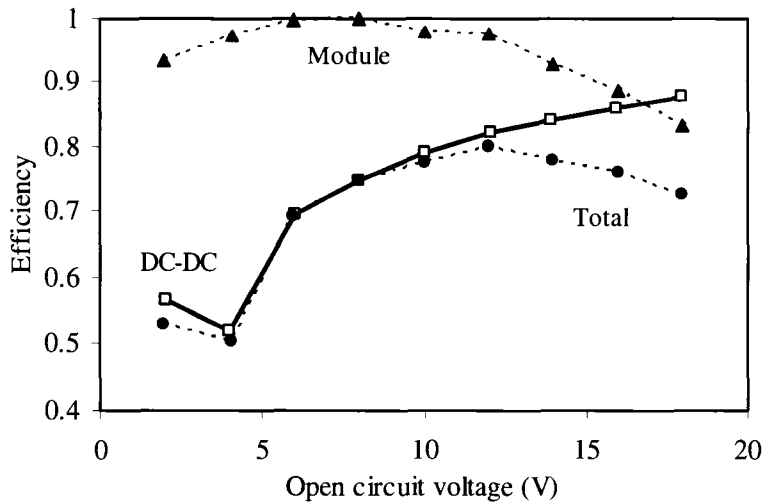


**Figure 5.29: Charging circuit characterization for original circuit with 40 mOhm current sense resistor**

### 5.1.6 Stove Temperature Characterization

In order to incorporate the stove into the system model, the hot gas temperature and mass flow rate through the stove were required. The temperature data was taken from field test data. The hot gas temperature over a five-week period was analyzed to create a “typical day” temperature profile. This was necessary for modeling purposes to convert the 10,000 points of data over five weeks into a more manageable number. Initially, the goal was to create an average cooking cycle. However, the starting point, peak and duration of each cooking cycle vary. If many cycles are averaged, the resulting cycle becomes close to a flat line at the average stove temperature, as shown in Figure 5.30. This method loses the temperature information (specifically the peaks) and results in a cycle that is not representative of any of the individual cycles.

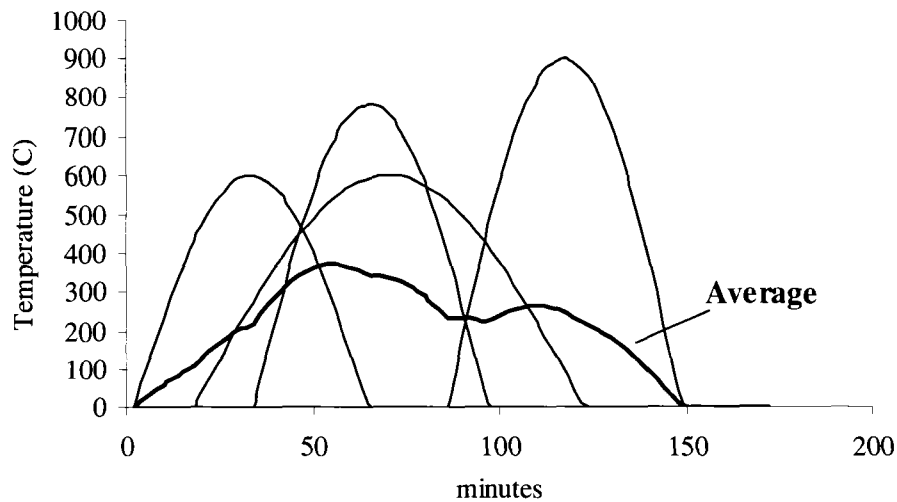


**Figure 5.30: Averaging multiple cycles**

In order to maintain as much temperature information as possible and still come up with a representative daily profile, a temperature histogram was created. Over the five-week period, the total number of minutes spent at a particular temperature interval was calculated. These values were then divided by the number of days. The temperature histogram for House #7 and House #8 from Nicaragua, as well as their average, is shown in Figure 5.31.

From the temperature histogram, an average daily cycle can be created that preserves all the temperature information and combines it into one cycle. This is accomplished by inverting Figure 5.31, dividing the times in half and creating a mirror image. In this case the time values are added to give the total cycle time, which comes out to be about 10 hours since the cool down periods are also included (down to 40 C). The average cycle and resulting hot side temperature using the generation 1 system is shown in Figure 5.32. The resulting net power from this cycle

is shown in Figure 5.33. In reality, the peak of 17 W is never achieved due to thermal capacitance of the system, and is closer to 15 W.

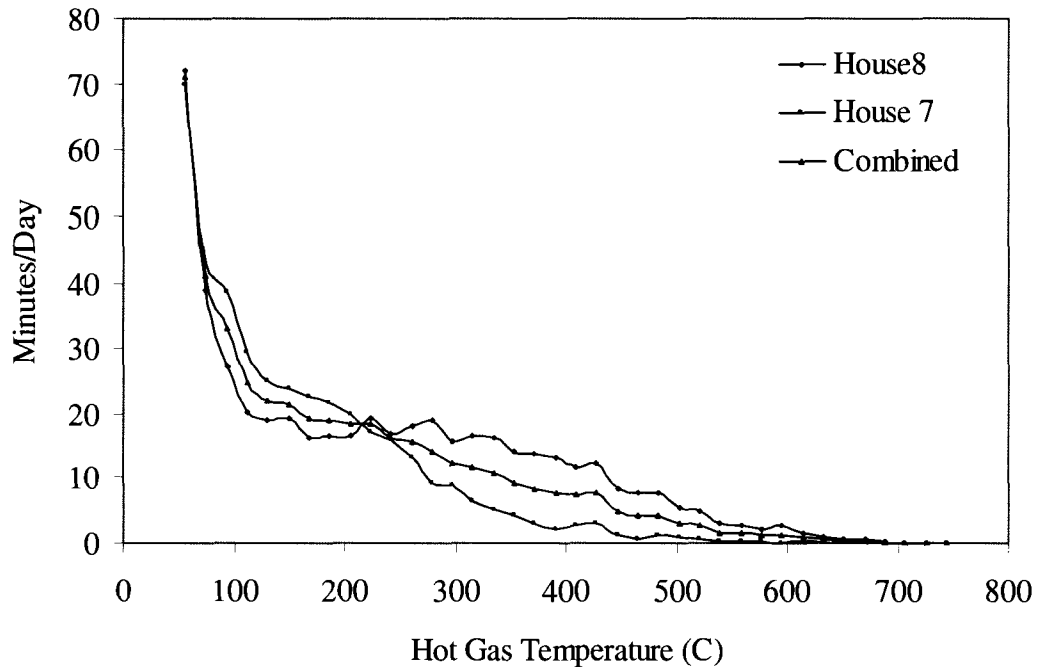


**Figure 5.31: Temperature histogram for Nicaragua field test data**

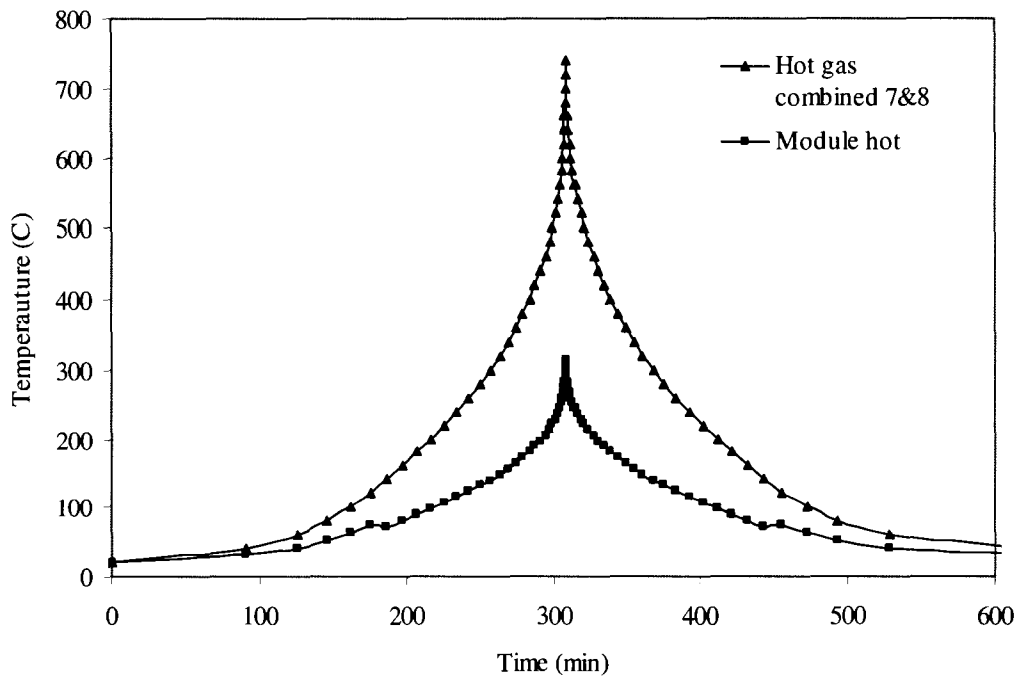


Figure 5.32: Average daily cycle for Nicaragua House 7 & 8

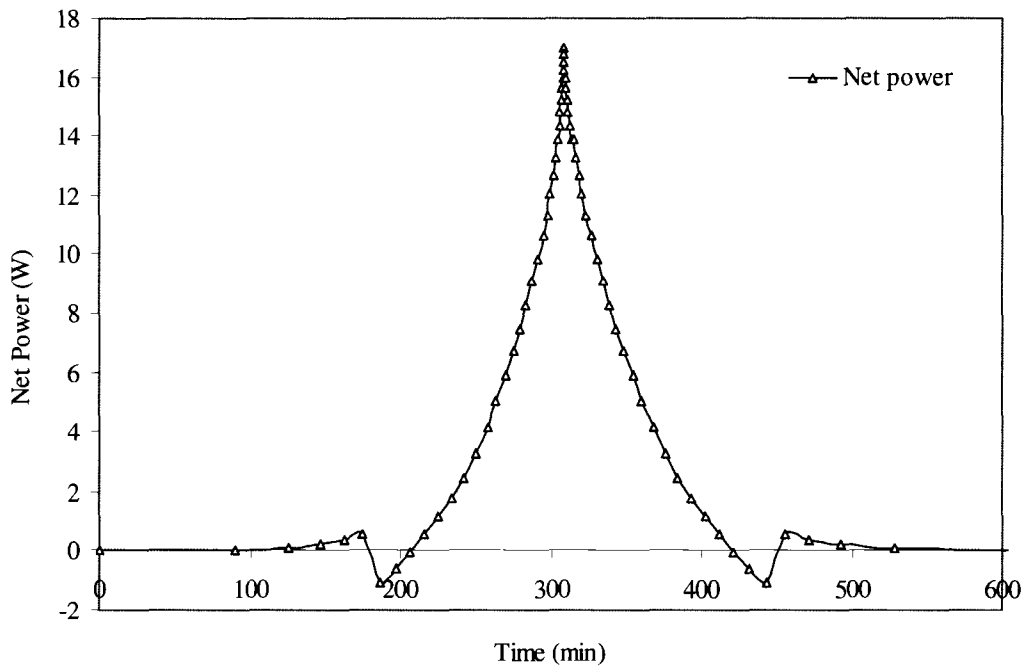
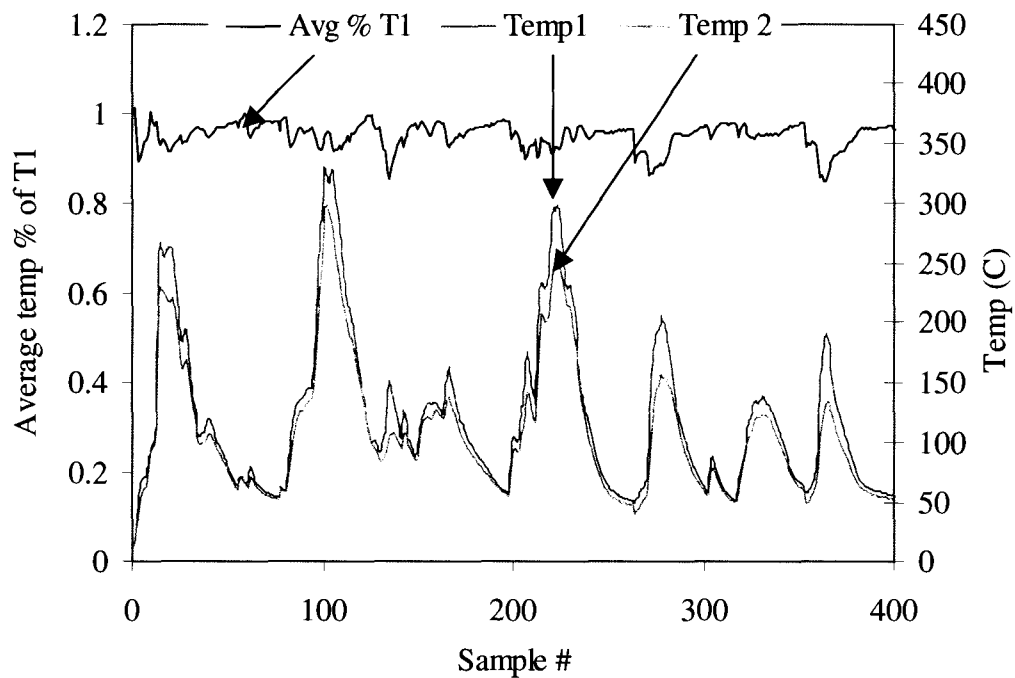


Figure 5.33: Resulting net power for average daily cycle

During stove testing, it was noticed that the temperature of the two hot-side heat sinks could vary significantly due to uneven temperature and flow distribution within the stove. From previous data taken from India where temperature on both hot-side heat sinks was measured, a significant difference was observed. Over two weeks of data, the average temperature was approximately 95% of the measured temperature (Temp1). This also has implications in the design of the generator, since one heat sink can be 10% hotter than the other. It will be important to include measures in the next stove design to create a more uniform temperature between the two heat sinks to maximize power without damaging one of the modules.



**Figure 5.34: Average temperature as a percentage of Temp 1**

## 5.2 System Model Architecture

Once each component in the system had been characterized through a bench test or model, they were combined in a comprehensive system model. The system model simultaneously solved all the governing equations for the thermal and electrical portions of the system. This was necessary to capture the non-linear effect of temperature on the module properties and the affect of the module properties on the charging circuit. The model was written in EES (Engineering Equation Solver) where the module properties, heat sink properties, charger properties, stove properties, etc. could all be included in subprograms or parametric tables that could be called by the main solver. The solver would then solve the system of equations simultaneously while calling the component subprograms. A schematic of the solver portion of the program is shown in Figure 5.35.

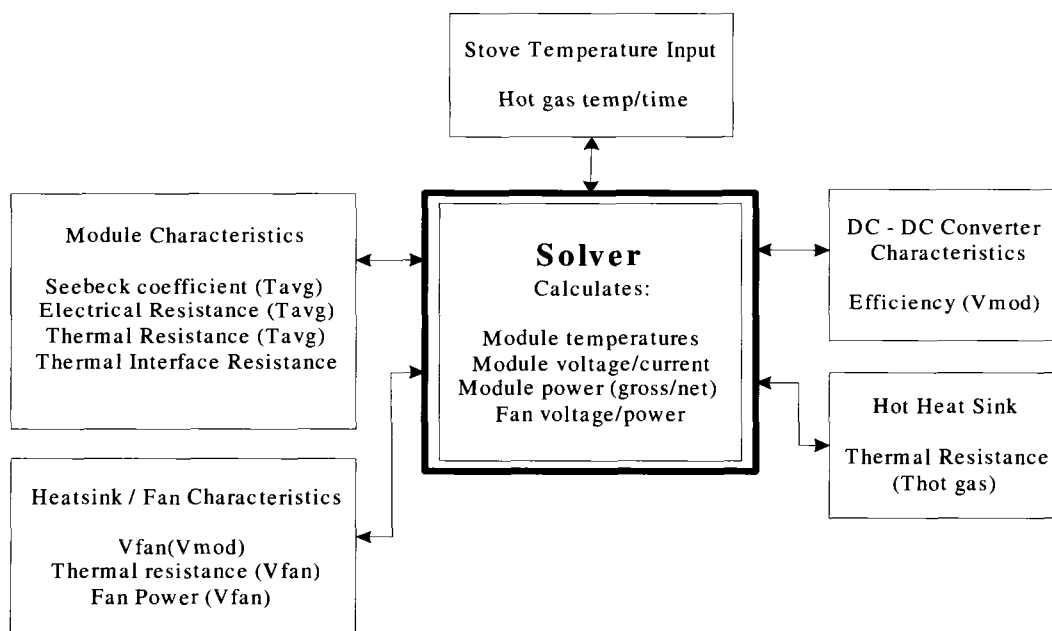
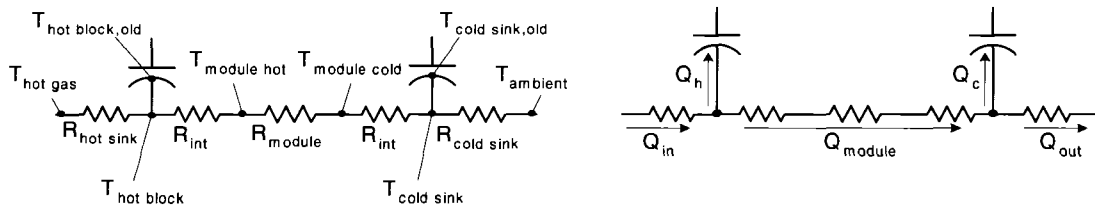


Figure 5.35: System power/temperature solver schematic

To solve the thermal portion of the system a thermal resistance circuit as described in Section 2.2.3 is used. For transient analysis, a series of capacitors were added to the thermal circuit to represent the thermal mass of the heat sinks. Since most of the mass is in the heat sink base, the capacitors were placed at the module hot and cold side temperatures. The revised thermal circuit with capacitance is shown in Figure 5.36. To solve the equations for the transient circuit, the temperatures from the previous iteration were used as the temperature at the capacitor. To solve the thermal circuit, a set of equations for the heat flux into and out of each node were written, along with equations for the flux of energy into and out of the entire system. The flux of energy between each node was governed by the thermal resistance between the nodes for the resistors. For the heat flux to the capacitor, the heat flux is proportional to the thermal mass ( $m \cdot C_p$ ) and the temperature difference between the nodes.



**Figure 5.36: Thermal circuit with capacitance**

### 5.3 Model Validation

To validate the system model, the hot gas temperature from field test data was fed into the model and the computed power levels and system temperatures were compared to the measured values. The model was run with and without the thermal

capacitance model. Due to the complexity of the hot sink thermal resistance as described in Section 5.1.4, a constant value for the hot side heat sink of .88 was used for validation of the model. The actual hot and cold side temperatures using the model are compared to those from the field data in Figure 5.37. The hot gas temperature is the only input to the model. A comparison of the model with and without thermal capacitance is shown in Figure 5.38. Overall the agreement is very good, and the thermal capacitance model does a good job of smoothing out the extreme peaks seen in the hot gas data. The errors in the hot gas temperature are due to the assumption of a constant hot sink thermal resistance, and due to the hot gas temperature samples being five minutes apart.

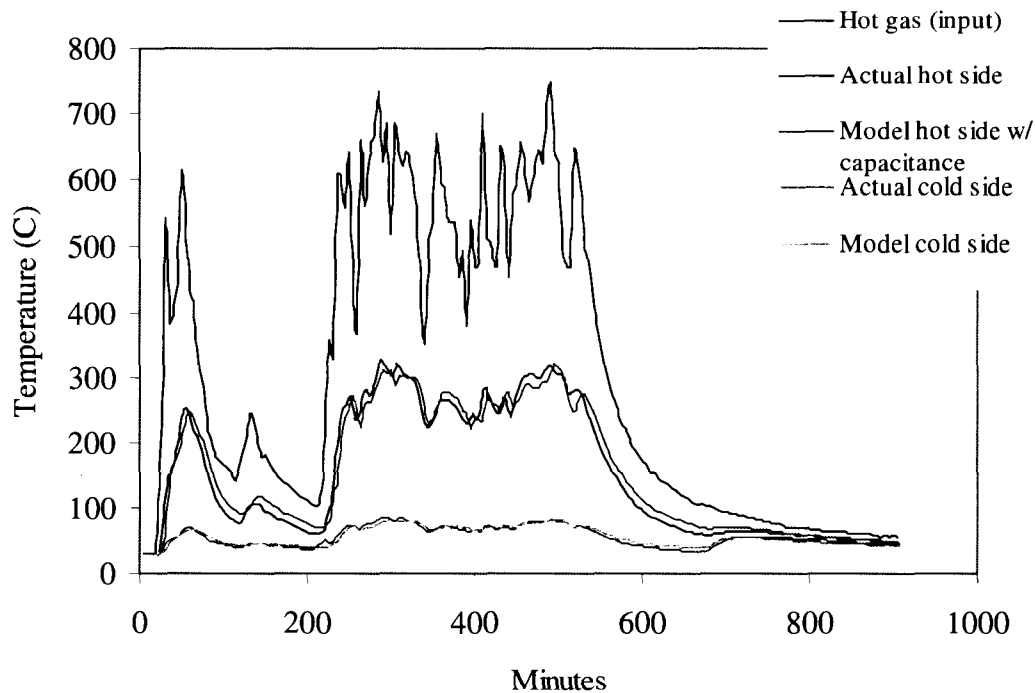
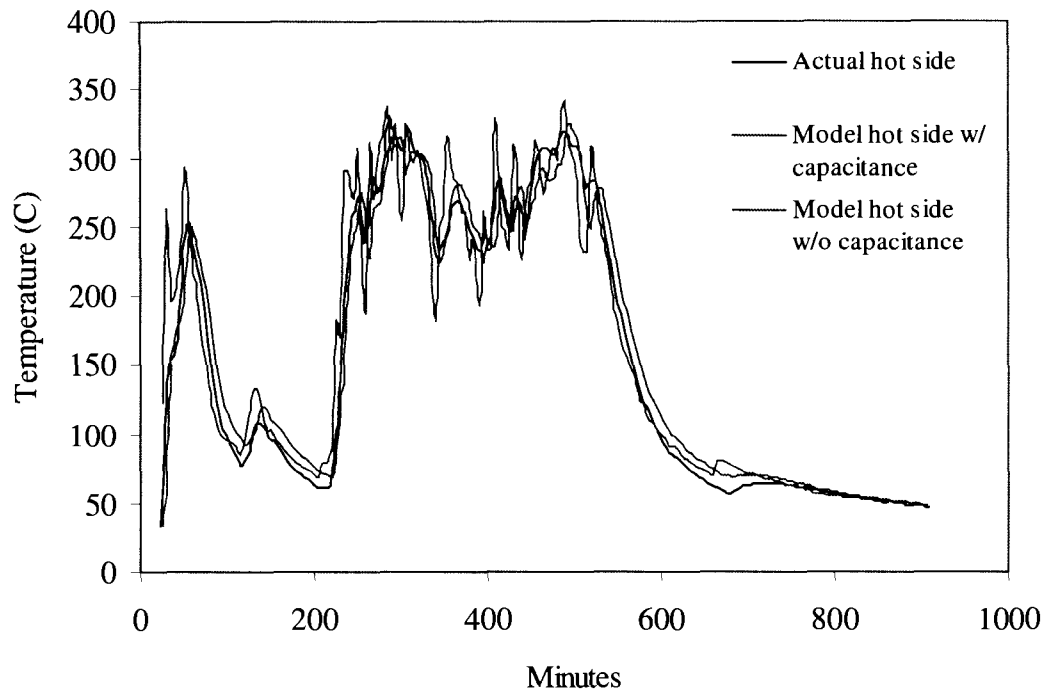
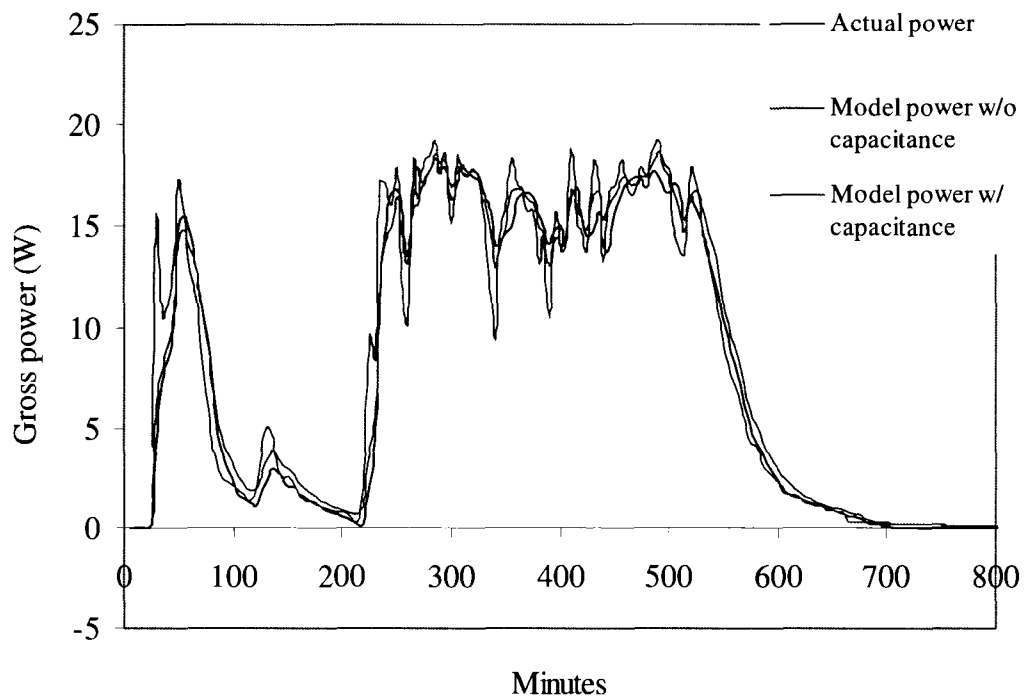


Figure 5.37: Comparison of hot and cold side temperatures using hot gas data



**Figure 5.38: Comparison of model with and without thermal capacitance**

With good agreement on the temperature data, the power data was examined next. The actual power from the logger and the model results (with and without thermal capacitance) are shown in Figure 5.39. The agreement between the field data and the model are very good, especially with the thermal capacitance model. The error in power is neither consistently high nor low, and follows the error in the predicted hot side temperature. Therefore, the only significant source of error in the model is the simplification of using a constant value for the hot sink resistance. Even with this error in the hot sink model, the overall energy calculation is very accurate both with and without thermal resistance, as shown in Table 5.3. Even the model without thermal capacitance makes a good energy prediction since the peaks and troughs tend to cancel each other out.



**Figure 5.39: Gross module power from field data and from the system model**

**Table 5.3: Model % error on total energy with and without thermal capacitance**

	Gross Energy (W-hr)	% Error
Actual Measured	104.6	
Model w/capacitance	108.4	3.7%
Model w/o capacitance	107.1	2.5%
Net Power	70.5	N/A

With good agreement demonstrated between the field data and the model for a single day, the next step was to see how accurate the model would be when predicting the energy generated over a week or month using the temperature histogram method described in Section 5.1.6. For this calculation the energy associated with each hot side temperature, and time spent there, is added up for the entire week. Given the

input as shown in Figure 5.40, the error in the predicted energy value was only 1.7%. This is a very good agreement, and validates the model as well as the histogram method for making energy calculations. This calculation is even more accurate than for the single day, possibly due to the averaging of data over many days. For all subsequent modeling, this was the method used to estimate the effect of improvements and predict energy generated over the life of the system.

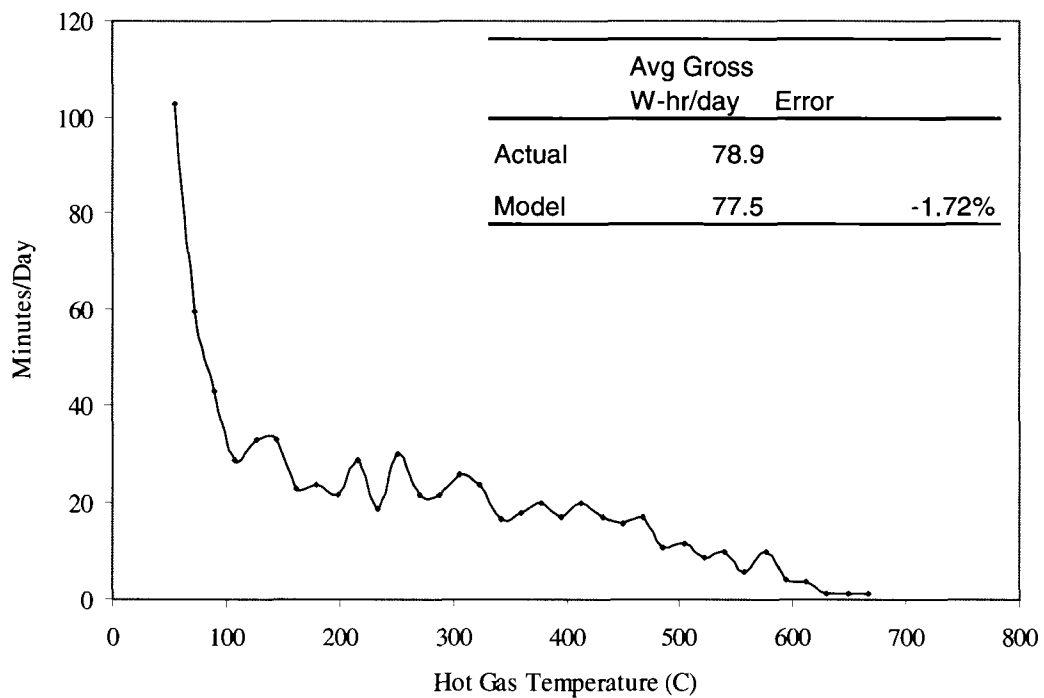


**Figure 5.40: Temperature distribution during week 1 with average energy per day (House #8)**

## 6 Generation 2 Circuit Design

Of all the system components, the circuit was seen as the one with the most potential for improvement with the least amount of added cost. After analyzing the field test results, a number of critical design modifications to the circuit were recognized. These were:

- Integration of charger, signal conditioner, and meter
- Peak power tracking
- Variable fan control
- Hysteresis on startup, buzzer and light control
- Adaptive battery capacity adjustment
- Low power operation

### ***6.1 Peak Power Tracking***

In the first generation circuit, the current to the battery was controlled by the value of a current sense resistor in the circuit. Although the current limit could be set to give maximum power through a small range of temperatures, it could not maintain peak power operation throughout. To maintain peak power through all operating temperatures, an active method for peak power tracking (PPT) was necessary. Peak power tracking was accomplished through adjusting the duty cycle on the PWM signal driving the DC-DC converter. By varying the duty cycle of the converter, the output voltage of the circuit can be varied, affecting the voltage and current

demanded from the module. For control of the DC-DC converter, a microcontroller with hardware PWM and 10 bit analog-to-digital (A/D) conversion was used (Microchip PIC-16F886). For current measurement, a 5 V current sense amplifier was selected to amplify the voltage across a current sense resistor (Maxim 4173). A logic-level, n-type MOSFET (Fairchild FDU6680A) was selected for the DC-DC converter with a small on-voltage (2.5 V) and small on resistance (.007 mOhm).

Several methods were considered and tested for peak power tracking. These methods varied in the hardware requirements and in the PPT algorithm. The first method considered computed the power from voltage and current measurements. The duty cycle would be incremented and the new power would be calculated. If the power increased, the duty would be incremented in the same direction again. If the power decreased, the duty cycle would be incremented in the opposite direction. This method has been successfully employed by Gitano et al. [78], and is shown in Figure 6.1 (direct power control).

The direct power control method was adequate for achieving near peak power operation; however, there were several problems with the method. Significant error could be introduced into the power calculation from signal noise and by the resolution of the A/D conversion. This error was magnified at low voltage or low current operation. In addition, the error could be magnified since the voltage and current readings were multiplied. On average, the power would drift between 90% and 100% of peak power. In some cases, the PWM duty would settle near a local peak caused by noise/resolution errors that was significantly off of the peak power point.

An alternative, but similar, method to the direct power method was to control the PWM duty based on the current delivered to the battery as shown in Figure 6.1. This method was used by Eakburanawat and Boonyaroonate [77]. In this method, the power delivered to the battery is maximized rather than the power from the module. Since the voltage of the battery is nearly constant, the power is proportional to the current into the battery. This means only one A/D reading must be taken, reducing the effect of measurement errors. This method was a significant improvement over the direct power method. However, it was still susceptible to measurement error. Using this method the power would drift between 95% and 100% of peak power as shown in Figure 6.2. This method was also more accurate at higher voltages and currents, but still had significant error at these points as the circuit noise was increased at higher currents. Although this method may be capable of achieving 100% peak power operation through a better circuit design minimizing noise, alternative methods less sensitive to measurement errors were investigated.

The third method evaluated for peak power tracking was the open circuit voltage method. In this algorithm, the charger is turned off and isolated for an instant and the open circuit voltage of the module is measured. The charger is turned back on and the duty cycle is adjusted until the voltage of the module is exactly half of the open circuit voltage, achieving peak power operation. The advantage of this method is that the power is less sensitive to errors in the voltage measurement. For example, a 5% error in the voltage measurement still results in 99.7% of peak power. The disadvantage of this method is that the circuit has to be periodically stopped and re-started. If it is not stopped often enough, it may not be able to track the peak power

during transients. Further work would need to be conducted in order to determine the optimal frequency of the measurement. There may also be potential to damage circuit components from voltage spikes during stopping and starting of the circuit. This would also need further investigation before implementing this strategy long term.

The final method investigated was the load resistance method. In this method the module resistance is calculated based on the module voltage (this curve is programmed into the controller). The PWM duty cycle is then adjusted until the computed load resistance (based on the voltage and current measurement) matches the computed module resistance. Although the computed module resistance is incorrect when the module is not operating at peak power, the computed value sends the circuit in the correct direction. This method also shows a high tolerance for measurement error, being slightly better than the voltage based control. However, this method also has some disadvantages. Since the module resistance has to be programmed into the software, it is very specific to the particular module being used. This would mean a different programming would be required any time a different module configuration was used, making it less universal. More importantly, it would not account for variability between modules, and increasing module resistance over time. Therefore, the accuracy of this method would degrade over time with the module.

The advantages and disadvantages of each method are summarized in Table 6.1.

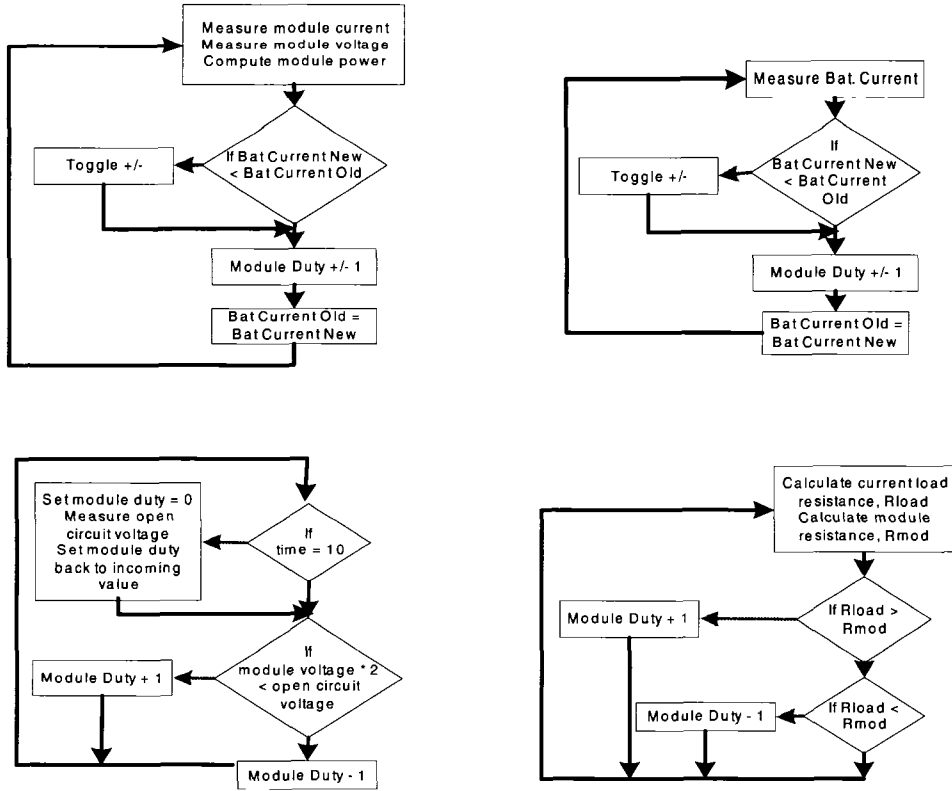


Figure 6.1: Peak power tracking methods. Clockwise from upper right: direct power control, battery current control, load resistance control and open circuit voltage control.

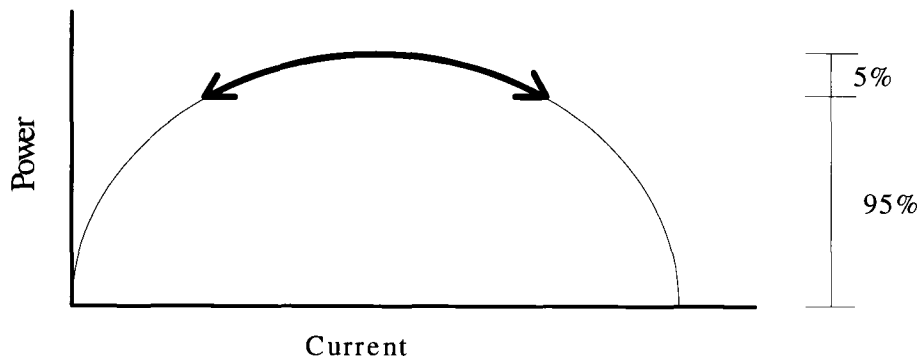
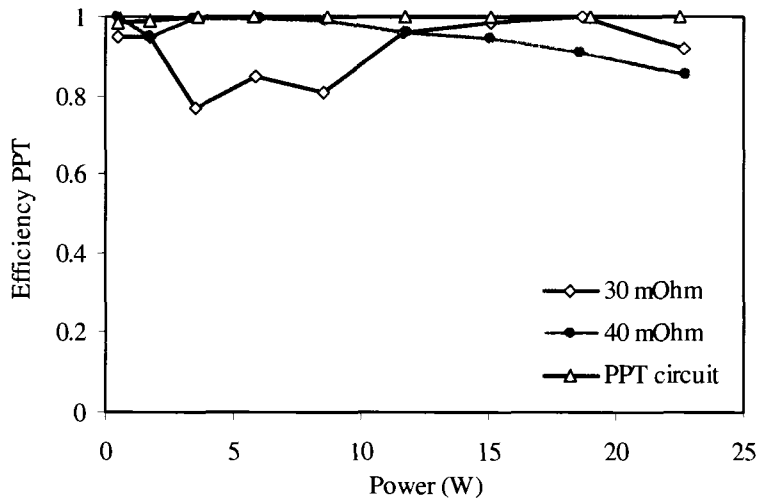


Figure 6.2: Power drift using battery current control

**Table 6.1: Comparison of PPT methods**

Method	Advantages	Disadvantages
Direct power control	Effective with changing module properties	High sensitivity to measurement error and measurement resolution
Battery current control	Requires only one measurement Effective with changing module properties	Moderate sensitivity to measurement error and measurement resolution
Open circuit voltage control	Does not require current sense resistor or amplifier Low sensitivity to measurement error Effective with changing module properties	Requires stopping the circuit which could lead to circuit damage
Load resistance control	Low sensitivity to measurement error	Module specific Does not track changes to module properties



**Figure 6.3: Peak power tracking effectiveness of PPT circuit compared to first generation circuit with 30 mOhm and 40 mOhm current sense resistors**

The results from circuit testing using load resistance control are shown in Figure 6.3, compared to the results from the first generation circuit. In order to achieve acceptable performance at module voltages below about four volts, it was necessary to configure the microcontroller to 10-bit resolution on the PWM duty cycle. It was found that an 8-bit resolution was too coarse, causing the circuit to bounce between values that were significantly (~20%) off of the peak power point. In order to achieve 10-bit resolution, the PWM frequency had to be reduced. The effects of PWM frequency are detailed on Section 6.2.

## ***6.2 Circuit Efficiency Optimization***

In addition to maximizing the power delivered from the module, it was also important to maximize the efficiency of the DC-DC converter by selecting the best components. The losses in the circuit arise from  $I^2R$  losses through the individual components. In general, the components with the lowest resistance possible were chosen. The critical components were the MOSFET, the capacitors, the diode and the inductor. Of these components, the inductor was the one with the largest resistance, and the largest affect on the circuit behavior. A larger valued inductor gives less ripple, which means less current into and out of the capacitors [79][80]. This improves the circuit efficiency and improves performance at low input voltages. However, larger valued inductors have more windings and larger internal resistance. At high current values, the larger inductor will result in less efficiency. Therefore, there is a tradeoff between low voltage efficiency and high voltage efficiency with

different inductor sizes. This tradeoff was examined using the peak power tracking circuit with different values of inductors. The points tested were for a voltage/current source equivalent to two TEP1-0.8 modules in series. The efficiency with four inductor values is shown in Figure 6.4 as a function of the module open circuit voltage and as a function of module current. From this figure, it can be seen that there is a consistent increase in efficiency on the low voltage and high voltage side from 38  $\mu\text{H}$  to 330  $\mu\text{H}$ . From 330  $\mu\text{H}$  to 1000 $\mu\text{H}$  there is little improvement on the low voltage end, and a significant loss on the high voltage end due to the added resistance of the inductor. For this particular module configuration, the 330  $\mu\text{H}$  inductor has the best performance, followed by the 100  $\mu\text{H}$  inductor.

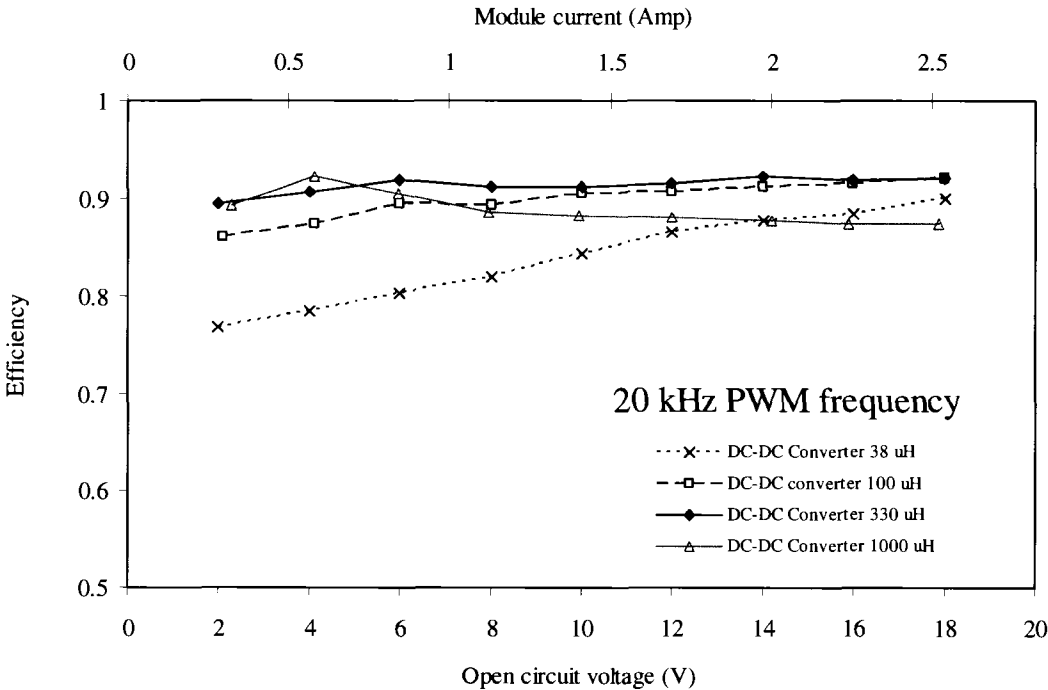


**Figure 6.4: Effect of inductor value on DC-DC converter efficiency**

The effect of the MOSFET PWM frequency was also investigated since it can have the same effect as increasing the inductor size, without the drawback of added resistance (REF). However, running at frequencies higher than 20 kHz with the microcontroller used, required the PWM resolution be reduced to 8-bit. This had a negative effect on the peak power tracking portion of the circuit. The frequency parametric study was performed first using the 330 uH inductors. The test was repeated using the 100 uH inductor to see if it would perform better than the 330 uH inductor if driven at the higher frequency. These results are shown in Figure 6.5 and Figure 6.6. In both cases, there was a significant increase in efficiency going from 4.8 kHz to 20 kHz, but little to no improvement going from 20 kHz to 78 kHz. Therefore, 20 kHz was used in the circuit to keep the 10-bit PWM. Also, the 330 uH inductor is still performing better than the 100 uH inductor even at the high frequency (78 kHz).

The final circuit efficiency at 20 kHz and 330 uH inductor is shown in Figure 6.7 compared to the generation 1 circuit. The total circuit efficiency (PPT efficiency + DC-DC converter efficiency) is shown in Figure 6.8.

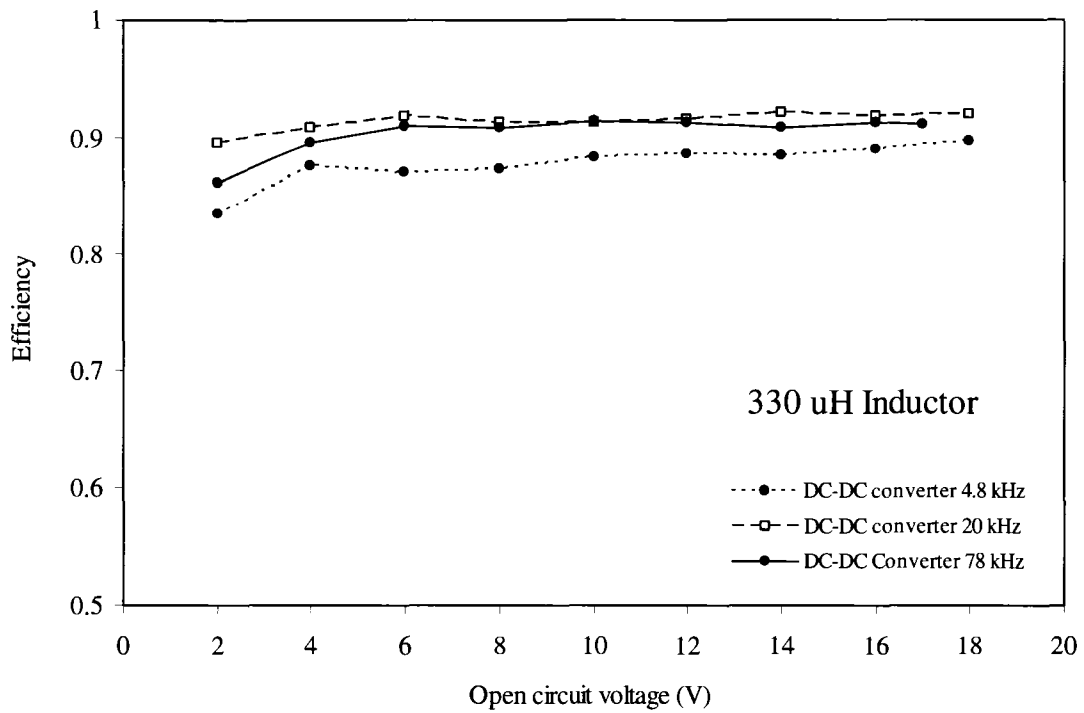


Figure 6.5: Effect of PWM frequency on charger efficiency (330 uH inductor)

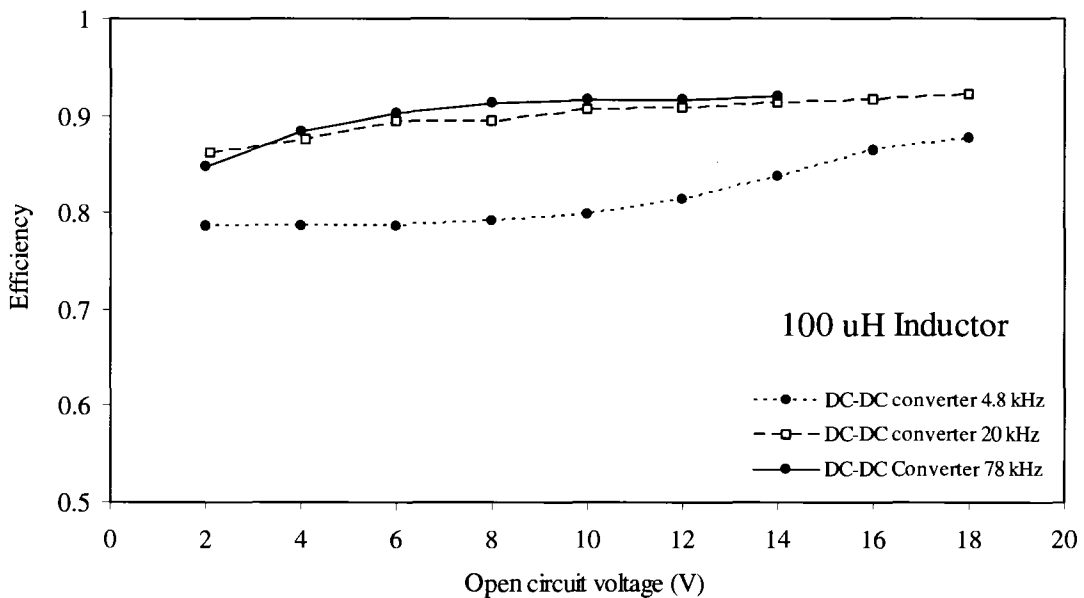


Figure 6.6: Effect of PWM frequency on charger efficiency (100 uH inductor)

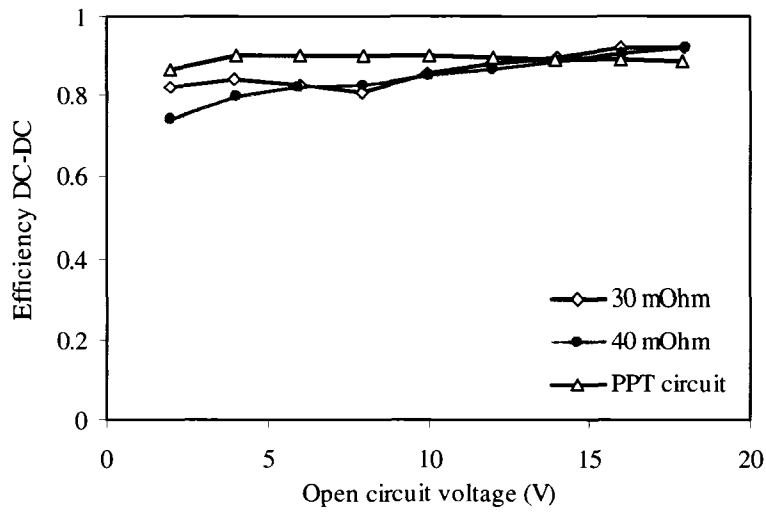


Figure 6.7: Comparison of Gen2 and Gen1 DC-DC converter efficiency

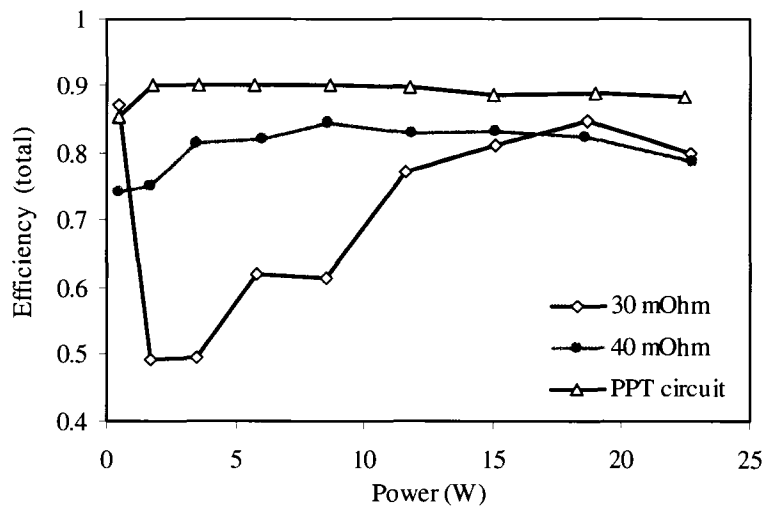
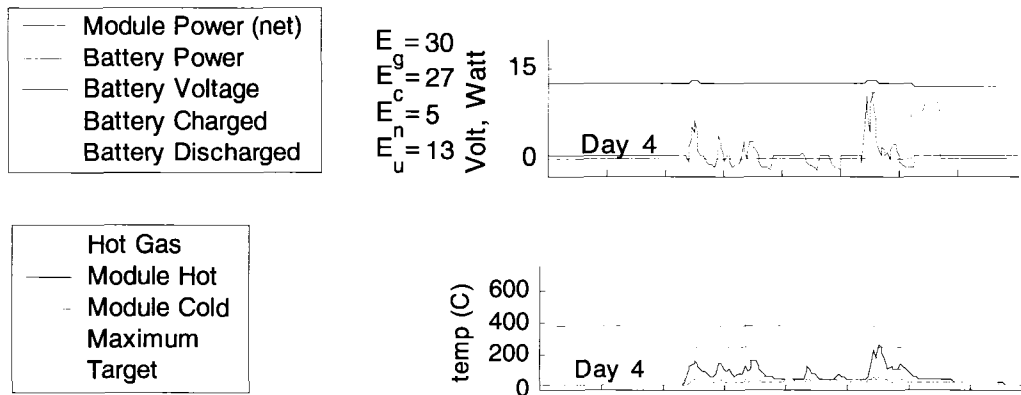


Figure 6.8: Comparison of Gen2 and Gen1 total circuit efficiency (PPT and DC-DC)

### 6.3 Variable Fan Control

From examination of the field test data, one of the largest opportunities for improvement was in the control of the fan. In many cases, the lack of precise control over the fan resulted in long periods of time spent at low or negative power. An

example of this is shown in Figure 6.9 where the stove was operated for the majority of the day at low temperature (hot side less than 150 C). Although 26 W-hr were passed through the charger, the net energy for the day was only 5 W-hr due to the power requirement for the fan.



**Figure 6.9: Example of continued low temperature operation leading to near zero net power (Nicaragua house 7, day 4)**

In the first generation circuit, the fan control was strictly on/off. The voltage to the fan was equal to the battery voltage, which could vary between 10 V and 13.8 V. At low module voltages, there is clearly an advantage to operating the fan at a reduced voltage or reduced duty cycle. The effect of fan voltage on net power from the system is shown in Figure 6.10 (2 TEP1-0.8 modules in series with 85% efficient DC-DC converter). Even with a fan voltage as low as 6 V, the net power at 40 C is negative. At 80 C, what would be a negative power at 12 V becomes positive at 6 V. Although the net difference is only 3 W, the stove can spend a very large amount of time at these conditions, especially when cooling down (see Figure 5.31). In addition to regulating the fan voltage, turning the fan on later and off sooner would also improve the net power of the module. However, with the fan off the heat sink thermal resistance is very large, and the voltage that can be produced with the fan off

thermal resistance is very large, and the voltage that can be produced with the fan off is very limited. If the threshold was set too high, the hot and cold heat sinks could continue to increase in temperature with little increase in the temperature difference. Also, when the fan is turned off there is a heat soak into the cold sink since the stove can still remain hot for a long time. After the fan is shut down there is a temperature spike on the cold sink as shown in Figure 6.11. The cold side of the module has a limitation of 160 C, due to the epoxy used to bond the elements to the ceramic wafer. Therefore, it is important to keep the cold sink below about 150 C on shutdown.

For the second generation circuit, the fan voltage was set to come on once the module could make enough power to result in net zero power. This gave the largest possible net energy over a cooking cycle. The fan voltage was also set to be a function of the module voltage. For a given module voltage, the program would calculate the optimal fan voltage. It would drop the voltage from the battery to the desired level through a buck-converter. The PWM duty cycle for the converter would be calculated based on the battery voltage and the desired fan voltage. The fan control portion of the circuit is shown in Section 6.8.

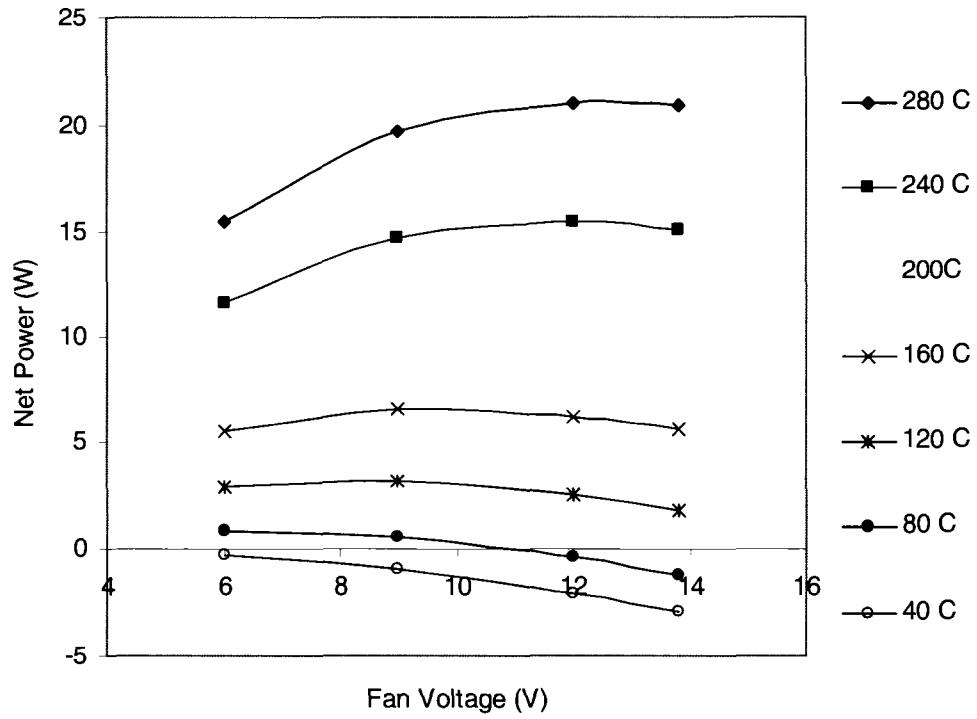


Figure 6.10: Net module power vs. fan voltage at various hot side temperatures (2 TEP1-0.8 modules in series, Thermaflo E1456 16.25 cm heat sink, Mechatronics fan, 85% efficient charger)

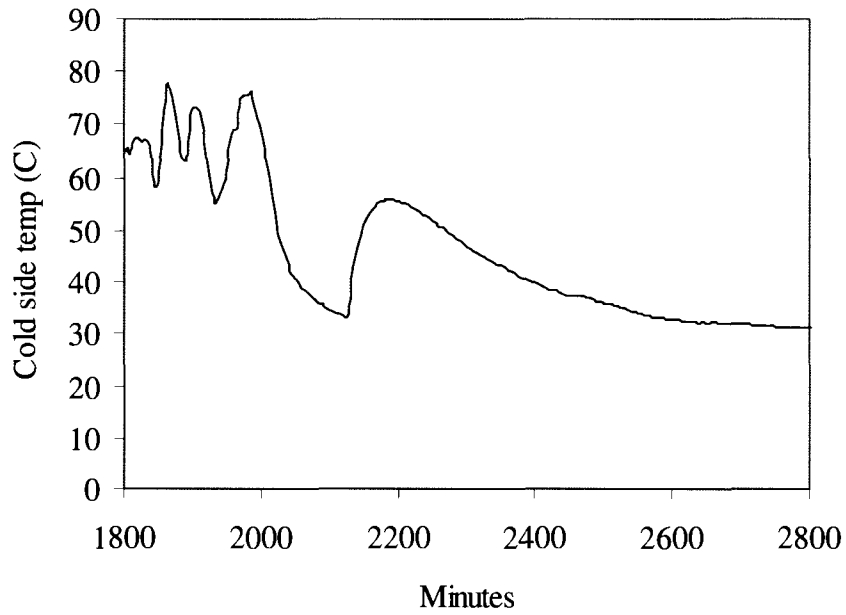


Figure 6.11: Example of temperature spike after fan is shut off on cool-down

## **6.4 Hysteresis**

Another important modification made to the circuit was the addition of Hysteresis thresholds on the battery management, and DC-DC converter startup/shutdown processes. In the first generation circuit, comparators were used to turn the buzzer/light/fans on and off. When the voltage reached these thresholds, the buzzer/light/fan would cycle on and off rapidly for a period of time. For example, when the light reached the threshold value it would be cut off, resulting in an increase in the voltage which would cause the light to come back on. This cycle would be repeated at high frequency until the battery was sufficiently drained. Similar effects were seen as the module voltage reached the threshold to turn the fans/charger on. As the voltage reached the threshold the circuit would turn on, dropping the voltage and turning the circuit back off. These oscillations were seen as nuisance and sign of poor quality. This effect could also cause potential damage to the components such as the circuit, fan or light.

For the battery, Hysteresis thresholds were created for the buzzer, light cutoff and charger cutoff. During charging the charger enters “charged = 1” state once the charged voltage threshold is reached. The charger is not turned on again until the battery voltage passes the “Hysteresis 1” threshold and enters the “charged = 0” state. This process is illustrated in Figure 6.12.

When the battery was being drained the buzzer and light cutoffs would be triggered at the same levels as before. Once the buzzer threshold was passed, the charger would go into “discharged = 1” state and the circuit would not return to

normal operation until it passed the Hysteresis 2 threshold and entered the “discharged = 0” state.

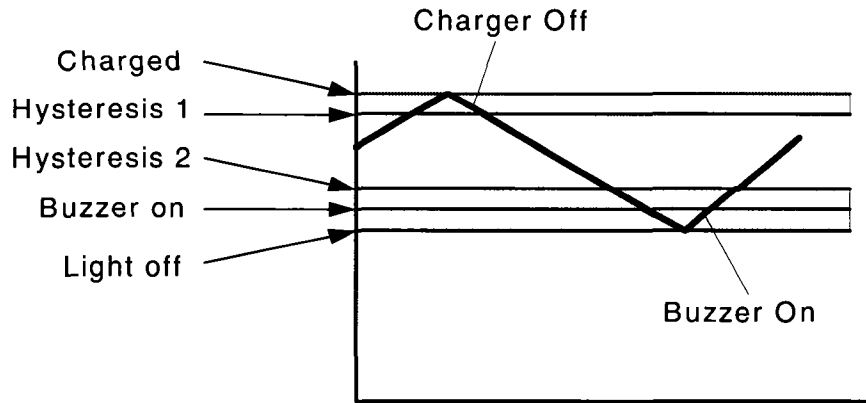


**Figure 6.12: Battery control Hysteresis**

A similar method is employed on the charging circuit to reduce bounce on startup and shutdown. The circuit will start in “ramp-up” mode, where it waits for the module voltage to reach the ramp-up threshold. Once this threshold has been reached the charger and fans turn on dropping the voltage. Once the charger is tuned on it will enter “ramp down” mode, where it uses the ramp-down threshold. This way, once the circuit comes on it will remain on. It was also important to limit the PWM frequency of the DC-DC converter on startup to ensure that the voltage would not drop below the ramp-down threshold once it was started. For two TEP1-0.8 modules in series and two Mechatronics fans coming on at 6 V, the ramp-up voltage was 2.4 V, the ramp-down voltage was 1 V and the maximum duty cycle was .927%.

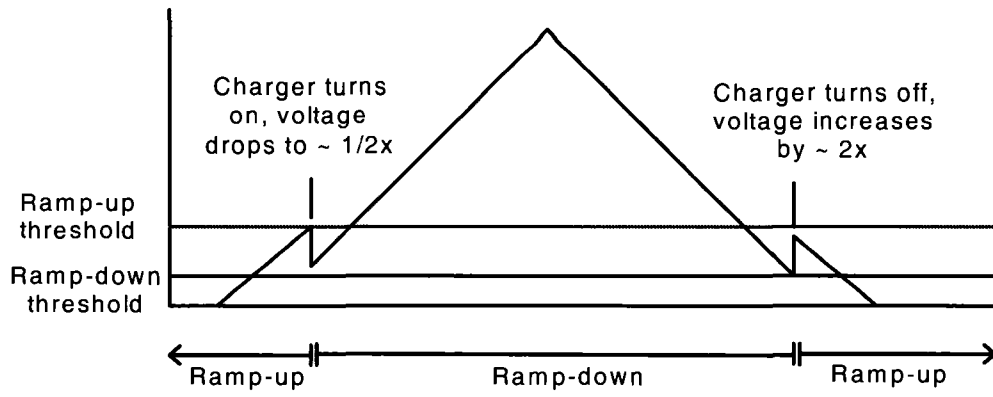


**Figure 6.13: Module start-up Hysteresis**

## 6.5 Battery Charge Control -- Adaptive Battery Capacity

The most consistent and detrimental failure observed during field testing was the failure of the battery. There were a number of causes for these battery failures identified by investigating the field test data. The first was caused by continuously partially charging the battery (Figure 6.14). It is well known that a lead-acid battery must be fully charged periodically in order to maintain battery [76]. There are a number of reasons why the battery never reached full charge. These are: too large of a battery, too low of a battery cutoff, lower than anticipated module power, lower than anticipated stove usage or light usage while the generator is running (directly powering device). Due to this multitude of potential causes, it is practically impossible to select a perfectly matched battery to prevent this condition without significantly under-sizing the battery.

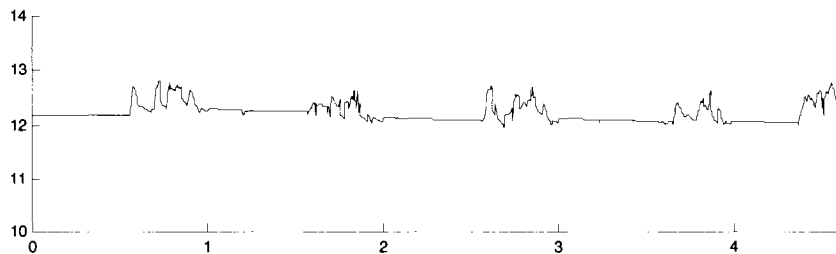


**Figure 6.14: Field data illustrating too large of battery capacity**

To get around this dilemma, an adaptive battery capacity concept was implemented in the second generation circuit program. The program works by monitoring whether the battery has reached full charge over the course of a day/week. If the battery is not charged, the cutoff threshold is moved up to increase the chances

of the battery being charged during the next cycle as illustrated in Figure 6.15. If the battery is consistently being charged, there is a chance that the threshold is too high, resulting in lost energy that could be stored in the battery. In this case, the battery threshold would be moved down as in Figure 6.16. The advantage of this algorithm is that it will adapt to the users power generation and usage habits, which can vary significantly from one house to the next even in the same region.

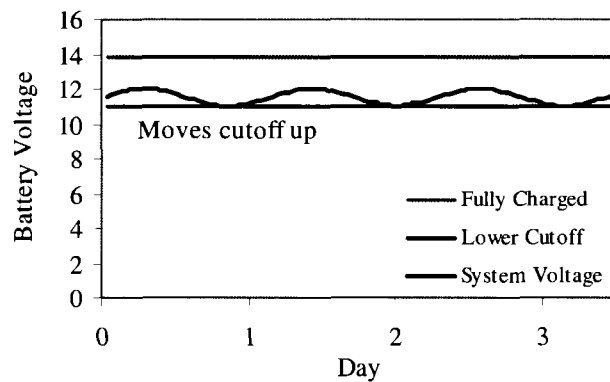


**Figure 6.15: Adaptive capacity concept -- threshold moves up**

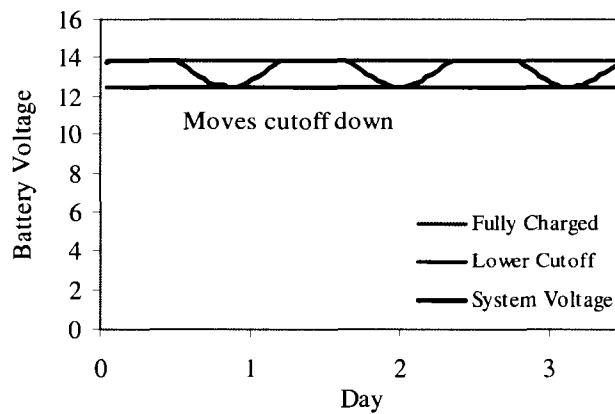


**Figure 6.16: Adaptive capacity concept -- threshold moves down**

Another cause of battery damage is over-charging. Although much less common in this round of field testing, there was one failed battery that was likely from over-charge (see Nicaragua House #3). With the two TEP1-0.8 modules in

series, the open circuit voltage could reach up to 17 V at open circuit. Once the battery is charged the current could drop, meaning the voltage from the modules could reach the open circuit value. When this happened the battery could be damaged since the charging circuit had no way to isolate the modules from the battery. In the generation two circuit a module isolation circuit was added through the use of a p-type MOSFET on the outlet of the DC-DC converter. To make the p-type MOSFET operate from a 5V signal from the controller, a voltage divider circuit in combination with a n-type MOSFET had to be used to create the desired gate-to-source voltage. This portion of the circuit is shown in Section 0. As with all circuit components in the module's current loop, a MOSFET with the lowest possible resistance was chosen to maximize the circuit efficiency.

The final cause for battery failure was substantial battery drain after the light had been cut off. This was due to high circuit operating power, and is covered in Section 6.6.

## ***6.6 Low Power Operation***

Another flaw of the generation one circuit that led to battery and generator failure was the excessive power draw of the charging circuit and the power meter. These components together consumed about 4 W-hr per day. Based on the initial calculations, it was estimated that around 40 W-hr a day would be generated, so the 4 W-hr consumed by the circuit would be relatively small. However, in most of the field tests the power generated was much less, and also included multiple consecutive days where the stove was not used (Figure 6.17)

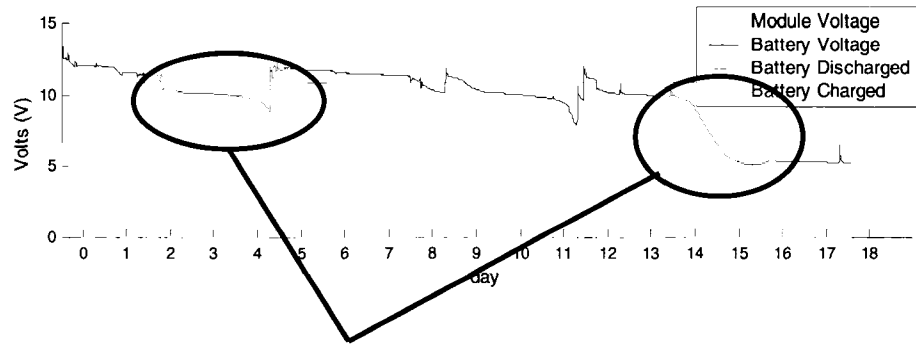


**Figure 6.17: Battery voltage drop from charger circuit power consumption over multiple days**

A component by component analysis was performed on the original and new circuit to determine where power savings could be made. The largest power consumers were the 5 V regulator, the amplifiers, the LEDs and the microcontroller. The original 5 V regulator was replaced by a ultra-low power regulator. In addition, since the new circuit combined the charger and meter circuits, one 5V regulator was eliminated.

The second generation circuit also utilizes a low power sleep mode to reduce power consumption when the charging circuit is not operating. In this case, the only function of the circuit is to monitor and control the battery functions. In this mode, the oscillator is switched from the 20 Mhz external oscillator to a 1 MHz internal oscillator. This reduces the power consumed by the controller from 8 mW to 1 mW. For the sleep mode, the amplifiers used for current measurements are switched off. This required that the 5 V power for both amplifiers be configured as outputs on the microcontroller. In sleep mode, the current sense amplifier for the battery is switched on briefly every second to take a measurement, and is then switched back off.

The result of these improvements to the circuit was a reduction in operating power to less than 1/10 the original amount as shown in Table 6.2.

**Table 6.2: Circuit improvements to reduce operating power**

<b>Old Meter + Charger</b>			
Component	Voltage	Current (ma)	Power mW
5V reg charger	12	2	24
5V reg meter	12	6	72
Amps	5	0.84	4.2
PIC 8 pin 4MHz	12	2	24
Diode leakage	12	0.7	8.4
LED 50% duty	3	2	6
Other			32
		Total (mW)	170.6
		W-hr/day	4.09

<b>New Meter + Charger</b>			
Component	Voltage	Values during "sleep mode"	
		Current (ma)	Power mW
5V reg	12	0.12	1.44
Amp1 10% duty	5	0.042	0.21
PIC 18 pin 1MHz	12	0.8	9.6
LED 10% duty	2	0.20	0.4
Other			2
		Total (mW)	13.65
		W-hr/day	0.33

## 6.7 Program Architecture

The controller program was written in the PICBASIC Pro programming language in Microcode Studio software by Micro Engineering Laboratories. Much of the program was written using PICBASIC commands to configure the controller's registers. However, configuration of the I/O, 10-bit PWM, and oscillator had to be done manually to get the desired functionality. The program code is presented in Appendix 12.1. A program flow chart is shown in Figure 6.18 where it is broken in to the three major components: battery management, peak power tracking, and the sleep/awake function.

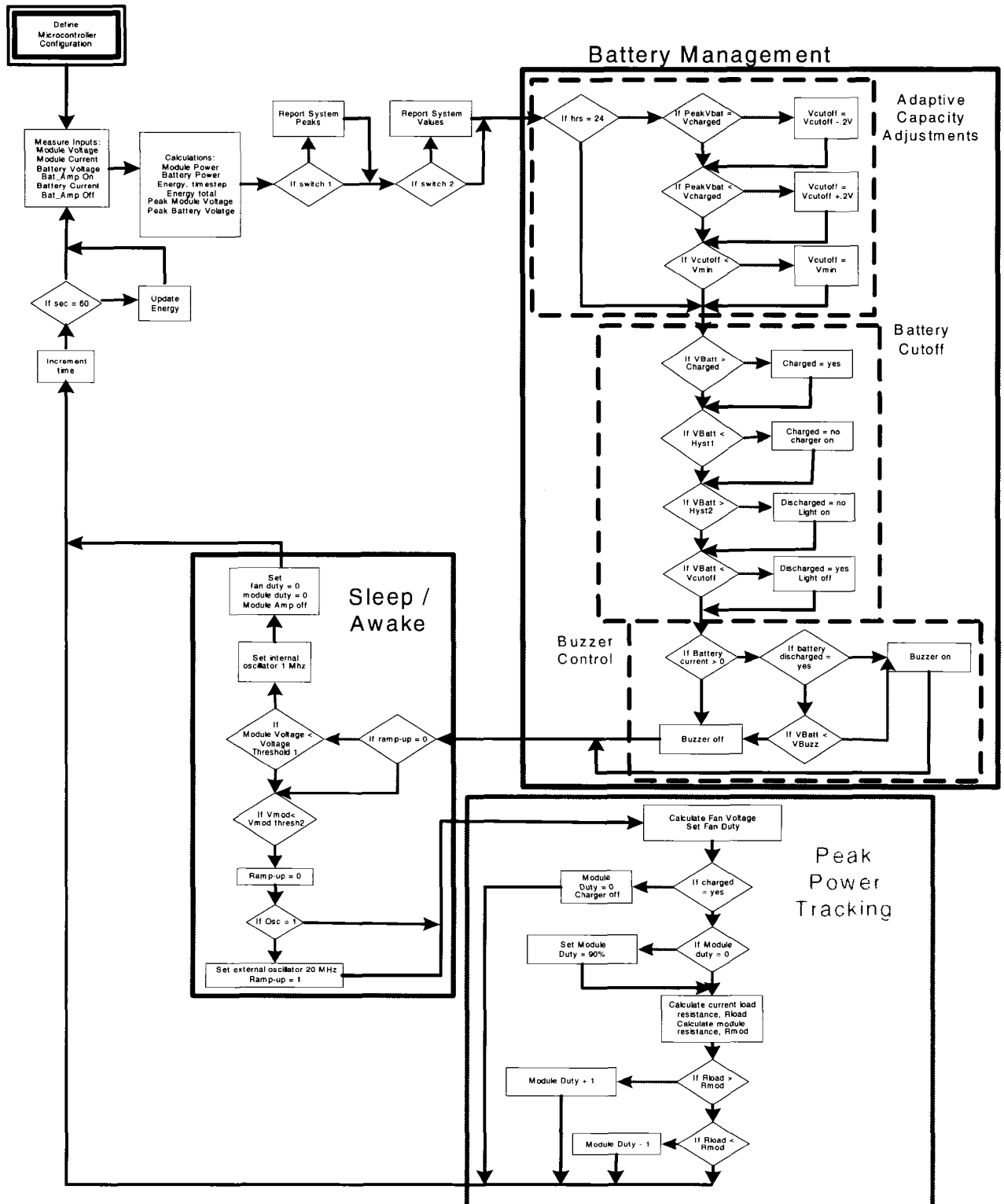


Figure 6.18: Program flow chart

## 6.8 Circuit Design

The circuit board was designed using Express PCB software. The board is a two layer board with the bottom layer being the ground plane to reduce signal noise. The board layout is shown in Figure 6.19, and the detailed circuit schematic is shown in Figure 6.20. The microcontroller chosen was the PIC16f886 by Microchip. The PIC16f886 is a 28 pin device with the necessary analog, digital and PWM channels for the controller program. The controller program requires the following I/O:

- 4 analog inputs
  - 1 for measuring module voltage
  - 1 for measuring battery voltage
  - 1 for measuring module current
  - 1 for measuring battery current
- 2 hardware PWM channels
  - 1 for driving the charger DC-DC boost converter
  - 1 for driving the fan control DC-DC buck converter
- 13 digital outputs
  - 2 for powering the current amplifiers
  - 2 for powering the red and green LEDs
  - 6 for driving the LCD display
  - 1 for the charger cutoff/module isolation
  - 1 for the buzzer control
  - 1 for the battery cutoff
- 3 digital inputs
  - 1 for the reset button
  - 1 for display setting #1
  - 1 for display setting #2

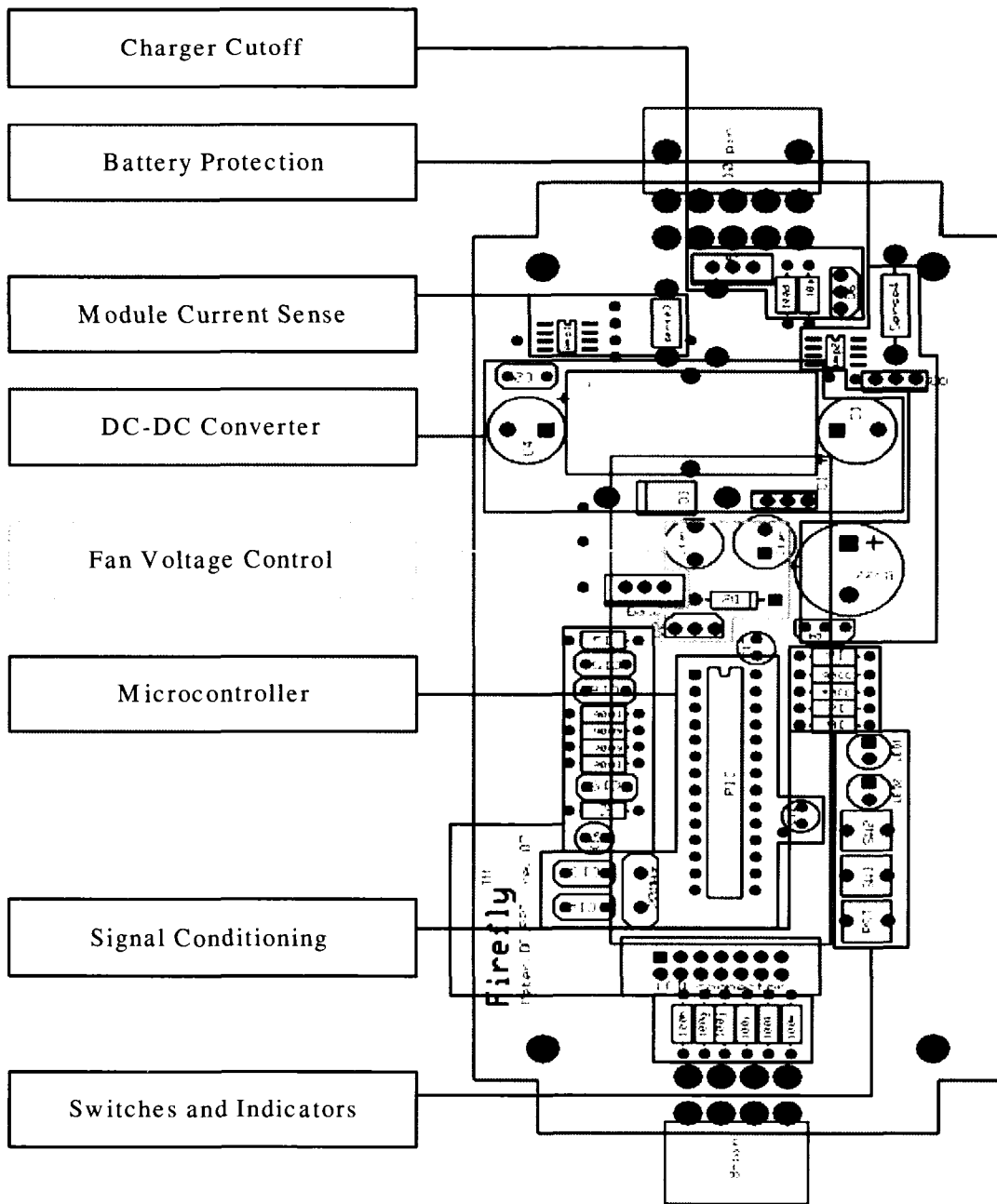


Figure 6.19: Generation two circuit elements and layout



## **6.9 Overall Net Energy Gains from Generation 2 Circuit**

The system level model was run to quantify all the improvements made between the generation 1 and generation 2 circuits. The model was run using the average daily temperature distributions for House#7, House #8 and the House #7&8 combined data to see how the different circuit improvements affect the two houses differently. The model was run starting with the original circuit (generation 1), and then run after adding each additional feature. The total energy percent increase was calculated after each component was added. By using this method, the percent change from each circuit improvement could change depending on what order they are implemented. However, it is believed this is the order these functions would be implemented based on the field test data. It should also be noted that the average daily temperature distributions include 1-2 days per week where the stove was not used. Therefore, on the days where the stove is used the energy values would be around 15% higher.

The first addition was the low power operation. As expected, for House #7 where the stove was not run as much or as hot, the low power operation more than doubled the net daily energy. The percent change on House #8 was much less since they were starting at a much higher net energy.

The second circuit addition was the variable fan control. As in the case of the low power operation, it had a much greater effect on the House #7 energy. This is due to the fact that House #7 spent a large amount of time at low stove temperatures where the original circuit would be near zero or negative power. With this addition,

the system can generate a significant net positive power at these conditions, increasing the energy generated by 79%. House #8 also saw an improvement, but not as much at 20%. This is because House #8 spent much more time at high temperatures.

The next circuit addition was peak power tracking (PPT). The increase due to PPT was surprisingly low. In fact, for House #7 it was near zero. The comparison for the two circuits (with and without PPT) is shown in Figure 6.3. Both House #7 and House #8 used the 40 mOhm current sense on the original circuit. With the current system, the peak power of the modules was about 16 W. At this point the PPT circuit generates about 10% more power. House #8 spent enough time at the higher power levels to see a 3% improvement from the PPT circuit. However, the over the range of 5-10 W, the generation 1 circuit and PPT circuits are the same. This is where the House #7 generator spent most of its time, so it saw no additional improvement from the PPT circuit. This should not be taken as evidence that PPT is not important. In this case, it is showing that the ability to set a current sense limit on the generation 1 DC-DC converter is very effective in approximating a PPT circuit. If the PPT circuit was compared to a DC-DC converter with no current limit, the PPT circuit would be dramatically better.

Finally, the optimized DC-DC converter with the new inductor, capacitor, and PWM frequencies was modeled. The new circuit gained 13% for House #7 and 6% for House #8.

In all, the circuit improvements had the most dramatic effect on House #7, which saw a 350% improvement in the net energy generated. This was expected

since most of the circuit improvements were made to improve the generators performance at lower temperature levels. The regions where this extra energy is generated is shown graphically in Figure 6.21 for the House #7&8 temperature distribution. This improvement is important in making the generator work for everybody, regardless of their cooking style. The new generator also significantly improved the energy generated for House #8, with a 50% increase in net energy.

**Table 6.3: Resulting energy gain for circuit improvements compared to original generation 1 circuit**

\*\* Values are average daily values, but include 1-2 days/week of no usage

Circuit Improvement	House 7+8 data			House 8 Data			House 7 data		
	Avg Gross W-hr/day	Avg Net W-hr/day	% gain	Avg Gross W-hr/day	Avg Net W-hr/day	% gain	Avg Gross W-hr/day	Avg Net W-hr/day	% gain
Original Circuit	29.5	11.39		42	20.24		17	2.54	
Low Power Mode	29.5	14.45	27%	42	23.3	15%	17	5.60	120%
Fan Optimization	26.2	19.00	32%	38.1	28	20%	14.2	10.05	79%
Peak Power Tracking	27.14	19.6	3%	39.7	28.8	3%	14.56	10.1	0%
New DC-DC components	27.74	20.7	6%	40.4	30.4	6%	14.86	11.4	13%
<b>Total Improvement</b>			<b>82%</b>			<b>50%</b>			<b>348%</b>

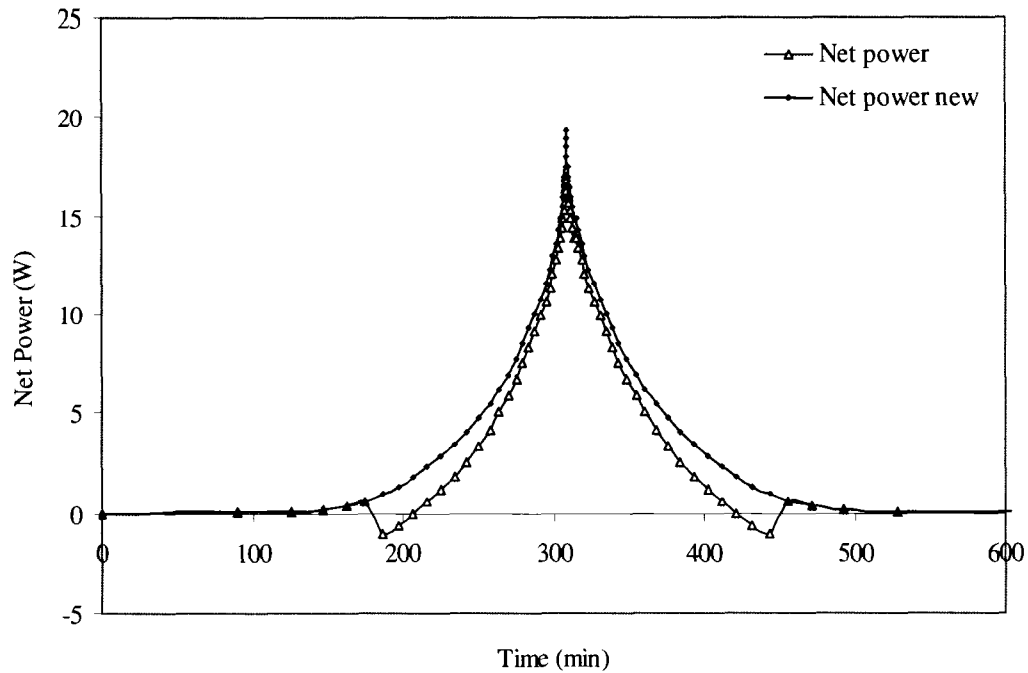


**Figure 6.21: Resulting net power for typical day (House 7+8) using generation 1 and generation 2 circuits**

## 7 Endurance Testing

### 7.1 Test Apparatus

For endurance testing, eight of the bench top module testers were constructed and incorporated into a Labview controlled system. A National Instruments (NI) PXI 1002 chassis with PXI 6225 and PXI 6025 I/O cards were used for data acquisition and temperature control. Hot block and cold sink temperatures were measured continuously on each apparatus, as well as ambient temperature. Cartridge heaters were used to heat the modules to the desired temperatures and 16.25 cm E1456 heat sinks with Mechatronics fans were used for the cold side of the modules. Cartridge

heater power varied from about 350 – 600 W, depending on the module type and maximum temperature. The heaters were turned on and off by activating 5V solid state relays through the NI system. The ramp rate of the heaters was controlled by regulating the heater power through dimmer switches in line with the heaters. Typical cycle time was kept around 30 minutes for a complete cycle.

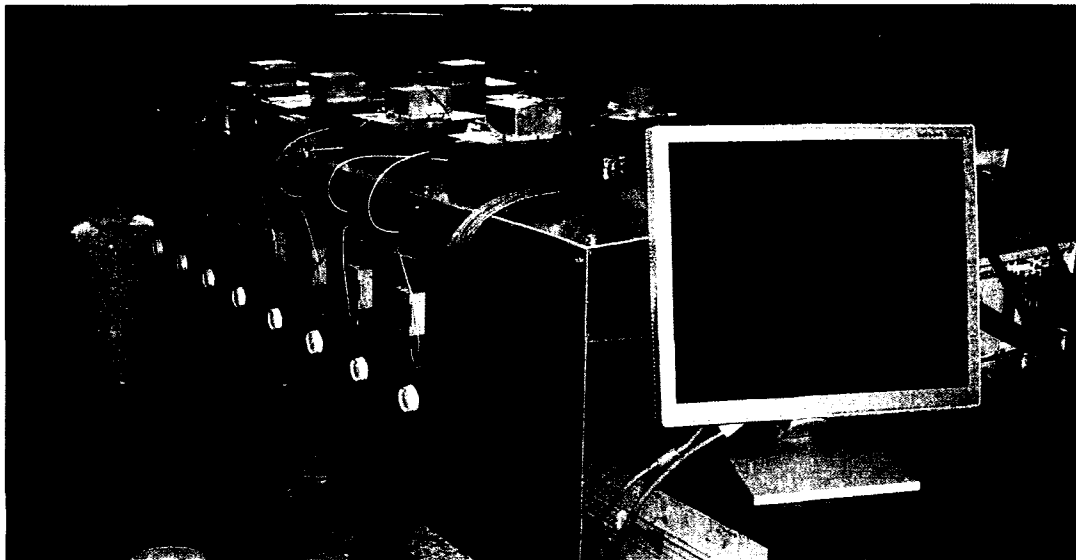


**Figure 7.1: Endurance test setup (heater insulation not shown)**

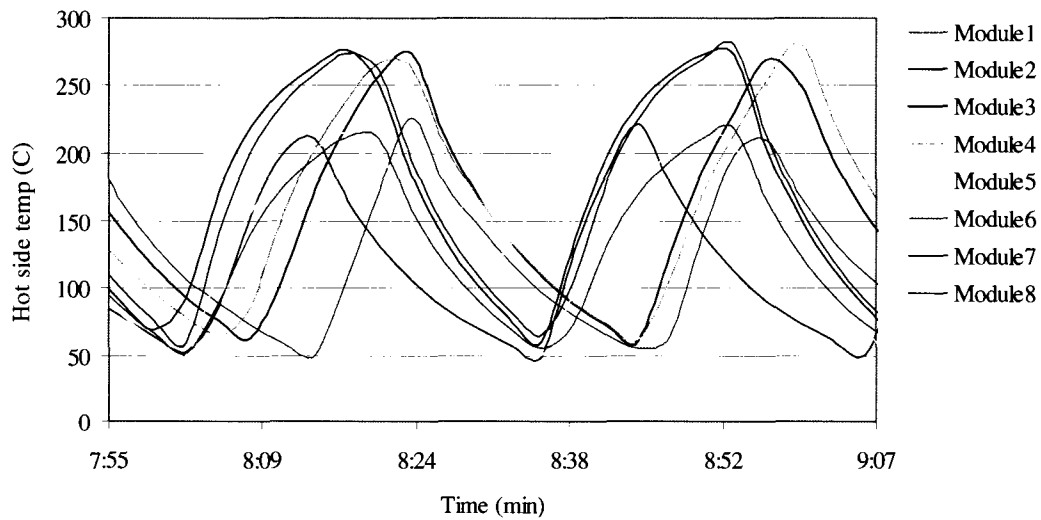


**Figure 7.2: Plot of temperature limits and typical cycle times**

## **7.2 Test Matrix and Methodology**

The objectives of the endurance testing were to compare manufacturer types, the effect of temperature on degradation, and the effect of cycling on the thermal interface. A total of eleven modules were tested, with two identical modules for each condition except the Hi-Z module at 340 C. Two of each module were tested to get an impression of module variability, and to prevent misleading conclusions in the case of a bad module or equipment malfunction. The test matrix is shown in Table 7.1. For both modules, the recommended peak continuous operating temperature was 250-260 °C. For testing, a point 30 C above (280 C) and 30 C below (220 C) were chosen as the high temperature and low temperature conditions. An extreme temperature of 340 C was run for each module type for 600 cycles as well. For comparison of interface materials, two modules were assembled with graphoil patches in addition to a light layer of grease. These modules could be compared to identical modules at the same temperatures using grease only. The expectation was that the modules with the graphoil patch would maintain a good thermal interface for longer, since the patch would fill any macroscopic gaps in the interface where the grease would eventually evaporate.

**Table 7.1: Endurance test matrix**

Module #	Manufacturer	Module	Max cycle temp (C)	Interface
1	Thermonamic	TEP1-0.8	220	Grease
2	Thermonamic	TEP1-0.8	220	Graphite + grease
3	Thermonamic	TEP1-0.8	280	Grease
4	Thermonamic	TEP1-0.8	280	Graphite + grease
5	Thermonamic	TEP1-0.8	340	Grease
6	Thermonamic	TEP1-0.8	340	Grease
7	Hi-Z	HZ-14	220	Grease
8	Hi-Z	HZ-14	220	Grease
9	Hi-Z	HZ-14	280	Grease
10	Hi-Z	HZ-14	280	Grease
11	Hi-Z	HZ-14	340	Grease

From this test matrix, the following comparisons were made:

- Effect of temperature (1,2 vs. 3,4 vs. 5,6) and (7,8 vs. 9,10 vs. 11)
- Grease vs. graphoil + grease (1 vs. 2) and (3 vs. 4)
- Thermonamic vs. Hi-Z at low temperature (1,2 vs. 7,8)
- Thermonamic vs. Hi-Z at high temperature (3,4 vs. 9,10 and 5,6 vs. 11)

Module properties were measured as described in Section 5.1.2 at zero cycles, and at approximately 600 cycle intervals. For each round of module testing, the module properties were measured at three different temperature values to get a better average reading. For the low and medium temperatures (220 and 280 C), the modules were run for 3000 cycles to get a good trend line for the damage, and since

the majority of the cycles the module sees will be between these values. The high temperature cycles (340 C) were only run for 600 cycles since the slope was much higher for these cases, and fewer of these would be seen in an application.

### **7.3 Results**

The results from the endurance testing were overall quite encouraging. Although the modules did see a measurable increase in thermal resistance and interface resistance, only one module failed during the duration of the test, which was the Thermonamic module at 340 C. This module failed after only 200 cycles, while the second module under the same conditions lasted over 1000 cycles (with substantial damage). Interestingly, the module that failed had a lower initial resistance and higher initial Z value as measured by the Z-meter. This indicates that the Z-meter may not be a reliable way to detect weak modules.

The raw data from the tests for percent change in electrical resistance and thermal resistance are shown in Figure 7.3 and Figure 7.4. Due to the difficulty in taking steady state readings and in making calculations of electrical resistance, there is a noticeable amount of scatter in the data. This is especially noticeable in the case of the low temperature Hi-Z modules where the values actually went down by 2 % in some cases. This is within the error of the measurement, and should be interpreted as nearly 0% change.

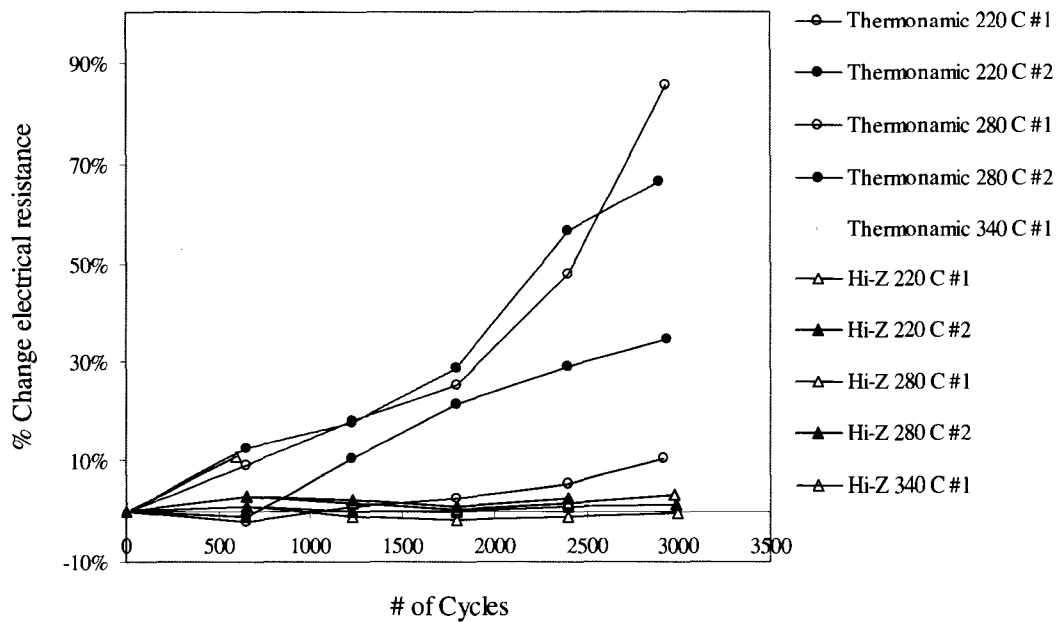


**Figure 7.3: % change in electrical resistance with number of cycles**

As expected, the higher cost Hi-Z modules performed better at all temperatures. At 220 C, the damage to electrical resistance of the Thermonamic modules was about 5 times greater per cycle. At 280 and 340 C, the damage to the Thermonamic modules was about 20 times greater per cycle. There are a number of explanations for this. First, the Hi-Z module uses fewer elements which reduces the probability of damage. The Hi-Z modules also use a different binding material to protect the modules from water vapor and oxidation. Lastly, the process of hot-pressing the conductor strips to the elements used by Hi-Z may be a superior method.

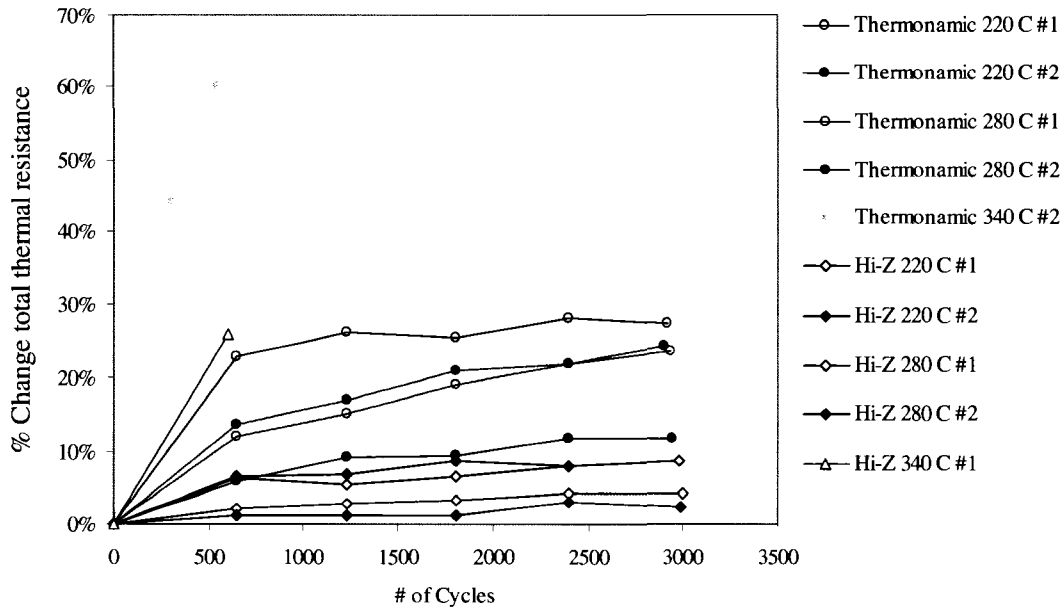


**Figure 7.4: % change in total thermal resistance (Module + interface) with number of cycles**

The Hi-Z modules also show a superior performance on thermal resistance change of 2.5 to 4 times. This large difference was not expected for thermal resistance. The percent change shown here is the change in the module + interface resistance. Since the thermoelectric elements will not change in thermal resistance, this increase is solely caused by the thermal interface degrading. The thermal interface resistance can be increased in several ways: loss of clamping pressure, loss of thermal grease, separation of the module elements from the conductor strips, and separation of the conductor strips from the ceramic wafer (Thermonamic module only). Since the same screws and clamping assembly were used for both types, this could be ruled out as the cause for the difference. Likewise, the same thermal grease was used for both types, but if the Hi-Z modules had a better flatness then the loss of the thermal grease would not be as detrimental. A separation of the module elements from the conductor strips can be inferred from the increase in electrical resistance so

this would also cause a difference between the modules. Finally, Thermonamic holds the module together by using a high temperature epoxy to secure the elements to the ceramic wafer on the cold side. Although this is fine from a temperature standpoint, it may be poor in a fatiguing application. The Hi-Z module is referred to as a “skeleton” module, where the binder between the elements holds the module together.

At 2400 cycles, the screws were re-torqued to their original value and the thermal resistance was measured. It was found that one screw on module #1 was loose, which would explain why this module showed a higher degradation than any of the others. No other screws were found to be loose in the other modules, so it is suspected that this screw may have been loose from the beginning. After re-torquing the screws, no measurable change in thermal resistance was seen. From this it was assumed that the change in thermal interface resistance was not caused by loss of clamping pressure, and that the Bellville washer assembly was performing perfectly. However, on disassembly of the modules many of the screws were very difficult to remove. This means there is a possibility that when the screws were re-torqued they did not move since they were seized up, not because they had retained their tightness. A separate experiment may be necessary to better understand and quantify the cause of the thermal degradation, possibly with and without a module.

Another goal of the endurance testing was to compare the use of thermal grease to a graphoil patch for the thermal interface. Modules 2 and 4 had the graphiol patch, while modules 1 and 3 did not. Comparing modules 1 and 2 is not valid since module one is clearly a bad data point, being worse than the modules cycled to higher temperatures. On the other hand, looking at modules 3 and 4 the module with the

patch has a higher degradation on average. From this data, it is hard to make any conclusions about whether the graphiol patch is an advantage or not. However, it does not appear to be a dramatic improvement in either case, and may not be necessary.

## **8 Parametric Studies and Component Optimization**

### ***8.1 Damage Modeling -- Module and Temperature Selection***

To model the damage caused to thermal cycling, trend lines were fit to the endurance test data to determine a percent damage per cycle for the various modules and temperatures tested. The trend line fits for electrical resistance increase and thermal resistance increase are shown in Figure 8.1 and Figure 8.3. From the slopes of these curves, the damage per cycle as a function of temperature was plotted for each module type as shown in Figure 8.2 and Figure 8.4. This data shows that the damage per cycle for both module types has an exponential dependence on temperature. These plots also concisely demonstrate the superior performance of the Hi-Z modules compared to the Thermonamic modules. The Hi-Z modules do not start to show significant damage until about 300 C for electrical resistance. The difference between the two on thermal resistance is not as large, but still significant.

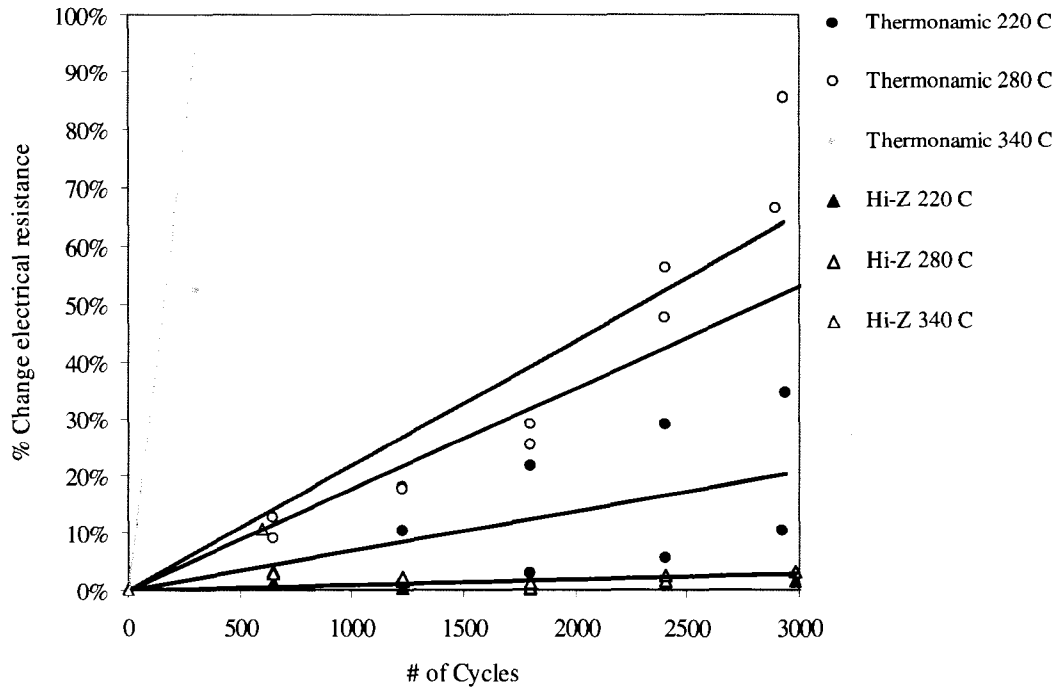


**Figure 8.1: Trend line fits for electrical resistance increase per cycle**

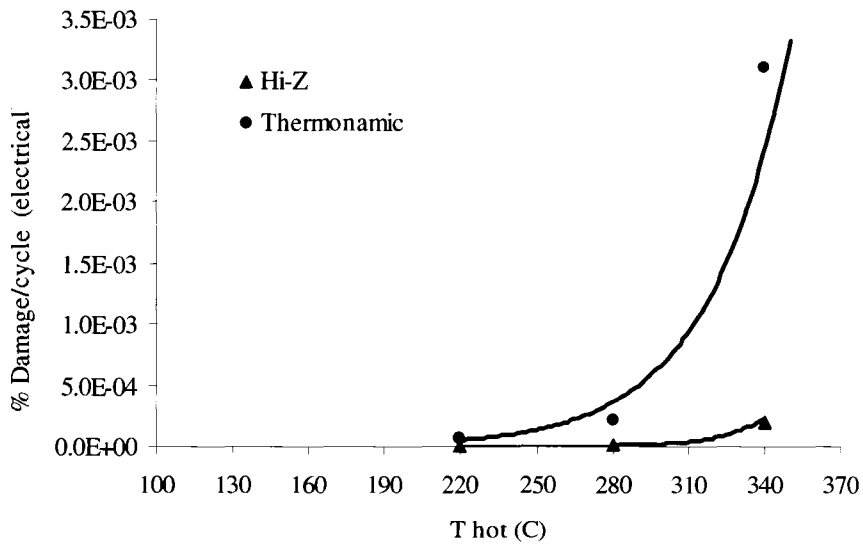


**Figure 8.2: Damage per cycle (electrical) as a function of maximum temperature**

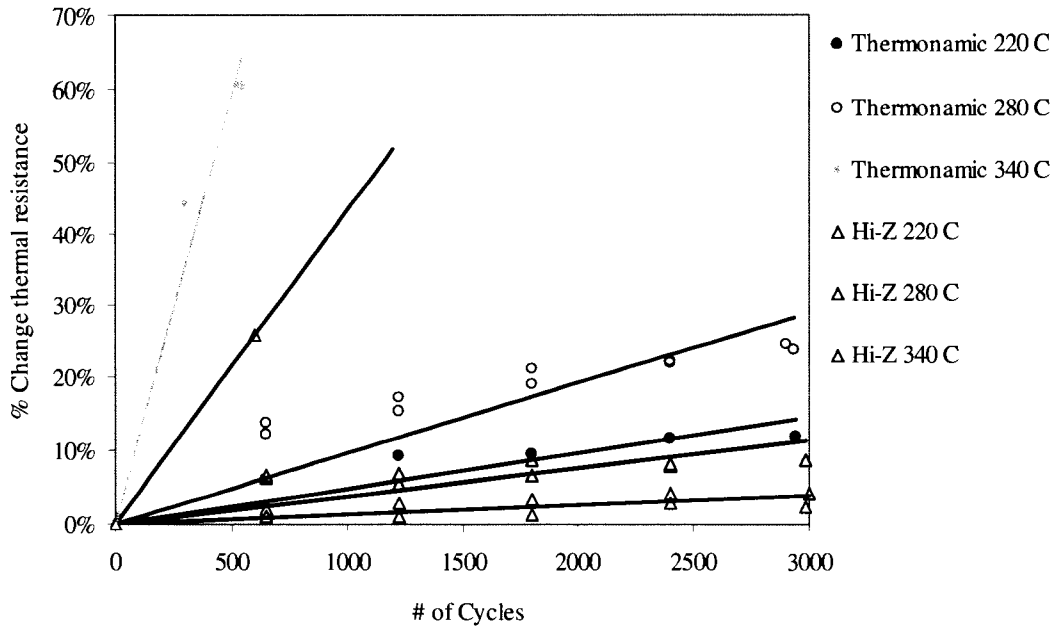


**Figure 8.3: Trend line fits for total thermal resistance increase per cycle**

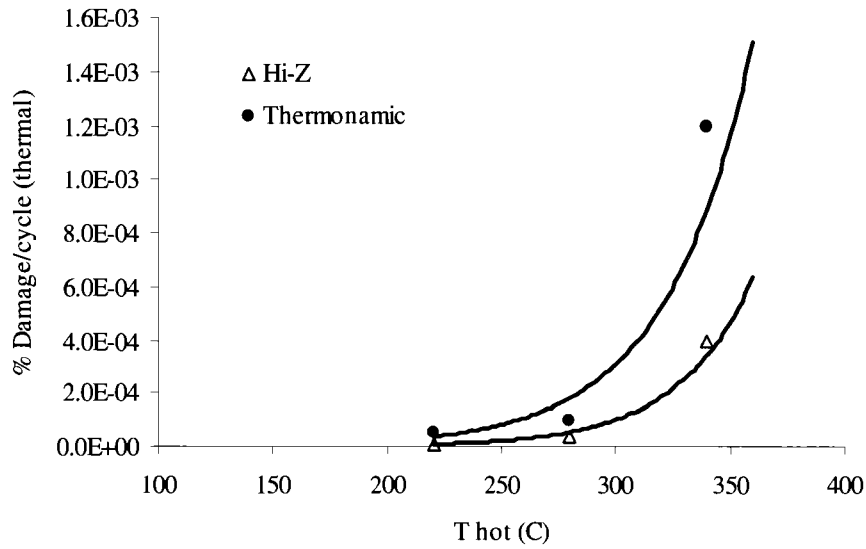


**Figure 8.4: Damage per cycle (thermal) as a function of maximum temperature**

From these figures, a good estimate for the damage caused by a cycle to any given temperature could be made. To apply this model to the field data, the number

of cycles to a specific temperature interval was required. For determining the energy generated during the month an average cycle as described in Sections 5.1.6 and 5.3 was effective. However, this average cycle assumes that the hot gas temperature reaches the max temperature (740 C) every cycle (for less than 1 minute). In reality, the stove may only reach this temperature a few times per month. To calculate damage a different approach was used. For the first month of data, the number of cycles peaking at various temperature intervals was recorded for House #7 and House #8. These are shown in Figure 8.5 and Figure 8.6. The combined data is shown in Figure 8.7, where the total number of cycles was normalized to give two cycles per day. This data shows the stark contrast between the usage habits in the two different houses, and why House #7 generated so little power.

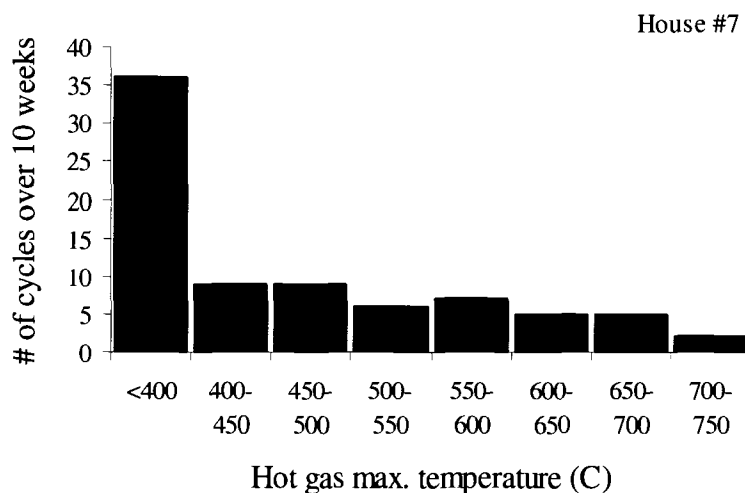


**Figure 8.5: Number of cycles peaking at various temperature intervals (House #7)**

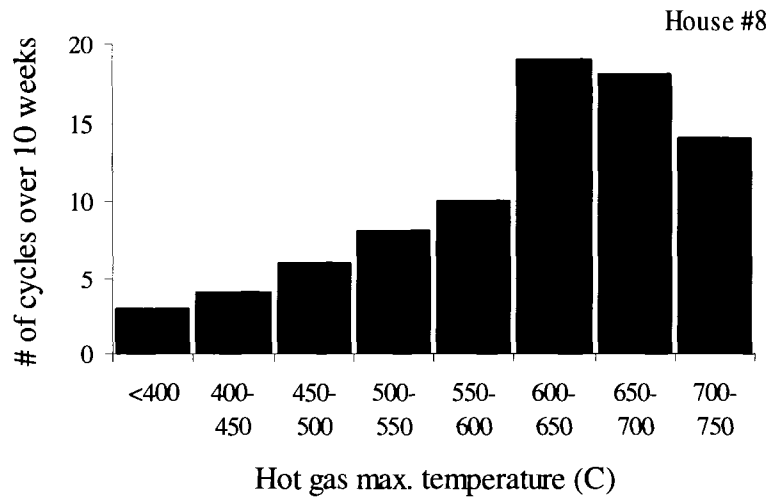


**Figure 8.6: Number of cycles peaking at various temperature intervals (House #8)**

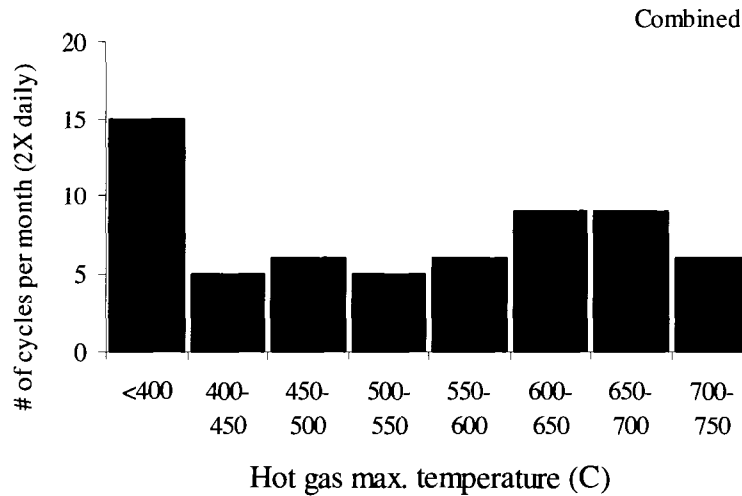
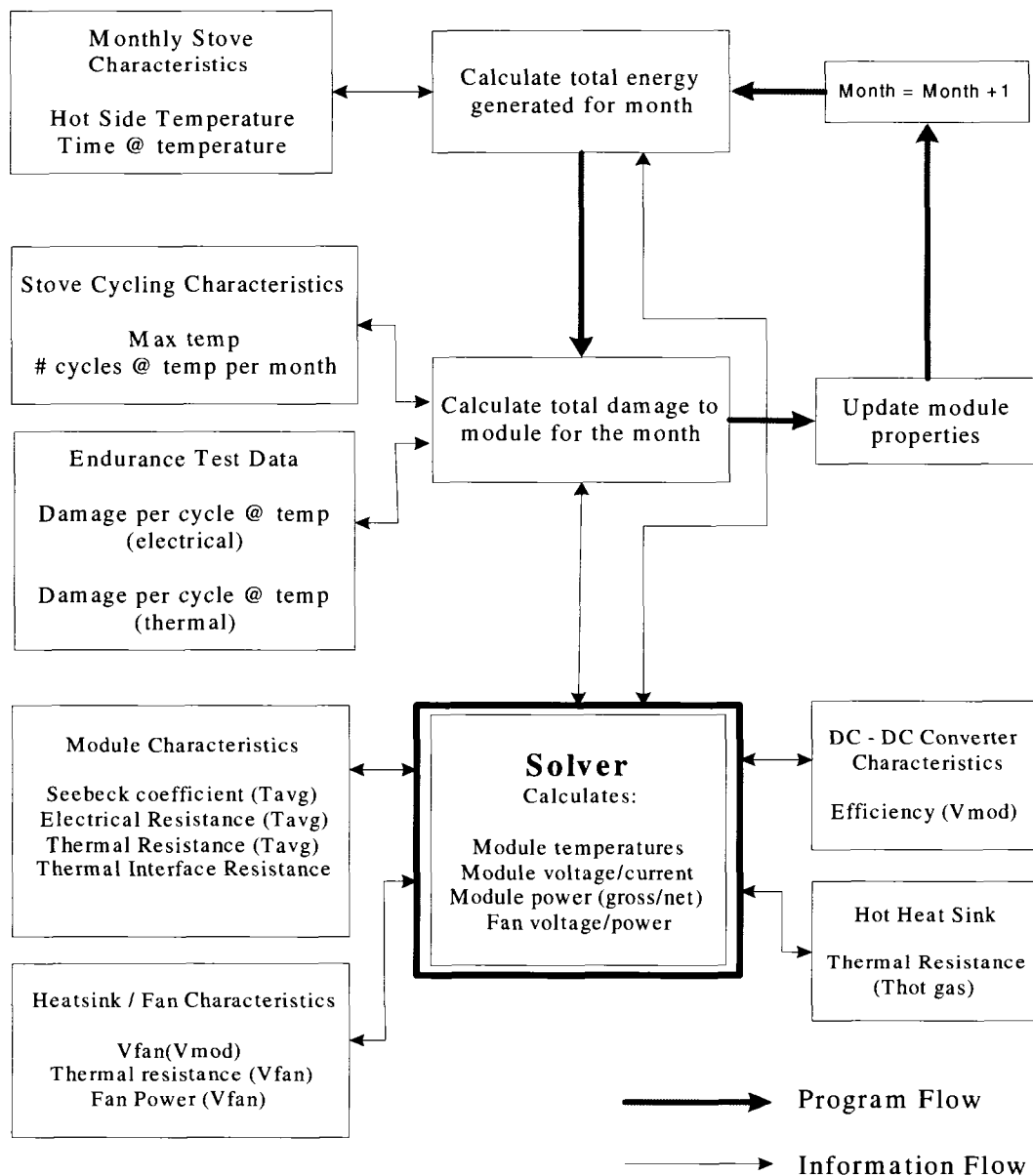


**Figure 8.7: Number of cycles peaking at various temperature intervals (House #7&8, normalized for 2 cycles per day)**

Using this data, the corresponding hot side temperature for these hot gas temperatures was calculated using the system model. Using the module hot side temperatures and number of cycles at that temperature, the total amount of damage to the module for that month could be calculated. The thermal damage to the module would be calculated as a % of the module resistance as done in the endurance testing

and the amount of thermal resistance increase would be added to the interface resistance.

Using the combined models for monthly energy generated and the progressive damage model, the performance over a five-year period was modeled for several modules and peak operating temperatures. A schematic of the model architecture is shown in



The damage model was run for three different modules (Thermonamic 10 W, Thermonamic 14 W, Hi-Z 14 W) with three different peak module temperatures (280 C, 310 C, 340 C). The model was run for a two module system using the Thermaflo E1456 16.25 cm heatsinks and the Mechatronics fans. The model was run for 60 months, and the resulting energy generated for each month was recorded. The resulting monthly energy trends for each case are shown in Figure 8.8, and the accumulated energy over the five year period is shown in Figure 8.9.

The Thermonamic modules show a rapid decrease in performance at 340 C and at 310 C. The energy generated by these modules decreases to 50% within one year at a 340 C peak. This is most likely the trajectory of several of the units in the field tests that consistently saw these high temperatures. On the other hand, the Hi-Z modules show very good performance over the five year period, even at 310 C and 340 C. In fact, the slope of the line for the Hi-Z module at 310 C is roughly equal to the slope for the Thermonamic module at 280 C. The module with the best performance is the Thermonamic 14 W module run at 280 C. Since this is a higher power module than the Hi-Z 14 (due to how they are rated) it can produce more power at a lower temperature. Even though the Thermonamic modules show a much worse response to cycling, if the temperature is kept below 280 C the total reduction over the five year period is held to 20%. Since the Thermonamic 10 W and 14 W modules are the same cost, it is clearly better to run the 14 W module at a lower temperature than the 10 W module at a higher temperature.

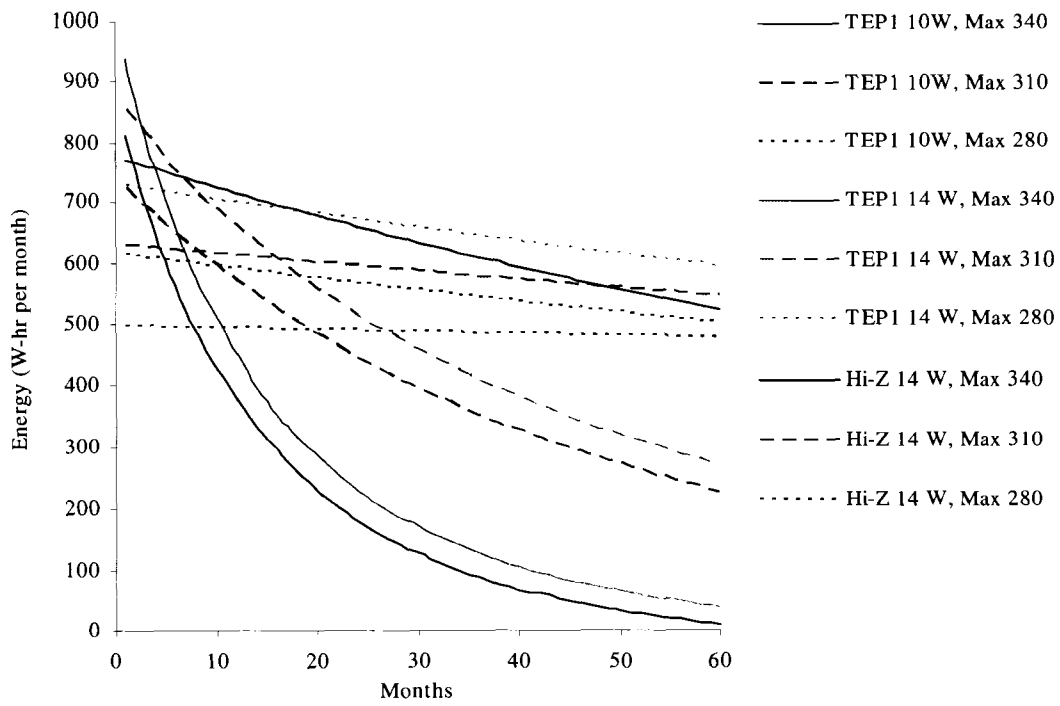


**Figure 8.8: Reduction in monthly energy as a result of module damage for different maximum temperatures**

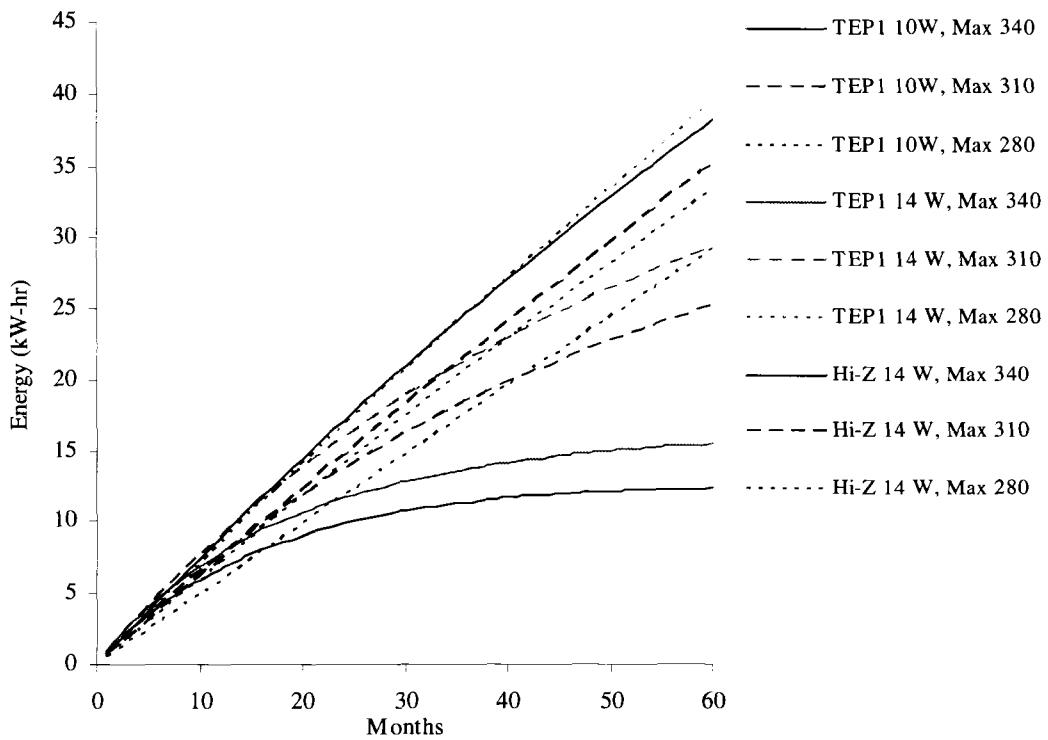


**Figure 8.9: Total energy generated over a five year period with different maximum temperatures**

Although the Thermonamic module at 280 C appears to be the best performer, the difference between 280 C and 310 C is dramatic. Therefore, any design using the Thermonamic module may need additional precautions to ensure that the module does not exceed this temperature. Differences in stove usage and fuel type could make this 280 C target very difficult to hit exactly. If the maximum temperature is less the energy generated will fall off rapidly. If the temperature is higher, the module lifetime will be reduced dramatically. This is the subject of Section 8.3 which addresses over temperature protection. For a more forgiving design, the Hi-Z module would be preferred. In addition, some applications may see a very different temperature distribution than used in this model run (shown in Figure 8.7). If the frequency of the high temperature cycles is increased significantly this may force an even lower temperature for the Thermonamic module, making the Hi-Z module the best performer. Unfortunately, the Hi-Z module is currently approximately three times the cost (based on costs at 10,000 units). From a cost perspective, the added cost of the Hi-Z module may be better spent on over-temperature protection for the Thermonamic module.

## ***8.2 Heat Sink Selection***

The first parametric study in the heat sink investigation was a comparison between the Melcor 15 cm bonded heat sink and the Thermaflo E1456 extruded heat sink at 16.25 cm length. In the generation 1 design, these heat sinks were compared, but only at full fan power where the Thermaflo heat sink is slightly better. However,

at low fan voltage, the Melcor heat sink is slightly better since it has a larger fin spacing. The thermal resistance of the two heat sinks is shown in Figure 8.10. As was shown in the charging circuit analysis, the performance of the generator at low temperatures can have a major effect on the overall energy generated each day.

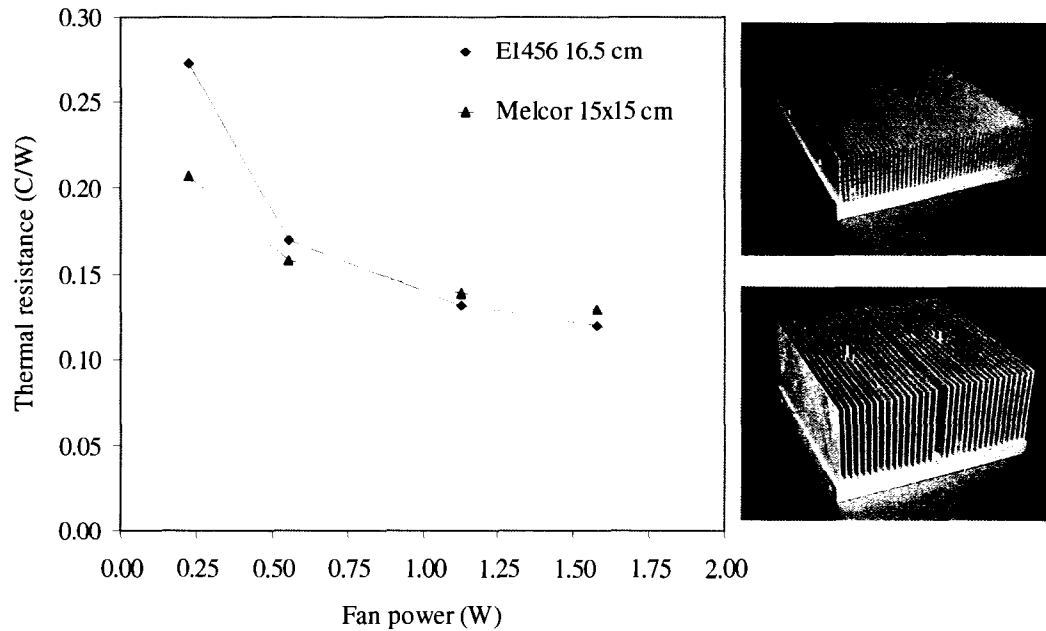


**Figure 8.10: Thermaflo E1456 16.5 cm(top) and Melcor 15 cm(bottom) heat sink thermal resistance with Mechatronics fan**

To evaluate the two heat sinks the standard daily temperature distribution was used as presented in Section 5.1.6. The heat sink study was run with 2 of the Thermonamic 14 W modules at a peak temperature of 280 C. The power curves are shown in Figure 8.11. As expected, the Thermaflo heat sink generates more power at high temperatures, and the Melcor performs better at low temperatures. However, this difference is much smaller than anticipated. The net result is that the Melcor heat sink generates approximately 0.9 W or 3.4% more energy. This small difference would not be enough to justify one heat sink versus the other, since other factors such as cost, manufacturability, natural convection performance and lifetime must also be

considered. The two heat sinks use approximately the same amount of material, and should ultimately be about the same cost. The Melcor heat sink has better performance before the fans turn on for a faster startup, but has the disadvantage of bonded fins which can come loose over time. Another advantage of the Melcor heat sink is that it would be less susceptible to clogging up with dust over time since the fin spacing is much larger.

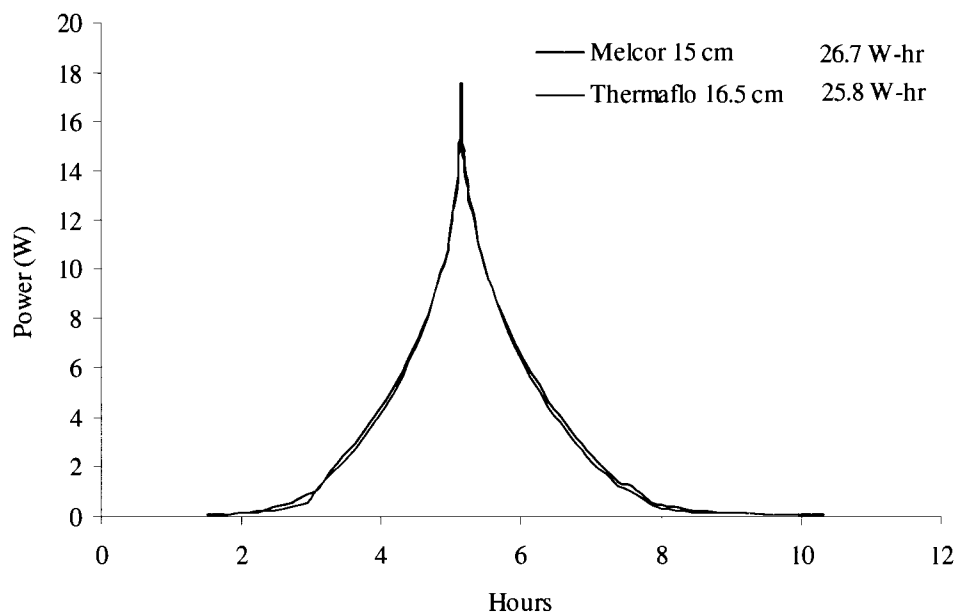


**Figure 8.11: Power curves for Melcor and Thermaflo heat sink comparison**

The next study in the heat sink analysis was to evaluate the cost effectiveness of different heat sink lengths. In Section 5.1.3 it was shown that for the E1456 heat sink the minimum thermal resistance occurred at a length of 16.25 cm. For the heat sink length study the 9.5, 12.5 and 16.25 cm heat sinks were used in the model. Moving to a smaller heat sink does reduce the system power, but it also reduces the system cost since the cold heat sink is the second most expensive component in the system. To

quantify this tradeoff the three heat sink lengths were run in the model to find the total W-hr/day that would be generated with each. The total system cost was then computed with various heat sink cost estimates. Depending on the place of manufacture, manufacturing method and quantity the cost of the heat sink could vary significantly. To observe this sensitivity the heat sink costs were calculated using \$5/kg, \$10/kg, and \$15/kg. The results from this analysis are shown in Figure 8.12. The component costs, total system costs and system cost effectiveness are shown in Table 8.1.

It is interesting that although the energy generated is affected by the heat sink length, the resulting tradeoff in cost almost perfectly balances out this reduction in energy. The result is that the total system cost effectiveness is not very sensitive to the heat sink length. For the cheaper heat sink costs, the longest heat sink results in the best system cost effectiveness. It isn't until the cost is increased to \$15/kg that the shorter heat sinks are favored.

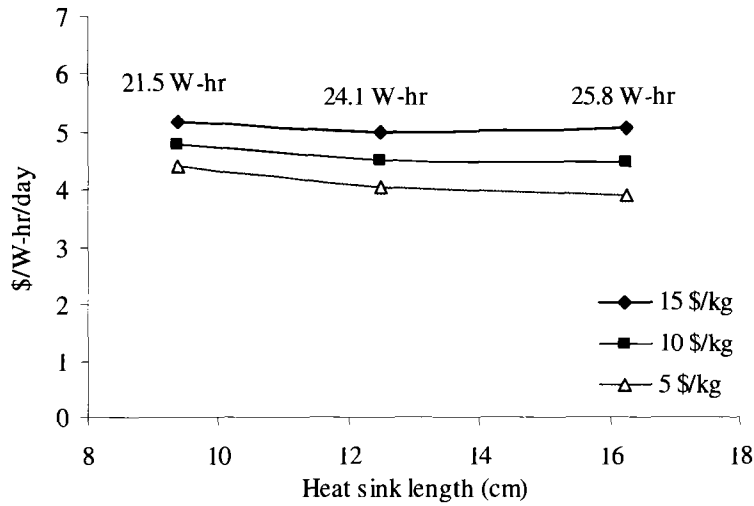


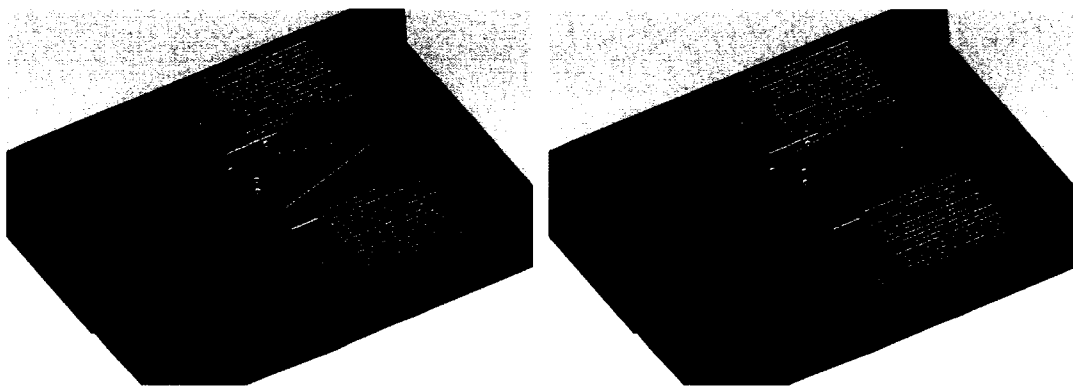
Figure 8.12: Heat sink cost effectiveness at various manufacturing costs

Table 8.1: System cost effectiveness with different heat sink lengths

Fixed Costs	each	total	16.25 cm length		25.8 W-hr
			Heat sink cost (for two) (\$15/kg)	System Cost	Cost/W-hr
Battery	\$10.00	\$10.00	44.17	130.17	5.05
Fan	\$3.00	\$6.00	33.98	119.98	4.98
Hot sink	\$5.00	\$10.00	25.48	111.48	5.17
Circuit	\$10.00	\$10.00			
Module	\$25.00	\$50.00			
		\$86.00			
			12.5 cm length		24.1 W-hr
			Heat sink cost (for two) (\$10/kg)	System Cost	Cost/W-hr
			29.45	115.45	4.48
			22.65	108.65	4.51
			16.99	102.99	4.78
			9.5 cm length		21.5 W-hr
			Heat sink cost (for two) (\$5/kg)	System Cost	Cost/W-hr
			14.72	100.72	3.91
			11.33	97.33	4.04
			8.49	94.49	4.38

### **8.3 Over-Temperature Protection**

Data from field testing showed significant variations in the peak temperature of the stoves. These differences were a result of regional usage (heating and cooking vs. cooling only), individual user habits (types of food cooked, number in family, etc.), variations in fuel wood and minor variations in stove construction. Results from endurance testing and damage modeling show a rapid destruction of the module if the hot side temperature exceeds 280 C (for the Thermonamic modules). These two factors suggest a means of over-temperature protection will be necessary to get the most energy from the system while ensuring a long lifetime. The addition of over-temperature protection will not only increase the lifetime of the modules, it could also significantly increase the energy generated at lower stove temperatures. The most practical means of over-temperature protection is to use a bimetallic material to open a heat sink bypass when the temperature reaches a certain level. This concept is shown in Figure 8.13.



**Figure 8.13: Bimetallic bypass in closed (left) and open (right) positions**

The actual implementation of this concept could vary significantly from the concept shown. The deflection of the bypass “doors” can be engineered to give

almost any desired deflection/temperature profile by changing the material type, coil length, thickness and preload.

Although the calculation for the deflection of the bimetallic strip as a function of temperature is very straightforward, the resulting hot-sink resistance once the bypass is opened is a very complex problem. To accurately tune the deflection of the bimetallic strip for a specific thermal resistance profile would take a significant amount of CFD modeling and experimentation as was shown in Section 5.1.4. This will be left as topic of future work. For this study, several potential hot-sink thermal resistance profiles were proposed and modeled in the system model. The first one was the fixed heat sink (current design). The second was a linear increase in thermal resistance as the temperature increases. The third was a toggle concept, where the bypass would toggle open and closed at a specific temperature. The last was a delayed linear increase where the bimetallic strip would have an initial offset or preload so it wouldn't begin to move until a certain temperature. For the delayed linear model, initial heat sink resistances of 0.6 and 0.4 were used, representing two different heat sinks. The hot-sink resistance as a function of gas temperature is shown in Figure 8.14. For this model, the heat sink resistances were chosen so that the peak module temperature never exceeded 280 C. The model was run with the standard time/temperature profile with the Thermonamic 14 W module, Thermaflo 1456 heat sink, and Mechatronics fan. The resulting module hot side temperatures are shown in Figure 8.15 with a close up view in Figure 8.16. The resulting power and energy generated with each concept are shown in Figure 8.17.

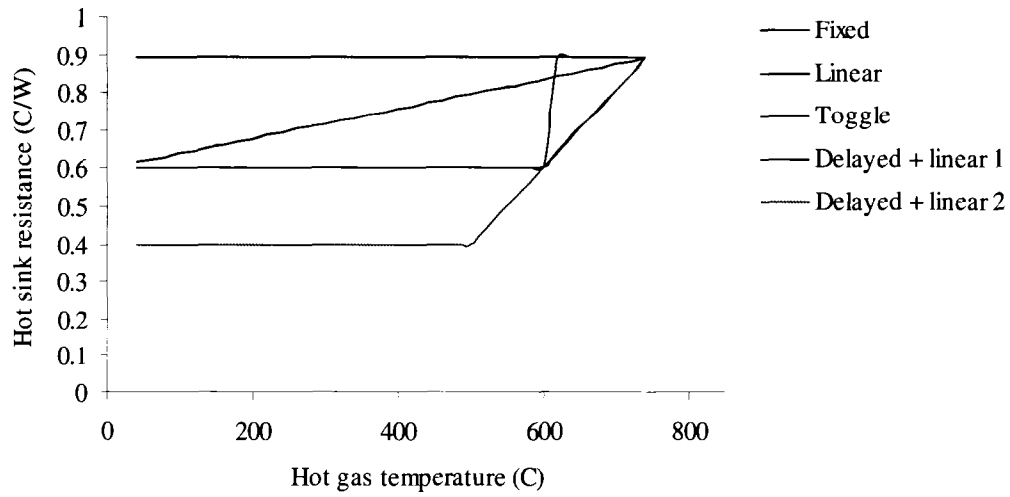


**Figure 8.14: Hot sink thermal resistance as a function of temperature with three different bimetallic concepts**

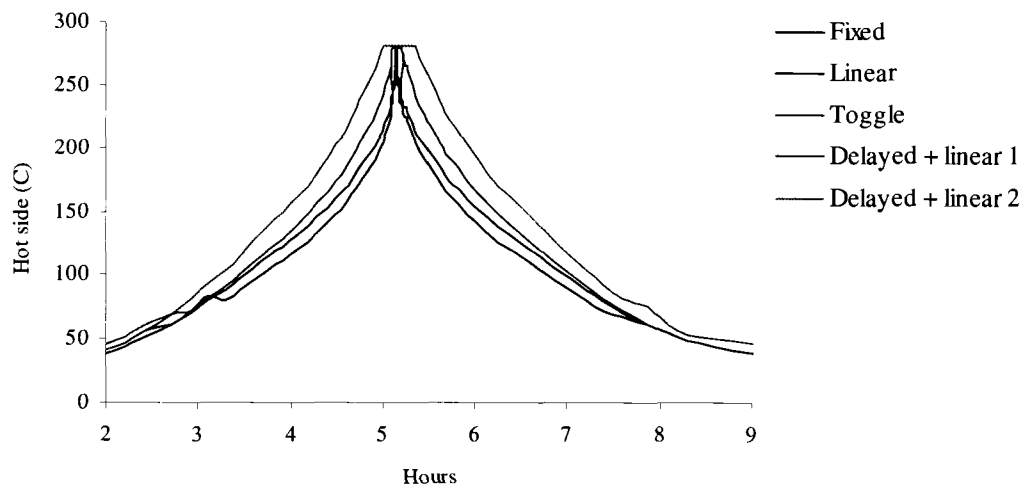


**Figure 8.15: Module hot side temperature with three different bimetallic concepts**

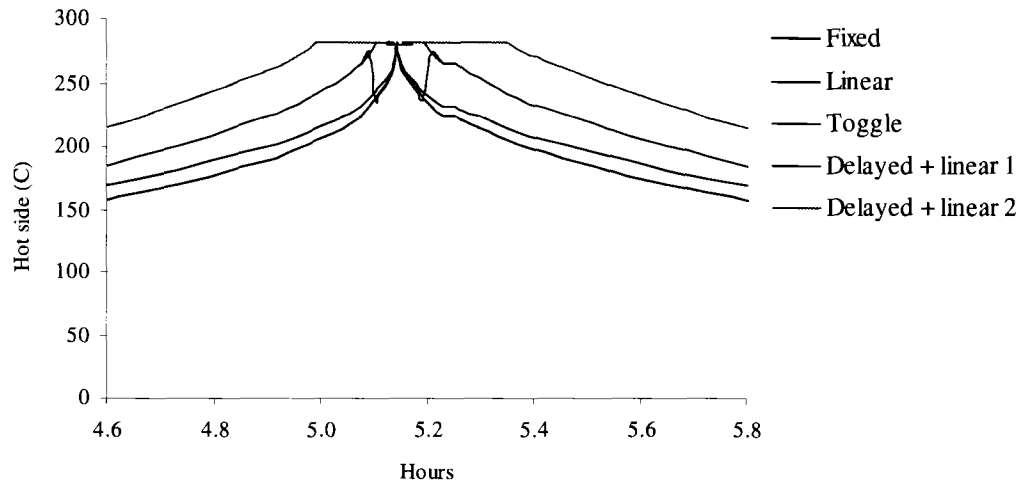


**Figure 8.16: Close up of module hot side temperature with fixed and variable hot sink resistance**

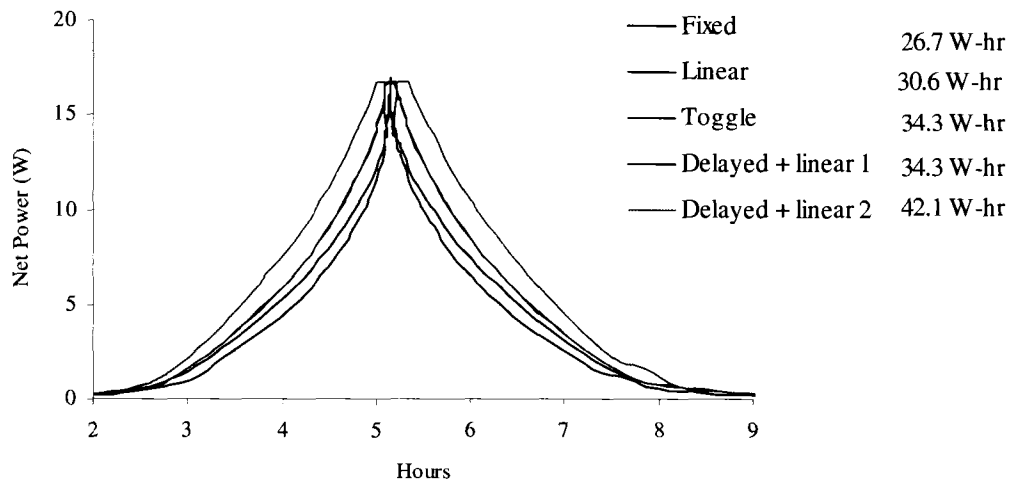


**Figure 8.17: Module net power with fixed and variable hot sink resistance**

As shown in Figure 8.16, the variable heat sink resistance does a good job of maintaining the module temperature below 280 C. The delayed + linear profile does a perfect job of holding the temperature right at 280 C, while the toggle concept briefly drops the module temperature back to 240 C immediately after the bypass is

opened. In this case, the loss of power during this brief drop is insignificant in the total energy production. As seen in Figure 8.17, the total energy generated by the two concepts (toggle and delayed + linear 1) is the same since the amount of time spent at the highest temperatures is so small. It is also interesting that the linear concept only increases the energy by 4 W-hr, or 15%. The toggle and delayed linear concept increase the energy by 7.6 W-hr, or 30%. Finally, the delayed linear 2 concept increases the energy by 15.4 W-hr, or 57%.

To achieve the thermal resistance of .6 C/W and .4 C/W, a more efficient heat sink than what is currently being used would be required. Two heat sinks that have the potential to reach these numbers are shown in Figure 8.18 along with the current heat sink used (Aavid 61085). The manufacturer data for these heat sinks at ambient temperatures are shown in Figure 8.19. Although previous tests and modeling have shown the manufacturer data is not valid at elevated temperatures and low velocities, the relative differences between the three heat sinks is believed to be accurate.

The Thermaflo E1441 heatsink is only 100 mm wide, and would be a good candidate for the bimetallic concept since it would leave enough room for two heat sinks side by side, with a 100 mm gap between them. This is the heat sink modeled in Figure 8.13. The Aavid 82525 may be necessary to reach the .4 C/W target, however, its width may not leave enough room for the bypass around the heat sink if two are used. For single module stoves, the Aavid 82525 may be a very good option, and is a way to increase the output of the single module stove with little additional cost. These larger heat sinks also have much lower pressure drops since they have a larger flow area. This could improve the stove performance by introducing less

restriction to the flow through the stove. However, these heat sinks are also much taller, and would require a much deeper channel to sit in. This may lead to lower temperatures on the stove top over the heat sinks, and may require a redesign of this portion of the stove.

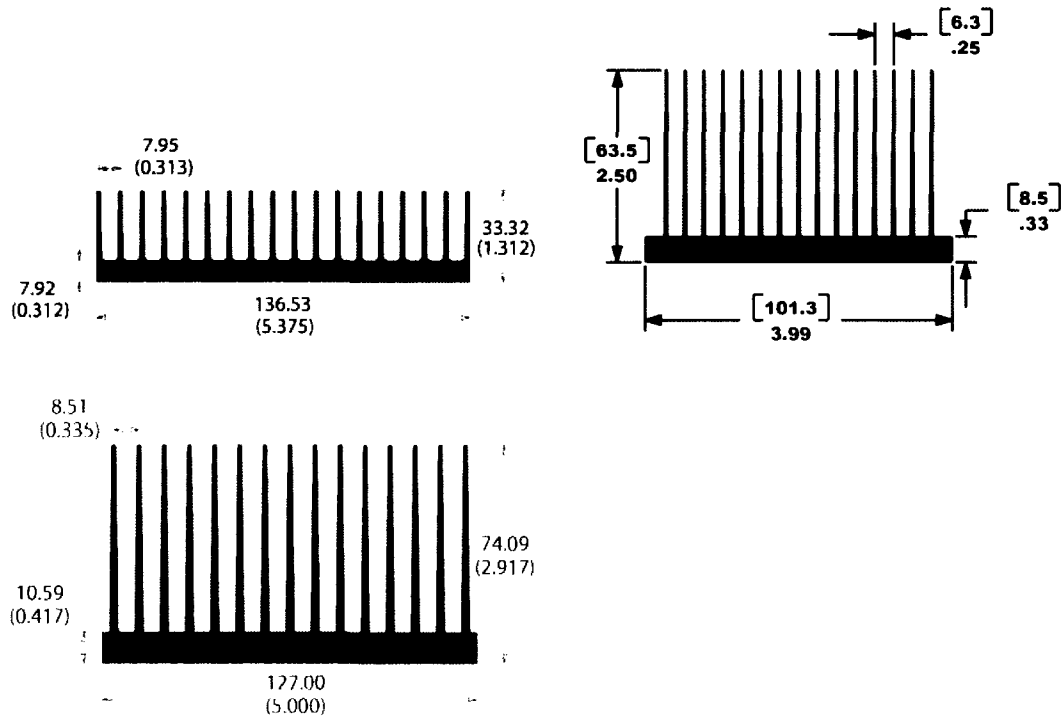


**Figure 8.18: Hot side heat sinks: Aavid 61085 (upper left), Thermaflo E1441 (upper right), Aavid 82525 (bottom). (Dimensions in mm and inches)**

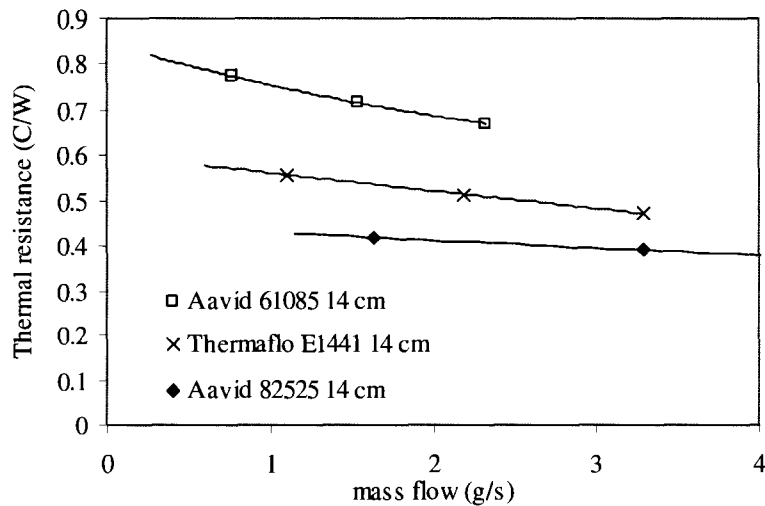


**Figure 8.19: Hot sink thermal resistance (manufacturer data at 20 C)**

## 9 Future Work

- Further endurance testing to understand the relative contributions of cycling and continuous time at elevated temperatures. This work is important in understanding if a 15 minute cycle to 280 degrees has the same damage as a 2 hour cycle to 280 degrees.
- Further endurance testing to isolate factors in thermal interface deterioration. This testing should include tests with different thermal greases with and without modules. The tests could be conducted at constant temperatures (non-cycling).
- Integration of the bimetallic concept into the design. This would also require further development of the modeling tools for the hot side heat sink and the stove.

- Endurance testing of the battery to validate the adaptive capacity concept and better understand how to extend battery lifetime under varying conditions. This work should also include a more detailed examination into alternative battery materials.
- Further field testing without TEGs installed in the stove to build a better model of stove usage. It would also be important to understand how the user's habits change with the TEG stove by taking data before and after - something that was not done during this work.

## **10 Summary & Conclusions**

In summary, this work has demonstrated that a stove-powered thermoelectric generator is a technically and economically feasible method for generating power. This technology has been tested and demonstrated in the lab, as well as in multiple field test locations around the world. Detailed data has been gathered from field test installations and has been used to drive design improvements through system level modeling.

A methodology for modeling and optimization of a stove-powered generator has also been developed. This method integrates component bench test data, endurance test data, and field test data into a system optimization process. The system level model was used to understand the cost-benefit trade-offs for various module sizes, module styles, operating temperatures, heat sink styles and heat sink sizes.

As a major component to this work the first published module lifetime predictions for high-temperature generator modules has been conducted. This type of testing and analysis currently does not exist in the literature. Two different module types were tested at three different hot side temperatures and the resulting damage was tracked. The data from this test was then combined with field test data in a progressive damage model to predict the performance of the modules at different peak hot side temperatures.

Finally, an over-temperature protection concept was presented and modeled for further improving the power output and extending the lifetime of the thermoelectric generator.

Some highlights from the various stages of this work are outlined below:

### Generation 1 Design

The generation 1 design was successful in integrating all the system components into a working system that could be used for laboratory and field testing. The generation 1 design was based on limited component tests as well as estimated field stove temperatures. The actual energy generated by the generation 1 design was significantly less than predicted for a few reasons. The power from the modules was predicted using manufacturer data for the modules and assuming constant properties with temperature. When the modules were tested in the stove they were tested in the open circuit configuration and the max power was calculated based on the specified internal resistance. This led to over predicting the power since the module thermal

resistance is higher under open circuit conditions. Also, the module electrical resistance was higher than the manufacturer data, especially at higher temperatures. Another shortcoming of the generation 1 design was the accumulation of power losses through each component of the system. Although the loss through any one component was small, after combining them all the energy generated was only about one third of the initially predicted value.

### Field Testing

The field testing was very productive and critical in gaining an understanding of how the stoves were being used, and what scenarios could lead to system failures. In addition, important feedback from the users was documented that will go into future improvements in the functionality of the stoves. The most important observations (regarding the generator) from the field testing were:

- Loosening of the generator components from thermal cycling, leading to increased thermal resistance between the parts.
- Excessive power consumption from the circuit and the fans at low stove temperatures which could offset any power generated at high stove temperatures.
- The inability of the design to function well under various user cooking styles and user habits. The design was optimized for a very specific temperature range, which was not consistently achieved by all users. This also highlighted the need to optimize the design for the low temperature conditions as well

- Battery failures due to incomplete charging of the battery. This was caused by lower than predicted power levels and people using the light/TV while the stove was running. One failure was also seen from over-charging the battery since the modules could not be isolated from the battery.

These lessons learned from the field test have all been successfully addressed by the generation 2 design.

### System Modeling

The system modeling for the generation 2 design incorporated a much more thorough component testing procedure than used for the generation 1 design.

- Heat sinks were tested at varying lengths with various fans at varying voltage to create a wide array of potential heat sink performance capabilities.
- A maximum effective heat sink length was identified after which the thermal resistance started to increase.
- Five commercially available high temperature modules were tested at varying average temperatures. The module properties were seen to change significantly with temperature, which was very important to account for in the system model.
- Stove testing showed a very complex interaction between stove flows and stove temperature due to thermal transients throughout the stove. Creating a

direct correlation between stove flows and gas temperature was not possible, and would require a complete stove thermal model.

- Hot heat sink thermal resistance was very difficult to predict. The manufacturer data had significant error, and does not account for variations seen at high gas temperatures. To predict the thermal resistance of the heat sink at high temperatures and high heat flux, a CFD model is necessary. The current CFD model had reasonable agreement with experimental results (within 20-25%), but needs more refinement
- The overall system model did a very good job in predicting system temperatures and power levels given field test stove temperature data. The addition of a simple thermal capacitance to the thermal circuit was very effective in further increasing the models accuracy. The model was able to predict the overall system energy within 5% of the field data for a daily transient cycle as well as for weekly average data.

### Generation 2 Circuit Design

The generation 2 circuit design incorporated important design changes brought to light by the field testing. First, the three circuits from the field testing (charger, power meter and signal conditioner) were integrated into one circuit. The generation 2 circuit included:

- Low power operation to prevent discharging the battery when the stove is not used for several days

- Variable power control for the fans to prevent negative net power and improve performance at low stove temperatures. This was seen to have a profound effect on the net system power over a typical daily cycle.
- Hysteresis on startup/shutdown for smoother operation
- Adaptive battery cutoff that accounts for users generation and consumption habits for extended battery life
- Peak power operation for improved performance across the range of operating temperatures

These improvements to the circuit were predicted to lead to a 350% increase in net power for users such as House #7 in Nicaragua, and a 50% increase for users such as House #8 in Nicaragua.

### Endurance Testing

The endurance testing performed showed very dramatic effects of maximum temperature and module type on the lifetime of the module.

- The higher cost Hi-Z modules showed approximately 20 times lower electrical resistance damage per cycle at each operating temperature and 3 times lower thermal interface damage per cycle.
- The effect of peak temperature on damage/cycle was exponential.
- The addition of a graphoil patch did not show any definitive improvement in thermal interface resistance over time.

- Separate tests may be required to better understand the thermal interface degradation

#### Parametric Studies and Component Optimization

The parametric studies incorporated all the results from the individual component tests with the field test temperature data. A progressive damage model was created to evaluate the energy generated by the module over a five year period.

The results of this model were:

- For the Thermonamic module, the maximum temperature cannot exceed 280 C in order to keep the damage below 20% over five years. Any higher temperature and the damage increases dramatically
- For the highest power over the life of the generator, it is better to run the larger module at a lower temperature than the small module at a high temperature.
- Although the Hi-Z module had much better performance at every temperature, it was still possible to match the power and lifetime with the Thermonamic module run at lower temperatures.

A parametric study was also run on the heat sink to examine the sensitivity of the total system cost/Watt to heat sink length. As the heat sink is made shorter, the power is reduced as well as the cost. From this analysis it was concluded that the total system cost effectiveness is fairly insensitive to the heat sink length, even at high heat sink cost. Therefore, the heat sink length can be selected to meet the specific

cost of power targets of the system, without changing the overall system cost effectiveness

Finally, a method for over-temperature protection was proposed using a bimetallic strip to actuate a bypass and vary the hot sink resistance. It was shown that this addition could increase the energy generated by the module by up to 57%. This addition would be a very cost effective improvement to the design since it would only add an additional few dollars to the cost. In some cases, this may be preferred to adding a second module, since it almost doubles the energy. It was also shown that the bypass should be a delayed action rather than a linear increase with temperature. In fact, the bypass could simply toggle open at a fixed temperature to give very good results.

#### Optimal System Configuration

The final result of the various component optimizations resulted in the optimal system configuration shown below.

Module	Thermonamic "14 W" module
Hot heat sink	R = .88 for max hot side temperature 280 C at 740 C max hot gas temperature
Cold heat sink	Thermaflo E1456 @ 16 cm length
Fan	Mechatronics fan (variable power)
Charger	Peak Power Tracking (Res. match method or VOC method) with 330 uH inductor @ 20 kHz PWM frequency

## 11 Works Cited

- [1] [www.tellurex.com](http://www.tellurex.com) August 2006
- [2] [www.hi-z.com](http://www.hi-z.com) August 2006
- [3] [www.powersonic.com](http://www.powersonic.com) August 2006

### **Stoves Background**

- [4] Smith, K. R. 1987. *Biofuels, Air Pollution, and Health: A Global Review* Plenum Press, New York
- [5] Narain, S. 2003. Put an End to India's Cooking-Stove Pollution, Down to Earth, July 2003
- [6] Desai, M. A., Mehta, S., Smith, K. R. 2004. Indoor Smoke from Solid Fuels: Assessing the Environmental Burden of Disease at National and Local Levels, World Health Organization, Protection of the Human Environment, Geneva 2004
- [7] Bhatt, S. M. 1990. Towards the Design of High Efficiency Woodstoves, *International Journal of Energy Research*, (14): p. 629-649
- [8] Kandpal, J. B., Maheshwari, R. C., Kandpal, T. C. 1994. Comparison of CO, NO<sub>2</sub> and HCHO Emissions from Biomass Combustion in Traditional and Improved Cookstoves, *Energy* 19(11): p. 1151-1155
- [9] LaFontane, H. 1991. An Inverted Downdraft Wood-Gas-Stove and Charcoal Producer, *Energy from Biomass and Wastes*, (25): p. 1023-1049
- [10] Bond, T., Venkataraman, C., Masera, O. 2004. Global Atmospheric Impacts of Residential Fuels, *Energy for Sustainable Development*, 8(3)

### **Thermoelectric Applications**

- [11] Hall H. 1995. Terrestrial Applications of Thermoelectric Generators. In: Rowe D, editor, *CRC Handbook of Thermoelectrics*. London, CRC Press, p. 503-513
- [12] McNaughton A. 1995. Commercially Available Generators. In: Rowe D, editor, *CRC Handbook of Thermoelectrics*, London, CRC Press, p. 459-469
- [13] Rahman M, Shuttleworth R. 1995. Thermoelectric Power Generation for Battery charging, *Proceedings of the International Conference on Energy Management and Power Delivery*, (1): p. 186-191

- [14] Killander A, Bass J. A. 1996. Stove-Top Generator for Cold Areas, 15<sup>th</sup> International Conference on Thermoelectrics, p. 390-393
- [15] Nuwayhid R, Rowe D, Min G. 2003. Low Cost Stove-Top Thermoelectric Generator for Regions with Unreliable Electricity Supply, *Renewable Energy*, (28): p. 205-222
- [16] Nuwayhid R, Shihadeh A, Ghaddar. 2005. Development and Testing of a Domestic Woodstove Thermoelectric Generator with Natural Convection Cooling, *Energy Conversion and Management*, (46): p. 1631-1643
- [17] Eakburanawat J, Khedari J, Hirunlabh J, Maneewan S, Daguinet M, Teekasap S. 2003. Solar-Biomass Thermoelectric Power Generation Simulation, 22<sup>nd</sup> International Conference on Thermoelectrics: p. 582-584.
- [18] [www.research.philips.com/newscenter/archive/2006/060227-woodstove.html](http://www.research.philips.com/newscenter/archive/2006/060227-woodstove.html), February 2006
- [19] Bargaen D. 1963. Thermoelectric Generators for Battery-Charging Applications, *Advanced Energy Conversion*, 3(2): p. 507-514.
- [20] Allen D, Haugeto R, Kajor M, Namazian M. 2002. Small Thermoelectric Generators, 21<sup>st</sup> International Conference on Thermoelectrics, Long Beach, CA, August 2002, p. 424-426.
- [21] Allen D, Mallon W. 1999. Further Development of "Self Powered Boilers," 18<sup>th</sup> International Conference on Thermoelectrics, Baltimore, USA, August 29-September 2, p. 80-83.
- [22] Ewell R, Zoltan A. 1996. SP-100 Thermoelectric Cell Testing, *Journal of Propulsion and Power*, 12(5), p. 911-917
- [23] Bass J, Campana R, Elsner N. 1991. Thermoelectric Generator development for Heavy-Duty truck Applications, *Proceedings of the Annual Automotive Technology Development Contractors' Meeting*, Dearborn, Michigan, October 28-31, p. 743-748.
- [24] Doloszeski M, Schmidt A. 1997. The Use of Thermoelectric Converters for the Production of Electricity from Biomass, 16<sup>th</sup> International Conference on Thermoelectrics, Dresden, Germany, August 26-29, p. 607-610
- [25] Furue T, Hayashida T, Imaizumi Y, Inoue T, Nagao K, Nagai A, Fujii I, Sakurai T. 1998. Case Study on Thermoelectric Generation System Utilizing the Exhaust Gas of Internal-Combustion Power Plant, 17<sup>th</sup> International Conference on Thermoelectrics, Nagoya, Japan, May 24-28, p. 473-478.
- [26] Roth W, Kugele R, Steinhuser A, Schulz W, Hille G. 1997. Grid-Independent Power Supply for Repeaters in Mobile Radio Networks using Photovoltaic/Thermoelectric Hybrid Systems, 16<sup>th</sup> International Conference on Thermoelectrics, Dresden, Germany, August 26-29, p. 582-585.

## **Module Design and Analysis**

- [27] Angrist S. 1982. Direct Energy Conversion. Boston, Allyn and Bacon.
- [28] Rowe D. 2006. General Principles and Basic Considerations, In: Rowe D, editor, Thermoelectrics Handbook, Macro to Nano. Florida, CRC press.
- [29] Soo S. 1968. Direct Energy Conversion, Englewood Cliffs, New Jersey, Prentice-Hall.
- [30] Pollock D. 1995. Thermoelectric Phenomena. In: Rowe D, editor, CRC Handbook of Thermoelectrics. London, CRC Press, p. 7-17.
- [31] Matsuura K, Rowe D. 1995. Low Temperature Heat Conversion. In: Rowe D, editor, CRC Handbook of Thermoelectrics. London, CRC Press, p. 573-593.
- [32] Rowe D. 1995 Miniature Semiconductor Thermoelectric Devices. In: Rowe D, editor, CRC Handbook of Thermoelectrics. London, CRC Press, p. 441-458
- [33] Min G, Rowe D. 1995. Peltier Devices as Generators. In: Rowe D, editor, CRC Handbook of Thermoelectrics. London, CRC Press, p. 479-488.
- [34] Rowe D, Min G. 1996. Design Theory of Thermoelectric Modules for Electrical Power Generation, IEEE Proceedings: Science, Measurement and Technology, 143(6): p. 351-356.
- [35] Min G, Rowe D. 1992. Optimization for Thermoelectric Module Geometry for 'Waste Heat' Electric Power Generation, Journal of Power Sources, 38, p. 253-259.
- [36] Min G, Rowe D. 2002. Recent Concepts in Thermoelectric Power Generation, 21<sup>st</sup> International Conference on Thermoelectrics, Long Beach, CA, August 2002, p. 365-373
- [37] Buist R, Lau P, 1997. Thermoelectric Power Generator Design and Selection from TE Cooling Module Specifications, 16<sup>th</sup> International Conference on Thermoelectrics, Dresden, Germany, August 26-29, p. 551-554.

## **Advanced Materials**

- [38] Tse J, Klug D. 2006. Recent Trends for the Design and Optimization of Thermoelectric Materials – A Theoretical Perspective, In: Rowe D, editor, Thermoelectrics Handbook, Macro to Nano. Florida, CRC press.
- [39] Nolas G, Sharp J, Goldsmid H. 2001. Thermoelectrics: Basic Principles and New Materials Developments, Berlin, Springer-Verlag.
- [40] Hicks L, Harman T, Sun X, Dresselhaus. 1996. Experimental Study of the Effect of Quantum-Well Structures on Thermoelectric Figure of Merit, 15<sup>th</sup> International Conference on Thermoelectrics, Pasadena, California, March 25-28, p. 450-453.

- [41] Venkatasubramanian R, Colpitts T, Watko E, Hutchby J. 1996. Experimental Evidence of High Power Factors and Low Thermal Conductivity in  $\text{Bi}_2\text{Te}_3/\text{Sb}_2\text{Te}_3$  Superlattice Thin-Films, 15<sup>th</sup> International Conference on Thermoelectrics, Pasadena, California, March 25-28, p. 454-458.
- [42] Sugihara S, Tomita S, Asakawa K, Suda H. 1996. High Performance Properties of Sintered  $\text{Bi}_2\text{Te}_3$ -Based Thermoelectric Material, 15<sup>th</sup> International Conference on Thermoelectrics, Pasadena, California, March 25-28, p. 46-51
- [43] Krommenhoek D, Ghamaty S, Bass J, Elsner N, Jovanovic V. 2006. Predicted Performance of Quantum Well Thermoelectrics for Power Generation, 4th International Energy Conversion Engineering Conference and Exhibit (IECEC), San Diego, California, June 26-29, AIAA-2006-4046

### **Module Testing and Reliability**

- [44] Leavitt F, Elsner N, Bass J. 1996. Use, Application, and Testing of the HZ-14 Thermoelectric Module, 15<sup>th</sup> International Conference on Thermoelectrics, Pasadena, California, March 25-28, p. 378-383.
- [45] Rowe D, Min G. 1998. Evaluation of Thermoelectric Modules for Power Generation, *Journal of Power Sources*, 73, p. 193-198.
- [46] Ritzer T, Lau P, Bogard A. 1997. A Critical Evaluation of Today's Thermoelectric Modules, 16<sup>th</sup> International Conference on Thermoelectrics, Dresden, Germany, August 26-29, p. 619-623.
- [47] Ritzer T. 1999. Quick Method for Determining the Reliability of a Thermoelectric Module via Pulse Testing, 18<sup>th</sup> International Conference on Thermoelectrics, Baltimore, Maryland, August 29-September 2, p. 432-435.
- [48] Ritzer T, Nagy M, Bruist R. 1996. Evaluation of Thermal Junction Quality in Thermoelectric Assemblies using Transient Analysis Technology, 15<sup>th</sup> International Conference on Thermoelectrics, Pasadena, California, March 25-28, p. 293-297.
- [49] Hori Y, Kusano D, Ito T, Izumi K. 1999. Analysis on Thermo-Mechanical Stress of Thermoelectric Modules, 18<sup>th</sup> International Conference on Thermoelectrics, Baltimore, Maryland, August 29-September 2, p. 328-331.
- [50] Anatyshuk L, Luste O. 1997. Problems of Thermoelectric Devices Reliability, 16<sup>th</sup> International Conference on Thermoelectrics, Dresden, Germany, August 26-29, p. 632-635.
- [51] Vazquez J, Palacios R, Sanz-Bobi A, Arenas A. 2003. Test Bench for Measuring the Electrical Properties of Commercial Thermoelectric Modules, 22<sup>nd</sup> International Conference on Thermoelectrics, Hérault, France, August 2003, p. 589-593.

- [52] Sharp J, Volckmann E, Lyon H, Gillespie D, Kamm G, Ehrlich A. 1996. Validation of Thermoelectrics Measurements II, 15<sup>th</sup> International Conference on Thermoelectrics, Pasadena, California, March 25-28, p. 417-421.
- [53] Anatyshuk L, Luste O. 1996. Reliability Theory in Thermoelectricity, 15<sup>th</sup> International Conference on Thermoelectrics, Pasadena, California, March 25-28, p. 243-246.
- [54] Stapfer G, Truscello V. 1971. Performance Testing and Evaluation of a High Temperature Silicon Germanium Thermoelectric Generator, Intersociety Energy Conversion Conference, Boston, p. 512-19.
- [55] Gromov G, Kondratiev D, Rogov A, Yershova L. 2001. Z-Meter: Easy-to-use Application and Theory, Proceedings of the Sixth European Workshop on Thermoelectricity of the European Thermoelectric Society, Freiburg, Sept. 20-21, p. 1-8
- [56] Harman T, Cahn J, Logan M. 1959. Measurement of Thermal Conductivity by Utilization of the Peltier Effect, Journal of Applied Physics, 30(9), p. 1351-1359

### **Heat Exchangers**

- [57] Esarte J, Min G, Rowe D. 2001, Modeling Heat Exchangers for Thermoelectric Generators, Journal of Power Sources, 93, p. 72-76.
- [58] Zheng W, Xu G. 1996. Influence of Air Heat Sink Geometry on the Performance of Thermoelectric Cooling Modules, 15<sup>th</sup> International Conference on Thermoelectrics, Pasadena, California, March 25-28, p. 311-314.
- [59] Ritzer T, Nagy M, Lau P. 1994. Economic Optimization of Heat Sink Design, 13<sup>th</sup> International Conference on Thermoelectrics, Kansas City, Missouri, August 30 – September 1
- [60] Buist R, Nagy M. 1994. Thermoelectric Heat Sink Modeling and Optimization, 13th International Conference on Thermoelectrics, Kansas City, Missouri, August 30 - September 1

### **Stirling Engines**

- [61] Cengel Y, Boles M. 2001. *Thermodynamics: An Engineering Approach*, New York, McGraw-Hill
- [62] Walker G. 1980. *Stirling Engines*, Oxford, Clarendon Press.
- [63] Mills D. 2004. Advances in Solar Thermal Electricity Technology, Solar Energy, 76, p. 19-31.
- [64] Kongtagool B, Wonwises S. 2003. A Review of Solar-Powered Stirling Engines and Low Temperature Differential Stirling Engines, 2003, Renewable and Sustainable Energy Reviews, 7, p. 131-154

- [65] Senft J. 1991. An Ultra Low Temperature Differential Stirling Engine, Proceedings of the Fifth International Stirling Engine Conference, Paper ISEC 91032, Dubrovnik, May 1991
- [66] Prodesser E. 1999. Electricity Production in Rural Villages with Biomass Stirling Engine, Renewable Energy, 16, p. 1049-52.
- [67] Dixit D, Ghodke S. 1992. Renewable Energy Powered Stirling Engines-A Viable Energy Alternative, In: Sayigh AAM, editor, Renewable Energy Technology and the Environment. Proceedings of the Second World Renewable Energy Congress, 2, p. 934-8.
- [68] Lane N, Beale W. 1999. A Biomass-Fired 1 kWe Stirling Engine Generator and Its Applications in South Africa, Presented at: 9<sup>th</sup> International Stirling Engine Conference, South Africa, June 2-4.
- [69] Lane N, Beale W. 1997. Micro-Biomass Electric Power Generation, Presented at: Third Biomass Conference of the Americas, Montreal, Canada.
- [70] Incopera F, Dewitt D. 2002. Fundamentals of Heat and Mass Transfer, New Jersey, John Wiley & Sons.

### **Lighting**

- [71] <http://www.lumileds.com/> August 2006
- [72] [http://www.netl.doe.gov/ssl/PDFs/energyEfficiency\\_oct25\\_06.pdf](http://www.netl.doe.gov/ssl/PDFs/energyEfficiency_oct25_06.pdf) August 2006
- [73] [http://www.rightlight6.org/english/proceedings/Poster\\_Session/CCFL\\_Light\\_Bulb\\_for\\_General\\_Lighting/f070guan.doc](http://www.rightlight6.org/english/proceedings/Poster_Session/CCFL_Light_Bulb_for_General_Lighting/f070guan.doc) August 2006
- [74] Dutt G. 1994. Illumination and Sustainable Development. Part 1: Technology and Economics, Energy for Sustainable Development, 1(1), p. 23-35

### **Textbooks**

- [75] F. White, *Fluid Mechanics*, McGraw-Hill, New York, 1999.
- [76] Bode H, *Lead-Acid Batteries*, John Wiley & Sons, New York, 1977.

### **Peak Power Tracking**

- [77] Eakburanawat J, Boonyaroonate I. 2005. Development of a Thermoelectric Battery-Charger with Microcontroller-Based Maximum Power Point Tracking Technique, Applied Energy, 83, p. 687-704
- [78] Gitano H, Taib S, Khdeir M. 2007. Design and Testing of a Low Cost Peak-Power Tracking Controller for a Fixed Blade 1.2 kVA Wind Turbine. 5<sup>th</sup> International Conference-Wokshop CPE 2007

- [79] Agrawal J. P. 2001. *Power Electronic Systems Theory and Design*, New Jersey, Prentice Hall
- [80] Wildi T. 2001. *Electrical Machines, Drives and Power Systems*, New Jersey, Prentice Hall

## 12 Appendix

### 12.1 Microcontroller Code (PicBasic)

```

*****
* Name   : Meter_PPT_Res_07           *
* Date   : 11/10/2007                 *
* Version : 1.0                       *
* Notes  : This program is configured *
*          : to use the resistance      *
*          : tracking method of PPT for *
*          : 2 Thermonamic 10W        *
*          : modules in series         *
*****

Define OSC 20
trisa = %11001111           'Setting port A inputs
ADCON1 = %10000000         ' Set PORTA analog
ANSEL = %00001111
trisb = %00110000          'Setting inputs and outputs on portB
ANSELH = %00000000        'Setting pins portB 0,1,2,3,4,5 digital %--543210

'----- PWM Setup -----
TRISC.1 = 0
TRISC.2 = 0                 ' Set PORTC.2 (CCP1) to output
CCP1CON = %00001100        ' Set CCP1 to PWM
CCP2CON = %00001100        ' Set CCP2 to PWM
T2CON = %00000100          ' Turn on Timer2, 00 Prescale=1, 01 pS=4
PR2 = 255                  ' Set PR2 to get 10 bit

'-----Define ADCIN parameters-----
Define  ADC_BITS      10    ' Set number of bits in result
Define  ADC_CLOCK     0     ' Set clock source (3=rc)
Define  ADC_SAMPLEUS  50    ' Set sampling time in uS

'-----[ LCD Setup ]-----
DEFINE LCD_DREG PORTC      ' Set LCD Data port
DEFINE LCD_DBIT 4          ' Set starting Data bit (0 or 4) if 4-bit bus
DEFINE LCD_RSREG PORTC    ' Set LCD Register Select port
DEFINE LCD_RSBIT 0        ' Set LCD Register Select bit
DEFINE LCD_EREG PORTC     ' Set LCD Enable port
DEFINE LCD_EBIT 3         ' Set LCD Enable bit
DEFINE LCD_BITS 4         ' Set LCD bus size (4 or 8 bits)
Define LCD_LINES 2

'-----Variable definitions-----
Fan Var portc.2
Light var portb.0
Buzz var portb.1
SW1 var portb.4           ' checks system values
SW2 var portb.5           ' checks peaks since last reset

```

```

Red var portb.7
Green var portb.6
Mod_Amp Var porta.4
Bat_Amp Var portb.2
charger var porta.5

Vmod var word ' Module voltage
V_OC var word ' Module Open circuit voltage
Vmod_raw var word ' Module voltage bits
Imod VAR WORD ' Module current
Imod_raw VAR WORD ' Module current bits
Imod_old var Word ' Used for peak power tracking
Vbat var word ' Battery voltage
PeakVbat var word ' Peak Battery voltage since reset
PeakVbat2 var word ' Peak Battery voltage for day
PeakVmod VAR word ' Peak Module voltage since last reset
MinVbat var word ' Minimum battery voltage
Ibat var word ' Current from battery
Pwr var word ' Power from module
Pwr_new var word ' new power value
Pwr_old var word ' old power value from last cycle
Pwr_raw var word ' product of raw voltage and current, lowest 16 bits
PeakPwr var word ' Peak power from module since last reset
Energy Var Word ' Energy generated over logging period
Rload var word ' Load resistance
Rmod var word ' module resistance
Mod_Duty var word ' Charger duty cycle
Dutyin var word ' duty into V_OC loop
Vfan var word ' desired fan voltage
Fan_duty var word ' Fan duty cycle
VCharged var word ' Voltage where battery is fully charged
VHyst1 var word ' Hysteresis voltage where charging is enabled again
VHyst2 Var Word ' Hysteresis voltage, battery is tuned back on again
VBuzz var word ' Battery voltage where buzzer sounds
VCutoff var word ' Battery voltage where battery shuts off
VMin var word ' Absolute minimum value for VCutoff
VMod_th1 Var Word ' Voltage where charging circuit "awakes"
VMod_th2 Var Word ' Voltage where charging circuit begins PWM
Charged var Bit ' Binary, 1 if completely charged state is reached
Discharged Var Bit ' Binary, 1 if completely discharged state is reached
Rampup var bit ' used as a hysteresis on startup
Rampdown var bit ' used as a hysteresis on ramp down
plus var bit ' used to increment duty
minus var bit ' used to decrement duty
t_Osc var Byte ' time multiplier for given oscillator setting
n var byte ' counter for open circuit voltage measurement
cyc var byte ' fractional seconds
s var byte ' seconds since last reset
minute var byte ' minutes since last reset
hr Var byte ' hours since last reset
day var byte ' days since last reset
volts con 205 ' divisor for A/D to convert from bit value to actual

```

----- initial values -----

```

Low Green
Low Red
Low Buzz
Low Fan
Low light
high charger

```

```

t_Osc = 20 'program starts at 20 MHz
n = 0
cyc = 0
s = 0
minute = 0
hr = 0
day = 0
Energy = 0
Pwr = 0

```

```

PeakPwr = 0
PeakVbat = 0
MinVbat = 13600

Mod_duty = 0
CCP2CON.4 = Mod_duty.0      ' Store duty to registers as
CCP2CON.5 = Mod_duty.1      ' a 10-bit word
CCPR2L = Mod_DUTY >> 2

Fan_Duty = 0
CCP1CON.4 = fan_duty.0      ' Store duty to registers as
CCP1CON.5 = fan_duty.1      ' a 10-bit word
CCPR1L = fan_duty >> 2

Charged = 1
Discharged = 0

Imod_old = 0 'used for Ibat PPT
Plus = 1     'used for Ibat PPT
Minus = 0    'used for Ibat PPT

Vcharged = 20000
Vhyst1 = 13100
Vhyst2 = 4000
Vbuzz = 4000
VCutoff = 4000
Vmin = 9000
VMod_th1 = 2400 'for 2 TEP1-0.8 and 2 mech fans @ 6V startup
VMod_th2 = 1000 'for 2 TEP1-0.8 and 2 mech fans @ 6V startup

V_OC = 0
Rampup = 0

Pause (500/20)*t_osc
    LCDOUT $FE, 1 'clear screen'
    LCDOUT "Initialized"
    High green
    Pause (1000/20)*t_osc
    Low green
'----- loop 1 -----
loop1:
'----- A-D measurements -----
Pause (200/20)*t_osc      'pause to let RC filter stabilize

Adcin 0, Vmod_raw          'reading module voltage pin A0
Vmod = Vmod_raw * 20      ' scaling 20 for 1/4, 29 for 1/6

ADCIN 1, Vbat              'reading battery voltage
Vbat = Vbat * 20          'scaling 20 for 1/4, 29 for 1/6

if cyc = 1 then
High Bat_amp
pause (200/20)*t_osc
cyc = cyc + 1

ADCIN 2, Ibat              'reading battery voltage pin A2
Ibat = Ibat * 39 / 10     'scaling .025 sense 50X amp
Low Bat_Amp
Endif

ADCin 3, Imod_raw          'reading module voltage
Imod = (Imod_raw/6) * 50  'scaling for .03 sense 20X amp

'-----Calculations-----
Pwr = (Vmod/32) * (Imod / 32)
'----defining peaks----
if pwr > PeakPwr then
Peakpwr = Pwr
endif

```

```

if Vbat > PeakVbat then
PeakVbat = Vbat
endif

if Vbat > PeakVbat2 then
PeakVbat2 = Vbat
endif

if Vmod > PeakVmod then
PeakVmod = Vmod
endif

if Vbat < MinVbat then
MinVbat = Vbat
endif

'-----Check Switch Status-----'
if SW1 = 0 and SW2 = 0 then

LCDOUT $FE, 1, "Vm=", #Vmod, " Im", #Imod
LCDOUT $FE, $C0, "P=", #Pwr, " Vb=", #Vbat

' other display options
'LCDOUT $FE, $C0, "Iraw ", #Imod_raw, " D", #Mod_Duty
'LCDOUT $FE, $C0, "Rm=", #Rmod, " R=", #Rload, " %", #Mod_duty

LCDOUT $FE, 1, "Vm=", #Vmod, " Im", #Imod
LCDOUT $FE, $C0, "Rm=", #Rmod, " R=", #Rload, " %", #Mod_duty

endif

'-----Report peaks-----

IF SW1 = 1 Then

LCDOUT $FE, 1, "PeakVbat ", #PeakVbat
LCDOUT $FE, $C0, "MinVbat ", #MinVbat
Pause (3000/20)*t_osc
LCDOUT $FE, 1, "PeakPwr ", #PeakPwr
LCDOUT $FE, $C0, "PeakVmod", #PeakVmod
Pause (3000/20)*t_osc

Endif

'-----system check-----
If SW2 = 1 Then
LCDOUT $FE, 1, "VCutoff ", #VCutoff
LCDOUT $FE, $C0, "Charg ", #Charged, " Disch ", #Discharged
Pause (3000/20)*t_osc
LCDOUT $FE, 1, #day, "day ", #hr, ":", #minute, ":", #s
LCDOUT $FE, $C0, "Energy ", #Energy, " W-min"
pause (3000/20)*t_osc
Endif

'-----Battery Management-----
'-----Adaptive Capacity Adjustments -----

if hr = 23 and minute = 59 and s = 59 then

if PeakVbat2 = Vcharged then
VCutoff = VCutoff - 200
endif

If peakVbat2 < Vcharged then
Vcutoff = Vcutoff + 200
endif

if Vcutoff < VMin then
Vcutoff = VMin

```

```

endif

endif
'-----light, buzzer, cutoff-----'
if Vbat > Vcharged then

pause 2000
LCDOUT $FE, 1, "Tripped ", #Vbat
ADCIN 1, Vbat           'reading battery voltage
Vbat = Vbat * 20        'scaling 20 for 1/4, 29 for 1/6

if Vbat > Vcharged then 'pause and check again for signal noise
Charged = 1
PeakVbat2 = Vbat
LCDOUT $FE, 1, "Charged ", #Vbat
pause 5000
low charger
Mod_Duty = 0
CCP2CON.4 = Mod_duty.0      ' Store duty to registers as
CCP2CON.5 = Mod_duty.1      ' a 10-bit word
CCPR2L = Mod_DUTY >> 2
Endif

endif

if Vbat < VHyst1 then
Charged = 0
high charger
endif

If Vbat > Vhyst2 Then
Discharged = 0
High Light
endif

If Vbat < VBuzz then
Discharged = 1
endif

If Vbat < VCutoff then
Low Light
endif

'-----Buzzer Setting-----
If Ibat > 100 then
  If Discharged = 1 then
    High Buzz
  endif
endif

  If Discharged = 0 Then
    If Vbat < VBuzz then
      High Buzz
    Endif

    If Vbat > VHyst2 then
      Low Buzz
    endif
  Endif

else
Low Buzz

ENDIF

'-----Sleep Mode-----
if rampup = 0 then
If Vmod < Vmod_th1 then
'Define CONFIG1 = %100
OSCCON = %1000111 'setting oscillator to internal, 1 MHz
t_Osc = 1

```

```

Low Mod_amp

fan_duty = 0
CCP1CON.4 = fan_duty.0      ' Store duty to registers as
CCP1CON.5 = fan_duty.1      ' a 10-bit word
CCPR1L = fan_duty >> 2

Mod_duty = 0
CCP2CON.4 = Mod_duty.0      ' Store duty to registers as
CCP2CON.5 = Mod_duty.1      ' a 10-bit word
CCPR2L = Mod_DUTY >> 2

goto time_inc

endif
endif

If Vmod < VMod_th2 then
Rampup = 0
endif

if t_osc = 1 then
'Define CONFIG1 = %010      ' setting oscillator to external, 20 MHz
OSCCON = %01101000
t_osc = 20
pause 100
Rampup = 1
High Mod_Amp
pause 100

endif

'-----Charging Circuit-----
'-----Setting fan-----
fan_duty = 500 + ((Vmod-2000)*5)/60

if fan_duty > 1020 then      'seting max fan duty, if >1024 it will go to 0
fan_duty = 1020
endif

CCP1CON.4 = fan_duty.0      ' Store duty to registers as
CCP1CON.5 = fan_duty.1      ' a 10-bit word
CCPR1L = fan_duty >> 2

'-----Charged battery exit-----
if charged = 1 then

Mod_duty = 0
CCP2CON.4 = Mod_duty.0      ' Store duty to registers as
CCP2CON.5 = Mod_duty.1      ' a 10-bit word
CCPR2L = Mod_DUTY >> 2
low charger
goto time_inc
endif

'-----Peak Power Tracking-----
High mod_amp

If Mod_Duty = 0 then      'lower limit on duty for faster recovery from 0 excursion

If VMod < 4000 then
Mod_Duty = 927      'set to maintain voltage over "on threshold"
endif

If Vmod > 4000 then
Mod_Duty = 500      'this is for the situation where the module voltage is
                    'high but the duty has been 0 because the battery is
If Vmod > 8000 then 'charged, when the battery voltage comes below the threshold
Mod_duty = 300      'the duty cannot be set to 927 or it will create too high
Endif              'a voltage on the battery and high current from the module

```

```

endif

CCP2CON.4 = Mod_duty.0          ' Store duty to registers as
CCP2CON.5 = Mod_duty.1          ' a 10-bit word
CCPR2L = Mod_DUTY >> 2

endif

'----- Adjusting Duty Cycle, Peak Power Tracking -----
Rload = Vmod / (Imod/10)        ' Calculating load resistance

Rmod = 20 + (((Vmod*3)/100)*6)/100 ' 2 + Vmod*.18 for 2 TEP1-0.8 in series
          ' Calculating module resistance

If Rload > Rmod then
Mod_duty = Mod_duty + 1        'adjusting duty for PPT
Endif

if Rload < Rmod Then
Mod_duty = Mod_duty - 1        'adjusting duty for PPT
endif

if Mod_Duty > 927 then          'setting max duty cycle
Mod_Duty = 927                 'set to maintain voltage over "on threshold"
plus = 0
minus = 1
endif

CCP2CON.4 = Mod_Duty.0          ' Store duty to registers as
CCP2CON.5 = Mod_Duty.1          ' a 10-bit word
CCPR2L = Mod_Duty >> 2

'----- Time/Energy update -----
time_inc:
cyc = cyc + 1
if cyc = 10 then
High green
pause (20 /20)*t_osc
Low green
cyc = 0
if t_osc = 20 then              'time is only added when module is on
s = s + 2
endif
endif

if s => 60 then
minute = minute + 1
s = 0
Energy = Energy + Pwr/1000 ' energy in W-min
endif

if minute = 60 then
hr = hr + 1
minute = 0
endif

if hr = 24 then
hr = 0
day = day + 1
endif

goto loop1

```

## 12.2 EES Model Code

"Note: All functions and procedures are defined first in the code, but are not solved in that order. This is how functions must be defined in EES. See chapter on modeling for program architecture"

```

"-----Writing variables to table-----"
function WriteVals(T_mod_hot, V_mod, V_fan, P_fan, P_net,i)

Lookup('Temptime7&8',i,3) = T_mod_hot
Lookup('Temptime7&8',i,4) = P_net
Lookup('Temptime7&8',i,5) = P_fan
Lookup('Temptime7&8',i,6) = V_mod
Lookup('Temptime7&8',i,7) = V_fan
WriteVals = T_mod_hot

end

"-----Write monthly energy totals-----"
function Monthly_Vals(Energy_net_tot,k)      "k = month"

Lookup('Month',k,1) = k                    "k = month"
Lookup('Month',k,2) = Energy_net_tot
Monthly_Vals = 0

end

"-----Monthly Increment-----"
Procedure month_inc (CS,M:Energy_net_tot,Energy_mod_tot)  "calculating energy generated each month"

k := 0
Dam_R_elec_tot := 0
Dam_R_therm_tot :=0

Repeat
k := k + 1      "k = month"

call damage(CS, M : Dam_R_elec, Dam_R_therm)      "calculating damage done that month"
Dam_R_elec_tot = Dam_R_elec_tot + Dam_R_elec      "adding monthly damage to total damage"
Dam_R_therm_tot = Dam_R_therm_tot + Dam_R_therm  "adding monthly damage to total damage"

call Monthtotals(CS,M, Dam_R_elec_tot, Dam_R_therm_tot : Energy_net_tot,Energy_mod_tot)

write2 = Monthly_Vals(Energy_net_tot,k)

Until (k=60)      "k = month"
END

"-----Damage Model-----"
Procedure damage(CS, M : Dam_R_elec, Dam_R_therm)

j := 0
REPEAT
j:=j+1

T_hotgas = Lookup('Cycle',j,1)
cycles = Lookup('Cycle',j,2)

Dam_R_elec := 0
Dam_R_therm := 0

Call Solver(CS,M,Dam_R_elec,Dam_R_therm,T_hotgas : P_fan,V_fan,V_mod,P_net, P_ml,P_mod, P_dc,Tot_cost,
T_mod_hot, Q)      "Calling main solver block to return system operating temperatures to be used in damage calcs"

Dam_R_elec = cycles * INTERPOLATE('Damage_TEP1','T_mod_hot',Dam_R_elec',T_mod_hot=T_mod_hot)
Dam_R_therm = cycles * INTERPOLATE('Damage_TEP1','T_mod_hot',Dam_R_therm',T_mod_hot=T_mod_hot)
Dam_R_elec = cycles * INTERPOLATE('Damage_Hi-Z','T_mod_hot',Dam_R_elec',T_mod_hot=T_mod_hot)
Dam_R_therm = cycles * INTERPOLATE('Damage_Hi-Z','T_mod_hot',Dam_R_therm',T_mod_hot=T_mod_hot)"
Dam_R_elec_arr[j] = Dam_R_elec
Dam_R_therm_arr[j] = Dam_R_therm

```

```

UNTIL ( j=8 )      "number of rows in Cycle, which is the hot gas temperature intervals"

Dam_R_elec = SUM(Dam_R_elec_arr[1..8])
Dam_R_therm = SUM(Dam_R_therm_arr[1..8])

END
"-----"
PROCEDURE Monthtotals(CS,M, Dam_R_elec, Dam_R_therm : Energy_net_tot,Energy_mod_tot)

i := 0
REPEAT
i:=i+1

T_hotgas = Lookup('Temptime7&8',i,1)  "Looking up values in Temptime table"
minutes = Lookup('Temptime7&8',i,2)   "Looking up values in Temptime table"

Call Solver(CS,M,Dam_R_elec, Dam_R_therm,T_hotgas : P_fan,V_fan,V_mod,P_net, P_ml,P_mod, P_dc,Tot_cost,
T_mod_hot, Q)      "Calling main solver block to return system operating conditions"

write = WriteVals(T_mod_hot, V_mod,V_fan, P_fan, P_net,i)   "writing results to table WriteVals"

Energy_ml = P_ml*minutes/60      "calculating energy from power"
Energy_mod = P_mod*minutes/60    "calculating energy from power"
Energy_net = P_net*minutes/60    "calculating energy from power"
Energy_dc = P_dc*minutes/60     "calculating energy from power"

Energy_net_arr[i] = Energy_net    "input energy values into array to be summed"
Energy_mod_arr[i] = Energy_mod    "input energy values into array to be summed"
"Energy_dc_arr[i] = Energy_dc"

UNTIL (i=73)      "number of rows in Temp-time"

Energy_net_tot = SUM(Energy_net_arr[1..73])
Energy_mod_tot = SUM(Energy_mod_arr[1..73])
Cost_Whr = Tot_cost/SUM(Energy_net_arr[1..73])

END
"-----Modules-----"
PROCEDURE Module_info(T_avg, M,Dam_R_elec,Dam_R_therm : Seeb,R_mod, R_elec, R_int, M_cost, mf, bf,
V_fan_on)

"TEPI-0.8"
IF M = 1 THEN
R_elec := (-1.6701E-08*T_avg^3 - 1.4944E-05*T_avg^2 + 8.1478E-03*T_avg + 7.5421E-01) * (1+Dam_R_elec)
Seeb := 3.7617E-09*T_avg^3 - 2.2317E-06*T_avg^2 + 3.1402E-04*T_avg + 3.5465E-02
R_mod := (-0.0006*T_avg + 0.6800)
R_int := .03 + (Dam_R_therm*R_mod)/2
M_cost = 20
mf = 2.2   "defining fan voltage curve"
bf = 6     "defining fan voltage curve"
V_fan_on = .8   "voltage where fans turn on"
ENDIF

"TEPI-0.6"
IF M = 2 THEN
R_elec := (-1.9542E-05*T_avg^2 + 7.2444E-03*T_avg + 4.7525E-01) * (1+Dam_R_elec)
Seeb := -1.9632E-08*T_avg^2 - 9.0824E-05*T_avg+ 5.8400E-02
R_mod := -8.1827E-04*T_avg + 5.0696E-01
R_int := .03 + (Dam_R_therm*R_mod)/2
M_cost = 20
mf = 2.2   "defining fan voltage curve"
bf = 6     "defining fan voltage curve"
V_fan_on = .6   "voltage where fans turn on"
ENDIF

"TEPI-1.5"
IF M = 3 THEN
R_elec := (-3.7075E-05*T_avg^2 + 1.3532E-02*T_avg + 1.2097E+00)*(1+Dam_R_elec)
Seeb := -4.8211E-05*T_avg + 5.1610E-02
R_mod := -1.4623E-03*T_avg + 1.0335E+00

```

```

M_cost = 10
mf = 2.6      "defining fan voltage curve"
bf = 6        "defining fan voltage curve"
V_fan_on = .8 "voltage where fans turn on"
ENDIF

"Hi-Z 14"
IF M = 4 THEN
R_elec := (5.1724E-04*T_avg + 1.1459E-01)*(1+Dam_R_elec)
Seeb := 7.5548E-06*T_avg + 1.5525E-02
R_mod := -4.2170E-04*T_avg + 5.1749E-01
R_int := .03 + (Dam_R_therm*R_mod)/2
M_cost = 80
mf = 6        "defining fan voltage curve"
bf = 6        "defining fan voltage curve"
V_fan_on = .17 "voltage where fans turn on"
ENDIF

"Hi-Z 9"
IF M = 5 THEN
R_elec := (2.5563E-07*T_avg^3 - 1.0014E-04*T_avg^2 + 1.4157E-02*T_avg + 8.3623E-01)*(1+Dam_R_elec)
Seeb := -5.9086E-05*T_avg + 4.7684E-02
R_mod := -2.1024E-03*T_avg + 1.0733E+00
M_cost = 100
mf = 2.0      "defining fan voltage curve"
bf = 6        "defining fan voltage curve"
V_fan_on = .8 "voltage where fans turn on"
ENDIF

END
"-----Coldsinks-----"
PROCEDURE Coldsink(CS,mf ,bf, V_fan_on ,V_mod, N_mod: R_coldsink, V_fan, P_fan,CS_cost)

V_fan := (V_mod-V_fan_on)*mf + bf      "Defining variable van voltage"
IF V_fan > 13 THEN                      "fan voltage cannot exceed battery voltage"
V_fan = 13
ENDIF
IF V_fan < 0 THEN                        "fan voltage cannot be negative"
V_fan = 0
ENDIF

" 6.5 E1456, mechatronics fan"
IF CS = 1 THEN
P_fan = (0.0139*V_fan^2 - 0.0848*V_fan + 0.2145)*N_mod
IF V_mod < V_fan_on THEN
V_fan := 0
P_fan := 0
ENDIF
R_coldsink := -2.799E-04*V_fan^3 + 1.111E-02*V_fan^2 - 1.527E-01*V_fan + 8.484E-01
CS_cost = 6.5*(20/6.5)
ENDIF

" 5 in E1456, mechatronics fan"
IF CS = 2 THEN
P_fan = (0.0139*V_fan^2 - 0.0848*V_fan + 0.2145)*N_mod
IF V_mod < V_fan_on THEN
V_fan := 0
P_fan := 0
ENDIF
R_coldsink := -3.090E-04*V_fan^3 + 1.180E-02*V_fan^2 - 1.562E-01*V_fan + 8.562E-01
CS_cost = 5*(20/6.5)
ENDIF

" 3.75 E1456, mechatronics fan"
IF CS = 3 THEN
P_fan = (0.0139*V_fan^2 - 0.0848*V_fan + 0.2145)*N_mod
IF V_mod < V_fan_on THEN
V_fan := 0
P_fan := 0
ENDIF

```

```

R_coldsink := -3.368E-04*V_fan^3 + 1.211E-02*V_fan^2 - 1.530E-01*V_fan + 8.456E-01
CS_cost = 3.75*(20/6.5)
ENDIF

" Melcor 6, mechatronics fan"
IF CS = 4 THEN
P_fan = (0.0139*V_fan^2 - 0.0848*V_fan + 0.2145)*N_mod
IF V_mod < V_fan_on THEN
V_fan := 0
P_fan := 0
ENDIF
R_coldsink := -1.760E-04*V_fan^3 + 6.406E-03*V_fan^2 - 8.224E-02*V_fan+ 5.076E-01
CS_cost = 6*(20/6.5)
ENDIF

END

"-----Hot Sink Properties-----"
PROCEDURE Hotsink(T_hotgas, T_mod_hot: R_hotsink)

R_hotsink = .6 "variable R hot using bimetallic"
IF T_hotgas > 580 THEN "variable R hot using bimetallic"
R_hotsink = .6 + .29*((T_hotgas-600)/140) "variable R hot using bimetallic"
"R_hotsink = .89" "fixed R hot"
ENDIF
END

"-----"
SUBPROGRAM Solver(CS,M,Dam_R_elec,Dam_R_therm,T_hotgas : P_fan,V_fan,V_mod,P_net, P_ml,P_mod,
P_dc,Tot_cost, T_mod_hot, Q)

Tot_cost = M_cost*N_mod + CS_cost
N_mod = 2
P_ml = I_m * V_mod*N_mod
P_mod = P_ml*eta_dc_mod
P_dc = P_ml * eta_dc
P_net = P_dc - P_fan

"collect module data"
CALL Module_info(T_avg, M,Dam_R_elec,Dam_R_therm : Seeb,R_mod, R_elec, R_int, M_cost, mf, bf, V_fan_on)
"collect heatsink/fan data"
CALL Coldsink(CS, mf, bf, V_fan_on, V_mod, N_mod: R_coldsink, V_fan, P_fan,CS_cost)
"collect hot sink data"
CALL Hotsink(T_hotgas, T_mod_hot: R_hotsink)

"eta_dc = INTERPOLATE('ChargerPPT','V_oc','Eff_dc',V_oc=V_oc)
eta_dc_mod = INTERPOLATE('ChargerPPT','V_oc','Eff_dc_mod',V_oc=V_oc)"
eta_dc =.89 "fixed converter efficiency"
eta_dc_mod =1 "fixed converter PPT efficiency"

I_m = V_oc/(2*R_elec)
V_oc = Seeb*(T_mod_hot - T_mod_cold)
V_mod = .5*V_oc

T_amb =20
T_hot_block= T_hotgas - (R_hotsink)*(Q)
T_mod_hot = T_hotgas - (R_hotsink + R_int)*(Q)
T_mod_cold = T_mod_hot - (R_mod*Q)
T_avg = (T_mod_hot +T_mod_cold)/2
Q = (T_hotgas - T_amb)/(R_tot)
R_tot = R_hotsink + 2*R_int + R_mod + R_coldsink

End

"-----"

CS = 4 "defining cold sink/fan combo"
M = 2 "defining module"

call month_inc (CS,M:Energy_net_tot,Energy_mod_tot)

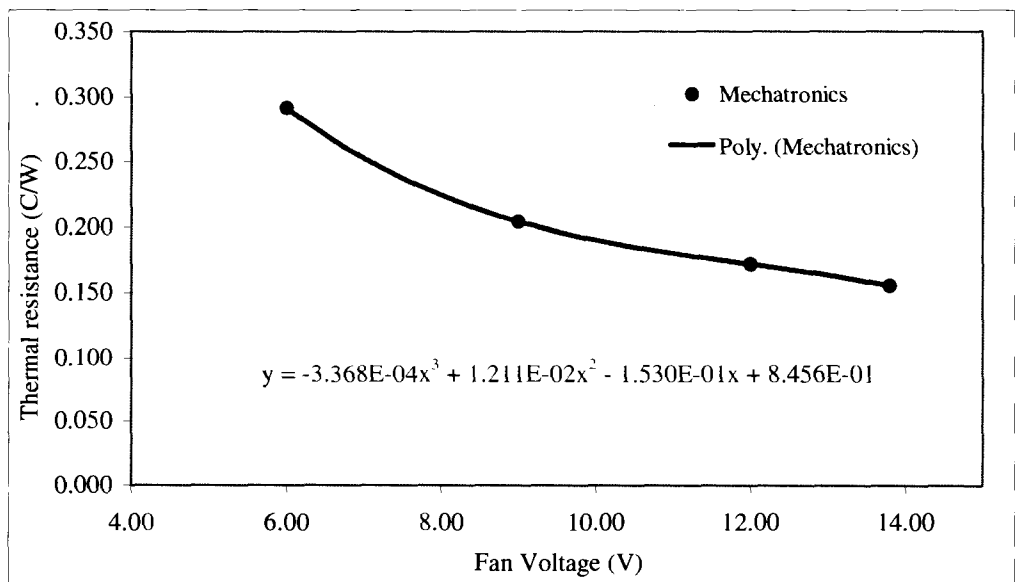
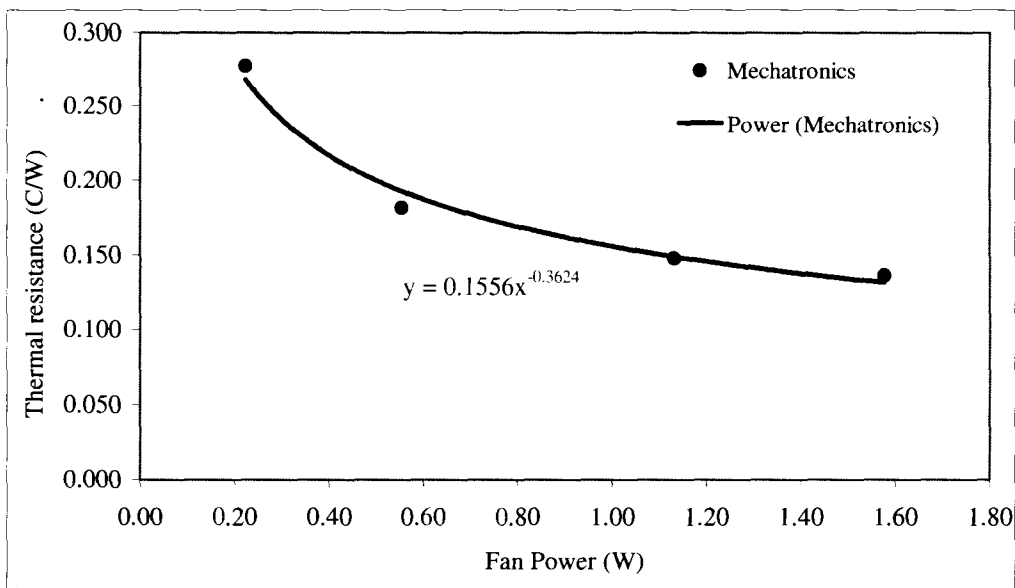
```

### 12.3 Heat sink data

#### Heatsink Thermaflo E1456 9.375 cm

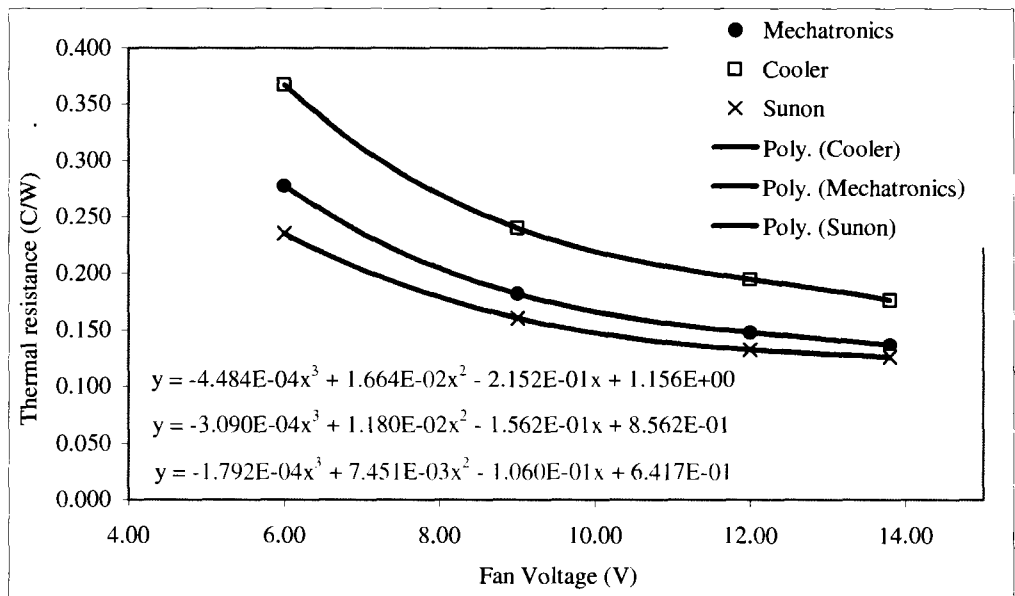
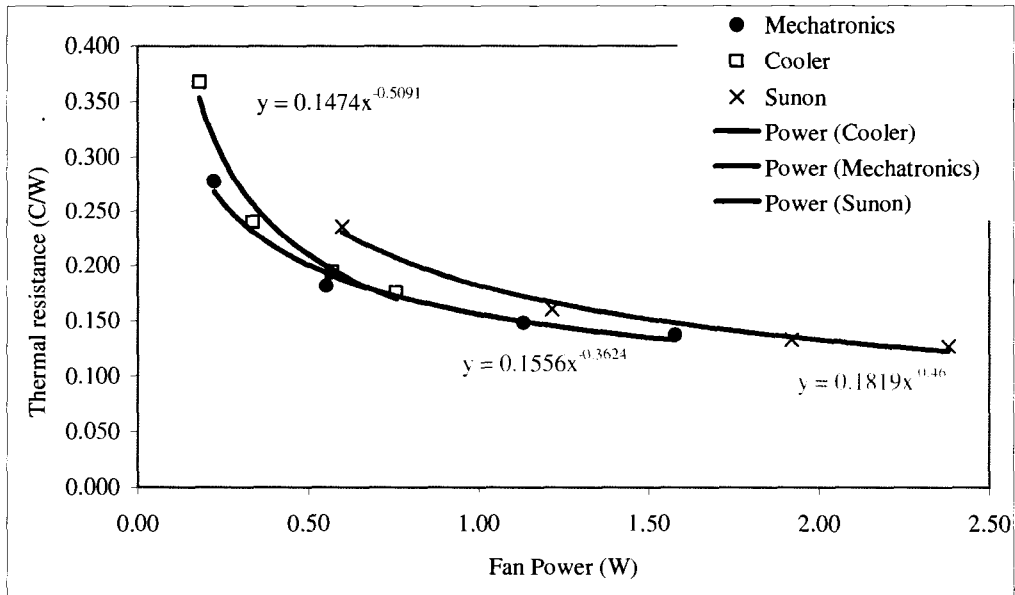
---

Length 9.375 cm (3.75 inch)  
Fan1 Mechatronics 1.2W



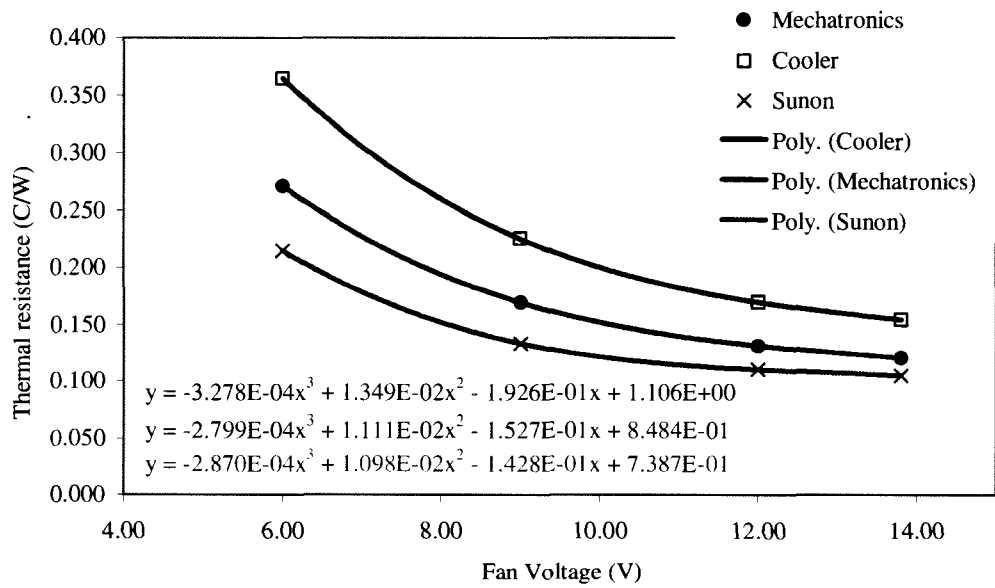
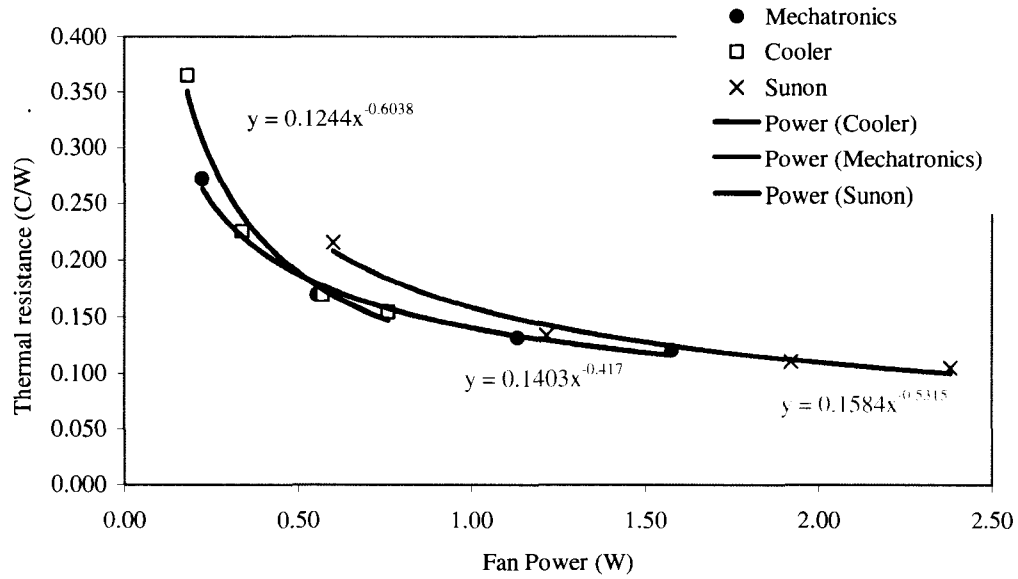
# Heatsink Thermaflo E1456 12.5 cm

Length	12.5 cm	(5 inch)
Fan1	Mechatronics	1.2W
Fan2	Cooler Master	0.6W
Fan3	Sunon	2.4W



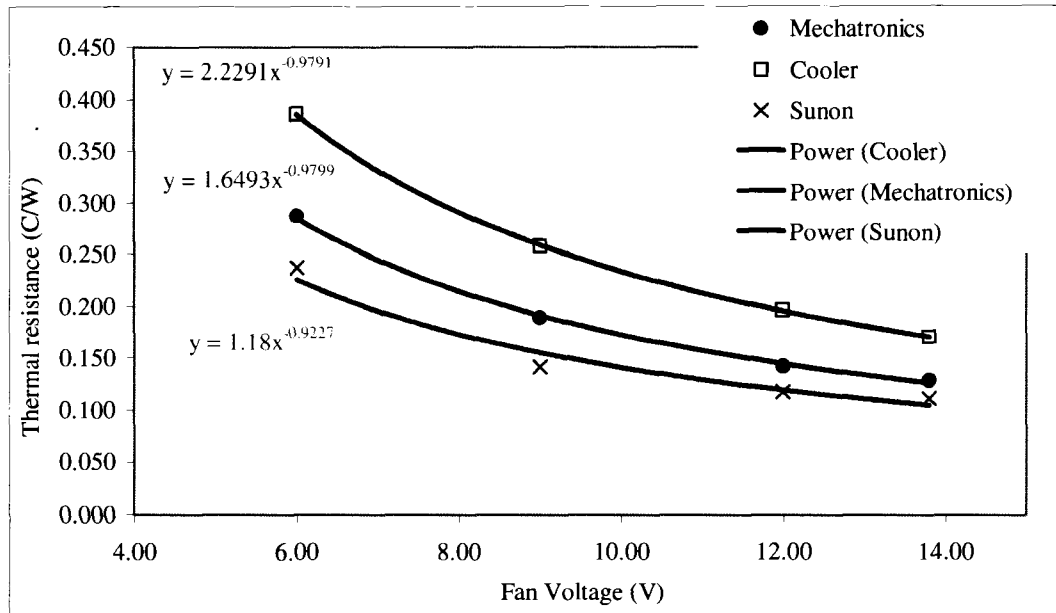
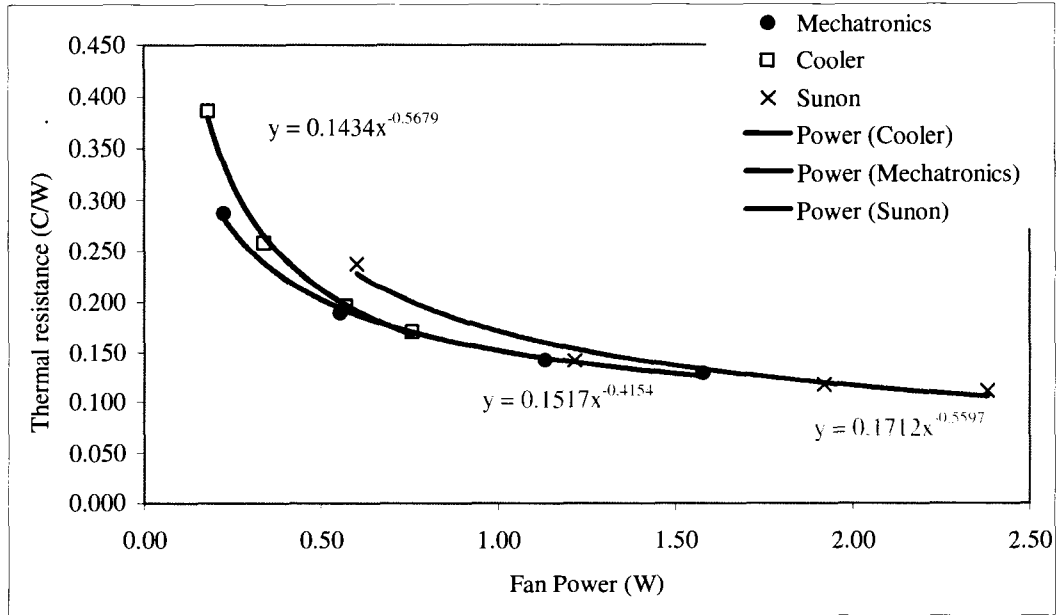
# Heatsink Thermaflo E1456 16.25 cm

Length	16.25 cm	(6.5 inch)
Fan1	Mechatronics	1.2W
Fan2	Cooler Master	0.6W
Fan3	Sunon	2.4W



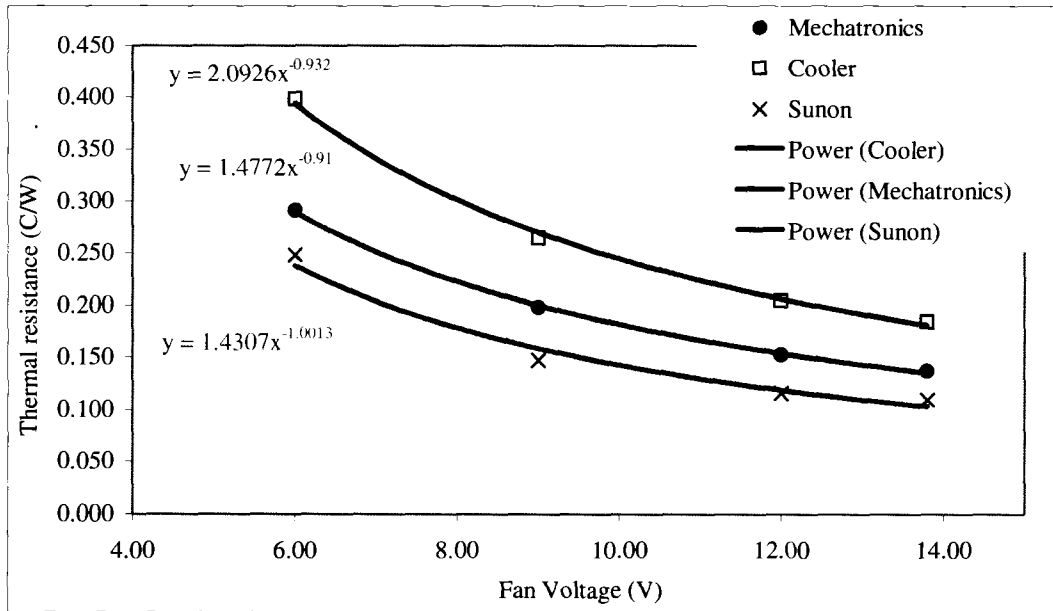
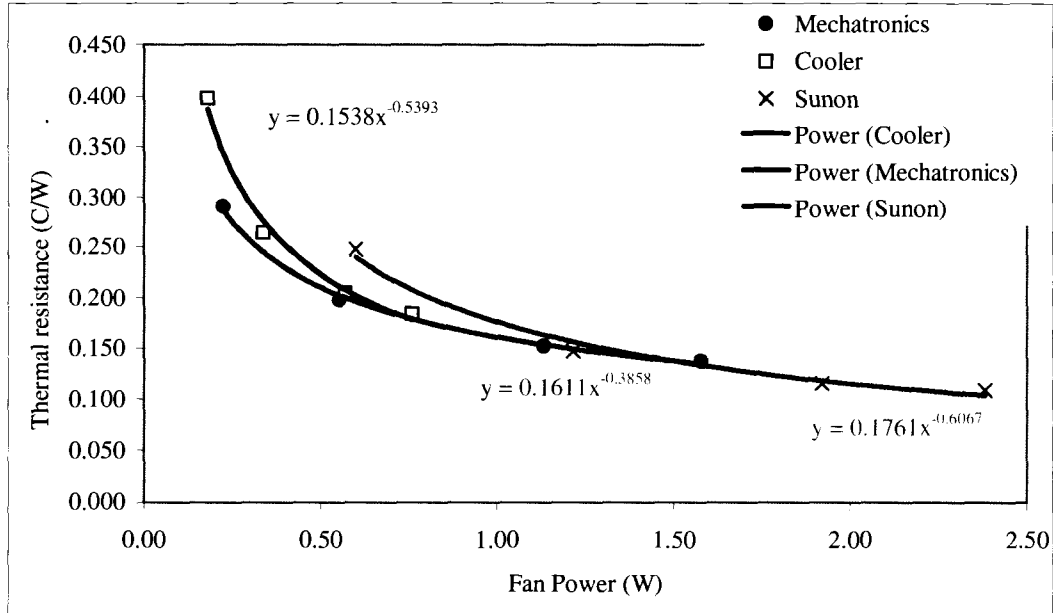
# Heatsink Thermaflo E1456 20 cm

Length	20 cm	(8 inch)
Fan1	Mechatronics	1.2W
Fan2	Cooler Master	0.6W
Fan3	Sunon	2.4W



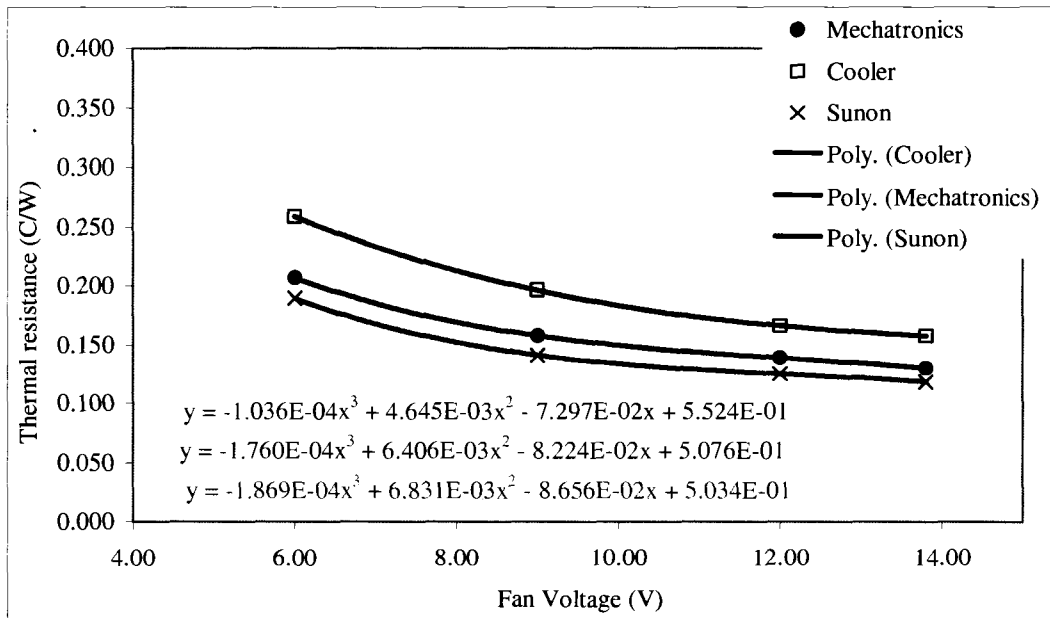
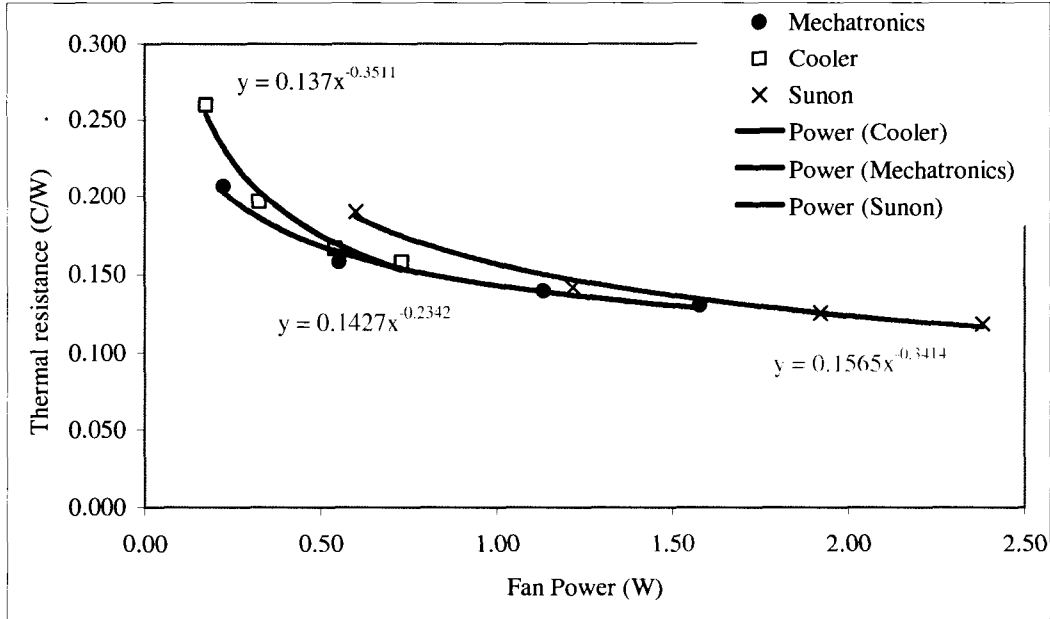
# Heatsink Thermaflo E1456 25 cm

Length	25 cm	(10 inch)
Fan1	Mechatronics	1.2W
Fan2	Cooler Master	0.6W
Fan3	Sunon	2.4W



# Heatsink Melcor Bonded 15 cm

Length	15 cm	(6 inch)
Fan1	Mechatronics	1.2W
Fan2	Cooler Master	0.6W
Fan3	Sunon	2.4W



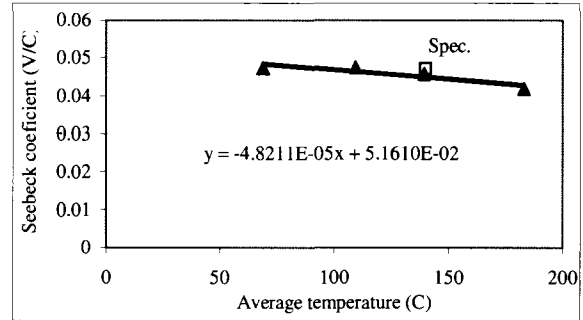
## 12.4 Module Data

Module TEP1-1.5

### Manufacturer Specs

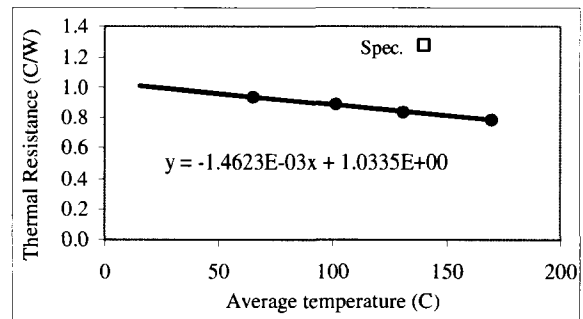
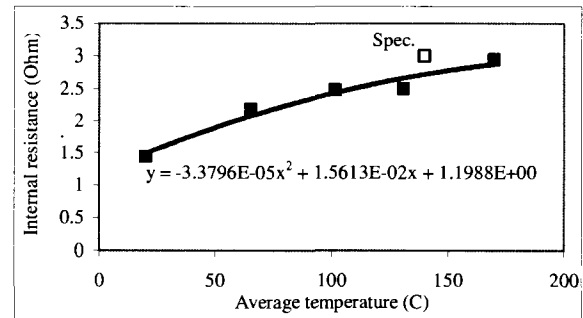
T hot (C)	230
T cold (C)	50
T avg (C)	140
Thermal Watts	140
Therm Res @match load (C/W)	1.28
Electrical Res (Ohm)	3
Voc @match load (V)	8.4
I @match load (Amps)	1.4
Seebeck coef. (V/C)	0.047
Efficiency	0.042
Power (W)	5.9

### Test Data



### Test Conditions

Heatsink	E1456 16.25cm
Fan	Mechatronics
Fan Voltage	12V

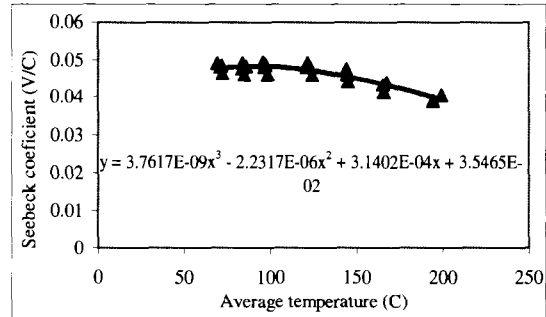


Module TEP1-0.8

Manufacturer Specs

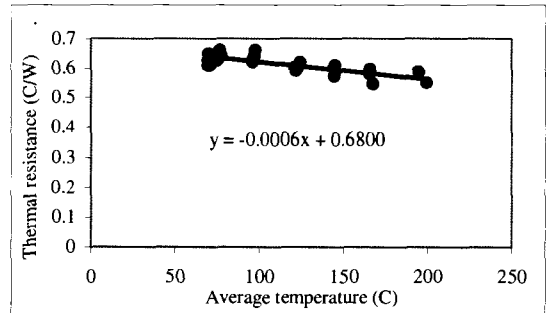
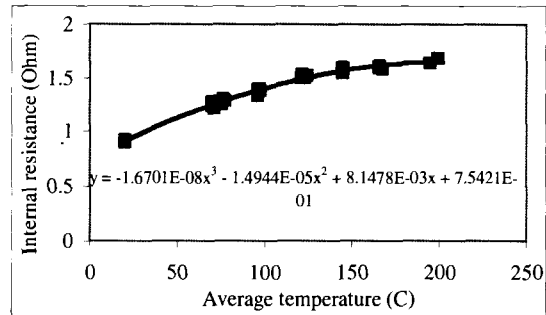
T hot (C)	230
T cold (C)	50
T avg (C)	140
Thermal Watts	240
Thermal Res @match load (C/W)	0.75
Electrical Res (Ohm)	1.7
Voc @match load (V)	8.4
I @match load (Amps)	2.5
Seebeck coef. (V/C)	0.046667
Efficiency	0.04375
Power (W)	10.5

Test Data



Test Conditions

Heatsink	E1456 16.25 cm
Fan	Mechatronics
Fan Voltage	12V

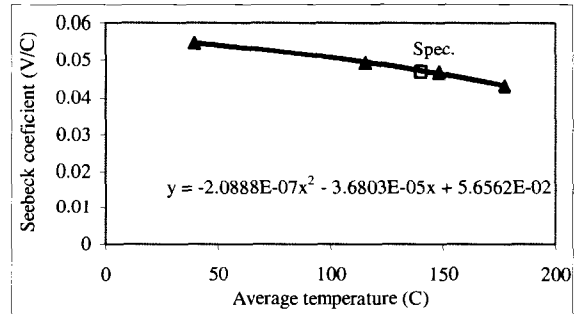


Module TEP1-0.6

Manufacturer Specs

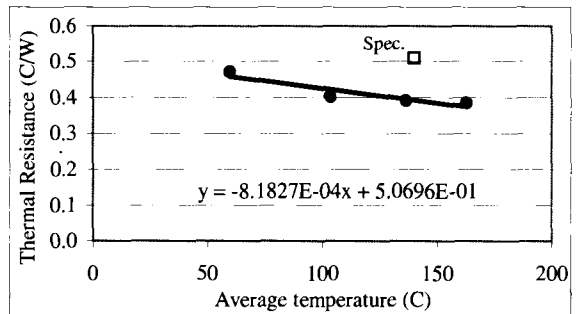
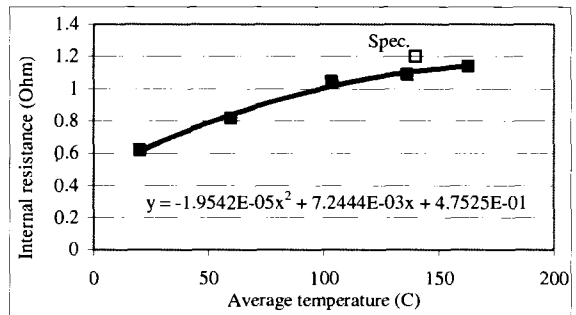
T hot (C)	230
T cold (C)	50
T avg (C)	140
Thermal Watts	350
Therm Res @match load (C/W)	0.5
Electrical Res (Ohm)	1.2
Voc @match load (V)	8.4
I @match load (Amps)	3.5
Seebeck coef. (V/C)	0.046667
Efficiency	0.042
Power (W)	14.7

Test Data



Test Conditions

Heatsink	E1456 16.25 cm
Fan	Mechatronics
Fan Voltage	12V





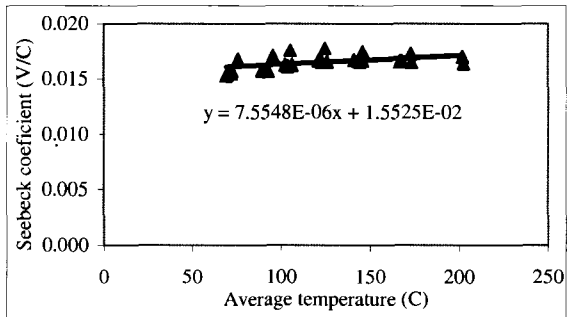
**Module** **HZ -14**

---

**Manufacturer Specs**

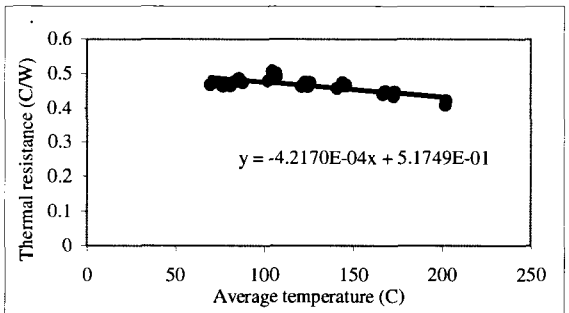
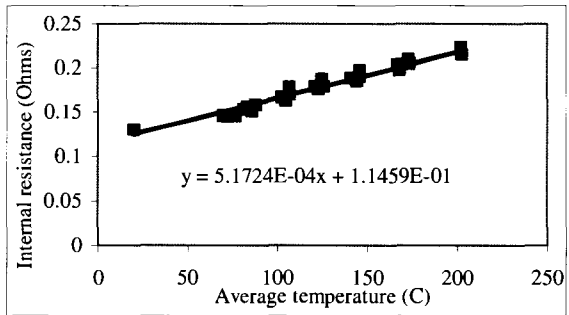
T hot (C)	230
T cold (C)	30
T avg (C)	130
Thermal Watts	375
Thermal Res @match load (C/W)	0.53
Electrical Res (Ohm)	0.15
Voc @match load (V)	3.3
I @match load (Amps)	8
Seebeck coef. (V/C)	0.0165
Efficiency	0.045
Power (W)	13.2

**Test Data**



**Test Conditions**

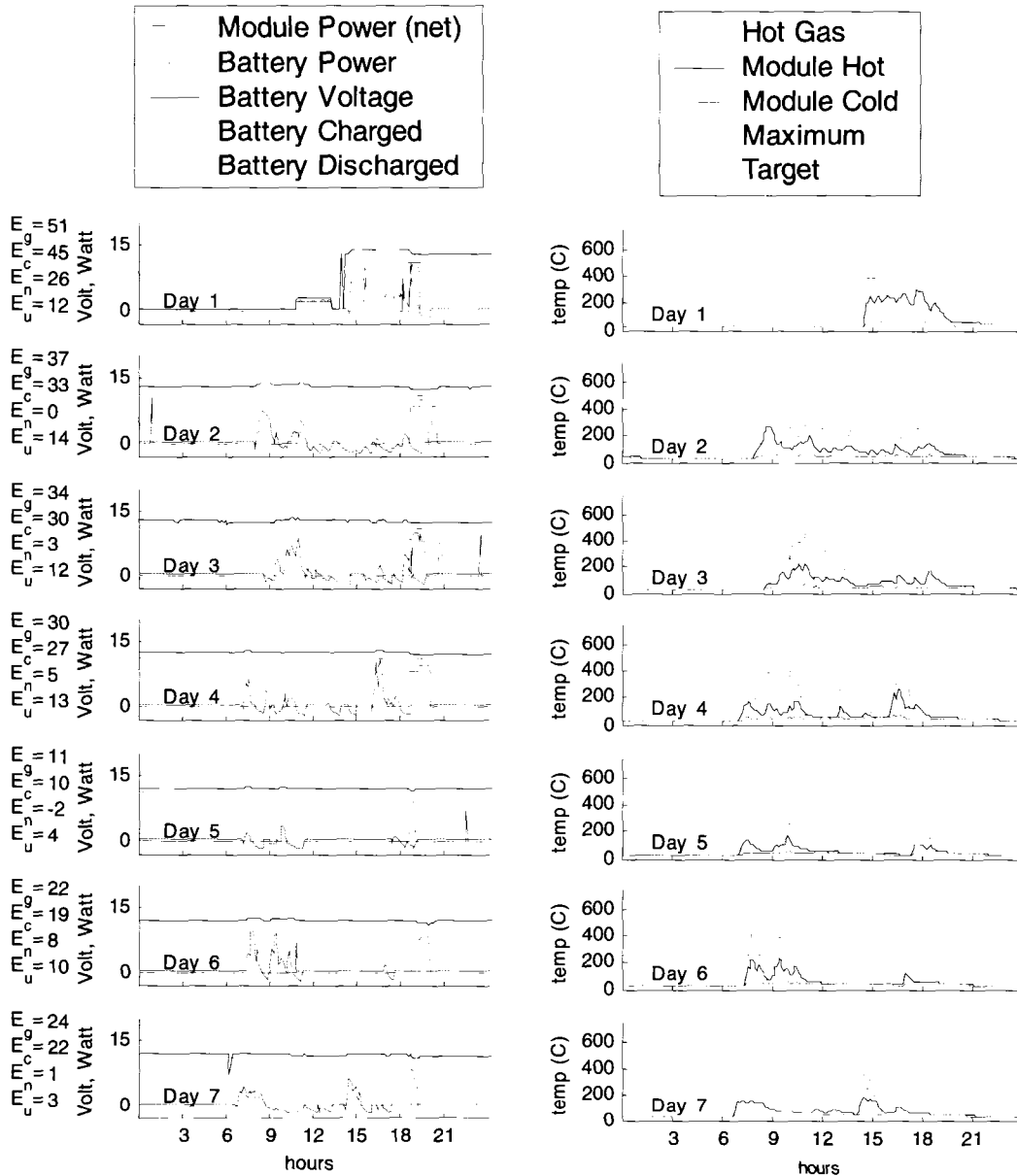
Heatsink	E1456 16.25 cm
Fan	Mechatronics
Fan Voltage	12V



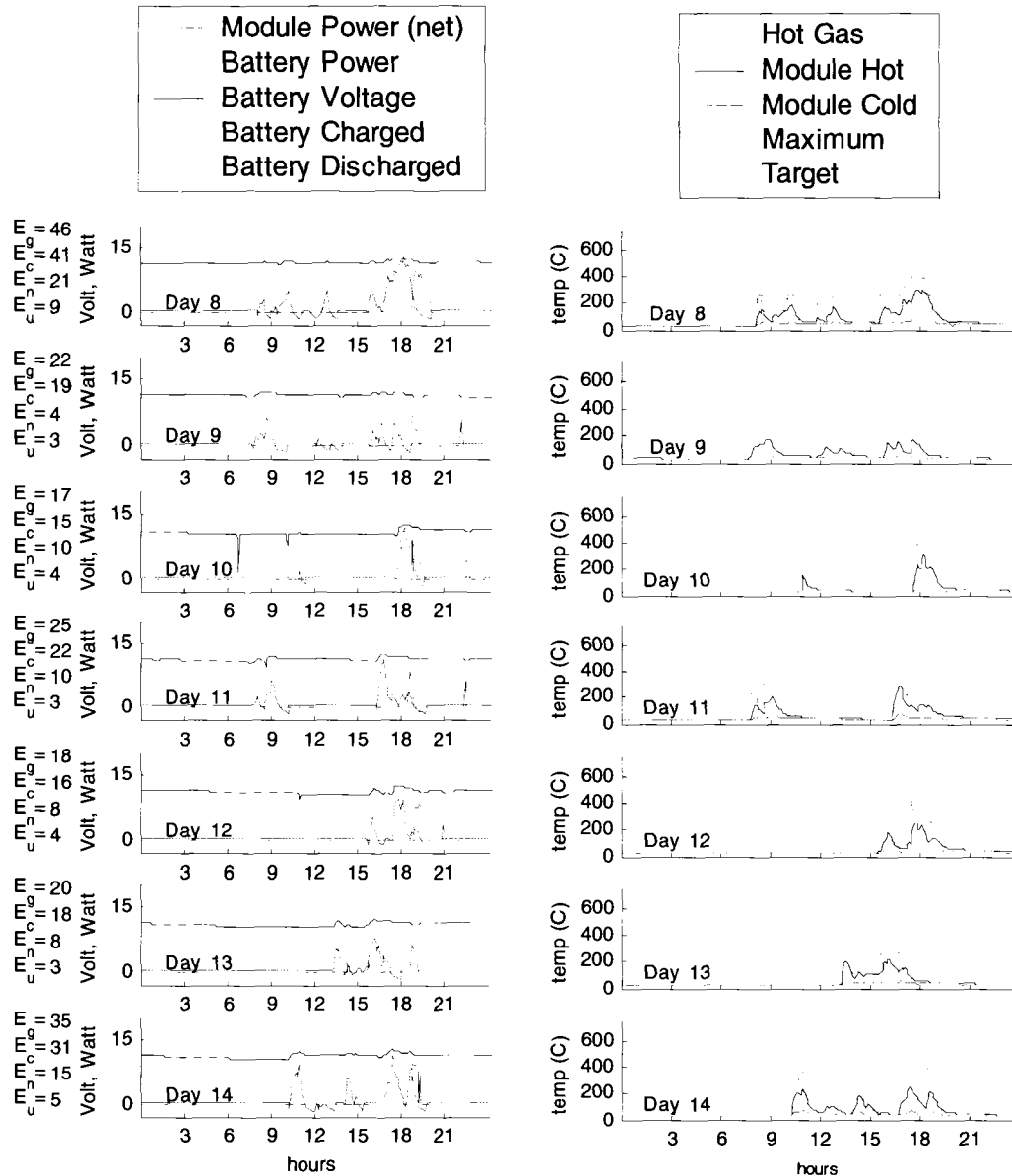
# 12.5 Nicaragua 5 Week Data House 7 and 8

## 12.5.1 House 7 Five Week Data

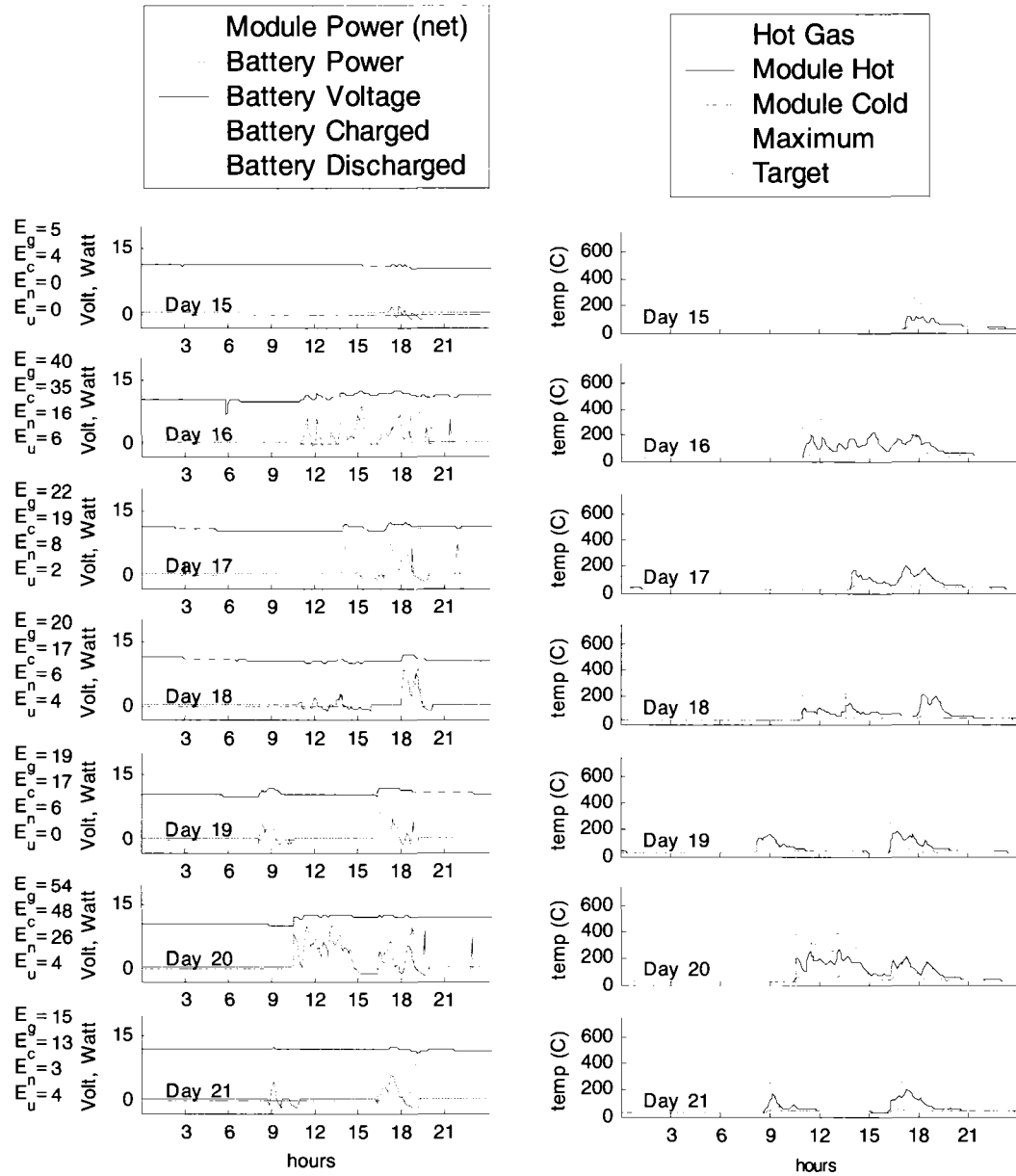
Week 1



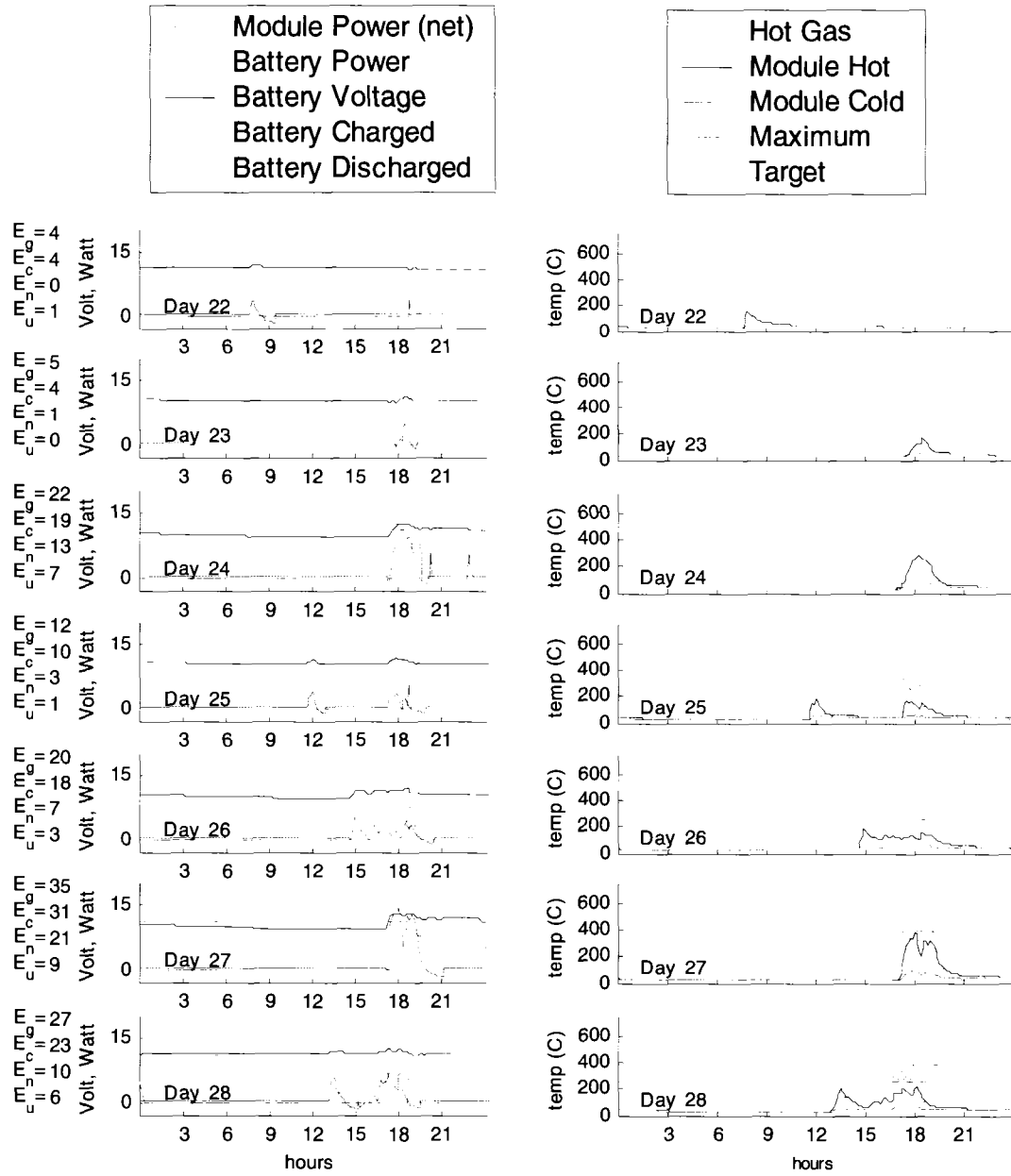
Week 2



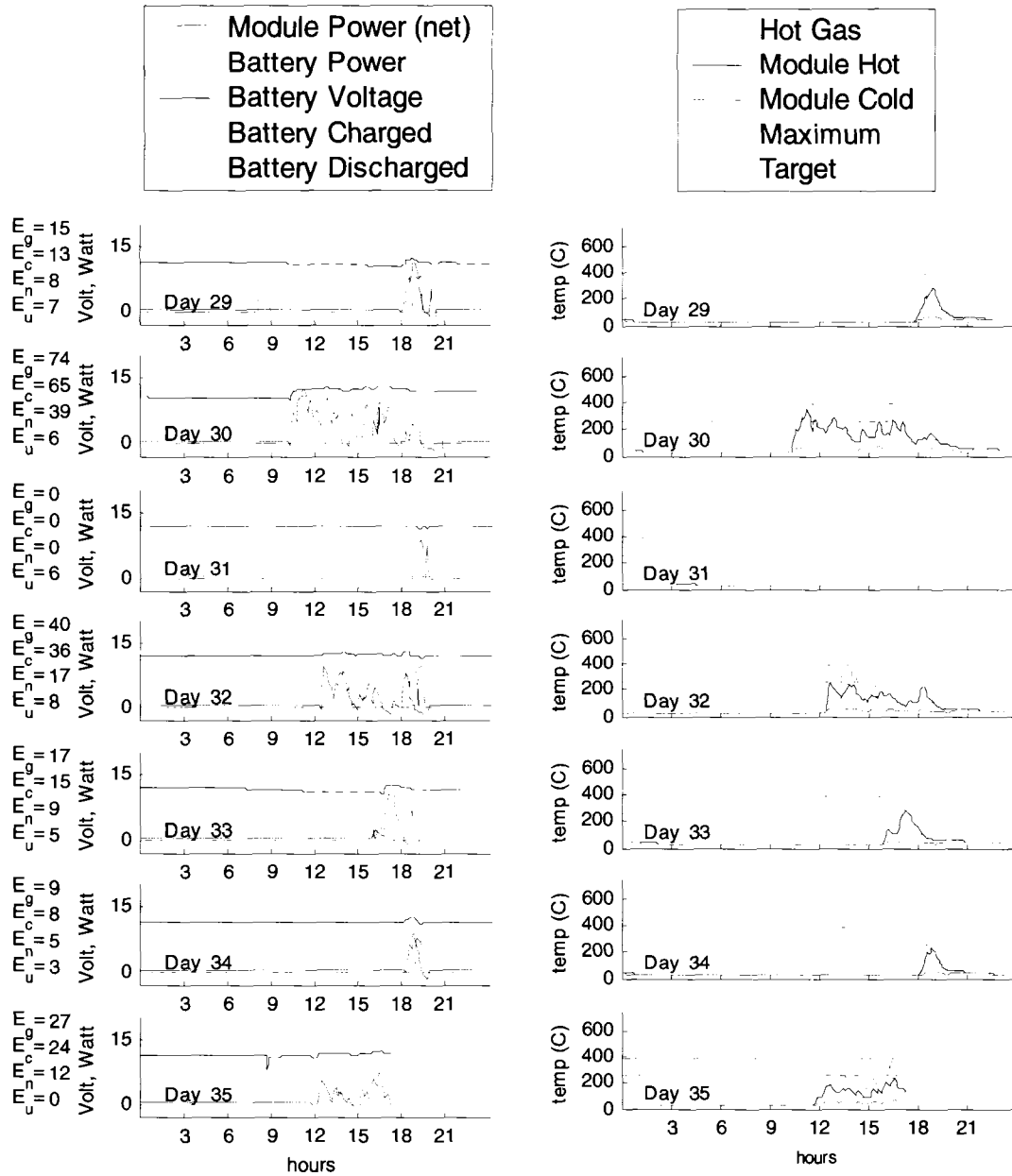
Week 3



Week 4

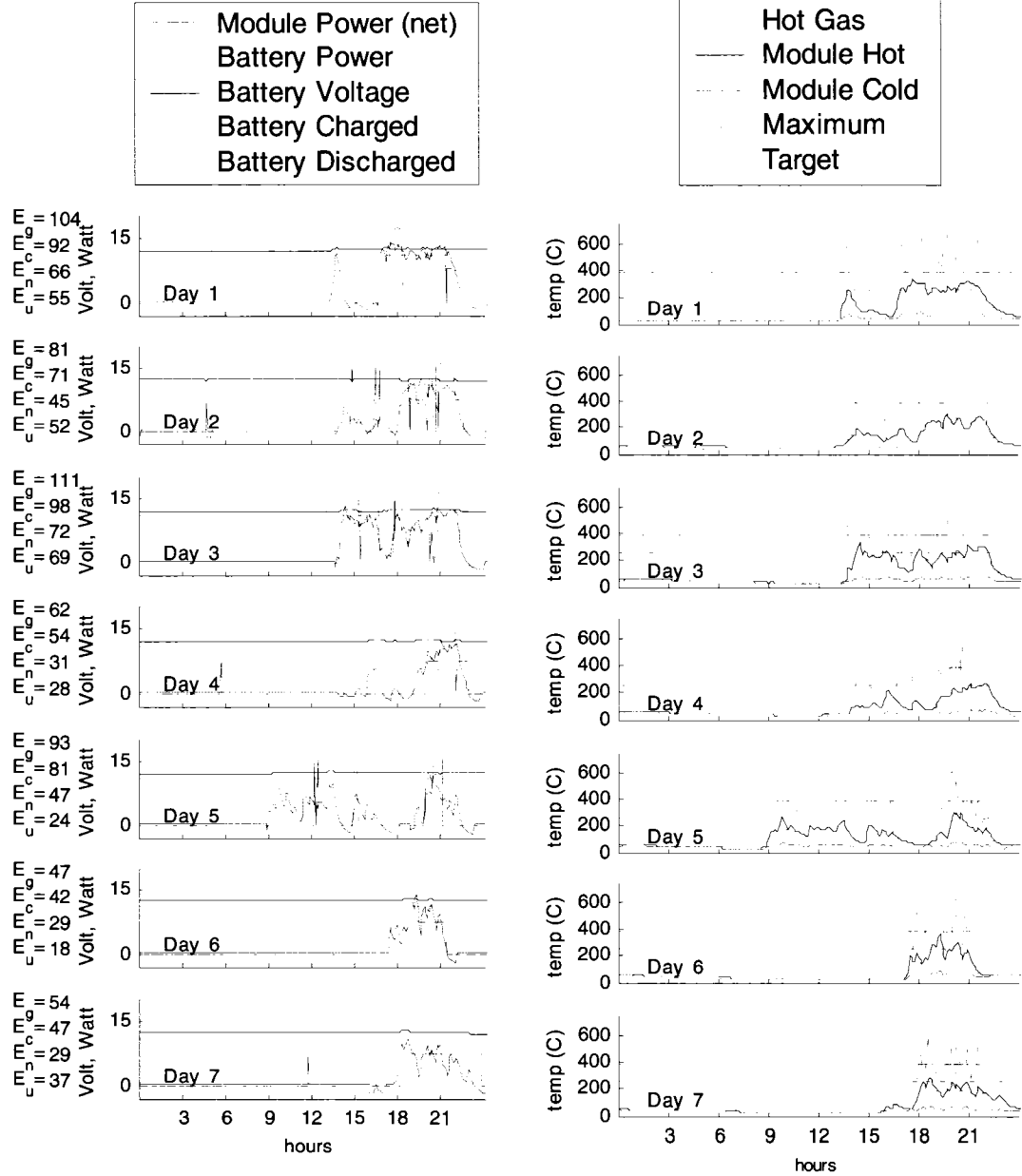


Week 5

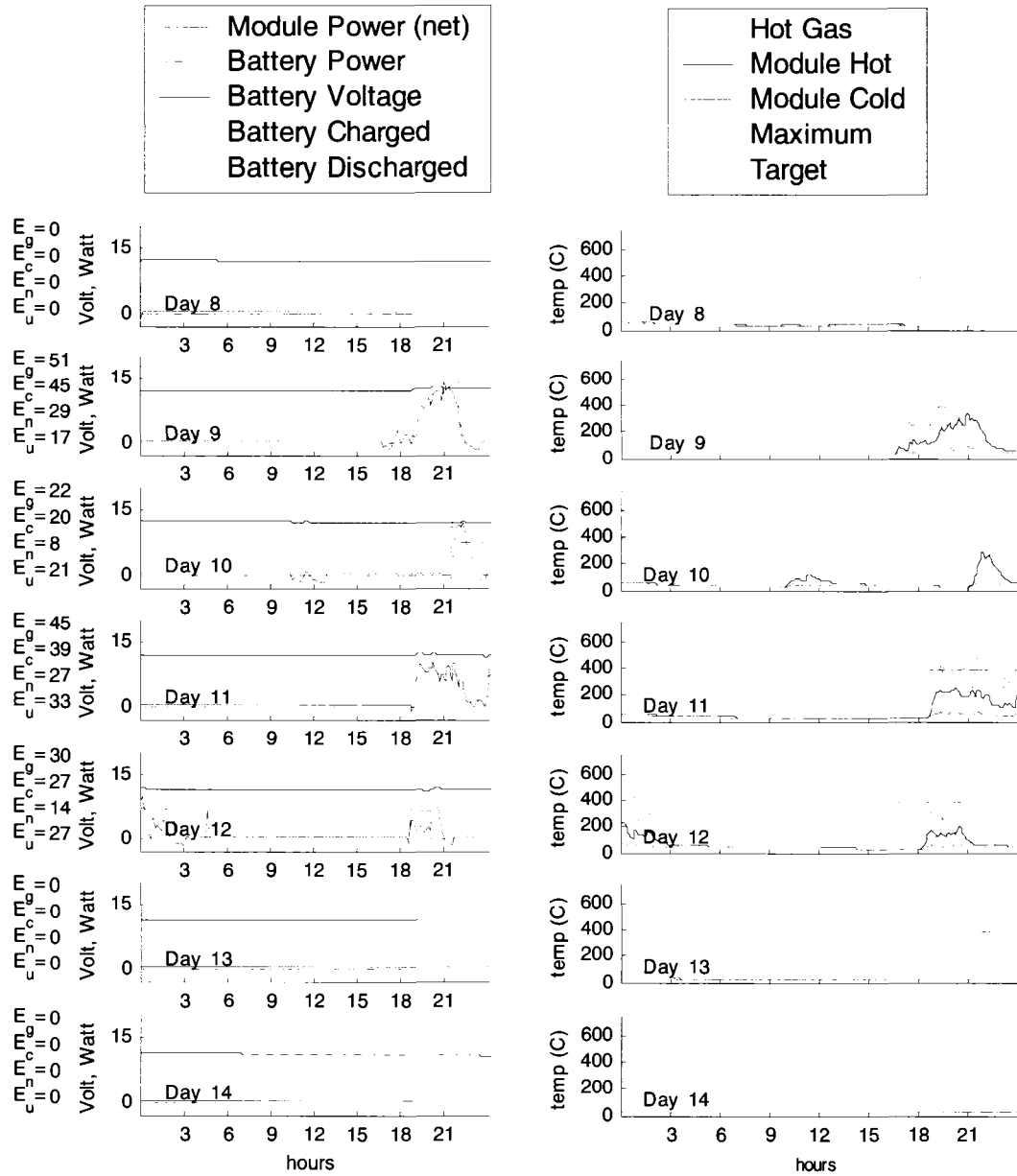


## 12.5.2 House 8 Five Week Data

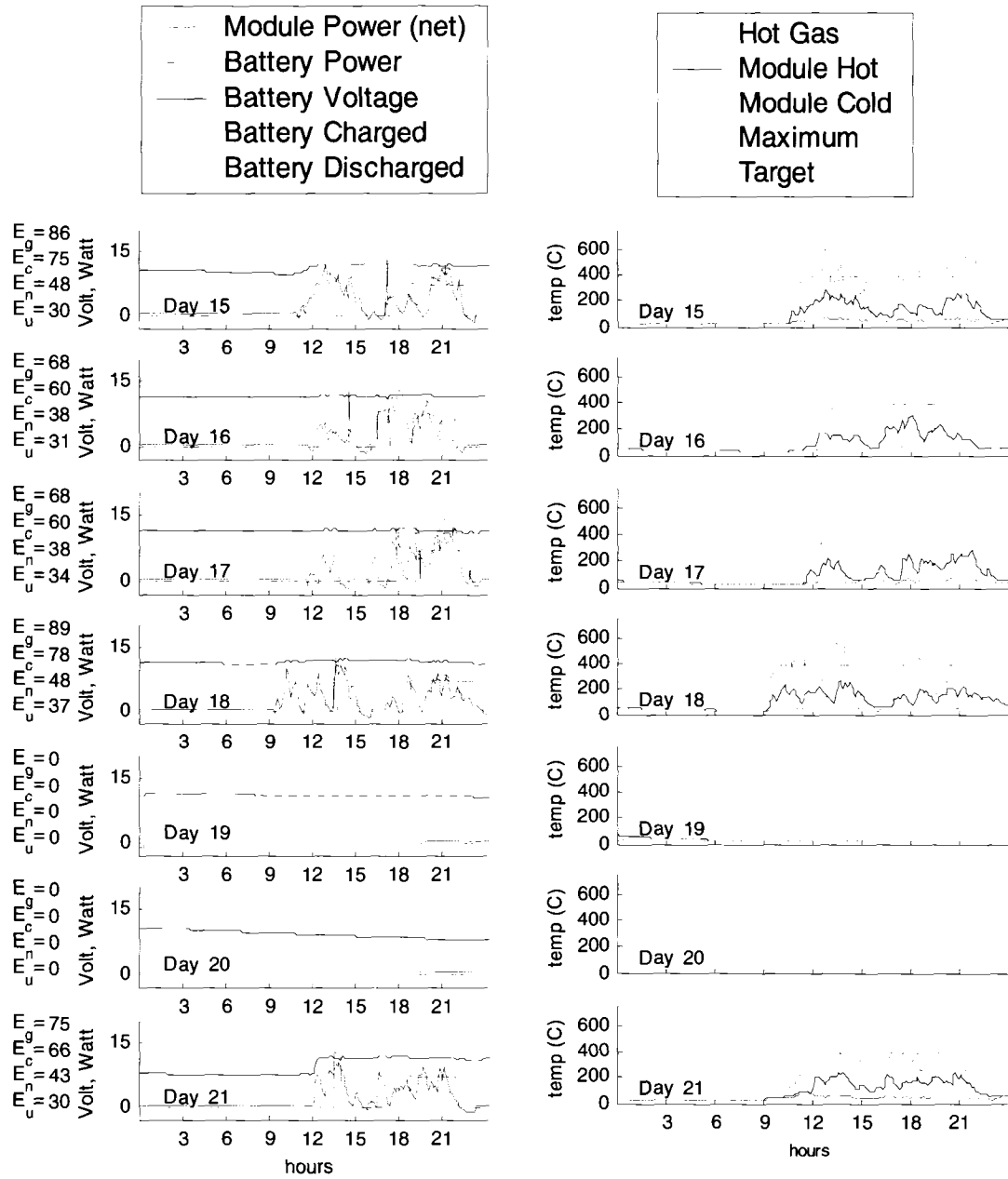
Week 1



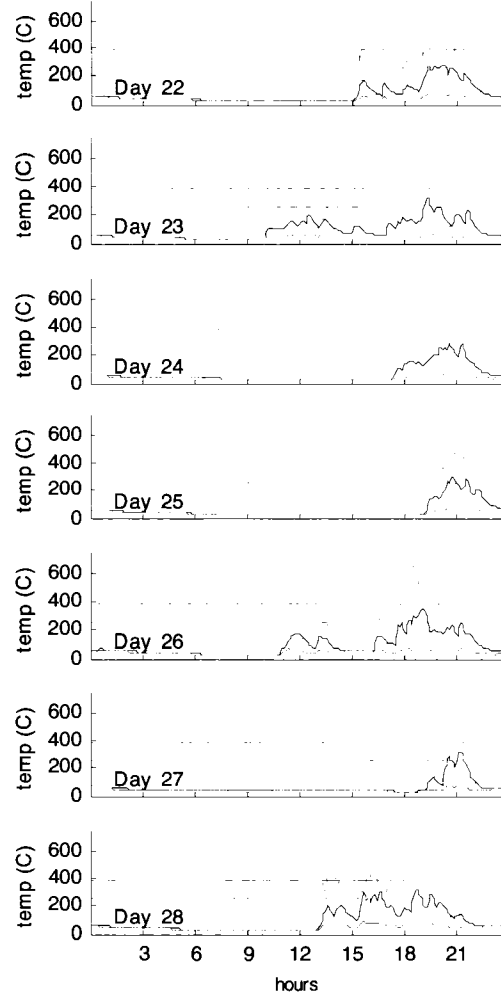
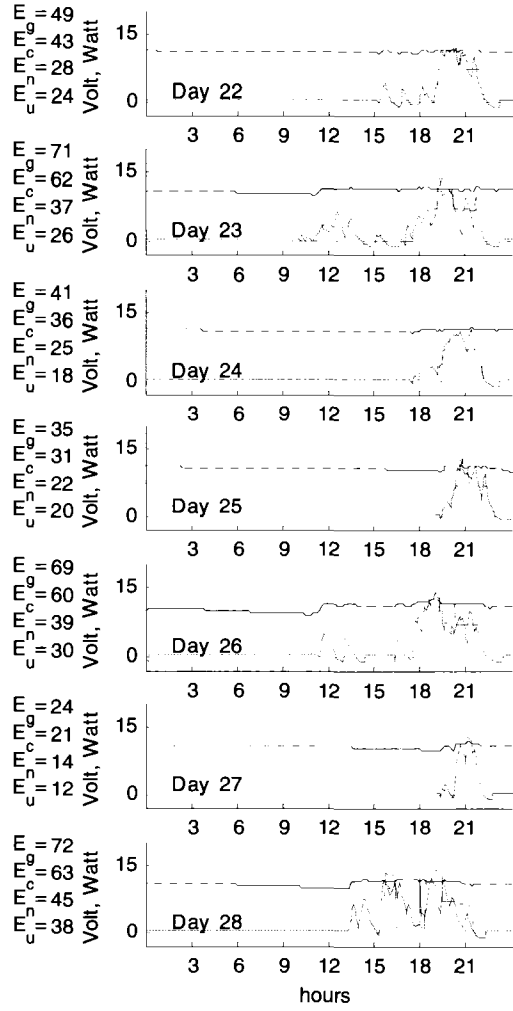
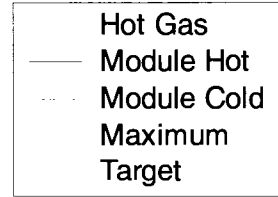
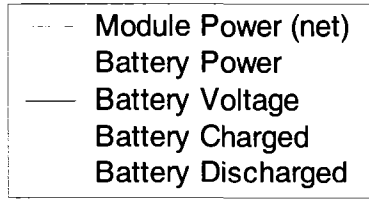
Week 2



Week 3



Week 4



Week 5

